Polymerization Kinetics and Properties of Vinyl Polymers

by

Ahmed Hazem Abdel-Alim, B.Sc.

A Thesis

Submitted to the Faculty of Graduate Studies

in partial fulfilment of the requirements

for the degree

Doctor of Philosophy

McMaster University

September 1973

DOCTOR OF PHILOSOPHY (1973) McMaster University

(Chemical Engineering) Hamilton, Ontario

TITLE: Polymerization Kinetics and Properties of Vinyl Polymers

AUTHOR: Ahmed Hazem Abdel-Alim

B.Sc. Chemical Engineering (Cairo University, Egypt)

SUPERVISOR: Professor A.E. Hamielec

NUMBER OF PAGES: (XV), 1-103, 11-56, 111-83

SCOPE AND CONTENTS

This thesis has been written as three self-consistent parts. Part One reports on experimental and theoretical investigation of the kinetics of the bulk polymerization of vinyl chloride. Part Two found its origin in Part One and resulted from the need of unambiguous characterization of the polymer synthesized. Molecular aggregation can interfere with the interpretation of all classical methods of polymer characterization in addition to gel permeation chromatography. Part Three resulted from an independent study performed by the author to broaden his knowledge in the field of polymer science and engineering in the area of polymer rheology. The results of this study were very successful and made a significant contribution to polymer rheology and therefore are reported herein. Some details of these three Parts follow under separate headings.

PART ONE - "Bulk Polymerication of Vinyl Chloride"

Herein reported is an experimental and theoretical study of the bulk polymerization of vinyl chloride using 2.2' - azobisisobutyronitrile initiator in the temperature range, 30°C to 70°C. Molecular weight averages and distribution were measured by gel permeation chromatography. A model has been proposed which accurately predicts both conversion and molecular weight distribution.

PART TWO - "Molecular Aggregation in Polyvinylchloride"

Herein is reported a comprehensive experimental study of the phenomenon of molecular aggregation in polyvinylchloride. Aggregate formation increases at lower polymerization temperatures. Syndiotacticity of the polymer measured by NMR was correlated with the aggregate content measured by gel permeation chromatography. At very low polymerization temperatures (-10°C) a second kind of aggregate was noticed. This type is larger in size and more temperature stable than aggregates formed at higher temperatures. Electron microscope examination supported the existence of at least two types of aggregates in accordance with GPC measurements. Techniques for disaggregating aggregates before polymer characterization are recommended.

PART THREE - "HIGH SHEAR VISCOMETRY"

A high shear couette viscometer with a very small gap between the cylinders (10^{-3} inch) was used to generate uniform shear rates up to 10^5 sec^{-1} making the following investigations possible:

I) Flow Properties of Polystyrene Solutions under High Shear Rates

Solutions of narrow polystyrene standards were sheared and the apparent viscosity versus shear rate was measured. Curves for different molecular weights and concentrations were found to overlap when plotted in dimensionless coordinates giving excellent agreement with the modified entanglement theory of Graessley.

II) Shear Degradation of Polyacrylamide

An equilibrium study of shear degradation was performed. Equilibrium molecular weight distributions at different shear rates and stages of degradation were measured by gel permeation chromatography. Measurements showed that the distributions tend to narrow on degradation in agreement with the midpoint break theory of Bueche. A correlation which relates the applied shear stress to the maximum stable molecular weight of the degraded polymer was found.

ACKNOWLEDGEMENTS

The author wishes to express his gratitude to those who contributed to this work. He is particularly indebted to:

His research director, Dr. A.E. Hamielec, for his enthusiasm, interest and guidance throughout the course of this study.

The members of the Ph.D. supervisory committee, Dr. J. Vlachopoulos and Dr. A.J. Yarwood for their advice in this study and in the final write-up of the thesis.

Dr. A. Grey of the Ontario Research Foundation for performing the NMR measurements.

Dr. S.T. Balke of Xerox Corporation, Rochester, for his assistance in the high shear viscometry investigation.

Imperial Oil Ltd., Canada, for financial support of projects reported as Parts (I) and (II).

McMaster University for providing financial assistance.

Special appreciation to Dr. C.M. Crowe for his advice during my stay at McMaster University.

Mrs. Sheelagh Courtney for her careful and concientious work in typing this dissertation.

TABLE OF CONTENTS

Part (I): Bulk Polymerization of Vinyl Chloride

Part (II): Molecular Aggregation in Polyvinyl Chloride

TABLE INDEX

FIGURE INDEX

PART 1

BULK POLYMERIZATION OF VINYL CHLORIDE

1.1 Introduction

1.1.1 General[1,2]

Polyvinyl chloride is an important member of a large family known as the vinyl polymers. These are the polymers containing the vinyl group (CH_2 = CH-). Other members of this family are, for example, polyethylene and polystyrene. Polymers containing the vinylidene groups (CH_2 = CR-) are also considered members of the same family. Polymethyl methacrylate and polyvinylidene chloride are examples of this second type.

Being a very distinguished member of the family, polyvinyl chloride (PVC) is usually referred to as "vinyl". Incorrectly the acronym PVC is often used to indicate the copolymers of polyvinyl chloride as well as the homopolymer.

Until recently, about thirty years ago, PVC was considered a laboratory curiosity. Today it ranks as the second most important polymer in use volume and the first on a compounded basis. In Europe PVC is the leading plastic material. In the U.S.A. the annual production rate is close to 3 billion pounds and this rate is increasing at about 20% each year.

PVC is currently used in the manufacture of flooring, furniture, hi-fi records, pipes, dolls garden hoses, balls, cans, toys, and of course, the wiring for sound and other appliances is vinyl-coated. The rapid growth of PVC production is usually attributed to the following factors:

1) Low Cost: PVC is among the least expensive polymers. In 1954 the selling price was about 38 cents a pound. In 1968 it sold for as low as 10 cents a pound. A current world shortage of vinyl chlordie has caused a recent price increase for PVC.

2) The ability to compound with plasticizers to give a range of flexibility.

3) Good physical, chemical and weathering properties of the compounded polymer.

4) Processability by a wide variety of techniques including calendering, extrusion, different types of molding, solution and latex coating and impregnation.

PVC has been extensively studied. Such studies deal with many areas, including polymerization kinetics, polymer characterization, degradation, rheology and processing. Despite the huge commercial production of PVC, some of the fundamental problems are not yet solved; for example, there is no model available that predicts conversion and molecular weight distribution accurately during free radical polymerization. Other problems are associated with the existence of molecular aggregates in the polymer during polymer characterization and processing. With the recent advent of improved analytical instruments and techniques it is possible to explore these important aspects with some hope of success.

Part (1) of this thesis reports on an experimental and theoretical study of the free-radical bulk polymerization of vinyl

chloride. Gel permeation chromatography was used to measure the molecular weight distribution (MWD) of the polymer. The purpose of the research was to develop a model capable of predicting with reasonable accuracy the conversion of monomer and molecular weight distribution of the polymer to limiting conversion. Part (II) reports an investigation of molecular aggregation of PVC.

1.1.2 Viny Chloride Monomer[1,2]

The monomer, $CH_2 = CHCl$ is a colourless, non-toxic gas with a faintly sweet odour. It may cause anesthesia at high concentrations. The main hazard is fire and explosion. Properties of vinyl chloride monomer are given in table 1.1.

Generally, vinyl chloride may be prepared by one of the following reactions:

a) Acetylene and HCl, to produce vinyl chloride directly:

$$CH \equiv CH + HCl \xrightarrow{HgCl_2} CH_2 = CHCl + \text{heat}$$

Acetylene gas may be obtained from either calcium carbide or petrochemical feedstock. It is then reacted with hydrogen chloride using mercuric chloride[3,4] or other heavy metal halides[5] as a catalyst. It is essential that the gas streams be dry and free from arsine, phosphine and sulfur compounds.

TABLE (1-1)

PROPERTIES OF VINYL CHLORIDE MONOMER

Normal boiling point	-13.7°C
Normal freezing point	-153.8°C
Density gm/cm^3	$\rho = 0.9479 - 0.00189\ t\ (t°C)$
Flash point	-78°C
Explosive limits in air	4-22% by volume
Vapor pressure, at 0°C	25.1 psi
at 20°C	49.2 psi
at 40°C	87.6 psi
Solubility	Aliphatic and aromatic hydrocarbons, ester, ketones, ethers, alcohols, chlorinated solvents, and most other organic solvents. Slightly soluble in water.
Viscosity at -10°C	0.25 Cps.
Molecular weight	62.5
Colour	Colourless
Odour	Pleasant, sweet
Heat of polymerization	23 kcal/mole
Index of refraction, 15°C	1.38

b) Ethylene and chlorine, to produce ethylene dichloride, followed by cracking to yield vinyl chloride and hydrogen chloride:

$$CH_2 = CH_2 + Cl_2 \longrightarrow CH_2Cl - CH_2CL \xrightarrow{500°C} CH_2 = CHCl + HCl$$

c) The balanced process. This is a combination of the above two methods where the hydrogen chloride produced as a byproduct in the second method is used as a reactant in the first method. This process is in actual use in one of the plants in Japan and a flowsheet is given by Buckley[6].

A review of some processes for making vinyl chloride was given by Albright[7].

1.1.3 Polymerization Processes[1,2]

Vinyl chloride can be polymerized by bulk, solution, suspension or emulsion techniques. Currently, the latter two methods are the most commonly used. The literature contains few details of commercial processes. However, a brief review of the processes and reactions may be found[8].

Bulk Process[9]

In this process the monomer is polymerized without diluents. An important advantage is the production of polymer free of impurities. However, the control of reaction rate and heat removal present serious difficulties. Bulk process began to become commercially important with the development of the Pechiney-St. Gobain process in France. In the original one-step Pechiney-St. Gobain process (PSG) which was practiced in France

and Germany, a 3000-gal ball mill was used as the reactor[10]. The balls densified the precipitated fluffy PVC to a fine powder, similar to general-purpose grade and suitable for extrusion or calendering. In 1960, PSG patented a continuous ball mill process[11] with a periodically opening discharge valve. This process did not become commercial. Further development led PSG to its two-step process[12]. One line consists of one 2000-gal rapidly agitated prepolymerization kettle and three or four 4200-5300-gal batch ribbon blender-type autoclaves. Usually, half of the monomer is fed to the prepolymerizer, furnished with a reflux condenser, and polymerized to 7% conversion by the addition of a fast initiator[13] in less than 1 hr. The speed of agitation determines the size of the polymer particles, which act as seeds in the second step[14]. The second half of the monomer is fed to the ribbon blender-type autoclave, and polymerization is completed in 5-9 hours. The reaction is simply stopped by evaporating the unreacted monomer, which is condensed and reused in the following batch. The resin is then discharged under agitation by pneumatic conveyors to screens for removing oversized particles. One line has a capacity of 35-45 million pounds per year dry-blend resin. PSG has also patented[15] a vertical reactor with two agitators - a slow turning top agitator and a faster turning bottom agitator, plus a reflux condenser. This reactor will be built as large as 10,000 gal and might replace the horizontal PSG reactors in the future.

Solution Process

This technique utilizes a solvent solution containing monomer. Depending on the choice of the solvent the polymer formed may dissolve

or precipitate. In either way it is easily separated and dried. This system permits efficient heat transfer. Highly uniform copolymer resins may be produced by this method. The main disadvantage is the high production cost due to the need for efficient solvent recovery.

Suspension Process

Currently this is the most important method for PVC production. About 85% of the PVC made in the U.S.A. and 50% of that made in Europe is produced by this process. This technique employs water as the continuous phase, with vinyl chloride monomer dispersed by means of suspending agents. Particle size range is considerably larger than for emulsion resins. Processing costs are low, level of suspending agent is low in the finished resin, and process control is good.

Emulsion Process

This process produces a fine particle size dispersion of polymer in water by using an emulsifying agent. The emulsion is coagulated and dried for processing applications, or it may be spray dried to produce plastisol resins. Extremely fine particle size types are also produced for latex application. As in suspension polymerization the presence of a continuous water phase permits the effective removal of heat during reaction. Disadvantages are high cost of manufacture and high emulsifier level in the final product.

1.1.4 Technology of PVC Plastics

PVC as such is not a very stable polymer. To make it useful for different applications certain ingredients should be added to it. Stabilizers are added to prolong the useful life of the product during heat fabrication and outdoor exposure. Plasticizers are added to convert the hard, brittle polymer to soft, flexible material. Other ingredients are often added to enhance the end-use properties of the plastic. The range of properties which can be built into a PVC product by selection of plasticizer and other formulation ingredients is quite remarkable. The volume of literature covering this subject is large[16-21].

Stabilizers

These are chemical compounds capable of reacting with and neutralizing the hydrochloric acid split off by the polymer[22]. Generally they are classified based on their chemical type. Table 1.2 lists some of the important stabilizer classes and typical examples. The exact stabilization mechanism is not fully understood yet. There is a theory that attributes the stabilization effect to the consumption of the first HCl formed which would normally act as an autocatalyst for further HCl formation.

Plasticizers

These are high molecular weight, nonvolatile liquids which solvate and soften the polymer. The most commonly used plasticizers are esters of di-or tribasic acids. Among the properties which are considered when selecting a plasticizer are the cost, performance, volatility, flamability,

TABLE (1-2)

POLYVINYL CHLORIDE STABILIZER CLASSES

CLASS	TYPICAL EXAMPLE
Basic lead compounds	Dibasic lead carbonate
Alkaline earth compounds	Barium stearate
Zinc and cadmium compounds	Cadmium stearate
Tin compounds	Dibutyltin maleate
Oxirane compounds	Epoxidized soybean oil

ease of compounding and heat and light stability. The softening effect or the "efficiency" of the plasticizer is often measured by determining the concentration required to produce a compound with a Type A durometer hardness of 80 (ASTM Method D1706-59T)[23]. Table 1.3 lists some of the most common plasticizers and their efficiencies.

Other Ingredients

Lubricants are usually employed in calendering and extrusion to aid release from metal surfaces of the equipment. These are usually fatty acids and their soaps. Fillers of various types can be used to reduce cost in certain cases. They may also improve some properties. For example, some clay minerals improve the electrical resistivity of insulation products. Other ingredients are light screening agents, antistatic agents and colourants. The resin may be processed by a variety of techniques depending on the application. Calendering[25] is used to make sheets. Extrusion[26] for wire coatings and pipes. Among the other techniques are injection molding[27], blow molding[28], and compression molding. An excellent review on PVC processing techniques may be found in reference (2).

1.1.5 Applications and Usage of PVC[1]

Polyvinyl chloride polymers are used in a variety of applications. Table 1.4 shows approximate percentages of PVC production used for different applications[1]. Welter[24] gives a general classification of PVC plastics according to use. He classified them as general purpose resin, dry-blend resin, and plastisol or organosol resin. To these types we can add rigid products and latex.

TABLE (I-3)

PLASTICIZER CONCENTRATION TO YIELD 80 DUROMETER HARDNESS, AT 23°C

Plasticizer	Parts Plasticizer per 100 Resins
Di-(2-ethylhexyl) adipate	40
Tri-(2-ethylhexyl) phosphate	47
Di-(2-ethylhexyl) phthalate	48
2-Ethylhexyl epoxy phthalate	50
Epoxidized soybean oil	50
Tri(cresyl) phosphate	56

TABLE (1-4)

PATTERN OF USAGE OF POLY VINYL CHLORIDE

Application	Percentage %
Calendering (film and sheeting)	28.2
Spreader coating (paper and cloth coating)	4.7
Flooring	21.4
Sound records	6.3
Wire and Cable	13.8
Slush molding	5.8
Other molding	16.4
Coatings, adhesives	3.4

General Purpose Resins (Melt Compounding)

These are made by suspension polymerization with coarse particles in the 75 to 150 micron range. Generally they are used in calendering. The particles are characterized by high porosity and surface area thus being able to absorb the plasticizer uniformly. The process consists of preparing a premix and fluxing of the mixture, followed by pelletizing or feeding the melt to process equipment.

Dry-Blend Resins

The ingredients are added to PVC to produce a granular, free flowing compound. In contrast to the melt compounding, the resin is not melted during the mixing process. The dry-blend mixture can be fed directly to an extruder for fabrication into wire insulation, garden hose or other final forms.

Plastisols and Organosols

Plastisols are mixtures of resins and other ingredients, solid at room temperature, but fusible to a fluid by heating. The polymer used here is usually made by emulsion polymerization. They are applied by dip-coating, slush-molding or casting. Organosols are made of plastisols by the addition of volatile organic diluents (Hydrocarbons) and dispersants (esters and ketones).

Rigid Products

These are usually made of unplasticized PVC. Examples are pipes and ducts. The resin can also be fabricated into film or blow-molded bottles.

Latex

Emulsion-polymerized PVC is produced and marketed as a colloidal emulsion in water. Solid content is about 50%. In this form PVC is mainly used in the coating industry for impregnation and coating of fibrous materials such as fabric, paper, and leather.

1.1.6 Copolymers of PVC

Vinyl chloride copolymerizes with other monomers readily and many commercial copolymers are available. A listing of reactivity ratios is given by Brandrup and Immergut[29]. The copolymers generally widen the area of application of polyvinyl chloride resins because specific comonomers are capable of imparting properties otherwise unattainable. Among the important comonomers are:

Vinyl Acetate

This usually increases the softness thus allows fabrication of unplasticized polymer at milder conditions. This copolymer is primarily used in sheets and phonograph records.

Propylene

This copolymer is recommended in making blown bottles. It is usually processed at temperatures lower than those required for PVC homopolymer. Scrap can be recycled more readily than with homopolymer.

Vinylidene Chloride

Copolymers of low PVC concentrations are used in making films and fibers. When the PVC concentration is above 60% the copolymer is used in solution coating applications.

Acrylonitrile

This copolymer is manufactured by Union Carbide Corporation and the product is called "Dynel fibers". Carpets and drapes made from Dynel are flame resistant. The major deficiency of these copolymers is poor colour and light stability.

1.2 Molecular Properties of PVC Homopolymer

Molecular properties are those class of properties associated with the arrangement of atoms in the molecules themselves. They are created during synthesis but once the polymer is made they cannot be changed by processing without bond breaking. These properties are chain configuration, branching and molecular weight distribution.

1.2.1 Chain Configuration

This refers to the structure of the polymer chain. Chain configuration includes:

Recurrence Regularity

If we consider the methylene group in vinyl chloride as the tail of the molecular and the carbon atom containing the chlorine atom as the head of the molecule, it is possible to describe the connecting monomer units as head-to-tail, head-to-head, or tail-to-tail structures:

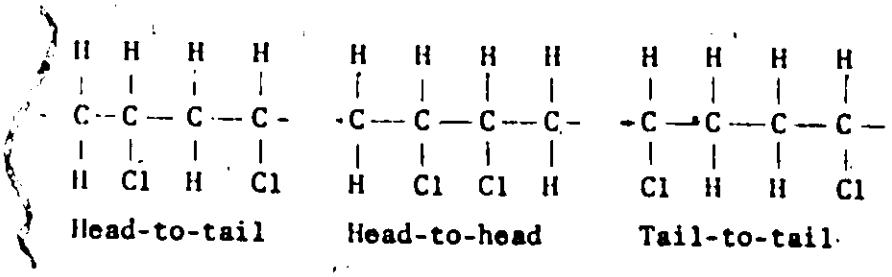

The existing evidence favours the head-to-tail addition, but is does not preclude the possibility of a certain amount of abnormal addition patterns.

Stereoregularity (Tacticity)

There are two different arrangements for the chlorine atom in the CHCl grouping in PVC. These are relative to the plane containing the backbone carbon-carbon bonds. When all the chlorine atoms are found in the same relative position, an isotactic chain results:

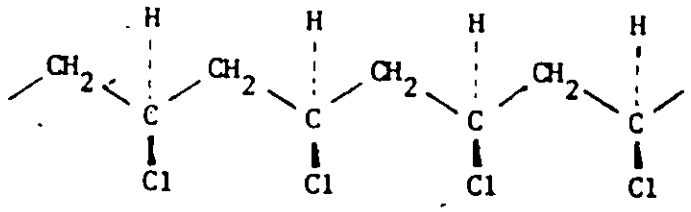

where all the carbon atoms lie in the plane of the paper. The bonds designated by dotted lines lie below the plane of the paper, and the bonds designated by the solid thin triangles lie above this plane. When the chlorine atoms are in an alternating configuration, a syndiotactic chain results:

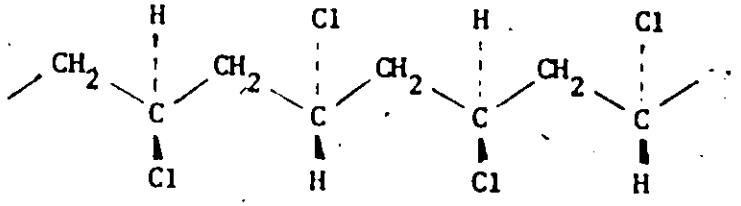

When the arrangement is random we get "heterotactic chain". An atactic polymer is one with 50% syndiotactic and 50% isotactic fractions.

Chain configuration will be discussed in more detail in Part II of this thesis.

1.2.2 Branching[1]

Branching results generally from the transfer reactions to polymer. In addition, the lower the polymerization temperature, the lower the degree of branching. The degree of branching is determined by infrared analysis on polyethylene obtained through reduction of PVC[30]. Infrared adsorption bands for the methyl group at 1378 cm^{-1} and for the methylene group at 1370 cm^{-1} are chosen for the analysis. Since a linear relationship exists between the methyl content (CH_3/100 CH_2) and the optical density ratio at these bands, calibration curves may be obtained by examination of the appropriate paraffin homologs[31].

Generally, branching is not highly prevalent in PVC polymerized below room temperature. Nakajima et al[31] conducted polymerizations at 90, 50, 20, -15, and -75°C. The degree of branching droped from 0.27 CH_3/100 CH_2 for the polymer prepared at 90°C to zero for the polymer prepared at -75°C. Cotman[30] found the degree of branching for a commercial polymer to be in the range of 0.4 to 1.1. Bier and Kramer[32] found a value of less than 0.5 for a commercial polymer. Pezzin and coworkers[33] found about 1.5 to 1.7 CH_3/100 CH_2 in certain fractions of a commercial PVC and there was no indication of a variation in degree of branching with molecular weight. Recently Lyngaae-Jorgensen[34] reported that the degree of branching in commercial PVC is 0.4 to 0.5 of which only about 10% are long branches and 90% short branches.

1.2.3 Molecular Weight Distribution (MWD)

Since it was shown experimentally that long branches exist only in negligible amounts in PVC, it can be concluded by simple kinetic analysis when transfer to monomer is dominant that the molecular weight distribution function is expressed as

$$W(r) = \frac{r}{(\bar{r}_n)^2} \exp(-\frac{r}{\bar{r}_n})$$

r, the chain length is the independent variable, W(r) is the weight fraction of chain length r and $\bar{r}_n$ is the number average chain length.

The ratio of the weight average molecular weight $\bar{M}_w$ to the number average molecular weight $\bar{M}_n$ obtained for such a distribution will be 2.0. Recently Lyngaae-Jorgensen[35] compared theoretical MWD with experimentally measured ones for different samples of PVC and found excellent agreement which supports this hypothesis. Pezzin, Talamini and Vidotto[36] examined the molecular weight distribution of different PVC samples and found that it does not vary during the course of the polymerization. The above discussion holds for PVC prepared by suspension polymerization as well as bulk polymerization.

1.3 Physical Properties of PVC Homopolymer

These are the class of properties associated with the physical behaviour of the polymer. They depend on the molecular properties but can be altered by processing. Examples of these properties are discussed below.

1.3.1 Crystallinity

Polyvinyl chloride is not generally classified as a crystalline polymer. As formed in the usual commercial polymerization, the polymer is highly amorphous with only a low degree of crystallinity. The crystallinity is associated with syndiotactic sequences[37,38]. PVC prepared at 40-75°C has about 10% crystallinity. At lower temperatures the degree of crystallinity is higher[31]. The crystal structure appears to be typical of syndiotactic polymers, with a repeat distance corresponding to four chain carbon atoms. A detailed study of the crystal structure in PVC may be found in reference (38).

Clark[39] reported the existence of spherulites (radial crystals) in thin films of PVC. This type of crystal was also noted by Utsuo and Stein[40]. Smith and Wilkes[41] prepared PVC single crystals by using n-butyraldehyde as a chain transfer agent. The single crystals were flat, rectangular in shape and had a thickness of about 100 Å.

1.3.2 Glass Transition Temperature (T_g)

This is defined as the temperature at which an amorphous polymer will change from its hard or glassy state to a rubbery soft material. Near this temperature certain properties undergo a remarkable change. For example, specific volume, mechanical loss and shear modulus are among the properties that change drastically near the glass transition temperature. For most commercial PVC the glass transition temperature is between 70 and 80°C[42-45]. Reding et al[44] showed that there is a

negative linear dependence of T_g on polymerization temperature. The addition of a plasticizer to the polymer significantly reduces the glass transition temperature[1]. The effect of pressure on T_g of PVC was studied by Heydemann and Guicking[46]. They showed that there is a slight linear increase in T_g with pressure in the order of 0.013 to 0.015°C per atmosphere.

1.3.3 Crystalline Melting Temperature (T_m)[1,47]

This is defined as the melting temperature of the crystalline domains of the polymer. The difference between T_m and T_g is better understood by considering the changes which occur in a liquid polymer as it is cooled. The translation, rotational, and vibrational energies of the molecules decrease on cooling. When both the translation and rotational energies are zero, crystallization is possible. The temperature at which this occurs is T_m. If certain symmetry requirements are not met, crystallization does not take place, but the energies of the molecules continue to decrease as the temperature decreases. A temperature is finally reached - the T_g - at which the segmental motion of the chains stop due to the cessation of bond rotations.

The melting point of PVC is markedly affected by polymerization temperature or more specifically by stereoregularity and crystallinity. The crystalline melting temperature cannot be measured by direct techniques because polymer decomposition is too rapid at elevated temperatures. Special methods for measuring it as a function of polymerization temperature may be found in the work of Reding and coworkers[44]. The melting point of commercial PVC (prepared at about 50-60°C) is about 200°C.

1.3.4 Solubility and Theta Solvents[1]

PVC is soluble in many ketones and esters. It swells in aromatic hydrocarbons, but is unaffected by alcohols or aliphatic hydrocarbons. The polymer is insoluble in some organic chlorides, including its own monomer but soluble in others, e.g. ethylene dichloride. Similar to other polymers, low molecular weight PVC is more soluble than high molecular weight in the same solvent. The preferred or most widely used solvents are tetrahydrofurane (THF) and cyclohexanone. Benzyl alcohol at 155.4°C is the only reported[48] theta solvent for PVC (a theta solvent is a solvent in which the dimensions of the molecular coils are unperturbed by solvent effects).

In benzyl alcohol at 155.4°C, the root mean square end-to-end dimension of PVC molecule is $0.906\ M^{1/2}$ Å where M is the molecular weight[48]. The calculated value for the "freely-rotating chain" is $0.296\ M^{1/2}$ Å. Data on polymer chain dimensions in other solvents are given in the polymer handbook[29].

1.3.5 Melt Viscosity[2]

Low melt viscosity permits good mixing, resulting in the development of uniform physical properties and permitting high processing rates. PVC is considered one of the difficult polymers to process, since it has a high melt viscosity. Lower melt viscosities are obtained through the use of copolymers and plasticizers. Factors contributing to an increase in melt viscosity are high molecular weight, long chain branching, cross-linked structure, and regularity. The presence of low molecular

weight PVC fractions reduces the melt viscosity. According to Rudd[49] melt viscosity at low shear rates is dependent on weight average molecular weight. At high shear rates, both the number average and the weight average are significant for melt viscosity.

1.4 Chemical Properties of PVC Homopolymer

PVC is generally considered to be quite insensitive to chemical attack compared to most commercial polymers. Its resistance to deterioration by air, peroxides or other oxidative reagents is especially significant. Aqueous acids produce no deleterious effects. In contrast to its relative inertness towards external reagents, PVC is considered a low stability polymer, for it decomposes readily and HCl is split off when the solid polymer is heated. For this reason stabilizers are usually added to PVC and an extensive technology of stabilization of PVC has been developed.

1.4.1 Thermal Dehydrochlorination

At about 250°C HCl molecules start to split off the polymer chains. The mechanism of the reaction is not yet fully clear. Stromberg[50] and Winkler[51] suggest mechanisms which involve the formation of a free radical on the polymer chain, followed by a re-arrangement and the split-off of a molecule of HCl. The reaction proceeds down the chain through a free radical mechanism in a zipper-like fashion, producing a conjugated unsaturated structure. Other data,

primarily by Gengaugh and Sharpe[52], signify a unimolecular process to be more plausible. They note that free radical sources such as azobisisobutyronitrile or benzoyl peroxide effect, at the most, only a mild acceleration of dehydrochlorination. Supporting evidence against a radical chain reaction is deduced from the effect of radical traps or inhibitors. The usual inhibitors have little or no effect on the rate.

It might be noted that it would be quite difficult to devise experiments which would differentiate zipper-like free radical mechanism from a straight-forward unimolecular decomposition proceeding along the chain by labilization of successive secondary allyl chlorides. A good survey paper on this subject was given recently by Braun[53].

1.4.2 Radiation-Induced Reactions

Irradiation of PVC may cause degradation of the polymer. The observable effects being discolouration, chain splitting, and cross-linking[21]. Kenyon[54] studied the mechanism of the reaction and found that the unstabilized polymer evolves no HCl when wavelengths shorter than 340 mμ are absent but light of shorter wavelengths induces HCl loss, the amount formed increasing with decreasing wavelength of the light employed. If oxygen is present, degradation and discolouration predominate.

I.4.3 Hydrogenation

When PVC is treated by lithium aluminium hydride in THF solution it is converted into the hydrogenated form through replacement of the chlorine by hydrogen [55]. The reaction can attain 97% conversion if done properly. This technique along with infra-red analysis are used to detect branching in polyvinyl chloride.

I.4.4 Chlorination

A resinous product may be obtained by treating PVC with chlorine. Post-chlorinated PVC has achieved some industrial importance since this resin has lower softening point and greater solubility than ordinary PVC. Infra-red and X-ray analysis showed that most of the chlorines substitute at the methylene sites [56]

I.5 Mechanism of Bulk Polymerization of Vinyl Chloride

Bulk polymerization of vinyl chloride is a typical example of what is known as "heterogeneous polymerization". Another example is the bulk polymerization of acrylonitrile. These systems have the following general characteristics:

1) The reaction is heterogeneous, meaning that the polymer is insoluble in its monomer. Since there is no solvent in bulk polymerization, the polymer precipitates during the reaction.

2) The reaction is autocatalytic. The rate increases with conversion until relatively high conversions then it starts to drop and finally a limiting conversion is reached.

3) The reaction order in the initiator is about 0.5.

Polymerization may be initiated chemically, that is through the use of an initiator, or by high energy sources, such as ultraviolet light or radioactivity (gamma rays). This latter method is effective for low temperature initiation. The chemical initiators may be activated by heat to produce free radicals. Usually chemical initiators are either organic peroxides or nitrogen compounds. Examples of the first type are benzoyl peroxide, lauroyl peroxide and decanoyl peroxide. An example of the second type is 2, 2' azobisisobutyronitrile (AIBN):

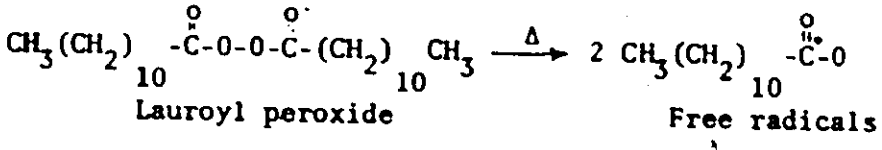

Lauroyl peroxide — Free radicals

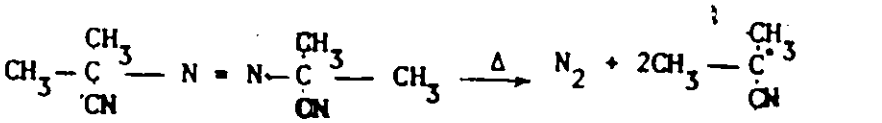

(AIBN) — Free radicals

Generally, nitrogen compounds are much safer in handling and use than the peroxides.

Molecular weight may be controlled by polymerization temperature therefore, an initiator is generally selected with the desired activity at the process temperature. New low temperature chemical initiators, such as IPP (isopropyl peroxydicarbonate), which requires special handling and storage, are now gaining importance. Polymers produced at lower temperatures have generally more heat stability.

Alkyl metal initiators, which do not involve free radical mechanisms may also be used. No commercial process or products have been developed to date, however.

Before describing the various proposed heterogeneous polymerization mechanisms, a review of the theory of homogeneous polymerization can be usefully given.

1.5.1 Theory of homogeneous bulk polymerization

It is well established that free-radical homogeneous bulk polymerization involves the following reactions (57):

Reaction Step		Reaction	Rate Constant
Initiation:	(I-1)	$\text{Initiator} \longrightarrow 2I^{\cdot}$	k_d
	(I-2)	$I^{\cdot} + M \longrightarrow R_1^{\cdot}$	
Propagation:	(I-3)	$R_1^{\cdot} + M \longrightarrow R_2^{\cdot}$	k_p
		$R_r^{\cdot} + M \longrightarrow R_{r+1}^{\cdot}$	
Chain Transfers:	(I-4)	$R_r^{\cdot} + M \longrightarrow P_r + M^{\cdot}$	k_{fm}
	(I-5)	$R_r^{\cdot} + I \longrightarrow P_r + I^{\cdot}$	k_{fI}
	(I-6)	$R_r^{\cdot} + P_s \longrightarrow P_r + P_s^{\cdot}$	k_{fp}
Termination:	(I-7)	$R_r^{\cdot} + R_s^{\cdot} \longrightarrow P_{r+s}$	k_{tc}
	(I-8)	$R_r^{\cdot} + R_s^{\cdot} \longrightarrow P_r + P_s$	k_{td}

where $I^{\cdot}$ is an initiator (incorrectly called catalyst) fragment radical, M and I are monomer, and initiator molecules respectively. $M^{\cdot}$ is monomer radical. $R_r^{\cdot}$ is a polymer radical containing r monomer units and P_r is a dead polymer molecule (usually called dead for irreversible polymerizations).

The initiation step is usually much more complex. For the present it will be assumed to involve thermal decomposition of the initiator molecule into two radical fragments. These radicals initiate a polymer chain by reacting with monomer molecules. Some radicals may undergo

side reactions (56). The initiator efficiency "f" is defined as the fraction of the radicals which initiates polymer chains.

The chain transfer step involves transfer of the radical activity from an active to an inactive species. The total number of free radicals does not change by transfer reactions, but the molecular weight distribution is strongly affected by them.

Equation (I-7) refers to termination by combination while equation (I-8) refers to termination by disproportionation. The relative rates of these two reactions affect the molecular weight distribution.

If we assume that:

1) kinetic stationary-state assumption is valid
2) velocity coefficients are independent of chain length
3) long chain approximation
4) volume change is negligible
5) chain transfer to dead polymer is negligible

We may write:

$$\frac{d[R^\cdot]}{dt} = R_I - (k_{tc}+k_{td})[R^\cdot]^2 \text{ with } R_I = (k_{tc}+k_{td})[R^\cdot]^2 >> \frac{d[R^\cdot]}{dt} \qquad (I\text{-}9)$$

$$\text{where } [R^\cdot] = \sum_{r=1}^{\infty} [R_r^\cdot] \qquad (I\text{-}10)$$

R_I = rate of initiation = $2f\, k_d[I]$

$[I]$ = initiator concentration

From (I-9):

$$\therefore [R^{\cdot}] = \sum_{r=1}^{\infty} [R_r^{\cdot}] = \left(\frac{R_I}{k_{tc} + k_{td}} \right)^{1/2} \qquad (I\text{-}11)$$

The rate of polymerization, in moles monomer consumed per unit volume per unit time is given by:

$$R_p = -\frac{d[M]}{dt} = k_p[M][R^{\cdot}] \qquad (I\text{-}12)$$

This is neglecting monomer consumed in other reactions (Long Chain approximation)

From (I-12) and (I-11):

$$\therefore R_p = -\frac{d[M]}{dt} = k_p[M] \left(\frac{R_I}{k_{tc} + k_{td}} \right)^{1/2} \qquad (I\text{-}13)$$

$$\therefore \left(\frac{R_p}{k_p[M]} \right)^2 = \frac{R_I}{k_{tc}+k_{td}}$$

$$\therefore R_I = R_p \left(\frac{k_{tc}R_p}{k_p^2[M]^2} + \frac{k_{td}R_p}{k_p^2[M]^2} \right)$$

If we call: $\dfrac{k_{td}R_p}{k_p^2[M]^2} = \alpha$

and $\dfrac{k_{tc}R_p}{k_p^2[M]^2} = \beta \qquad (I\text{-}14)$

$$\therefore R_p = \frac{R_I}{\alpha+\beta} \qquad (I\text{-}15)$$

For $[R_1^{\cdot}]$ we may write

$$[R_1^\cdot] = \frac{R_I + k_{fm}[M][R^\cdot]}{k_p[M] + k_{fm}[M] + k_{fI}[I] + (k_{tc} + k_{td})[R^\cdot]}$$

and for $r \gg 2$

$$[R_r^\cdot] = \frac{k_p[M][R_{r-1}^\cdot]}{k_p[M] + k_{fm}[M] + k_{fI}[I] + (k_{tc} + k_{td})[R^\cdot]}$$

$$= \phi[R_{r-1}^\cdot]$$

$$\therefore \quad [R_2^\cdot] = \phi[R_1^\cdot]$$

and in general

$$[R_r^\cdot] = \phi^{r-1}[R_1^\cdot]$$

If we define $T = \frac{k_{fm}}{k_p} + \frac{k_{fI}[I]}{k_p[M]}$ and $\tau = T + \alpha$ (I-16)

$$\therefore \quad \phi = \frac{1}{1 + \tau + \beta}$$

$$[R_1^\cdot] = \frac{(R_p/k_p[M])\ (\tau+\beta)}{1 + \tau + \beta}$$

The differential equations for dead polymer may be written as:

$$\frac{d[P_r]}{dt} = R_p\tau(\tau+\beta)\phi^r + R_p\frac{\beta}{2}(\tau+\beta)^2 r\phi^r \qquad \text{(I-17)}$$

The instantaneous differential molecular weight distribution (DMWD) may be written as:

$$W(r) = \frac{r[P_r]}{\int_0^t R_p dt} = \tau(\tau+\beta)r\phi^r + \frac{1}{2}\beta(\tau+\beta)^2 r^2\phi^r \qquad \text{(I-18)}$$

Where W(r) is the weight fraction of polymer of chain length r.

Consistent with the long chain approximation, we may write:

$$\phi^r = (1+\tau+\beta)^{-r} = \exp\left[-(\tau+\beta)r\right]$$

Then:

$$W(r) = \tau(\tau+\beta)[r \exp(-(\tau+\beta)r)] + \frac{1}{2}\beta(\tau+\beta)^2 (r^2 \exp[-(\tau+\beta)r]) \quad (I-19)$$

Applying the method of moments it may be readily shown that instantaneous average chain lengths may be expressed as:

$$\bar{r}_n = (\tau + \frac{\beta}{2})^{-1} \quad (I-20)$$

$$\frac{\bar{r}_w}{\bar{r}_n} = \frac{2(\tau + 3\beta/2)(\tau + \beta/2)}{(\tau+\beta)^2} \quad (I-21)$$

where $\bar{r}_n$ is the number average chain length, $\bar{r}_w$ is the weight average chain length, and $\bar{r}_w/\bar{r}_n$ is the polydispersity.

Equation (I-21) shows that the measured polydispersity gives a good idea about the mode of termination. For example:

if $\beta \gg \tau$ $\therefore \bar{r}_w/\bar{r}_n = 1.5$ $\therefore$ termination is by combination

if $\beta \ll \tau$ $\therefore \bar{r}_w/\bar{r}_n = 2.0$ $\therefore$ termination by combination is negligible in controlling MWD at polymer produced. If the polydispersity is equal to 2.0 at all conversions, transfer to monomer is dominant in controlling MWD.

1.5.2 Literature survey

Polymerization of vinyl chloride in sealed tubes was first done back in 1872 by Baumann [58]. It was further studied in detail in 1912 by Ostromislensky[59] who initiated the reaction by sunlight. In 1917, Klatte and Rollett[60] obtained a patent utilizing peroxides rather than sunlight for initiation of vinyl chloride polymerization. In 1922, Plausen[61] disclosed a process of direct polymerization to PVC from dry acetylene and hydrogen chloride under pressure at 150-200°C. Since then many workers have studied experimentally the bulk polymerization of vinyl

chloride[62-77]. A review of these works is given by Talamini and Peggion[78]. Most of the models proposed to date fit experimental rates only up to relatively small conversions. A comprehensive investigation of reaction parameters on molecular weight averages and distribution (MWD) has so far not been reported.

The reactions that have been proposed by various workers forthe bulk polymerization of vinyl chloride are given below[78]:

Reaction Step		Reaction	Rate constant
Reaction in liquid phase:			
Initiation	(I-22)	$I \longrightarrow R^{\cdot}$	k_d
Propagation	(I-23)	$R^{\cdot}+M \rightarrow R^{\cdot}$	k_p
Chain transfer to monomer	(I-24)	$R^{\cdot}+M \longrightarrow P+M^{\cdot}$	k_{fm}
Termination	(I-25)	$R^{\cdot}+R^{\cdot} \longrightarrow P$	k_t
Reaction in the polymer particles:			
Trapping of radicals by polymer particles	(I-26)	$R^{\cdot}+P \longrightarrow T^{\cdot}+P$	k_c
Propagation	(I-27)	$T^{\cdot}+M \longrightarrow T^{\cdot}$	k'_p
Chain transfer to monomer	(I-28)	$T^{\cdot}+M \longrightarrow P+M^{\cdot}$	k'_{fm}
Termination	(I-29)	$T^{\cdot}+T^{\cdot} \longrightarrow P$	k'_t
	(I-30)	$T^{\cdot}+M^{\cdot} \longrightarrow P$	k''_t

Reactions undergone by the monomeric radicals $M^{\cdot}$ in the polymer particles:

Propagation	(I-31)	$M^{\cdot}+M \longrightarrow T^{\cdot}$	k''_p
Chain transfer to polymer	(I-32)	$M^{\cdot}+P \longrightarrow T^{\cdot}$	k_{fp}
Escape to liquid phase	(I-33)	$M^{\cdot} \longrightarrow R^{\cdot}$	k_{esc}

Reactions (I-22) to (I-25) are typical of homogeneous free-radical polymerization. Reaction (I-26) indicates the formation of trapped free radicals in the polymer particles. Its rate is a function of the polymer concentration (i.e., of conversion). The trapped radicals may undergo propagation (I-27), chain transfer to the monomer (I-28), or termination (I-29, 30) with rate constants that may be different from those of the corresponding reactions in the liquid phase. Reactions (I-31) to (I-33) represent the possible reactions of monomeric radicals in the polymer particles. Some of the proposed models are discussed below.

Bengough and Norrish (1950)[64]:

They noticed that the increase in the rate of polymerization is proportional to the polymer concentration to the power two thirds. Accordingly they postulated that the trapping of the free radicals in the polymer particles is due to a chain transfer of radicals $R^{\cdot}$ to the polymer on the surface of the particles. If A is the total surface area of the particles, which is proportional to the polymer concentration to the 2/3 power ($A=k'\cdot[P]^{2/3}$), then,

$$\text{Trapping rate} = k_c F([P]) = k_{fp} A = k'.k_{fp}[P]^{2/3} \qquad \text{(I-34)}$$

[P] is the concentration of suspended polymer. As the polymerization occurs on the surface of the particles, a radical escapes (I-33) for each

chain transfer to the monomer (I-28). They assumed that $k'_t = k''_t = o$, $k_p = k'_p = k''_p$, $k_{fm} = k'_{fm}$ and equal monomer concentrations [M] in the liquid phase and in the polymer particles. On the assumption of the steady-state for all the radicals present, i.e.:

$$\frac{d}{dt}\left([R^{\cdot}] + [T^{\cdot}] + [M^{\cdot}]\right) = o$$

The polymerization rate may be derived as:

$$-\frac{d[M]}{dt} = (k_p + k_{fm})\left(\frac{f\,kd}{k_t}\right)^{1/2}\left[[M] + \frac{k_{fp}}{k_{fm}}k'[p]^{2/3}\right][I]^{1/2} \qquad (I\text{-}35)$$

This model fits experimental data only to small conversions. The main drawback of the model is that it assumes significant transfer to polymer. This would automatically lead to significant branching. This has been proven to be not valid for PVC.

Schindler and Breitenbach (1955)[68]

These workers assumed steady-state conditions for the radicals. They also assumed that $k'_t < k_t$. The rate acceleration is due to a decrease in the termination rate. k_t was assumed to decrease with conversion in the following empirical form:

$$(k_t)_{\text{over-all}} = \frac{k_{t_o}}{1+aX}$$

where k_{t_o} is the value of k_t at zero conversion, X is the conversion and a is an adjustable parameter. They also assumed that $k_p = k'_p = k''_p$, equal monomer concentrations in both phases and $k_{fm} = k'_{fm}$. The following expressions may be derived:

$$X = k_p \frac{[M]}{[M]_\circ} \left(\frac{fk_d[I]}{k_t}\right)^{1/2} \left[1+\frac{a}{4} k_p[M] \left(\frac{fk_d[I]}{k_t}\right)^{1/2} t\right] t \qquad (I-36)$$

where $[M]_\circ$ is the initial monomer concentration and [I] is the initiator concentration.

Magat (1955)[69]

He assumed that the steady-state approximation does not apply to the vinyl chloride bulk polymerization and that the termination constants are very low and all equal ($k_t = k'_t = k''_t$) and moreover, that there is no transfer reactions, i.e. $k_{fm} = k'_{fm} = o$, $k_{fp} = o$, and $k_p = k'_p$. This leads to a very simple mechanism. By integrating the system of differential equations the following expression is obtained:

$$X = \frac{k_p}{k_t} \ln \cosh \left[(fk_d k_t [I])^{1/2} t\right]$$

For small values of x, the above expression can be approximated by series expansion of the logarithm to give:

$$X = (1/2) f k_d k_p [I]^2 \qquad (I-37)$$

This model fits experimental data only to about 20 or 30% conversions, besides, it also ignores transfer reactions to monomer which have been proven to be significant.

Mickley, Michaels and Moore (1962)[70]

These workers assumed k'_t equal to $k''_t = o$, i.e. no termination in the polymer particles. They applied the steady-state hypothesis. The monomeric radicals formed in reaction (I-28) may undergo reactions

(I-31, 32, 33). In the last reaction k_{esc} is equal to $4\pi r D_L$, where r is the radius of the spherical polymer particle and D_L is the diffusion coefficient of monomeric radicals in the liquid phase. They suggested the following equations:

for [P] < 30 gm/liter

$$\therefore -\frac{d[M]}{dt} = k_p \left(\frac{fk_d[I]}{k_t}\right)^{1/2} \left[[M] + \frac{D'_L k_{fp}[T^\cdot] V_p}{D_L \bar{\alpha} k_{fm}}\right] \quad \text{(I-38)}$$

and for [P] > 60 gm/liter

$$\therefore -\frac{d[M]}{dt} = k_p \left(\frac{fk_d[I]}{k_t}\right)^{1/2} \left[[M] + \frac{D'_L k_{fp}[T^\cdot] \delta S_p}{D_L \bar{\alpha} k_{fm}}\right] \quad \text{(I-39)}$$

where D'_L is the diffusion coefficient of the chain radicals in the liquid phase. α is the ratio of monomeric radical concentration at the surface of the particles to the average concentration of monomeric radicals in the active volume. S_p is the total area, V_p is the total volume of the particles in a unit volume of suspension. δ is the depth of radical penetration into the particles. [P] is the polymer concentration. When [P] < 30 gm/liter, the radical activity involves the total volume of the polymer particles, and equation (I-38) is applicable; when [P] > 60 gm/liter, the radical activity is confined to a thin surface of thickness δ and equation (I-39) is applicable.

Such a model is most complicated and difficult to use. It fits data only up to moderate conversions, and does not attempt to predict molecular weights. It assumes no termination in the polymer particles and it over-emphasizes the diffusion of radicals between the liquid phase and the polymer particles (see Appendix (I-1)).

Cotman, Gonzalez, and Claver (1967)[73]

These workers attributed the auto-acceleration to a progressive reduction in termination rate. This reduction is due to the fact that as the reaction progresses and more polymer accumulates, there is a decrease

in probability that chain transfer of polymer radicals to monomer will generate a mobile radical, which can readily terminate an occluded free radical.

An interesting part of their work was the study of the precipitated polymer particles. They showed that the particles are spherical in shape and the diameter is a function of the conversion. The particles form and precipitate at the very early stages of the polymerization (conversion less than 0.01).

Talamini (1966)[72] & Grosato-Arnaldi, Gasparini, and Talamini (1968)[74]

This model proposed by Talamini and his co-workers is rather interesting. It states that the bulk polymerization of vinyl chloride takes place in two phases from very low conversions onwards. With increasing conversion the amount of the dilute phase decreases while that of the concentrated phase increases. The two phases have constant composition in the whole range of their co-existence. The termination rate is lower in the concentrated phase due to high viscosity (gel effect) accordingly the rate of polymerization is higher. Although the values of the termination constants are different in the two phases, the individual values will not be expected to vary up to about 70% conversion where dilute phase disappears. If M_o is the initial weight of monomer, X the conversion at time t, A the monomer/polymer ratio in the concentrated phase, R_d and R_c the specific polymerization rates (degree of conversion per unit time), respectively, in the dilute and concentrated phase, then the rate of reaction is the sum of the rates in both phases:

$$\therefore \quad M_o \frac{dX}{dt} = R_d(M_o - XM_o - AXM_o) + AXM_oR_c$$

This assumes phase separation occurs at zero conversion. This assumption was shown experimentally to be true, as the polymer starts to precipitate at practically the onset of the reaction.

$$\therefore \quad \frac{dX}{dt} = R_d\,(1-X-AX) + AXR_c$$

As mentioned above R_c and R_d are constant and moreover, we can write:

$$R_c = Q\,R_d$$

where Q is a constant greater than unity

$$\therefore \quad \frac{dX}{dt} = (1+qX)\,R_d$$

Upon integration with X = o at t = o

$$\therefore \quad X = \frac{1}{q}\left[\exp\,(qR_dt) - 1\right]$$

From the theory of homopolymerization, equation (I-13) can be expressed as:

$$R_d = k[I]^{1/2}$$

with $$k = k_p\left(\frac{fkd}{kt}\right)^{1/2}$$

$$\therefore \quad X = \frac{1}{q}\left[\exp\,(qk[I]^{1/2}t) - 1\right]$$

By expanding the exponential term in series:

$$\therefore \quad X = \frac{1}{q}\sum_{n=1}^{\infty}\frac{(qk)^n}{n!}\,[I]^{n/2}\,t^n \qquad (I\text{-}40)$$

This equation predicts conversion versus time data of bulk and suspension polymerization rather well [74] up to about 70% conversion. But the model again does not include a prediction of molecular weights.

Ugelstad et al (1971)[76] and (1973)[77]

The model proposed by these workers is similar to the one proposed by Mickley et al[70] and Talamini model[72]. This model also overemphasizes the transport of radicals to and from the polymer particles. In fact they assume that this process is controlling in determining the mass balance of radicals. Actually, the rate of radical production and destruction is much higher than the transport rate. This can be shown to be true by carrying out an order of magnitude calculation of these rates (see Appendix I-1). They also assumed that propagation rate constant k_p is the same in both phases. This assumption leads to an equilibrium ratio of the radicals in both phases. Talamini's model indicates an equilibrium ratio of reaction rates and accordingly of radical concentrations. Ugelstad's model also does not deal with polymer molecular weights. The rate expression of Ugelstad's model follows:

$$\frac{dX}{dt} = \left[\frac{k_d[I]}{V_L k_{tL} + V_p k_{tp} Q^2} \right]^{1/2} k_p (1-X-AX+QAX)$$

where V is the volume, L. refers to liquid phase, and P to polymer phase. Q is the equilibrium ratio of the radical concentration in polymer particles to the radical concentration in liquid phase. All other quantities have the same meaning as in Talamini's model.

I.6 Model development

The present model is similar to that of Talamini with some modifications regarding the change in volume during polymerization as well as the consumption of initiator. It is extended to cover the whole range of conversion up to the limiting values. The present model can also predict molecular weight distribution and averages.

I.6.1 Theory

Talamini's model assumes a two-phase polymerization, in a monomer-rich and polymer-rich phase. The polymer is treated as a single component with the concentration of monomer and polymer remaining constant during the polymerization. As reaction proceeds, the mass of polymer-rich phase grows while the monomer-rich phase diminishes. The initiator is assumed to have the same concentration in both phases. Experimental evidence indicates that the onset of two-phases begins after less than 1% conversion and lasts until between 70% and 80% depending on the temperature. Talamini's model can be represented on a binary, two-phase equilibrium diagram shown in Figure (I-1).

The present model assumes the presence of two phases in equilibrium, each is of constant composition (x_i & x_f polymer percent respectively), Figure (I-1). x_i is very small[74], so it is taken as $x_i = o$, that is the monomer-rich phase contains only monomer. Under these conditions, the polymer molecules come together and form monomer-swollen aggregates insoluble in the monomer. These aggregates are roughly spherical in shape, their size depends on the conversion since they grow a little after precipitation[75]. The size distribution of these aggregates is rather narrow[75]. The aggregate size, solubility and stability depend on the polymerization temperature through its effect on chain configuration. This will be discussed in more depth in the second part of this thesis. A material balance for polymer gives (nomenclature is given at the end of part I):

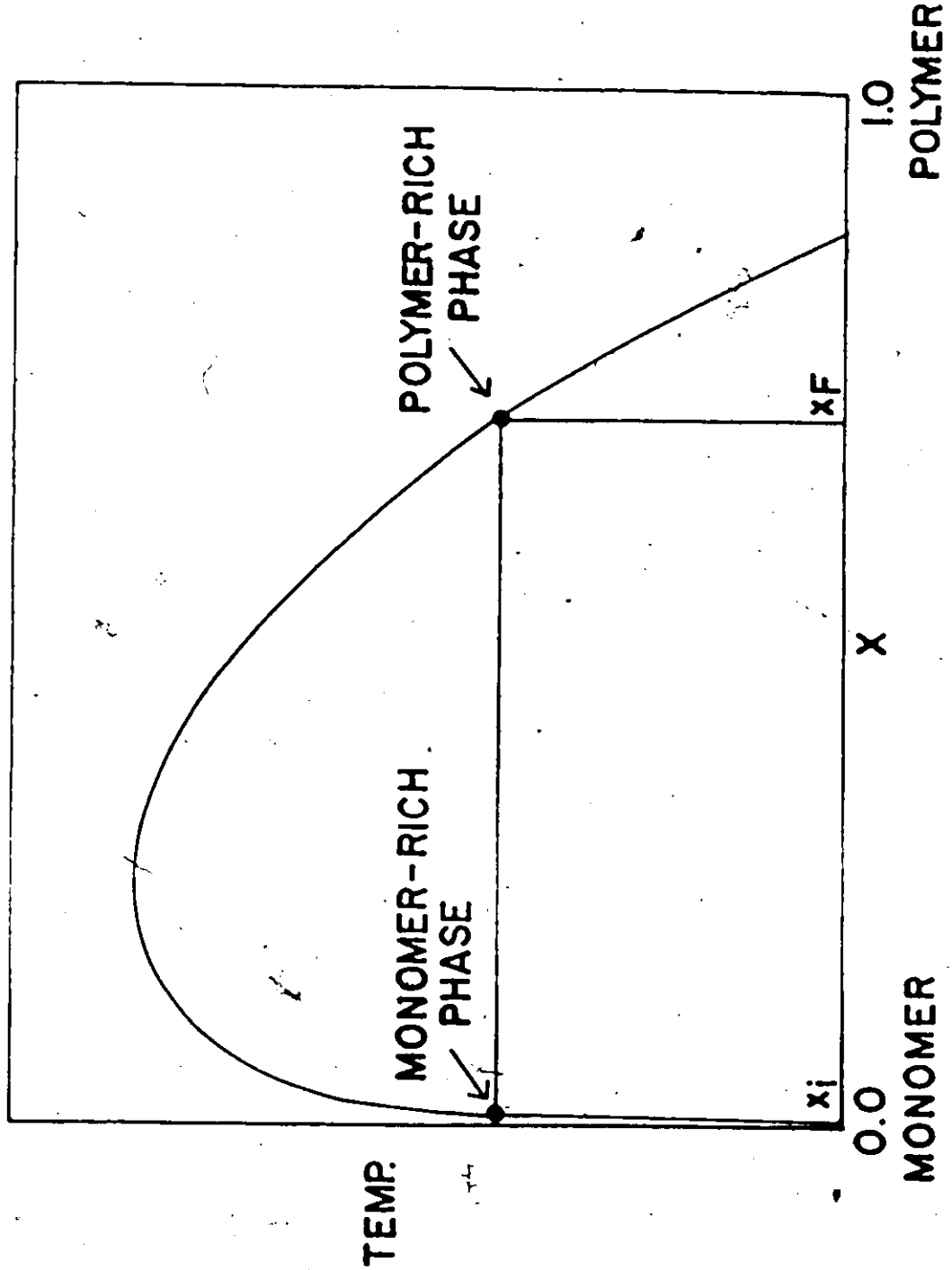
TEMP.
MONOMER-RICH PHASE
POLYMER-RICH PHASE
Xi
XF
X
0.0 MONOMER
1.0 POLYMER

FIGURE 1-1

$$xM_T = x_f M_2$$

$$\therefore M_2 = M_T \frac{x}{x_f} \qquad \text{(I-41)}$$

$$\therefore M_1 = M_T \frac{x_f - x}{x_f} \qquad \text{(I-42)}$$

The density of the mixture at conversion x is given by:

$$\frac{1}{\rho} = \frac{x}{\rho_p} + \frac{1 - x}{\rho_m} \qquad \text{(I-43)}$$

From which the change of volume with conversion is given by:

$$V = V_o (1 - Bx) \text{ where } B = \frac{\rho_p - \rho_m}{\rho_p} \qquad \text{(I-44)}$$

This relation was also used to calculate conversion using dilatometry. The concentration of monomer in monomer-rich phase clearly is unit mole fraction, it can be shown that monomer concentration in polymer-rich phase is given by:

$$[M_2] = \frac{\rho_2}{\rho_m} (1 - x_f) \quad \text{mole fraction} \qquad \text{(I-45)}$$

$$[M_1] = 1.0 \quad \text{mole fraction} \qquad \text{(I-46)}$$

where

$$\frac{1}{\rho_2} = \frac{x_f}{\rho_p} + \frac{1 - x_f}{\rho_m}$$

The mole fraction unit is a way of expressing dimensionless concentration. This is to be consistent since the initiator concentration is expressed in mole per mole, i.e. dimensionless. One mole fraction unit corresponds to ρ_m gm/cm^3. For unit volume of reaction mixture:

total moles of monomer = moles monomer in monomer-rich phase + moles monomer in polymer-rich phase.

$$\therefore \quad M_T \frac{dx}{dt} = R_{p_1} + R_{p_2}$$

$$R_{p_1} = R_1 M_T \frac{x_f - x}{x_f} \qquad \text{moles/time} \qquad \text{(I-47)}$$

$$R_{p_2} = R_2 M_T \frac{x}{x_f} (1-x_f) \qquad \text{moles/time} \qquad \text{(I-48)}$$

where R_1 & R_2 are expressed in conversion/unit time

$$\therefore \quad \frac{dx}{dt} = R_1 \left(\frac{x_f - x}{x_f}\right) + R_2 x \left(\frac{1 - x_f}{x_f}\right)$$

The polymerization in the polymer-rich phase might be diffusion controlled and therefore:

$R_2 = P R_1$ where P is a constant greater than unity

$$\frac{dx}{dt} = R_1(1 + Qx) \qquad \text{(I-49)}$$

where

$$Q = \frac{P(1 - x_f) - 1}{x_f} \qquad \text{(I-50)}$$

From the theory of homogeneous kinetics, equation (I-13):

$$R = k_p \left(\frac{f\, k_d\, I}{k_t}\right)^{1/2} = k\, I^{1/2} \qquad \text{(I-51)}$$

where

$$k = k_p (f.k_d/k_t)^{1/2} \qquad \text{(I-52)}$$

$$\therefore \quad R_1 = k_1 I^{1/2}$$

If we take into account the variation of the volume with conversion and the consumption of the initiator, then:

$$I = I_o \frac{\exp(-k_d.t)}{(1 - Bx)}$$

$$\therefore \frac{dx}{dt} = \frac{1 + Qx}{\sqrt{1 - Bx}} \cdot k_1 I_o^{1/2} \exp\left(\frac{-k_d.t}{2}\right) \qquad (I\text{-}53)$$

Substituting $x = 0$ in equation (I-53) yields:

$$\left(\frac{dx}{dt}\right)_o = k_1 I_o^{1/2}$$

This means that the constant k_1 is simply, the initial slope of the curve, x vs. $t\sqrt{I_o}$, Figures (I-3), (I-4).

Equation (I-53) describes the system up to conversion of x_f, it is easily solved analytically with the initial conditions $x = x_i = 0$ at $t = 0$. However, the solution is more readily obtained as t expressed as an explicit function of x rather than the reverse, it is given by:

$$t = -\frac{2}{k_d} \ln(1 - H) \qquad (I\text{-}54)$$

where:

$$H = \frac{k_d}{2k_1 I_o^{1/2}} \left\{ \frac{2}{Q}\left(\sqrt{1-Bx}-1\right) + \frac{\sqrt{Q+B}}{Q\sqrt{Q}} \ln\left[\frac{\sqrt{Q(1-Bx)} - \sqrt{Q+B}}{\sqrt{Q(1-Bx)} + \sqrt{Q+B}} \cdot \frac{\sqrt{Q} + \sqrt{Q+B}}{\sqrt{Q} - \sqrt{Q+B}} \right] \right\}$$

Undoubtedly k_t will continue to fall with conversion in the region $x > x_f$ and that near the glass transition point k_p will approach zero and the polymerization will cease. Because the contribution of transfer to monomer is so much greater than termination by disproportionation[79] with respect to the polymer molecular weights, we can assume that k is proportional to the monomer concentration with small error in the prediction of DMWD and

molecular weight averages. It is difficult to assess the error in prediction of conversion because f, k_t and k_p will all fall with conversion; it is decided for the present model to assume that the combined group k changes with (1-x), for x values greater than x_f.

Diffusion control in polymer-rich phase leads to a much lower k_t value which gives rise to a higher k value, accordingly:

$$k_2 = P.k_1 \tag{I-55}$$

for $x > x_f$: $\therefore \quad k \propto (1-x)$

$$\therefore \quad k = Pk_1 \frac{1-x}{1-x_f} \tag{I-56}$$

The rate of reaction can then be written as

$$\frac{-d[M]}{dt} = Pk_1 \left(\frac{1-x}{1-x_f}\right) I_o^{1/2} \frac{\exp\left(-\frac{k_d \cdot t}{2}\right)}{\sqrt{1-Bx}} \cdot M_T (1-x)$$

$$\frac{dx}{dt} = \frac{Pk_1}{1-x_f} I_o^{1/2} \frac{(1-x)^2}{\sqrt{1-Bx}} \exp\left(-\frac{k_d \cdot t}{2}\right) \tag{I-57}$$

Again, equation (I-57) is easily solved analytically and the solution is better expressed as t explicitly in x:

$$t = -\frac{2}{k_d} \ln (1 - HH) + t_f \tag{I-58}$$

where:

t_f is the time to reach x_f, and

$$HH = \frac{(1-x_f)k_d}{2\, Pk_1\, I_o^{1/2}} \left[\sqrt{\frac{1-Bx}{1-x}} - \sqrt{\frac{1-Bx_f}{1-x_f}} + \frac{B}{2\sqrt{1-B}} \ln \left\{ \frac{\sqrt{1-x} - \sqrt{1-B}}{\sqrt{1-x_f} - \sqrt{1-B}} \cdot \frac{\sqrt{1-x} + \sqrt{1-B}}{\sqrt{1-x_f} + \sqrt{1-B}} \right\} \right]$$

Molecular Weight Averages and Distribution

The measured molecular weights had a polydispersity of 2 or slightly higher; this suggests that the molecular weights are controlled principally by transfer to monomer with some contribution from disproportionation.

If polymer produced in each phase has a polydispersity of 2 the polydispersity of the mixed polymer will be equal to or greater than 2.

From the homogeneous kinetics, it can be shown that for termination by disproportionation and transfer to monomer (i.e. B = o, from equation (I-19):

$$W(r) = \tau^2 . r . \exp(-\tau . r) \qquad \text{(I-59)}$$

τ is given by

$$\tau = C_M + \frac{2(f . k_d . k_t)^{1/2}}{k_p} \frac{I^{1/2}}{[M]} \qquad \text{(I-60)}$$

where C_M = monomer transfer constant = k_{fm}/k_p

Substituting from equation (I-52) into (I-60):

$$\tau = C_M + \frac{2f\ k_d\ I^{1/2}}{k[M]} \qquad \text{(I-61)}$$

The instantaneous DMWD of the total polymer mixture is obtained from:

$$W(r) = m_1 . W(r)_1 + m_2 W(r)_2 \qquad \text{(I-62)}$$

It is assumed that C_M is the same in both phases. This assumption is confirmed by the work of Talamini[79] and Danusso[80] who obtained almost the same value of C_M by applying the Mayo equation to data from solution polymerization (homogeneous) and bulk polymerization (heterogeneous) respectively.

Since transfer to monomer plays the controlling role in MWD, it is reasonable to assume that the cumulative MWD is the same as the instantaneous one.

From equations (I-45), (I-46), and (I-61)

$$\tau_1 = C_M + \frac{2f\ k_d\ I_o^{1/2}}{k_1\sqrt{1-Bx}} \cdot \exp\ (-\frac{k_d.t}{2}) \qquad \text{(I-63)}$$

$$\tau_2 = C_M + \frac{2f\ k_d.\rho_m.I_o^{1/2}}{Pk_1.\rho_2(1-x_f)\sqrt{1-Bx}} \cdot \exp\ (-\frac{k_d.t}{2}) \qquad \text{(I-64)}$$

$$m_1 = \frac{mp_1}{M_T x}$$

$$mp_1 = \int_0^t R_{p_1}\ dt$$

$$= \frac{M_T}{Q^2 x_f}\ [(Qx_f + 1)\ \text{In}\ (1 + Qx) - Qx]$$

$$\therefore\ m_1 = \frac{(Qx_f + 1)\ \text{In}\ (1 + Qx) - Qx}{Q^2\ xx_f} \qquad \text{(I-65)}$$

Similarly: $M_2 = \frac{mp_2}{M_T x}$

$$mp_2 = \int_0^t R_{p_2}\ dt$$

$$m_2 = \frac{P(1-x_f)[Qx - \text{In}\ (1 + Qx)]}{Q^2\ xx_f} \qquad \text{(I-66)}$$

For the DMWD of equation (I-62), it can be shown that:

$$\int_0^\infty \frac{W(r)}{r}\ dr = m_1\ \tau_1 + m_2\tau_2$$

$$\int_0^\infty W(r)\ dr = 1.0$$

$$\int_0^\infty r.\ W(r)\ dr = 2\left(\frac{m_1}{\tau_1} + \frac{m_2}{\tau_2}\right)$$

$$\therefore \quad \bar{r}_n = \frac{1}{m_1\ \tau_1 + m_2\ \tau_2} \tag{I-67}$$

$$\bar{r}_w = \frac{2m_1}{\tau_1} + \frac{2m_2}{\tau_2} \tag{I-68}$$

$$r_w/r_n = \left(\frac{2m_1}{\tau_1} + \frac{2m_2}{\tau_2}\right)(m_1\ \tau_1 + m_2\ \tau_2) \tag{I-69}$$

This polydispersity will be equal to or greater than 2. For conversions higher than x_f, we assumed before that:

$$k \propto (1 - x)$$

with small error we can assume that the group $k_p^2\ I/k_t$ is constant:

$$\therefore \frac{fk_d}{k} \propto k$$

or

$$\frac{f\ k_d}{k[M]} = \text{constant for } x > x_f$$

$$\therefore \frac{f.k_d}{k[M]} \quad (\text{for } x > x_f) = \frac{f\ k_d}{Pk_1[M]} \quad (\text{at } x = x_f) \tag{I-70}$$

From equation (I-70) we can see that τ of the polymer produced after x_f will practically be the same as that which was produced in the polymer-rich phase. So, after x_f we still can differentiate between two kinds of polymers only, the one that was produced in the monomer-rich phase, and the one that was produced in the polymer-rich phase plus that polymer produced after x_f.

It can be shown that for $x > x_f$:

$$m_1 = (m_1)_{x=x_f} \cdot \frac{x_f}{x} \qquad (I.71)$$

$$m_2 = \frac{P(1-x_f)[Qx_f - \ln(1+Qx_f)] + Q^2 x_f(x-x_f)}{Q^2 x x_f} \qquad (I-72)$$

Equations (I-71) and (I-72) with equations (I-62), (I-63), (I-64), (I-67), (I-68) and (I-69) could be used to obtain the DMWD and molecular weight averages

1.6.2 Experimental

Reagents

The initiator 2, 2' azobisisobutyronitrile (AIBN), (Eastman Organic Chemicals) was recrystallized twice from absolute methanol. The solvent for GPC analyses was tetrahydrofurane (THF), Fisher purified grade. The monomer, vinyl chloride, was obtained from Imperial Oil Enterprises Limited, Sarnia Ontario. The analysis provided by Imperial Oil is given in Table (I-5) on the following page:

TABLE (I-5) ANALYSIS OF VINYL CHLORIDE MONOMER

Inspections	Unit	Limits
Acidity (as Hcl)	ppm	2 max.
Aldehyde (as Acetaldehyde)	ppm	5 max.
Acetylene	ppm	2 max.
Iron	ppm	0.15 max.
Sulphur (as SO_2)	ppm	3 max.
Water	ppm	100 max.
Non-volatile matter	ppm	100 max
Phenol	ppm	——
Appearance		clear, colourless, and free of suspended matter

Apparatus and Procedure

Polymerization was carried out in 12 inches long glass ampoules having 10 mm O.D. and 8 mm I.D. This size gave negligible calculated temperature rise during reaction. Since vinyl chloride is a gas at ordinary temperature and pressure, it must be condensed under vacuum. Figure (I-2) is a schematic diagram of the vacuum line used to fill the ampoules. The line is first evacuated to less than 10^{-4} mm Hg, filled with nitrogen and then evacuated again. This is to ensure the absence of oxygen which acts as an inhibitor to the polymerization reaction. Vinyl chloride gas from the cylinder is then allowed to enter the line. It passes through ammoniacal cuprous chloride solution, then silver nitrate solution, water and finally through anhydrous calcium chloride. This is to purify the monomer from the acetylene and aldehyde traces it contains. Prior to

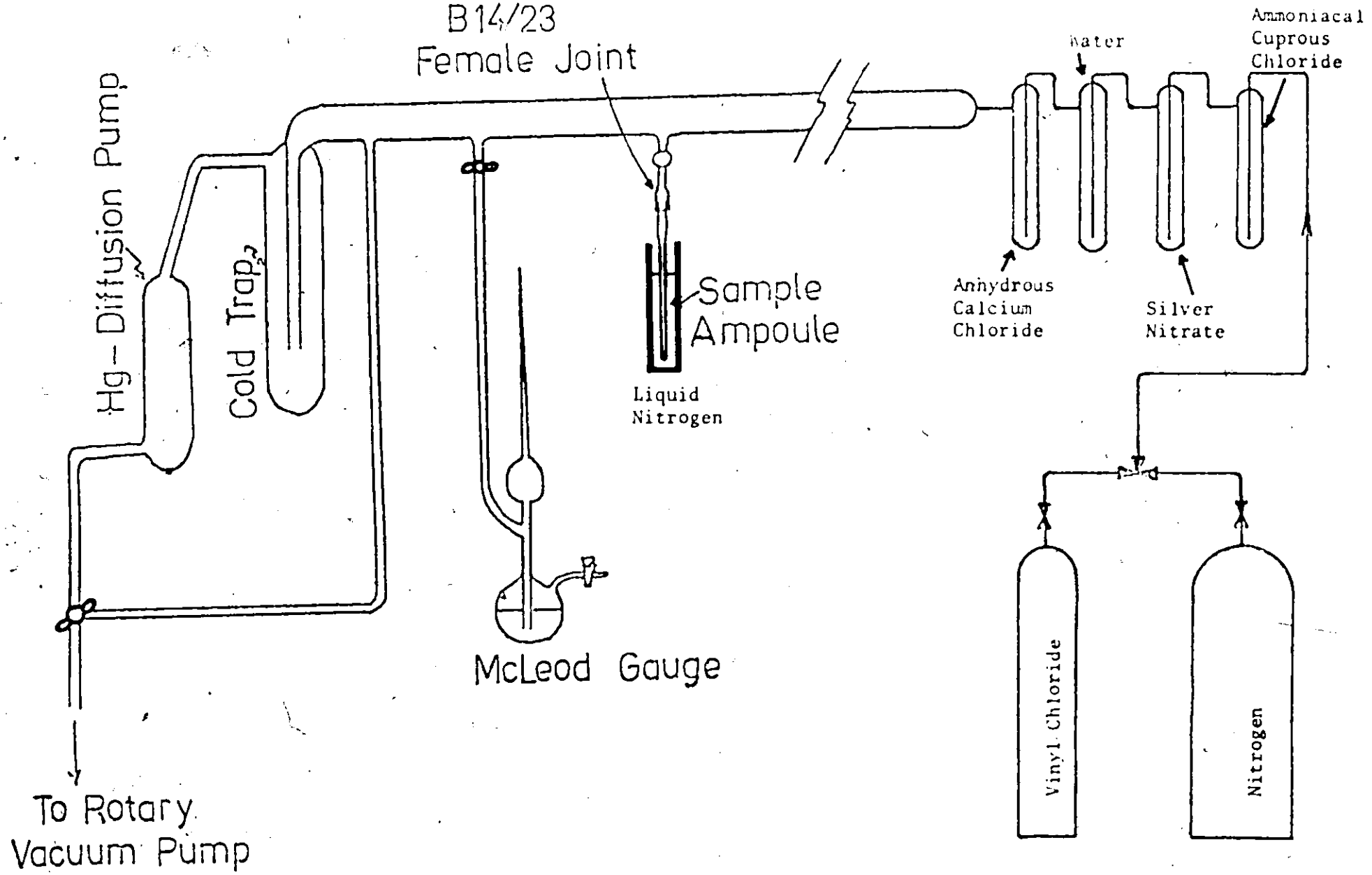
B14/23
Female Joint
Hg – Diffusion Pump
Cold Trap
Sample
Ampoule
Liquid
Nitrogen
Water
Ammoniacal
Cuprous
Chloride
Anhydrous
Calcium
Chloride
Silver
Nitrate
McLeod Gauge
Vinyl Chloride
Nitrogen
To Rotary
Vacuum Pump

FIGURE 1-2

evacuating the line, the required amounts of the initiator (AIBN) in chloroform solution are introduced into the ampoules and the chloroform removed by evacuation. Predetermined amounts of monomer are then condensed in the ampoules cooled by liquid nitrogen. The ampoules are then sealed off. They are put in a constant temperature bath controlled to ± 0.1°C where the reaction takes place.

Analytical Techniques

Conversion is determined gravimetrically. When the reaction time is over, the ampoule is taken out of the bath, quenched to stop the reaction, opened to let the unreacted monomer vent off. The polymer remaining is weighed and from the initial mass of monomer one calculates the conversion.

For conversions below about 20%, dilatometry was employed; dilatometers were 6 ml. in capacity, with a capillary of 2 mm I.D. The course of the polymerization was followed by the fall of the meniscus in the capillary through the use of a cathetometer. Conversion can be calculated by the equation:

$$\text{Conversion } \% = \frac{(V_o - V_t)\rho_p}{V_o\,(\rho_p - \rho_m)} \times 100$$

where V_o, V_t are the initial volume and the volume at time t; ρ_p and ρ_m are the polymer and monomer densities, respectively. Dilatometry, unfortunately, cannot be used for conversions higher than about 20% since the reaction mixture becomes quite turbid.

For MWD and averages waters model 200, GPC was used, THF as a solvent, Temp. 30°C, flowrate 3 ml/min. A train of 9 columns was used to give high resolution, these columns were:

Bio-glass	2500/1500	Å
CPG 10	2000/1250	Å
CPG 10	2000/1250	Å
CPG 10	2000	Å
CPG 10	700	Å
STYRAGEL	10^4	Å
STYRAGEL	800	Å
STYRAGEL	350/100	Å
STYRAGEL	350/100	Å

This column combination gave very good resolution. A universal calibration curve was first obtained using polystyrene standards, then an effective PVC calibration curve was obtained from it using the hydrodynamic-volume concept. A search was employed to get the best effective values of Mark-Houwink constants to fit PVC standards supplyed by T. Provder of Monsanto Co., St. Louis, Mo. U.S.A.:

PV1	$\bar{M}_w$ = 132,000	$\bar{M}_n$ = 54,000
PV2	$\bar{M}_w$ = 118,000	$\bar{M}_n$ = 41,000
PV3	$\bar{M}_w$ = 68,000	$\bar{M}_n$ = 25,500

This method was suggested by Provder[81]. It automatically corrects for axial dispersion. The Mark-Houwink values found were:

$K = 1.48 \times 10^{-4}$

$\epsilon = 0.768$

A non-linear calibration curve was obtained in the form:

$$\text{Mol.W.} = D_1 \exp(-D_2 v - D_3 v^2 - D_4 v^3)$$

Experimental Conditions

Factor	Levels
Polymerization temperature, °C	30, 50, 70
Initiator (AIBN) concentration, wt.%	0.35, 0.85, 1.75, 3.0

About 100 polymerization experiments were done covering the above levels and including replicates. Approximately 25 samples were analyzed by GPC for MWD and averages, including replicates.

I.6.3 Results

It is well established from previous work [74,82] that conversion curves completely overlap when they are plotted as x versus $t\sqrt{I_o}$. This was also observed in the present work. The solution of the proposed kinetic equations shows that the quantity $t\sqrt{I_o}$ assumes a constant value at a certain conversion and temperature, irrespective to the value of I_o in the working region. Accordingly, this type of plot was used in this work.

Figures (I-3) and (I-4) show the conversion curves for the three temperature levels 30°C, 50°C and 70°C. The theoretical curves are also

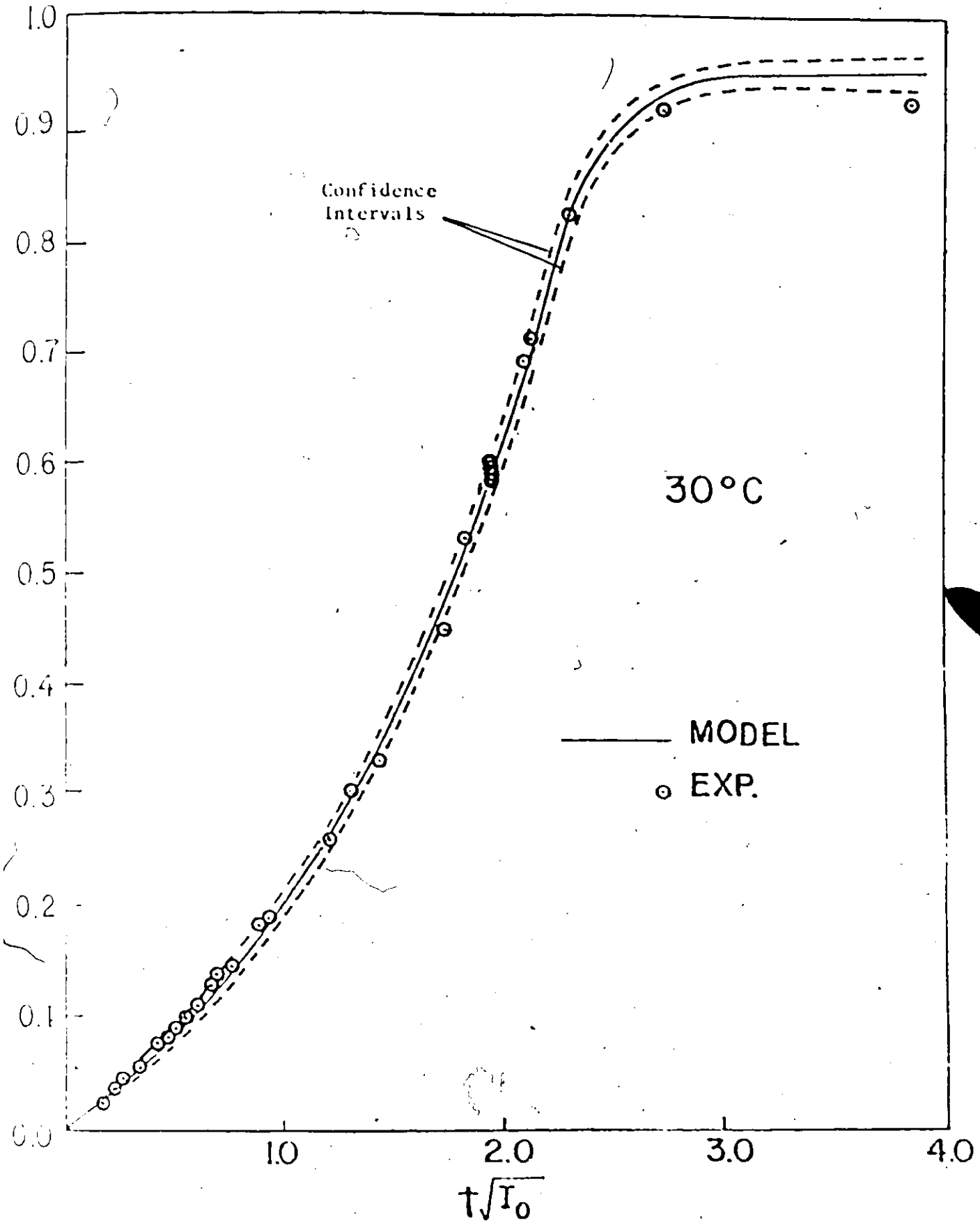
1.0
0.9
0.8
0.7
0.6
0.5
0.4
0.3
0.2
0.1
0.0
Confidence Intervals
30°C
MODEL
EXP.
1.0
2.0
3.0
4.0
$t\sqrt{I_0}$

FIGURE 1-3

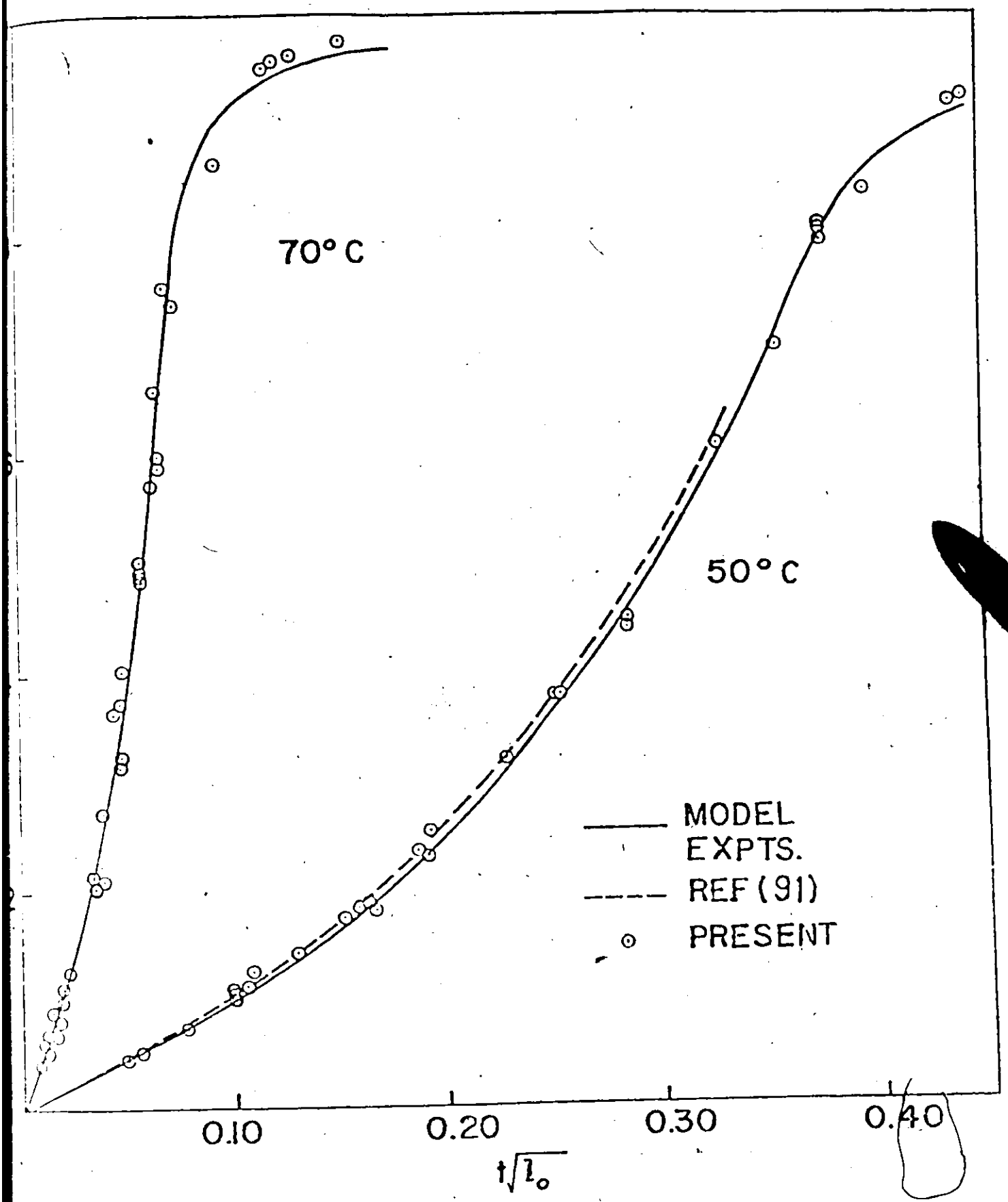

FIGURE I - 4

shown. These curves were fitted to the experimental points by using a non-linear, least-squares regression routine. This allows the estimation of model parameters. Confidence intervals of model response at 30°C are shown in Figure (I-3). Details of the statistical analysis are given in Appendix (I-2).

In Figures (I-5) to (I-9), experimentally measured molecular weight averages are shown. Theoretical curves are fitted to the data thus allowing C_M to be estimated. It should be mentioned here that the contribution of C_M in the quantity τ, equation (I-60), is much greater than the remaining term. In other words, the molecular weight averages are essentially determined by C_M alone[70, 79, 80]. This is obvious from the fact that the averages do not change with conversion and makes it possible to estimate C_M accurately using molecular weight averages. The remaining term is sensitive to conversion time data which is independent of C_M. Had the situation been different, it may have been necessary to consider a multi-response system where conversion data together with molecular weight averages are used to estimate simultaneously all the parameters including C_M[89, 90].

Figures (I-10) to (I-12) show a comparison between the measured and predicted MWD at 30°, 50° and 70°C., respectively. The theoretical distributions were obtained using the parameter values obtained as shown above. It is noted that the measured DMWD is shifted slightly to lower molecular weights; the reason for this could be small uncorrected axial dispersion effects, such as skewing in gel permeation chromatography.

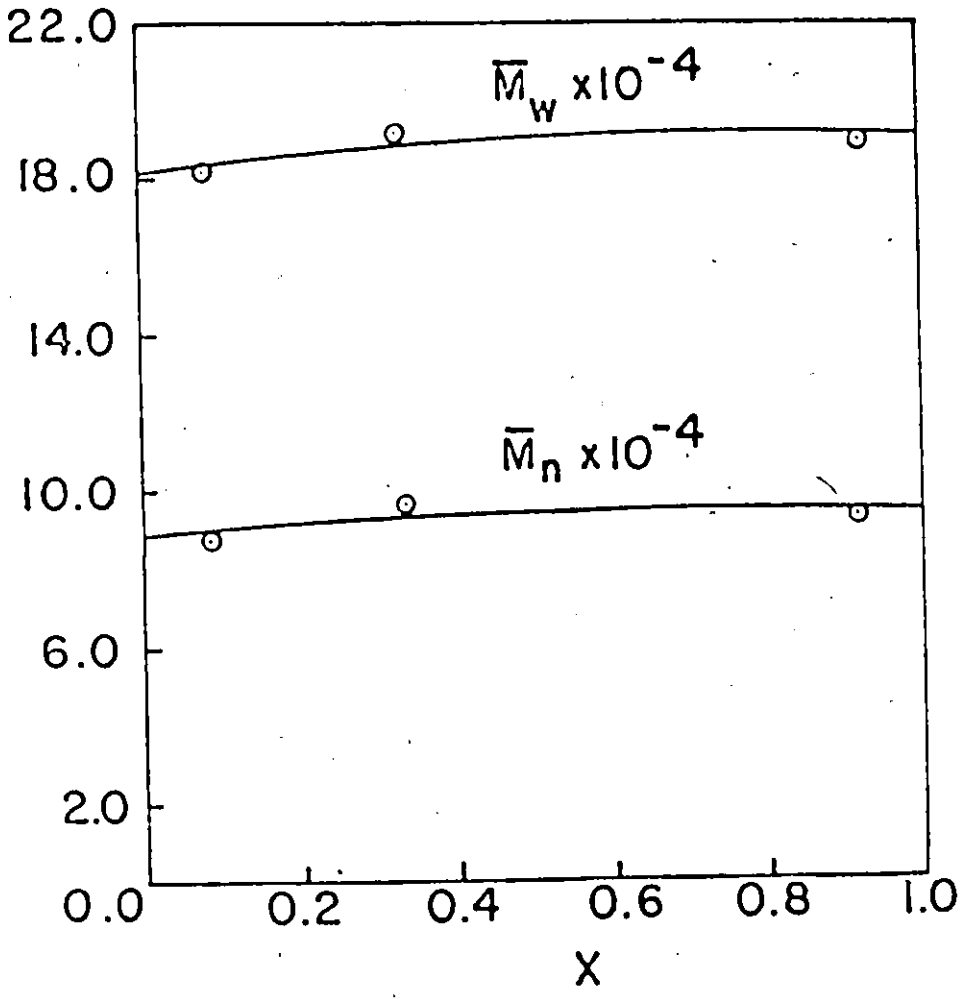
22.0
18.0
14.0
10.0
6.0
2.0
0.0
0.2
0.4
0.6
0.8
1.0
X
$\bar{M}_w \times 10^{-4}$
$\bar{M}_n \times 10^{-4}$
I_o = 0.85 wt %
30° C
MODEL

FIGURE I - 5

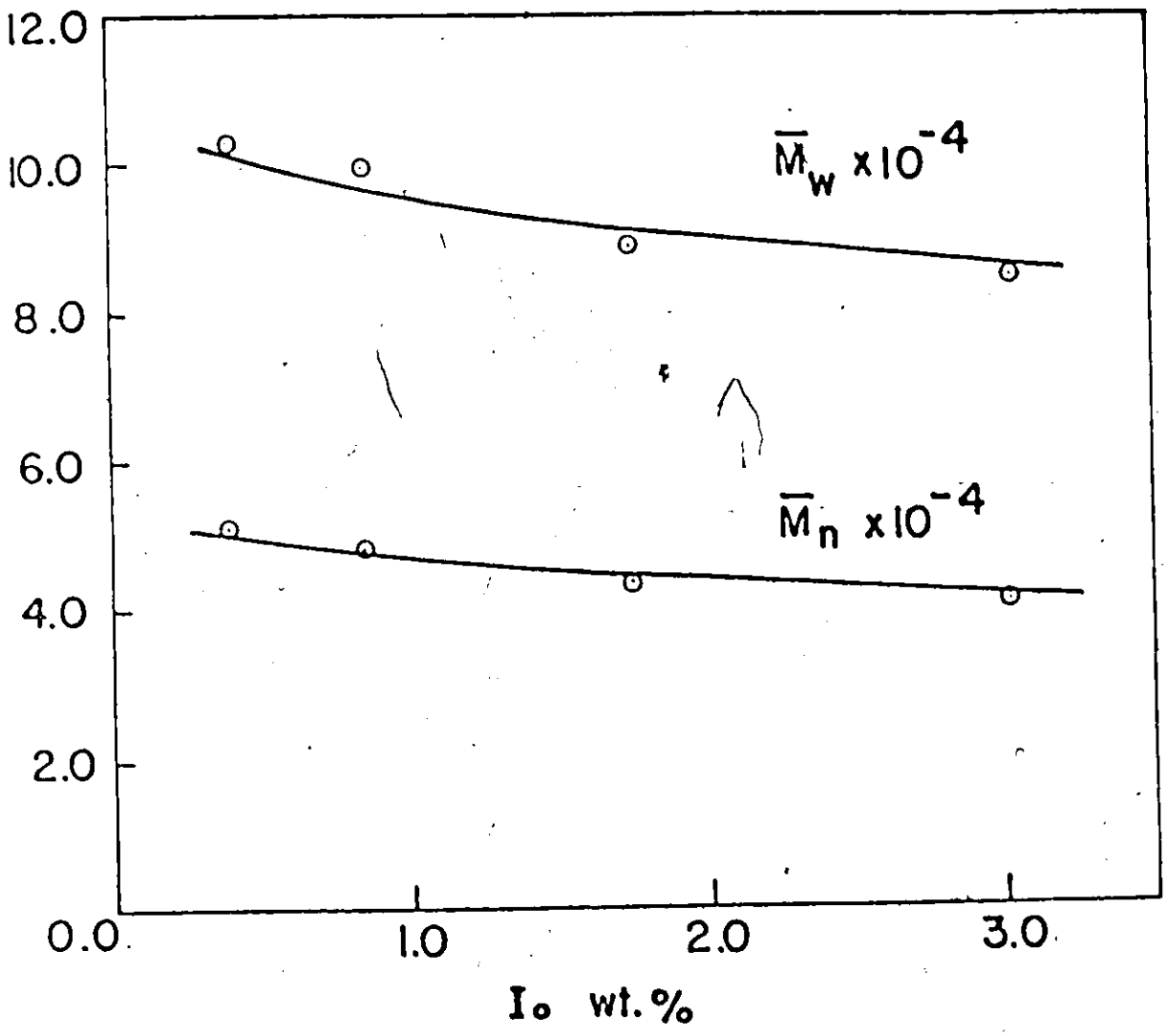

X = 0.18

50°C

_____ MODEL

FIGURE 1-6

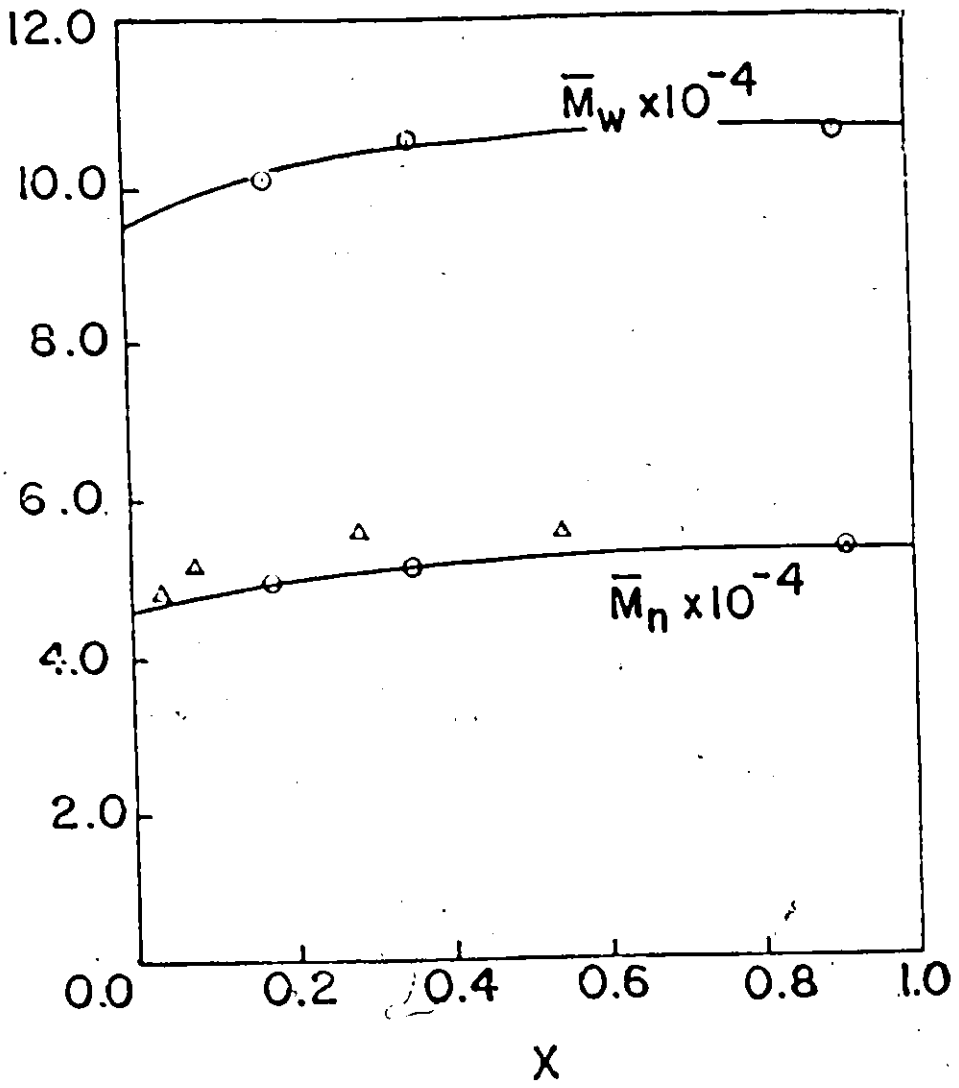

$I_o = 0.85$ wt.%

50 °C

EXPTS.

⊙ PRESENT (GPC) —— MODEL

△ REF (79) (VISC.)

FIGURE 1 - 7

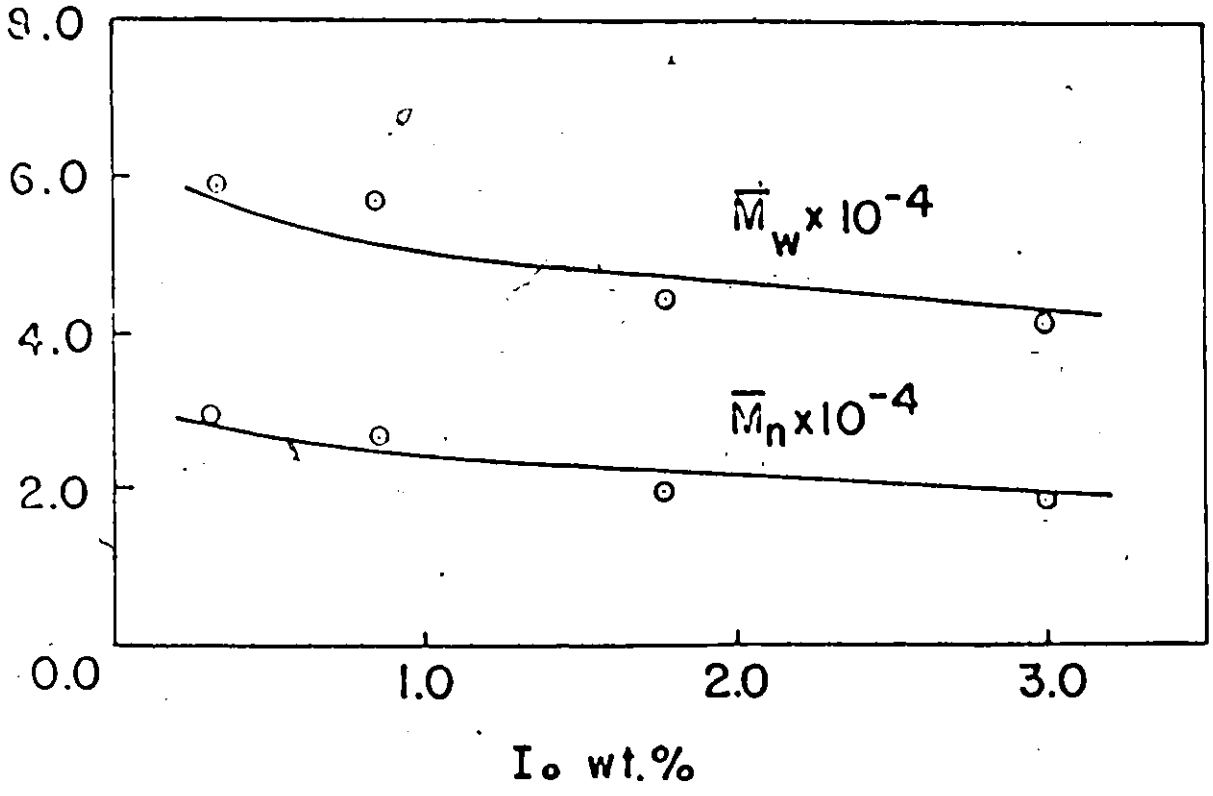
8.0
6.0
4.0
2.0
0.0
1.0
2.0
3.0
$\bar{M}_w \times 10^{-4}$
$\bar{M}_n \times 10^{-4}$
I_o wt.%
X = 0.21
70°C
—— MODEL

FIGURE 1-8

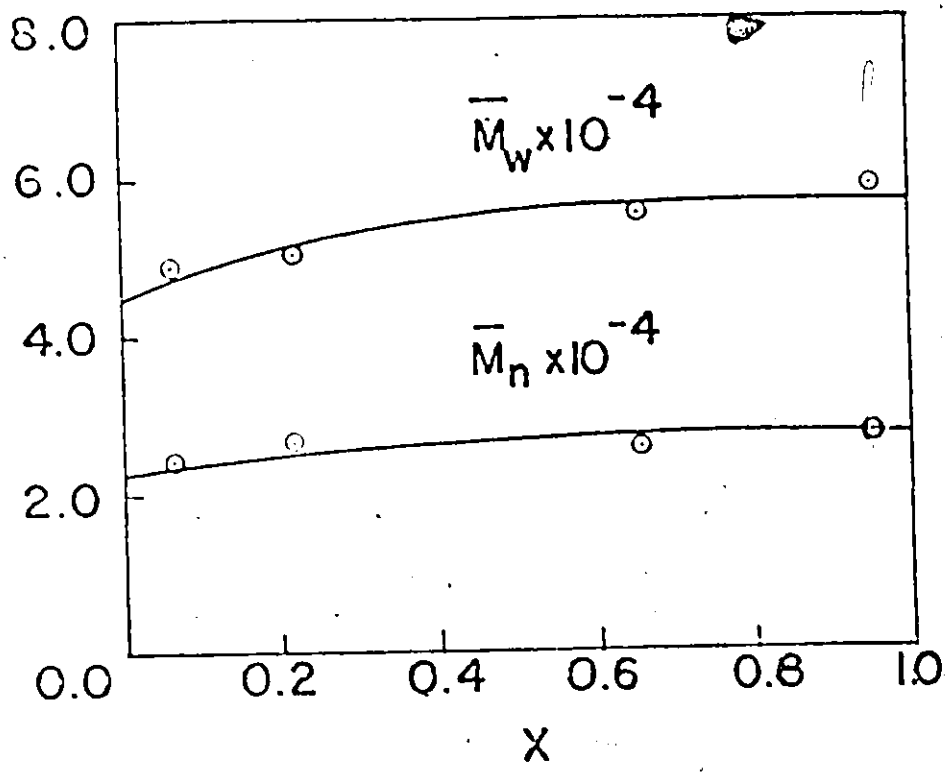

I_o = 0.85 wt.%
70°C
—— MODEL

FIGURE 1 - 9

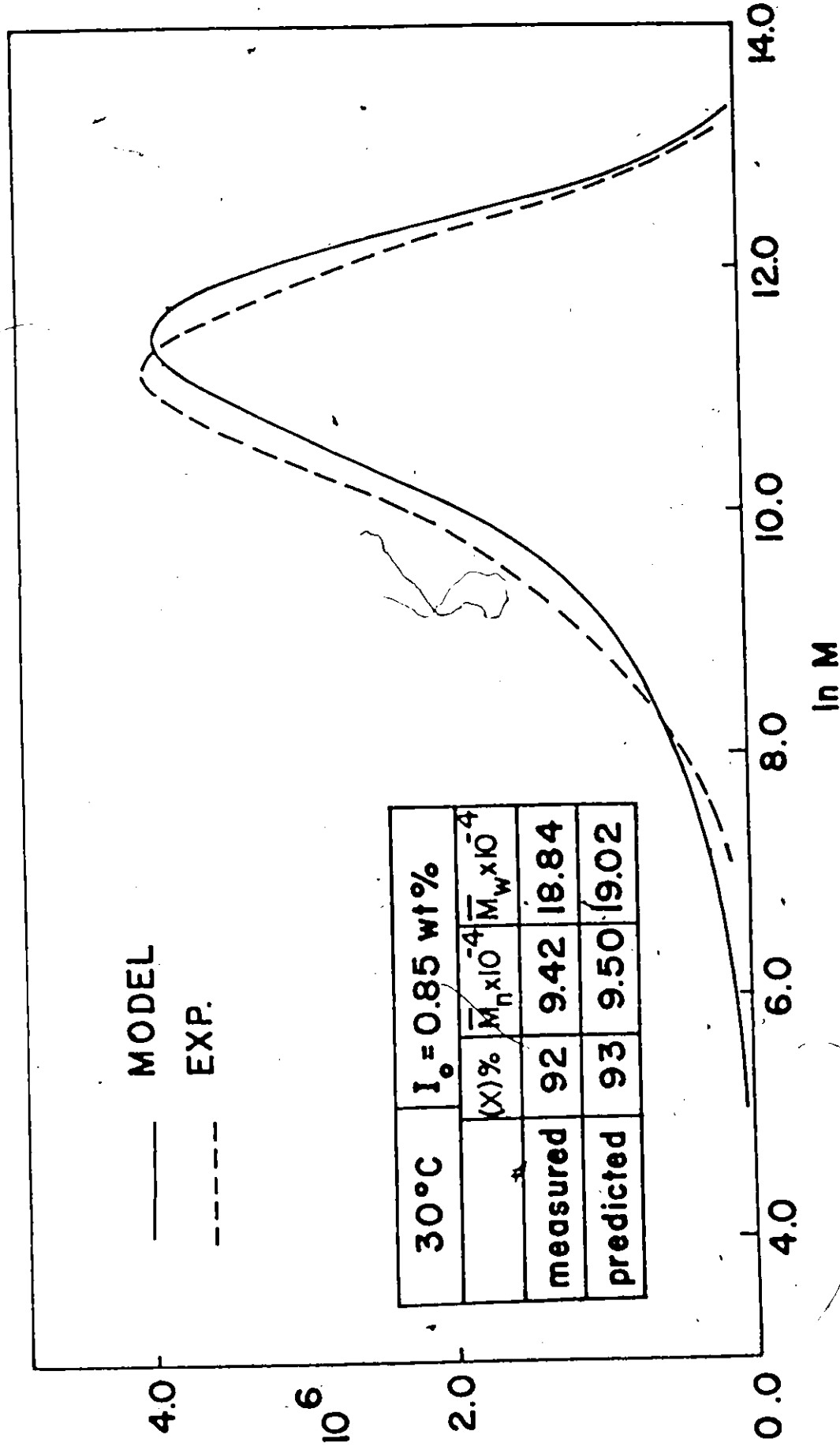
MODEL
EXP.
$W_M \times 10^6$
4.0
2.0
0.0
4.0
6.0
8.0
10.0
12.0
14.0
ln M
30°C
I_o = 0.85 wt%
(X)%
$\bar{M}_n \times 10^{-4}$
$\bar{M}_w \times 10^{-4}$
measured
92
9.42
18.84
predicted
93
9.50
19.02

FIGURE 1-10

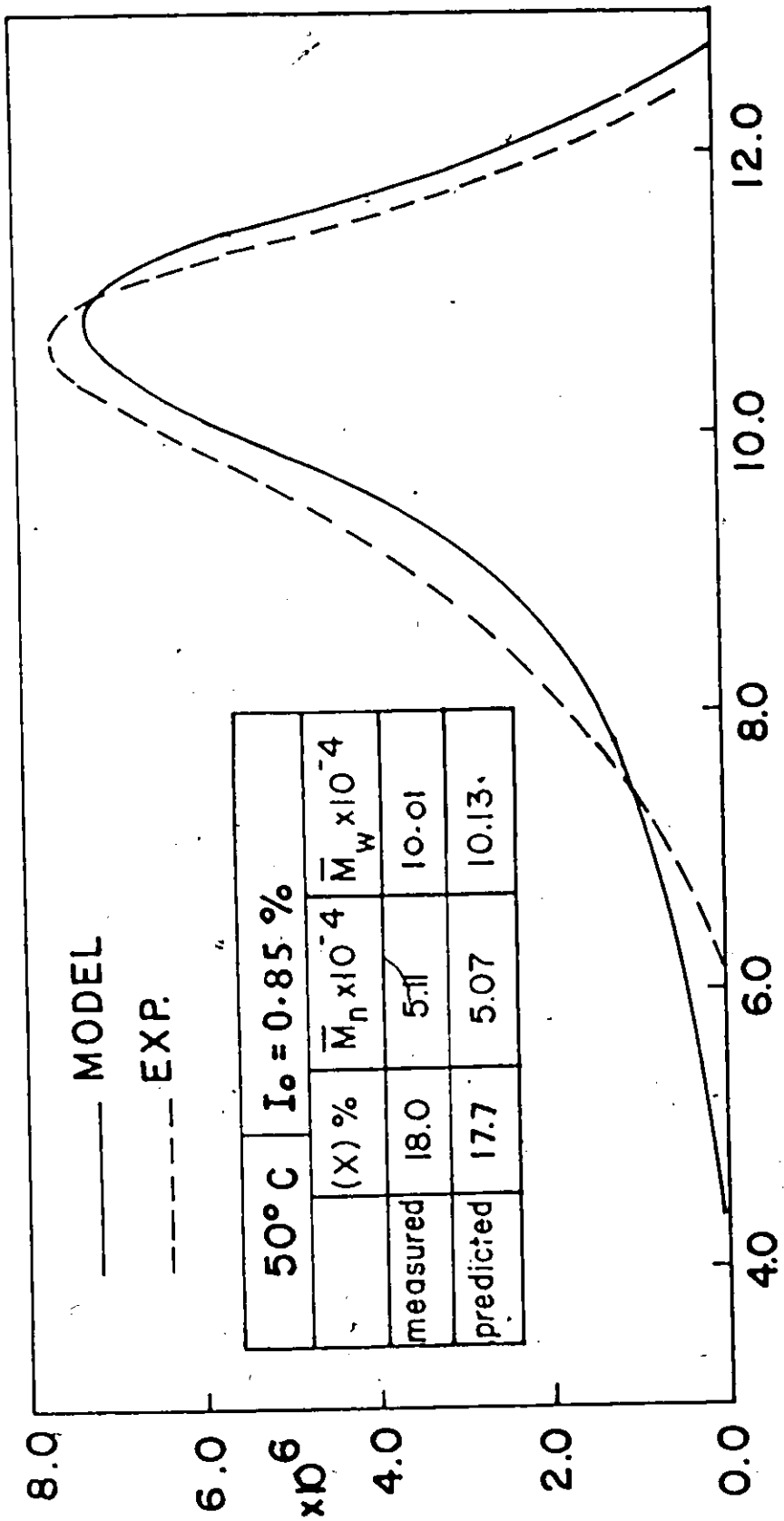
MODEL
EXP.
50° C
I_o = 0.85 %
(X) %
$\bar{M}_n \times 10^{-4}$
$\bar{M}_w \times 10^{-4}$
measured
18.0
5.11
10.01
predicted
17.7
5.07
10.13
$W_M \times 10^6$
8.0
6.0
4.0
2.0
0.0
4.0
6.0
8.0
10.0
12.0
ln M

FIGURE 1-11

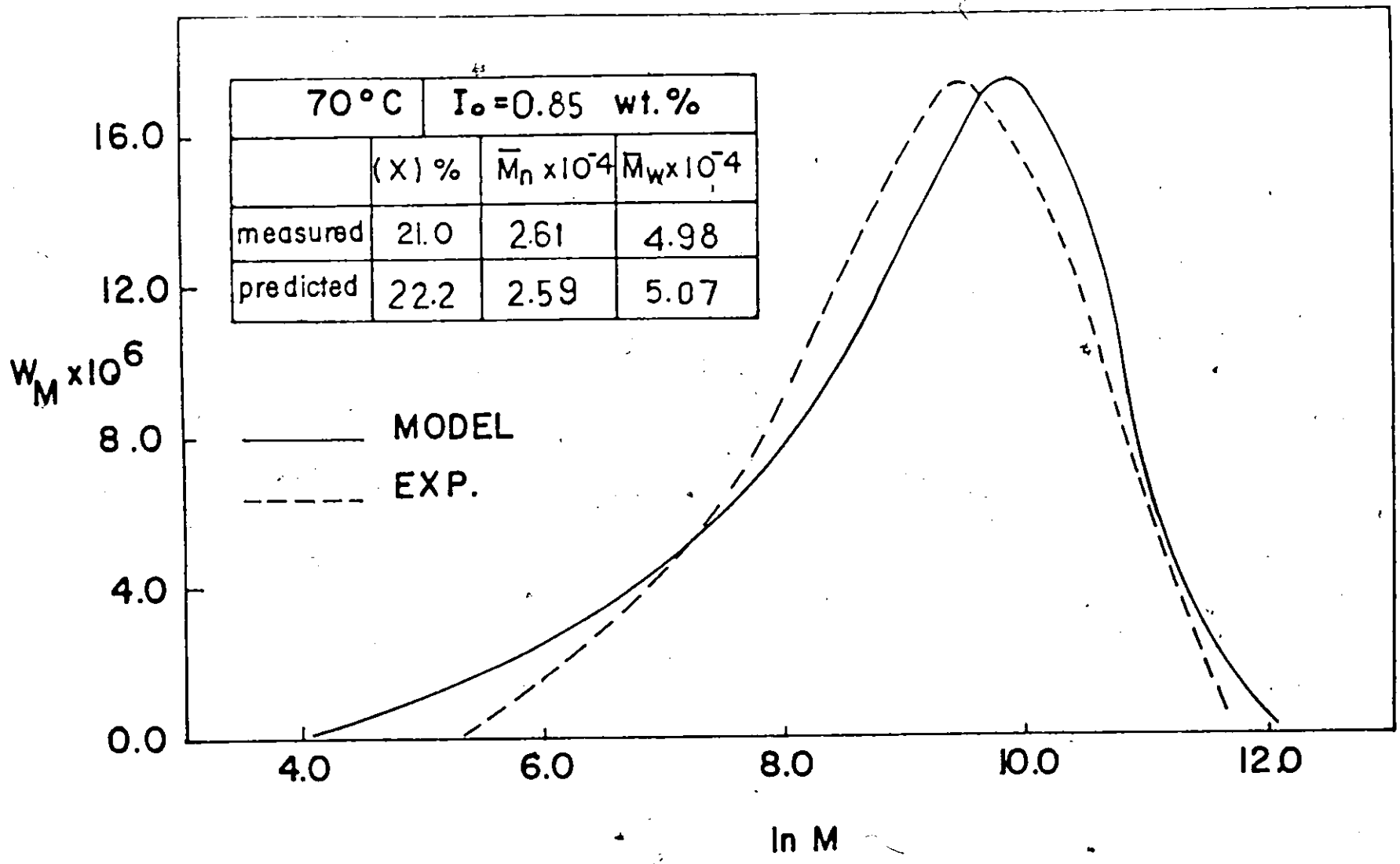
70°C
I_o=0.85 wt.%
(X) %
$\bar{M}_n \times 10^{-4}$
$\bar{M}_w \times 10^{-4}$
measured
21.0
2.61
4.98
predicted
22.2
2.59
5.07
MODEL
EXP.
$W_M \times 10^6$
16.0
12.0
8.0
4.0
0.0
4.0
6.0
8.0
10.0
12.0
ln M

FIGURE 1-12

The least-squares estimate of the parameters and their approximate individual confidence intervals are shown in Table (I-6).

Values of $k_p(f/k_t)^{1/2}$ and C_M are compared in Table (I-7) with values obtained by other workers. In converting the units from mole fraction to moles/liter, the density of the monomer at 50°C is taken as 0.853 gm/ml. This makes a unit mole fraction of monomer equal to 13.6 gm. moles/liter.

The functional relationships between the quantities k_d, C_M, $k_p(f/k_t)^{1/2}$ and temperature were established from their values at different temperatures and the expressions obtained are given below. These are usual Arrhenius-type relationships. Instead of presenting them in the form:

$$k = A \exp(-E/RT)$$

they are presented in the form

$$k = A^* \exp\left[-\frac{E}{R}\left(\frac{1}{T} - \frac{1}{T^*}\right)\right]$$

where T^* is an arbitrary reference temperature, usually chosen in the middle of the temperature range studied. This reparameterization process does not affect the prediction but makes calculations easier since there will be no huge numbers to deal with. A^* is simply the value of k at T^* where A is the value of k at infinite temperature. From a statistical point of view, the correlation coefficient between A^* and E will always be less than that between A and E[88]. It is believed that the second form is more convenient to use.

Table (I-6)

Parameters of Present Model

Polymerization temperature (C°)	Q	$k_p(f/k_t)^{1/2}$ (hr.mole fraction)$^{-1/2}$	$k_d \times 10^3$ (hr^{-1})	x_f	$C_M \times 10^3$	$P = \frac{Qx_f+1}{1-x_f}$	$k_1 = k_p(fk_d/k_t)^{1/2}$ (hr^{-1} mole fraction $^{-1/2}$)
30	4.5±0.11	13.75±0.62	0.28±0.01	0.8±0.01	0.63±0.02	23.0	0.23
50	5.5±0.12	15.52±0.64	6.6±0.17	0.77±0.009	1.1±0.03	22.7	1.25
70	5.1±0.11	19.00±0.57	106.8±3.6	0.72±0.008	1.8±0.05	16.7	6.21

$$k_d = 6.57 \times 10^{-3} \exp\left[\frac{-30.71 \text{ k cal/mole}}{R}\left(\frac{1}{T} - \frac{1}{323.16}\right)\right] \text{hr}^{-1} \qquad \text{(I-73)}$$

$$C_M = 1.098 \times 10^{-3} \exp\left[\frac{-5.448 \text{ k cal/mole}}{R}\left(\frac{1}{T} - \frac{1}{323.16}\right)\right] \qquad \text{(I-74)}$$

$$k_p\left(\frac{f}{k_t}\right)^{1/2} = 16.05 \exp\left[-\frac{1.718 \text{ k cal/mole}}{R}\left(\frac{1}{T} - \frac{1}{323.16}\right)\right] (\text{hr.mole fraction})^{-1/2} \qquad \text{(I-75)}$$

The reference temperature in all of the above expressions is 50°C.

Table (I-7)

Comparison of Present Parameter Values with Literature Values at 50°C.

Source	$k_p(f/k_t)^{1/2}$ (sec.mole/liter)$^{-1/2}$	$C_M \times 10^3$
Present work	0.070	1.1
Crosato-Arnaldi, et al[74]	0.069	---
Tkachenko, et al[84, 85]	0.089	---
Vidotto, et al[79]	0.076	1.1
Danusso, et al[83]	-----	1.035
Breitenbach[86]	-----	1.35
Uno and Yoshida[87]	-----	0.85

I.7 Discussion of Results

Figures (I-3) and (I-4) show the conversion curves for the three temperature levels 30°, 50°, and 70°C. Agreement between experimental curves and model predictions is satisfactory. Experimental data of Farber and Koral[91] for suspension polymerization at 50°C. using AIBN are also compared in Figure (I-4); the good agreement suggests that the

same kinetic model would apply as well for suspension polymerization.

In Figures (I-5) to (I-9), experimental and predicted molecular weight averages are shown. A slight increase in $\bar{M}_n$ and $\bar{M}_w$ is noted with conversion, it is more significant below about 20% conversion as was noticed by Danusso[80] at 50°C. Also, as expected, there is a slight decrease in $\bar{M}_n$ and $\bar{M}_w$ with increasing initiator concentration. This apparent independency of molecular weight averages on conversion or initiator concentration is certainly the result of the dominance of transfer to monomer[64, 70, 79].

Figure (I-7) shows also the results of Vidotto[79] for $\bar{M}_n$ values at 50°c (with lauroyl peroxide as initiator (0.89 wt%)) measured by viscometry. These values are slightly higher than the present values measured by GPC.

It was noticed that the variation of $\bar{M}_n$ and $\bar{M}_w$ with conversion is more pronounced at higher temperatures Figures (I-5), (I-7) and (I-9). The reason for this is that at lower temperatures C_M is much higher than $f\, k_d\, I^{1/2}/k[M]$ which is a function of conversion, accordingly, τ will not vary much with conversion, since C_M is assumed the same in both phases. τ_1 and τ_2 will be close to each other and varying little with conversion, hence molecular weight averages will vary little with conversion. At higher temperatures, the relative importance of $f\, k_d\, I^{1/2}/k[M]$ increases and τ_1 will not equal τ_2. This gives rise to a greater variation of molecular weight averages with conversion.

Table (I-8) shows the predicted variation of the polydispersity with conversion at 30°C, 50°C and 70°C. An increase in polydispersity with an increase in temperature is indicated. This observation is consistent with the above explanation.

Equation (I-73) indicates that the activation energy for the decomposition of the initiator (AIBN) E_i is equal to 30.71 k cal/gm mole. This is in excellent agreement with the value found in the literature 30.7 k cal/gm mole[29]. From equation (I-75), the quantity $(E_p - E_t/2)$ is equal to 1.718 k cal/gm mole, where E_p is the activation energy of propagation, and E_t is the activation energy for termination. Danusso and Sianesi[83] reported a value for $(E_p - E_t/2)$ of 1.5 k cal/gm mole. The overall activation energy of the reaction E_a may be calculated from[93]:

$$E_a = E_i/2 + E_p - E_t/2$$

The calculated value of E_a is 17.07 k cal/gm mole.

Applying the Model to Different Initiator Systems

In the present study experiments were done using (AIBN) as the initiator. As the proposed model indicates, different initiators give rise to different conversion curves due to different k_d values. All the other parameters are properties of the monomer-polymer system and not the initiator. It is possible therefore to predict conversion data using other initiators once k_d for the particular initiator is known.

Conversion data for different commercial initiators at 50°C, are available in the literature. This permits one to test the model over a wide range of initiator systems of commercial interest as shown in figures (I-13)

Table (I-8)

Polydispersity Predicted by Present Model

Conversion x	$\bar{M}_w/\bar{M}_n$ 30°C	50°C	70°C
0.00	2.0000	2.0000	2.0000
0.10	2.0028	2.0151	2.0492
0.20	2.0039	2.0199	2.0651
0.30	2.0043	2.0215	2.0699
0.40	2.0045	2.0217	2.0702
0.50	2.0045	2.0213	2.0686
0.60	2.0044	2.0207	2.0661
0.70	2.0043	2.0200	2.0632
0.80	2.0042	2.0192	2.0609
0.90	2.0040	2.0185	2.0579
0.99	2.0039	2.0171	2.0516

I_o = 0.85 wt %

Table I-9

Different Initiators Used for the Bulk Polymerization of VC at 50°C

Name	Formula Weight	Frequency Factor (A) hr^{-1}	Activation Energy (E) k cal/mole	k_d at 50°C (hr^{-1})	Data from Ref.	Concentration used mole/mole VC
Diisopropyl Peroxydicarbonate	$C_8H_{14}O_6$ 206.18	1.786×10^{18}	28.7	0.6931×10^{-1}	92	1.02×10^{-4}
Di(sec-Butyl) Peroxydicarbonate	$C_{10}H_{18}O_6$ 234.0	1.478×10^{17}	27.1	0.6931×10^{-1}	92	6.7×10^{-5}
t-Butyl Peroxy-Pivalate	$C_9H_{18}O_3$ 174.2	1.274×10^{18}	29.1	0.2652×10^{-1}	92	2.7×10^{-4}
Lauroyl Peroxide	$C_{24}H_{46}O_4$ 398.63	1.353×10^{19}	31.3	0.9158×10^{-2}	74 91 92	4.7×10^{-4} to 5.5×10^{-3}
Benzoyl Peroxide	$C_{14}H_{10}O_4$ 242	2.33×10^{17}	29.7	1.809×10^{-3}	74 63 68 82	7.5×10^{-4} to 10.3×10^{-3}

Figure (I-13)

Literature Data for Four Commercial Initiators Compared with Present Model Predictions

Curve A:	Diisopropyl Peroxydicarbonate	Ref. (92)
Curve B:	Di(sec-Butyl) Peroxydicarbonate	Ref. (92)
Curve C:	t-Butyl Peroxy-pivalate	Ref. (92)
Curve D:	Lauroyl Peroxide	Ref. (91)
Curve E:	Lauroyl Peroxide	Ref. (92)
• :	Lauroyl Peroxide	Ref. (74)
— :	Model Prediction	

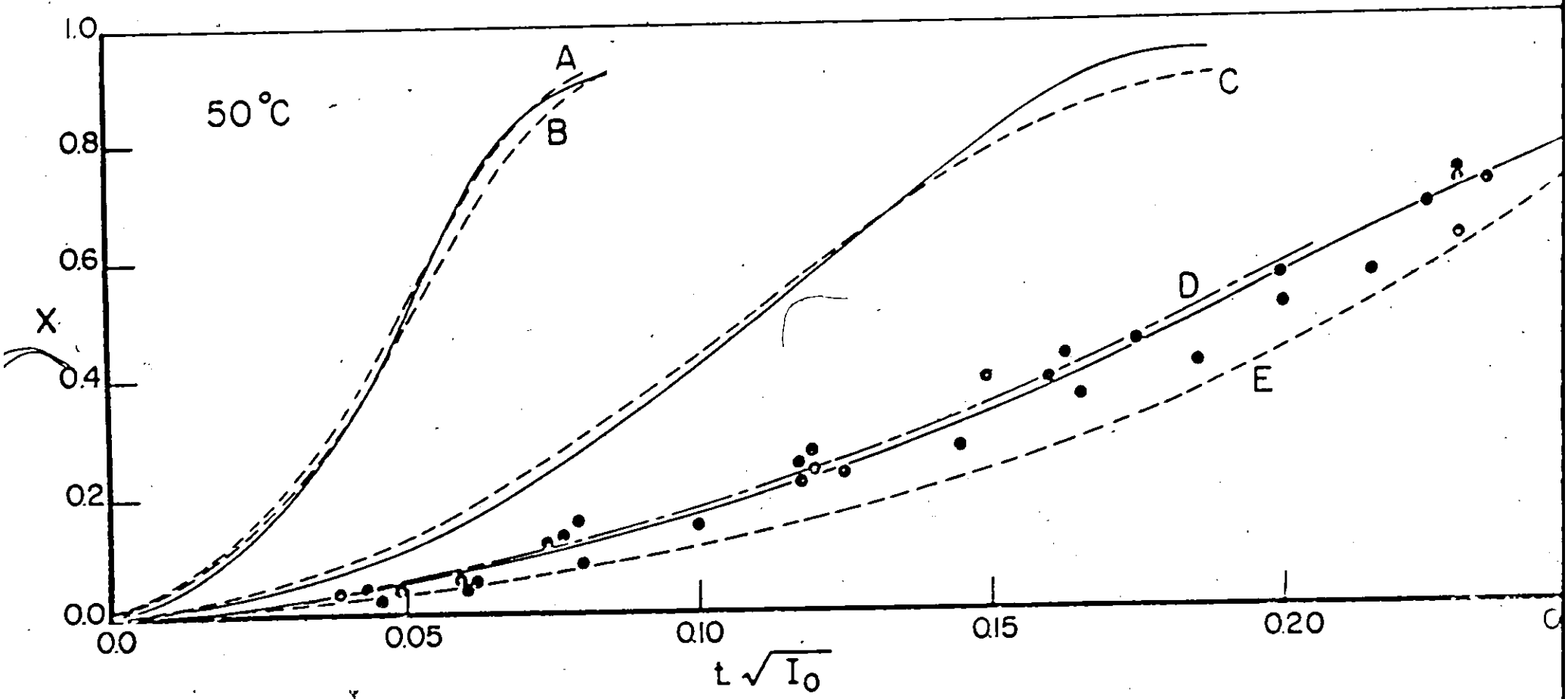

FIGURE 1-13

Figure (I-14)

Literature Data for Benzoyl Peroxide Compared with Present Model Prediction

Curve A: Ref. (82)

Curve B: Ref. (63)

Curve C: Ref. (68)

● : Ref. (74)

- - - : Model Prediction

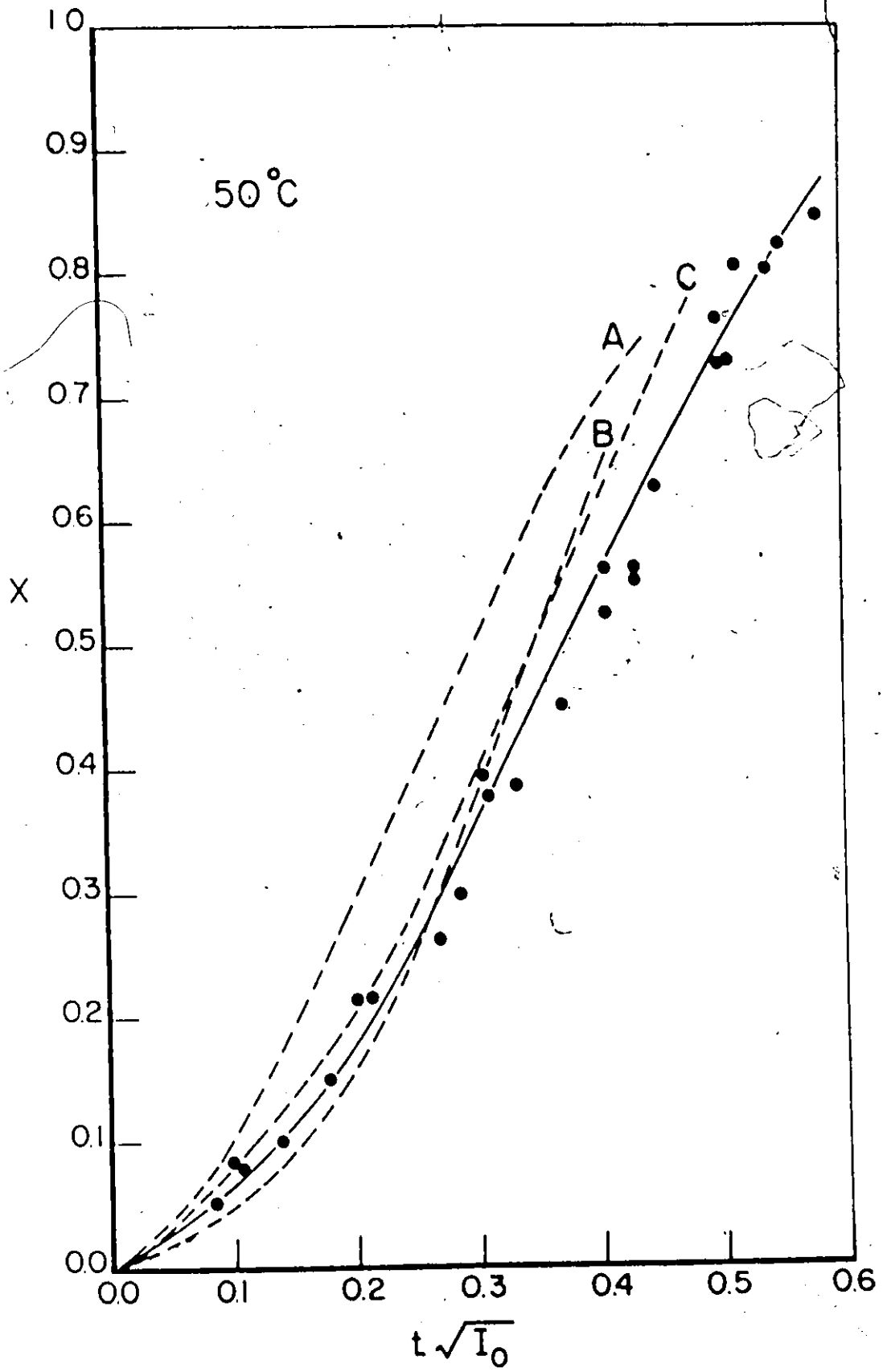

FIGURE 1 - 14

and (I-14). Data for five different initiators were examined. Table (I-9) lists these initiators, their decomposition characteristics and the source of the data.

The dashed lines and the dots are experimental data. The solid lines are the model predictions. These were not fitted to the experimental points but were generated using k_d values given in Table (I-9), as reported in the corresponding references. Values of the other parameters were taken from Table (I-6). k_d for the initiators in curves A and B is the same at 50°C, accordingly only one curve could be predicted. Although there is some scatter of the data obtained from different sources, the prediction seems quite reasonable. Data in Figure (I-14) are all for benzoyl peroxide at 50°C.

Scatter in data also exist in Figures (I-13) and (I-14), data for lauroyl peroxide and benzoyl peroxide respectively from reference (74) agree best with the present model predictions. In both figures, t is the reaction time in hours and I_o is the initial initiator concentration in gm moles/ gm mole VC.

I.8 Summary and Conclusions

Bulk polymerization of vinyl chloride was carried out to limiting conversions in isothermal batch reactors. Three levels of polymerization temperature were used, 30°, 50°, and 70°C. AIBN was the initiator. Molecular weight averages and MWD were measured by gel permeation chromatography. A kinetic model was developed based on a two-phase polymerization system; a

polymer-rich phase with high reaction rate and increasing volume with conversion and a monomer-rich phase with lower reaction rate and decreasing volume with conversion. The net effect is an acceleration in the overall rate of polymerization. This continues until a particular conversion X_f is reached when the rate of reaction starts to drop due to monomer depletion. The model gave good agreement with experimental data while at the same time, the rate constants agreed with literature values. The results obtained indicate that the molecular weight distribution is close to being the most probable distribution function. Transfer to monomer plays the major role in controlling molecular weights.

The following publications are based on the results of the investigation reported in Part (I) of this thesis.

1) Abdel-Alim, A.H., and A.E. Hamielec, "Bulk Polymerization of Vinyl Chloride", J. App. Poly. Sci., 16, 783, (1972).

2) Abdel-Alim, A.H., and A.E. Hamielec, "Bulk Polymerization of Vinyl Chloride" - "Commercial Initiator Systems", J. App. Poly. Sci. (in press).

I.9 Nomenclature

r	chain length, also radius of polymer particle
$w(M)$	weight fraction of polymer of molecular weight M
$w(r)$	weight fraction of polymer of chain length r
$\bar{r}_n$	number average chain length
$\bar{r}_w$	weight average chain length
$\bar{M}_n$	number average molecular weight
$\bar{W}_w$	weight average molecular weight
T_m	crystalline melting temperature
T_g	glass transition temperature
$[M]$	monomer concentration (Dimensionless, i.e. mole fraction)
$R_r^{\cdot}$	polymer radical containing r monomer units
$[I]$	initiator concentration
$M^{\cdot}$	monomeric radical
$I^{\cdot}$	initiator radical
P_r	dead polymer molecule containing r monomer units
k_d	initiator decomposition rate constant
k_p	propagation rate constant
k_{fm}	transfer to monomer rate constant
k_{fI}	transfer to initiator rate constant
k_{fp}	transfer to polymer rate constant
k_t	termination rate constant
f	initiator efficiency
t	reaction time
$[R^{\cdot}]$	total radical concentration

R_I	rate of initiation
R_p	rate of polymerization, in moles monomer consumer per unit volume per unit time
$T^{\cdot}$	trapped radicals
k_c	rate constant for radical trapping in polymer particles
k'_p, k''_p	propagation rate constant for radicals in polymer particles
k'_{fm}	transfer to monomer rate constant for radicals in polymer particles
k'_t, k''_t	termination rate constants for radicals in polymer particles
k_{esc}	rate constant for radicals escape to liquid phase
A	total surface area of polymer particles, also frequency factor
k'	constant, equation (1-34)
k_{t_o}	termination rate constant at t = o
X	conversion
D_L	diffusion coefficient of monomeric radicals in the liquid phase
D'_L	diffusion coefficient of chain radicals in the liquid phase
S_p	total particles surface area per unit volume of suspension
V_p	total volume of particles in a unit volume of suspension
R_c	specific polymerization rate in polymer phase (% per unit time)
R_d	specific polymerization rate in dilute phase (% per unit time)
Q, P	constants (equation 1-50), P also refers to polymer
M_T	total mass of the system
M_1	mass of monomer-rich phase
M_2	mass of polymer-rich phase

m_1	mass fraction of polymer produced in monomer-rich phase
m_2	mass fraction of polymer produced in polymer-rich phase
mp_1	mass of polymer produced in monomer-rich phase
mp_2	mass of polymer produced in polymer-rich phase
x_f	final conversion for the coexistence of two phases
V	volume
B	constant, equation (1-44)
k	kinetic parameter, equation (1-52)
K	Mark-Houwink constant
C_M	monomer transfer constant = k_{fm}/k_p
v	retention volume (counts)
D_1, D_2 D_3, D_4	regression coefficients of the GPC calibration curve
E	activation energy
T	absolute temperature °k
R	gas constant

Greek Symbols

α, β	kinetic parameters, equation (1-14)
τ, ϕ	kinetic parameters, equation (1-16)
α	ratio of monomeric radical concentration at the surface of the particles to the average concentration of monomeric radicals in the active volume
ρ	density of mixture

ρ_m	density of monomer
ρ_p	density of polymer
ρ_2	density of mixture at $x = x_f$
δ	depth of radical penetration into polymer particles
ε	Mark-Houwink constant

Subscripts

c	refers to combination
d	refers to disproportionation
i, 1	refer to monomer-rich phase, i also refers to initiation
f, 2	refer to polymer-rich phase
p	refers to polymer, also to propagation
m	refers to monomer
o	refers to initial conditions (t = o)
t	refers to termination
a	refers to overall

I.10 References

1. Koleske, J.V. and L.H. Wartman. "Poly(vinyl chloride)" Gordon and Breach Science publishers (1969).

2. H.A. Sarvetnick. "Polyvinyl chloride" Van Nostrand Reinhold Company (1969).

3. Barton, D.H.R. and M. Mugdan, J. Soc. Chem. Ind. (London), 69, 75, (1950).

4. Wesselhoft, R.D., J.M. Woods, and J.M. Smith, AIchE, 5, 361 (1959).

5. Gel'bshtein, A.I., Kinetika i Kataliz, 4, 149, (1963).

6. Buckley, J.A. Chem. Eng., 73, 102, (1966).

7. Albright, L.F., Chem. Eng., 74, 219, (1967).

8. Albright, L.F., Chem. Eng., 74, 151, (1967).

9. Platzer, N., Ind. Eng. Chem., 62, (1), 6, (1970).

10. Pechiney-St. Gobain, U.S. Patent 2, 715, 117 (1955); U.S. Patent 2, 856, 272 (1958).

11. Pechiney-St. Gobain, Belgian Patent 602, 397 (1960).

12. Pechiney-St. Gobain, British Patent 913, 724 (1962); Belgian Patent 644, 524 (1964); Belgian Patent 677, 869 (1966); Belgian Patent 677, 870 (1966); Belgian Patent 678, 172 (1966), ECN Large Plant suppl. 9/27/68; Hydrocarb. Proc., Nov. 1968, 192.

13. Pechiney-St. Gobain, Belgian Patent 674, 371 (1968); Belgian Patent 674, 372 (1965).

14. Thomas, J.C., SPE Journal, 61 (October, 1967)

15. Pechiney-St. Gobain, Belgian Patent 647, 821 (1964).

16. A guide to literature and Patents concerning PVC technology (Ed. Lloyd Whittington), Society of Plastic Engineers (1963).

17. Penn, W.S., "PVC Technology", Maclaren and Sons (1966).

18. Smith, W.M., Vinyl Resins, Reinhold Publishing Corp., (1958).

19. Kainer, H., "Polyvinyl Chloride and Vinyl Chloride Mischpolymerisate", Springer-Verlag, (1965).

20. Doditttle, A.K., "The technology of solvents and plasticizers", Wiley, (1954).

21. Chevassus, F. and DeBroutelles, R., "The Stabilization of polyvinyl chloride", St. Martin's Press, (1963).

22. Wartman, L.H., Ind. Eng. Chem., 47, 1013, (1955).

23. "Guide to plastics", by the editors of Modern Plastics Encyclopedia, McGraw-Hill, (1970).

24. Welter, C.R., "Modern Plastic Encyclopedia", McGraw-Hill, (1966), p. 129.

25. Meinecke, E., "Calendering", "Encyclopedia of polymer science and technology", 2, 802, (1966), John Wiley & Sons, Inc.

26. Fisher, E.G., "Extrusion of Plastics", London, Iliffe Books, Ltd., (1964).

27. Frimberger, H.H., "PVC Injection Molding Practices in Europe and the U.S.A.", paper presented at SPE RETEC, New York, (Nov. 18-19, 1965).

28. Lippens, A.M., "Parameters in Equipment Choice for PVC Blow Molding" paper presented at SPE RETEC, New York, (Nov. 18, 1965).

29. Brandrup, J. and E.H. Emmergut, "Polymer Handbook", Interscience, New York, (1966).

30. Cotman, J.D., Ann. N.Y. A Cod. Sci., 57, 417, (1953).

31. Nakajima, A., H. Hamada, and S. Hayaski, Makromol Chem., 95, 40, (1966).

32. Bier, G. and H. Kramer, Kunststoffe, 46, 504, (1956).

33. Pezzin, G., G. Sanmartin and F. Zilo-Grandi, J. App. Poly. Sci., 11, 1539, (1967).

34. Lyngaae-Jorgensen, J., J. Chrom. Sci., 9, 331, (1971).

35. Lyngaae-Jorgenson, J., J. Poly. Sci.(C), 33, 39, (1971).

36. Pezzin, G., G. Talamini, and G. Vidotto, Makromol. Chem., 43, 12, (1961).

37. Fuller, C.S., Chem. Rev., 26, 143, (1940).

38. Natta, G. and P. Corradini, J. Poly. Sci., 20, 251, (1956).

39. Clark, R.J., J. Poly. Sci., 51, S71, (1961).

40. Utsuo, A., and R.S. Stein, Polymer Letters, 3, 49, (1965).

41. Smith. R.W., and C.E. Wilkes, Polymer Letters, 5, 433, (1967).

42. Simril, V.L., J. Poly. Sci., 2, 142, (1947).

43. Keavney, J.J. and E.C. Eberlin, J. Appl. Poly. Sci., 3, 47, (1960).

44. Reding, F.P., E.R. Watter and F.J. Welch, J. Poly. Sci., 56, 225, (1962).

45. Pezzin, G., G. Sanmartin, and F. Zilio-Grandi, J. Appl. Poly. Sci., 11, 1539, (1967).

46. Heydemann, P. and H.D. Guicking, Kolloid Z., 193, 16, (1963).

47. Odian, G. "Principles of Polymerization", McGraw Hill, (1970).

48. Sato, M., Y. Koshushi, and M. Asahina, J. Poly. Sci., B1, 233, (1963).

49. Rudd, J.F., J. Poly. Sci., 44, 453, (1960).

50. Stromberg, R.R., S. Straus and B.G. Achhammer, J. Poly. Sci., 35, 355, (1959).

51. Winkler, D.E., J. Poly. Sci., 35, 3, (1959).

52. Bengaugh, W.Q. and H.M. Sharpe, Makromol. Chem., 66, 31, (1963).

53. Braun, A., "Thermal degradation of polyvinyl chloride", Main lecture given at the IUPAC conference, Prague, September, 1970.

54. Kenyon, A.S. National Bureau of Standards Circ., 528, 81, (1953).

55. Ostromislensky, J.J., J. Russ. Phys. Chem. Soc., 44, 204, 240, (1912).

56. Fuchs, W. and D. Louis, Makromal. Chem., 22, 1, (1957).

57. Bamford, C.H., W.G. Barb, A.D. Jenkis and P.F. Onyon, "The Kinetics of Vinyl Polymerization Radical Mechanisms", Butterworths, London, (1958).

58. Bauman, E., Annalen, 163, 312, (1872).

59. Ostromislensky, I., Chem. Zeitung, 36, 199, (1912).

60. German Patent 278, 249 (October 2, 1917).

61. U.S. Patent 1, 425, 130 (August 8, 1922).

62. Prat, J., M. Mem. Serv. Chim. Etat, 32, 319, (1946).

63. Jenckel, E., H. Eckmans, and H. Rumbac, Makromol. Chem., 4, 15, (1949).

64. Bengough, W.J. and R.G.W. Norrish, Proc. Roy. Soc. (London), A220, 301, (1950).

65. Breitenbach, J.W. and A. Schindler, Mh. Chem. 80, 429 (1949), 86, 437, (1955). J. Poly. Sci., 18, 435, (1955).

66. Arlman, J. and W.M. Wagner, J. Poly. Sci., 9, 581, (1951).

67. Danusso, F. and G. Perugini, Chim. Ind. (Milan), 35, 881, (1953).

68. Schindler, A. and J.W. Breitenbach, Ric. Sci. Suppl., 25, 34, (1955).

69. Magat, M., J. Poly. Sci., 16, 491, (1955).

70. Mickley, H.S., A.S. Michaels, and A.L. Moore, J. Poly, Sci., 60, 121, (1962).

71. Talamini, G., G. Vidotto, Makromol Chem., 50, 129, (1961), 53, 21, (1962).

72. Talamini, G., J. Poly. Sci., Part A2, 4, 535, (1966).

73. Ryska, M., C.M. Kolinsky, and D. Lim, J. Poly. Sci., C16, 621, (1967)

74. Crosato-Arnaldi, A., P. Gasparini, and G. Talamini, Makromol Chem., 117, 140, (1968).

75. Cotman, J.D., M.F. Gonzales, and G.G. Claver, J. Poly. Sci., Part A1, 5, 1137, (1967).

76. Ugelstad, J., H. Lervik, B. Gardinovacki, and E. Sund, Pure Appl. Chem., 25, 121, (1971).

77. Ugelstad, J., H. Flagstad, T. Hertzberg, and E. Sund, Makromol. Chem., 164, 171, (1973).

78. Talamini, G. and E. Peggion, in "Vinyl Polymerization", Vol. I, G. Ham, Marcel Dekker, New York, 1967, Chap. 5.

79. Vidotto, G., A. Crosato-Arnaldi, and G. Talamini, Makromol. Chem., 114, 217, (1968).

80. Danusso, F., G. Pajaro, and D. Sianesi, Chem. Ind. (Milan), 41, 1170, (1959).

81. Provder, T. and E.M. Rosen, ACS Symposium on GPC, Houston, Texas. February, 1970.

82. Danusso, F., and G. Perugini, Chim. Ind. (Milan), 35, 881, (1953).

83. Danusso, F., and D. Sianesi, Chim. Ind. (Milan), 37, 695, (1955).

84. Tkachenko, G.V., P.M. Khomikovkni, and S.S. Medveder, Zuhr. Fiz. Khim, 25, 823, (1951).

85. Tkachenko, G.V., G.G. Petlukov, and V.A. Dodonov, Vysokomol. Soedin, 3, 1549, (1961).

86. Breitenbach, J.W., Makromol. Chem., 8, 147, (1952).

87. Uno, T., and K. Yoshida, Kobunshi Kagaku, 15, 819, (1958).

88. Hunter, W.G., and Atkinson, A.C., Chemical Engineering, June 6 (1966), 159.

89. Box, G.E.P., and Draper, N.R., "Bayesian Estimation of Common Parameters from Several Responses", Biometrika, 52, 355, (1965).

90. Box. G.E.P., W.G. Hunter, J.F. MacGregor, and J. Erjavec, "Some Problems Associated with the Analysis of Multiresponse Data", Technometrics, 15, 33, (1973).

91. Farber, E., and M. Koral, Soc. Plast. Eng. Tech. Papers, 13, 398, (1967).

92. "LUCIDOL" bulletin for free radical initiators for PVC.

93. Flory, P.J., "Principles of polymer chemistry", Cornell University Press, Ithaca, N.Y., 1953.

94. Marquardt, D.W., J. Soc. Ind. Appld. Math., 11, 431, (1963).

95. Himmelblau, "Process analysis by statistical methods", J. Wiley, (1970).

96. Arita, K. and V. Stannett, J. Poly. Sci., 11, 1565, (1973).

I.11 Appendices

APPENDIX (I-1)

Material Balance for Radicals in Polymer Particles

As was shown in this text, the polymer (PVC) precipitates during polymerization in the form of aggregates. As will be shown in Part II of this thesis, these particles (aggregates) are spherical in shape with a diameter of about 2500 Å. We may write a material balance of the radicals in the polymer particles as follows:

At steady state and for a volume of one liter:

Rate of radical production by initiation + Rate of radical transport by bulk flow of monomer converting into polymer - Net rate of radical transport by diffusion out of the polymer - Rate of radical destruction by termination = 0

$$\therefore 2f k_d I + \left(\frac{\overline{dV}}{dt}\right) [R^\cdot]_1 - k_D a([R^\cdot]_2 - [R^\cdot]_1) - k_t [R^\cdot]_2^2 = 0 \qquad (I\text{-}76)$$

where I: the initiator concentration in moles/liter

$\left(\frac{\overline{dV}}{dt}\right)$: average rate of bulk flow of monomer converting into polymer, this is approximately equal to $1/t_1$, t_1 is the time required for one liter of monomer to convert to polymer. Units are mole/liter.

$[R^\cdot]_1$: radical concentration in monomer, gm mole/liter.

$[R^\cdot]_2$: radical concentration in polymer, gm moles/liter.

k_D : a constant representing radical transfer coefficient

a : mass transfer area per unit volume. Units of $k_D a$ are hr^{-1}.

An order-of-magnitude calculation will be carried out to assess the significance of each of the terms in equation (I-76) above. Let us consider bulk polymerization at 50°C. Initiator concentration is 0.8×10^{-3} mole AIBN/mole VC. Under these conditions the reaction time is about 10 hours[74].

k_t is in the order of 10^9 liter/mole.sec

k_d is in the order of 10^{-2} hr^{-1}

The radical transfer area per unit volume (a) is difficult to determine since it varies with time and depends primarily on the aggregation process. This area is a maximum if the surface area of all the spherical aggregates is available for transfer. Undoubtedly (a) will be much less than this extreme. For the purpose of the present rough calculations, this will be considered the case

$\therefore$ a = surface area of one spherical aggregate x number of aggregates per liter

$$= 4\pi (1250 \times 10^{-8})^2 \times \frac{1000 \times 0.5}{(4/3)\pi (1250 \times 10^{-8})^3}$$

The porosity is taken as 0.5

$\therefore$ a is in the order of 10^8 cm^2/liter

$$k_D = \frac{D}{r_o}$$

where D is the radical diffusion coefficient = 10^{-10} cm^2/sec.

r_o is radius of the spherical aggregate = 1250×10^{-8} cm

$\therefore$ k_D is in the order of 10^{-5} cm/sec

$[R^\cdot]_1$ and $[R^\cdot]_2$ are of the same order of magnitude, even though $[R^\cdot]_2$ is larger than $[R^\cdot]_1$. Accordingly $[R^\cdot]$ will be used for any of them or their difference.

$\therefore$ $2f k_d I$ is of the order of $2 \times \frac{1 \times 10^{-2}}{3600} \times \frac{0.8 \times 10^{-3}}{0.0625}$ i.e. 10^{-9} moles/sec

$(\frac{dV}{dt})$ $[R^{\cdot}]$ is of the order of $\frac{1}{10 \times 3600} [R^{\cdot}]$ i.e. $3 \times 10^{-5} [R^{\cdot}]$ moles/sec

$k_D a [R^{\cdot}]$ is of the order of $10^{-5} \times 10^{8} \times 10^{-3} [R^{\cdot}]$ i.e. $[R^{\cdot}]$ moles/sec

$k_t [R^{\cdot}]^2$ is of the order of $10^{9} [R^{\cdot}]^2$ moles/sec

When the above quantities are substituted in equation (I-76) and the equation is solved for $[R^{\cdot}]$, it is found that:

$[R^{\cdot}]$ is in the order of 10^{-9} moles/liter

This means that the transport by bulk flow is completely insignificant, initiation, termination and diffusion are of equal significance.

In the above calculations, (a) was taken as that of isolated spherical aggregates of diameter approximately 2500 Å. Particles of diameter 800 Å and less were recently reported[96] in γ-ray initiated bulk polymerization of vinyl chloride at zero °C. Obviously this leads to a very large surface area. It is highly unlikely that the particles are made up of single aggregates, especially in the absence of stabilizers. Actually, these aggregates agglomorate to form larger polymer particles of diameter ranging from 80 to 200 microns[10, 11, 12, 13, 14].

The above calculations may now be repeated for a more realistic case, namely, the particles having an average diameter of about 100 microns.

The quantity ($k_D a$) is inversely proportional to the diameter squared. This makes the diffusion term in equation (I-76) smaller by a factor of $(400)^2$ or 1.6×10^5. For this case the term $k_D a$ [R·] will be in the order of 10^{-5} [R·]. When equation (I-76) is solved for [R·] it is found that [R·] is again in the order of 10^{-9} gm moles/liter, but now the diffusion term is completely insignificant. This seems to be more realistic, since the polymer precipitated particles were noticed to be in the range of 100 microns in diameter.

APPENDIX (I-2)

Statistical Analysis

The objective of the present study has been the development of a kinetic model to predict conversion, molecular weight distribution, and molecular weight averages. The parameters in the model are to be estimated from the experimentally obtained data.

The ultimate goal is to develop a model which involves the true mechanism. Such a model would probably be very complex and extremely difficult to obtain. A good practical model, however, is one which is capable of predicting satisfactorily the quantities mentioned above. This appendix concerns the mathematical technique of model fitting.

The theory developed earlier in this text indicates that the model contains five parameters, Q, $k_p \left(\frac{f}{k_t}\right)^{1/2}$, k_d, x_f, and C_M.

The parameter C_M appears only in the expressions for the molecular weight averages. In fact, these averages (or the MWD) are governed almost entirely by C_M. The contribution of the other four parameters to the prediction of the MWD is minor. Although the situation is one of multiresponse, it will not be treated as one for the reason just mentioned. The first four parameters are estimated from conversion data., C_M is estimated from molecular weight averages using the estimated values for the other four parameters.

Explicit expressions for the variation of Q and x_f with temperature are not known. Accordingly, data at each temperature level is treated separately and the parameters are evaluated at each temperature level. Values of $k_p \left(\frac{f}{k_t}\right)^{1/2}$, k_d and C_M are then fitted to the usual Arrhenius form to evaluate the activation energies.

Since the model at hand is non-linear, the estimation is carried out using a non-linear least-squares regression routine.

The model may be written as:

$$\underline{y} = \underline{\eta}\ (\underline{x}, \underline{\beta}) + \underline{\xi} \qquad (1\text{-}77)$$

where $\underline{y}$ is a vector of observations, $\underline{x}$ is the matrix of the independent variables settings, $\underline{\beta}$ is a vector of parameters, and $\underline{\xi}$ is a vector of unobservable error. η is the expected value of y. If we have n observations, then for the $u^{\underline{th}}$ observation:

$$y_u = \eta(x_{1u}, x_{2u}, .., x_{ku}; \beta_1, \beta_2, .. \beta_p) + \xi_u \quad u=1 .., n$$

The following assumptions are made:

1) the settings of the independent variables are known fixed values without errors.

2) the model is correct, i.e. $\eta = E(y)$.

3) The errors, ξ, are independent random variables with equal variance from the same probability distribution.

4) The expected value of the errors is zero.

5) The errors are normally distributed with variance σ^2.

This shows that the model contains k independent variables, and p parameters. The least-squares estimate of the p parameters is that choice of $\underline{\beta}$ values that minimizes the quantity:

$$\sum_{u=1}^{n} \left[y_u - \eta(\underline{x}_u, \underline{\beta}) \right]^2 \qquad (I\text{-}78)$$

If the model is linear, it is possible to obtain explicit expressions for those $\underline{\beta}$ values. The model is non-linear however, so the estimation is characterized by the iterative nature.

The course of action followed here is that known as the "Marquard method"[94] which is a combination of linearizing the model and the steepest descent.

If the model is expanded in a Taylor series about some guessed values $\underline{\beta}^\circ$ for the $\underline{\beta}$, then truncating after the linear term:

$$\therefore \eta(\underline{x}_u, \underline{\beta}) \simeq \eta(\underline{x}_u, \underline{\beta}^\circ) + \sum_{i=1}^{p} \left[\frac{\partial \eta(\underline{x}_u, \underline{\beta})}{\partial \beta_i} \right]_{\underline{\beta}^\circ} (\beta_i - \beta^\circ_i)$$

$$\text{Let's define } X^\circ_{iu} = \left[\frac{\partial \eta}{\partial \beta_i} \right]_{\beta^\circ} \quad \text{and } \delta^\circ_i = \beta_i - \beta^\circ_i \qquad (I\text{-}79)$$

$$\therefore \eta(\underline{x}_u, \underline{\beta}) \simeq \eta(\underline{x}_u, \underline{\beta}^\circ) + \sum_{i=1}^{p} X^\circ_{iu} \delta^\circ_i$$

using = instead of $\simeq$ and bearing in mind the approximation involved:

$$\therefore \eta_u = \eta^\circ_u + \sum_{i=1}^{p} X^\circ_{iu} \delta^\circ_i$$

$$\therefore y_u = \eta^\circ_u + \sum_{i=1}^{p} X^\circ_{iu} \delta^\circ_i + \varepsilon_u$$

$$\therefore R^{\circ}_u = y_u - \eta^{\circ}_u = \sum_{i=1}^{p} X^{\circ}_{iu}\, \delta^{\circ}_i + \xi_u \qquad u=1, \ldots, n \text{ and } i=1, \ldots, p$$

This is the linearized form of the model (I-77), and it could be written as:

$$\underline{R}^{\circ} = \underline{X}^{\circ}\, \underline{\delta}^{\circ} + \underline{\xi} \qquad \text{(I-80)}$$

From the theory of linear models[95], the least-squares estimate of $\underline{\delta}^{\circ}$ is shown to be:

$$\hat{\underline{\delta}}^{\circ} = (\underline{X}^{\circ\prime}\, \underline{X}^{\circ})^{-1}\, \underline{X}^{\circ\prime}\, \underline{R}^{\circ} \qquad \text{(I-81)}$$

where $\underline{X}^{\circ\prime}$ is the transpose of $\underline{X}^{\circ}$

In the Marquardt method, $\hat{\underline{\delta}}^{\circ}$ are given by:

$$\hat{\underline{\delta}}^{\circ} = \left(\underline{X}^{\circ\prime}\, \underline{X}^{\circ} + \lambda I\right)^{-1}\, \underline{X}^{\circ\prime}\, \underline{R}^{\circ} \qquad \text{(I-82)}$$

where λ is a positive constant and I is the identity matrix. The introduction of λI represents the steepest descent part of the routine. The choice of λ indicates the contribution of each method.

For $\lambda \longrightarrow 0$ The method reduces to linearization only.

For $\lambda \longrightarrow \infty$ The method reduces to steepest descent only.

Once $\hat{\underline{\delta}}^{\circ}$ are obtained, an improved guess for $\underline{\beta}$ is obtained:

$$\underline{\beta}^{\circ\prime} = \underline{\beta}^{\circ} + \hat{\underline{\delta}}^{\circ} \qquad \text{(I-83)}$$

and the iteration is repeated. This continues until the $\underline{\beta}$ values converge within specified tolerance limits.

Usually the calculations start with relatively large value of λ, then decreasing it as we go along. This means that the contribution of the steepest descent method decreases during iteration. The reason for this is that the steepest descent method always moves towards the right solution regardless of how bad the initial guess is. Linearization if

used at the start may lead to instability if the initial guess was bad. As the right solution is approached, the contribution of the steepest descent should be decreased since it is a slower method than the linearization.

If $\underline{\hat{\beta}}$ are the least-squares estimate of the parameters, then based on the linear theory, the variance-covariance matrix for the $\underline{\hat{\beta}}$ is given by:

$$\text{Estimated Var } (\underline{\hat{\beta}}) = (X'X)^{-1} S^2 = C^{ij} S^2 \qquad \text{(I-84)}$$

Where S^2 is an estimate of σ^2 (the observations variance). This is obtained from the analysis of variance. C^{ij} is the symmetric matrix $(X'X)^{-1}$.

The approximate individual confidence intervals for the parameters are:

$$\beta_i = \hat{\beta}_i \pm t_{(n-p),\alpha/2} \sqrt{C^{ii} S^2} \qquad \text{(I-85)}$$

Where $t_{(n-p),\alpha/2}$ is the student t value obtained from tables for (n-p) degrees of freedom at the α level of significance. The approximate confidence intervals on the model response η at the $\underline{w^{th}}$ setting of the independent variables $\underline{X}_w$, is given by:

$$\eta_w = \hat{\eta}_w \pm t_{(n-p),\alpha/2} \sqrt{\underline{X}'_w (X'X)^{-1} \underline{X}_w S^2} \qquad \text{(I-86)}$$

The approximate correlation matrix for the estimated parameters is given by:

$$r_{ij} = \left\{ \frac{C^{ij}}{\sqrt{C^{ii} C^{jj}}} \right\} \qquad \begin{matrix} i=1, \ldots, p \\ j=1, \ldots, p \end{matrix} \qquad \text{(I-87)}$$

If $|r_{ij}|$ is close to one, then this is evidence that the parameters β_i and β_j are highly dependent.

The initial guesses of C_M and k_d were obtained from the literature. x_f was roughly taken as the inflexion point on the conversion curve. $k_p(f/k_t)^{1/2}$ was guessed as shown from equation (I-53), the value of k_1 at each temperature is the initial slope of the curve x versus $t\sqrt{I_o}$ for this temperature. In fact, equation (I-53) has the form:

$$\frac{dx}{dt} = \left(\frac{dx}{dt}\right)_o \cdot F(x, t)$$

Where x is the conversion and F(x, t) represents an acceleration function. From the value of k_1 and the corresponding k_d, initial guess for $k_p (f/k_t)^{1/2}$ may be obtained. Initial guesses for Q were obtained from Talamini's results[74].

For estimating the parameters Q, x_f, k_d, $k_p (f/k_t)^{1/2}$ the function to be minimized was:

$$\sum_{u=1}^{n} (x_{u\ exp.} - x_{u\ model})^2$$

$x_{exp.}$ is the experimentally-measured conversion and x_{model} is the model prediction at the same value of the independent variable $t\sqrt{I_o}$. This was obtained from equations (I-54) or (I-58) depending on whether x is higher or smaller than x_f. A small subroutine was used to iterate on these equations in order to solve for x at any desired $t\sqrt{I_o}$.

For estimating C_M, the following function was minimized:

$$\Sigma \left[(\bar{M}_{n\ GPC} - \bar{M}_{n\ model})^2 + (\bar{M}_{w\ GPC} - \bar{M}_{w\ model})^2 \right]$$

$\bar{M}_{n\,model}$ and $\bar{M}_{w\,model}$ were obtained from equations (I-67) and (I-68) respectively.

Table (I-10) lists the residuals, defined as the differences between the experimental conversions and the fitted conversions. The appearance of residuals in Table (I-10), together with Figures (I-3) and (I-4) show that the fit is satisfactory and there are no trends.

Table (I-11) shows the analysis of variance performed in this study. In estimating the pure error variance, replicates were made as follows:

At 30°C, 4 replicates at $t\sqrt{I_o} = 1.94$ hr(gm/gm VC)$^{1/2}$

At 50°C, 3 replicates at $t\sqrt{I_o} = 0.1$, and 3 replicates at $t\sqrt{I_o} = 0.337$

At 70°C, 4 replicates at $t\sqrt{I_o} = 0.0625$ hr(gm/gm VC)$^{1/2}$

The "F" tests indicate the absence of lack-of-fit.

Table (I-12) lists the correlation matrices $\{r_{ij}\}$ for the parameters Q, $k_p\,(f/k_t)^{1/2}$, k_d, and x_f at the three temperature levels.

Table (I-13) lists the estimated activation energies and the pre-exponential factors for the parameters k_d, C_M, and $k_p\,(f/k_t)^{1/2}$.

Experimental and Fitted Conversions

30°C				50°C				70°C			
$t\sqrt{I_o}$	x exp.	x model	Residual	$t\sqrt{I_o}$	x exp.	x model	Residual	$t\sqrt{I_o}$	x exp.	x model	Residual
.1800	.025	.0271	-.0021	.0510	.043	.0441	-.0011	.0100	.041	.0425	-.0015
.2500	.037	.0386	-.0016	.0580	.051	.0505	.0005	.0125	.059	.0546	.0044
.2800	.045	.0437	.0013	.0780	.074	.0719	.0021	.0135	.056	.0596	-.0036
.3600	.057	.0578	-.0008	.1000	.101	.0971	.0039	.0150	.068	.0673	.0007
.4400	.077	.0726	.0044	.1000	.092	.0971	-.0051	.0175	.071	.0807	-.0097
.5000	.088	.0843	.0037	.1000	.098	.0971	.0009	.0176	.088	.0812	.0068
.5100	.099	.0863	.0127	.1070	.110	.1063	.0037	.0200	.084	.0948	-.0108
.5600	.105	.0965	.0085	.1100	.117	.1094	.0076	.0220	.100	.1066	-.0066
.6200	.118	.1092	.0088	.1300	.140	.1359	.0041	.0225	.110	.1097	.0003
.6750	.133	.1213	.0117	.1500	.170	.1649	.0051	.0250	.125	.1254	-.0004
.7000	.139	.1269	.0121	.1580	.180	.1773	.0027	.0375	.215	.2180	-.0030
.7800	.162	.1457	.0163	.1620	.185	.1837	.0013	.0380	.210	.2222	-.0122
.8900	.186	.1733	.0127	.1650	.180	.1885	-.0085	.0400	.220	.2397	-.0197
.9400	.190	.1866	.0034	.1870	.234	.2264	.0076	.0430	.272	.2676	.0044
1.200	.260	.2639	-.0039	.1890	.230	.2300	.0000	.0480	.316	.3185	-.0025
1.310	.305	.3014	.0036	.1910	.246	.2337	.0123	.0490	.325	.3294	-.0044
1.425	.335	.3439	-.0089	.2250	.310	.3021	.0079	.0510	.364	.3520	.0120
1.720	.471	.4721	-.0011	.2520	.373	.3653	.0077	.0520	.369	.3637	.0053
1.820	.533	.5228	.0102	.2530	.370	.3678	.0022	.0550	.402	.4006	.0014
1.940	.590	.5896	.0004	.2840	.445	.4525	-.0075	.0625	.512	.5059	.0061
1.940	.601	.5896	.0114	.2850	.440	.4555	-.0155	.0625	.493	.5059	-.0129
1.940	.587	.5896	-.0026	.3270	.607	.5964	.0106	.0625	.488	.5059	-.0179
1.940	.576	.5896	-.0136	.3550	.700	.7111	-.0111	.0625	.495	.5059	-.0109

2.090	.691	.6833	.0077	.3370	.793	.8079	-.0149	.0674	.570	.5865	-.0165
2.130	.729	.7105	.0185	.3370	.809	.8079	.0011	.0690	.614	.6152	-.0012
2.290	.822	.8259	-.0039	.3370	.817	.8079	.0091	.0695	.611	.6245	-.0135
2.720	.920	.9306	-.0106	.3980	.840	.8608	-.0208	.0710	.654	.6530	.0010
3.840	.948	.9732	-.0252	.4380	.920	.9093	.0107	.0750	.750	.7340	.0160
				.4420	.925	.9123	.0127	.0760	.742	.7518	-.0098
								.0950	.892	.8944	-.0024
								.1240	.950	.9446	.0054
								.1260	.955	.9463	.0087
								.1360	.968	.9537	.0143
								.1600	.977	.9652	.0118

$\Sigma(\text{Residuals})^2 = 2.66 \times 10^{-3}$ $\Sigma(\text{Residuals})^2 = 2.13 \times 10^{-3}$ $\Sigma(\text{Residuals})^2 = 3.00 \times 10^{-3}$

Table (I-11)

Analysis of Variance (ANOVA)

Temp.	Source	Sum of Squares (SS)	Degrees of Freedom (ν)	Mean Squares MS=SS/ν	$\frac{(L.O.F.)MS}{(P.E.)MS}$	$F_{0.95}(\nu_{L.O.F.}, \nu_{P.E.})$	Is the model adequate?
	Residuals	2.66×10^{-3}	24	1.11×10^{-4}			
30°C	Pure Error(P.E)	3.17×10^{-4}	3	1.06×10^{-4}	1.06	8.65	YES
	Lack of Fit (L.O.F.)	2.34×10^{-3}	21	1.12×10^{-4}			
	Residuals	2.13×10^{-3}	25	8.50×10^{-5}			
50°C	Pure Error(P.E)	3.41×10^{-4}	4	8.52×10^{-5}	0.998	5.79	YES
	Lack of Fit (L.O.F.)	1.79×10^{-3}	21	8.49×10^{-5}			
	Residuals	3.00×10^{-3}	30	1.00×10			
70°C	Pure Error(P.E)	3.26×10^{-4}	3	1.09×10^{-4}	0.912	8.62	YES
	Lack of Fit (L.O.F.)	2.68×10^{-3}	27	9.91×10^{-5}			

Table (I-12)

Parameters Correlation Matrix $\{r_{ij}\}$

Temp.		Q	$k_p(f/k_t)^{1/2}$	k_d	x_f
30°C	Q	1.000	-0.561	-0.416	-0.394
	$k_p(f/k_t)^{1/2}$		1.000	-0.698	-0.205
	k_d			1.000	-0.274
	x_f				1.000
50°C	Q	1.000	-0.623	-0.472	-0.377
	$k_p(f/k_t)^{1/2}$		1.000	-0.702	-0.214
	k_d			1.000	-0.293
	x_f				1.000
70°C	Q	1.000	-0.594	-0.448	-0.369
	$k_p(f/k_t)^{1/2}$		1.000	-0.683	-0.209
	k_d			1.000	-0.280
	x_f				1.000

Table (I-13)

Arrhenius Expressions for k_d, C_M, and $k_p(f/k_t)^{1/2}$

$$\text{Parameter} = A^* \cdot \text{Exp}\left[-\frac{E}{R}\left(\frac{1}{T} - \frac{1}{T'}\right)\right]$$

$$T' = 50°C + 273.16$$

Parameter	A^*	E Cal/gm mole	Correlation Coefficient
k_d	$(6.57 \pm 0.04)\times10^{-3}$ hr^{-1}	30710 ± 563	-0.692
C_M	$(1.098 \pm 0.003)\times10^{-3}$	5448 ± 36	-0.658
$k_p(f/k_t)^{1/2}$	16.05 ± 0.77 $(hr.mole\ fraction)^{-1/2}$	1718 ± 126	-0.417

PART (11)

MOLECULAR AGGREGATION IN POLYVINYL CHLORIDE (PVC)

11.1 Introduction

It has been known for some time that PVC molecules form aggregates and that these supermolecular entities dissolve very slowly in good solvents such as THF and cyclohexanone. The discovery of PVC aggregates dates back to the early work of Doty[1]. The presence of these aggregates leads to difficulties in measurements using dilute PVC solutions, e.g. a downward curvature was noticed[2-5] in the plot of $KC/R\theta$ vs. $\sin^2(\theta/2)$ for light-scattering measurements, the suggested cause was microgel particles with a diameter of 2500 Å and a molecular weight of the order 10^8. Hengstenberg[6], using different measuring techniques, concluded that these aggregates are made up of associated molecules and have a diameter between 140 and 180 Å and a weight between 11 and 25 times that of a single molecule.

It was noticed[6-8] that heating dilute solutions of PVC in THF as well as other solvents will dissolve these aggregates, however, these authors suggest different heat treatments. Crugnola and Danusso[9] showed that polymers produced at very low temperatures, e.g. -40°C did not disintegrate by heating at 150°C for two hours while atactic polymers, produced at 30 - 50°C, readily disintegrate to single molecules by heating. More recently, workers have become aware of the need to disintegrate these aggregates into single PVC molecules to preclude anomolous molecular weight measurements[10,11,12]. Lyngaae-Jorgensen[13] did rheological measurements on PVC melts containing aggregates and found

that flow properties were significantly affected. He employed light scattering techniques and estimated the aggregates to have the shape of a star branched polymer with approximately 24 long branches of random length held together in a crystalline nucleus. It is the syndiotactic placement (figure 11-1) that is responsible for the formation of these crystallites[14].

Part (11) of this thesis is a study of the properties of these aggregates using GPC and electron microscopy.

11.2 Polymer Stereo-Chemistry[15]

11.2.1 Chain Conformation versus Configuration

As shown in figure (11-1), polymer stereo-chemistry covers both chain conformation and chain configuration.

In dilute solution, where the polymer chain is surrounded by small molecules, or in the melt, where it is in an environment of similar chains, the polymer molecule is in continual motion because of its thermal energy, thus assuming different conformations.

Configuration, on the other hand, reflects geometrical regularity and is fixed by the polymerization conditions.

Conformation may be changed by altering the environment, but changing the configuration requires breaking of bonds.

11.2.2 Tacticity

Tacticity is determined by the configuration of the successive "asymmetric" carbon atoms along the chain. As in figure (11-1), if the R groups are randomly distributed above and below the planar zig-zag polymer main chain, the polymer does not have order and is termed atactic.

POLYMER STEREO - CHEMISTRY

- CHAIN CONFORMATION:
  - STRAIGHT CHAINS
  - HELICAL CHAIN
  - RANDOM COIL
- CHAIN CONFIGURATION
  - RECURRENCE REGULARITY
    - head-to-tail: $-CH_2-\underset{R}{CH}-CH_2-\underset{R}{CH}-CH_2-\underset{R}{CH}-$
    - head-to-head, tail-to-tail: $-CH_2-\underset{R}{CH}-\underset{R}{CH}-CH_2-CH_2-\underset{R}{CH}-$
  - STEREOREGULARITY (TACTICITY)
    - Isotactic
    - Syndiotactic
    - Atactic

FIGURE (11-1)

Two types of ordered or tactic polymer structures may occur - isotactic and syndiotactic. An isotactic structure occurs when the site of steric isomerism in each repeating unit in the polymer chain has the same configuration. All the R groups will be located in one side of the plane of the carbon-carbon polymer chain - either all above or all below. A syndiotactic structure occurs when the site of steric isomerism in each repeating unit in the polymer has the opposite configuration of that in the preceding repeating unit. The R groups are located alternately above and below the plane of the polymer chain.

Two ways are generally used to describe the degree of syndiotactic or isotactic regularity. One is the diad tacticity defined by Natta[16] as the fractions of the adjacent monomer units (diads) which are placed isotactic or syndiotactic to one another:

Isotactic Syndiotactic

where the horizontal line represents a segment of the polymer chain and each vertical line represents the configuration at the site of steric isomerism in a monomer unit. The fractions of isotactic and syndiotactic diads are usually designated as I and S respectively.

The second definition of tacticity is the triad tacticity suggested by Bovey and Tiers[17]. Isotactic, syndiotactic, and heterotactic triads are defined by:

Isotactic Syndiotactic

Heterotactic

and designated as i, s, and H, respectively. The following relations hold:

$$I + S = 1 \tag{11-1}$$

$$i + s + H = 1 \tag{11-2}$$

$$I = i + \frac{1}{2} H \tag{11-3}$$

$$S = s + \frac{1}{2} H \tag{11-4}$$

Tacticity is usually measured by nuclear magnetic resonance (NMR). Whether one determines the diad or triad tacticities by NMR depends on the particular polymer and on the sensitivity of the NMR instrument used. As the resolution of NMR instruments increases, tacticity of longer sequences than diads and triads will be analyzed[18]. Recently, pentades have been measured in PVC[19].

11.2.3 Radical Polymerization

During propagation, the terminal carbon-carbon bond, as in figure (11-2) is freely rotating. This means that the configuration of a monomer unit in the polymer chain is not determined during its addition to the radical center but only when the next monomer molecule adds to it.

Figure (11-2) shows the two placements - syndiotactic and isotactic taking place with rate constants k_s and k_i, respectively. Whether or not the same placement is propagated through the successive additions of monomer units determines the stereo regularity of the final polymer

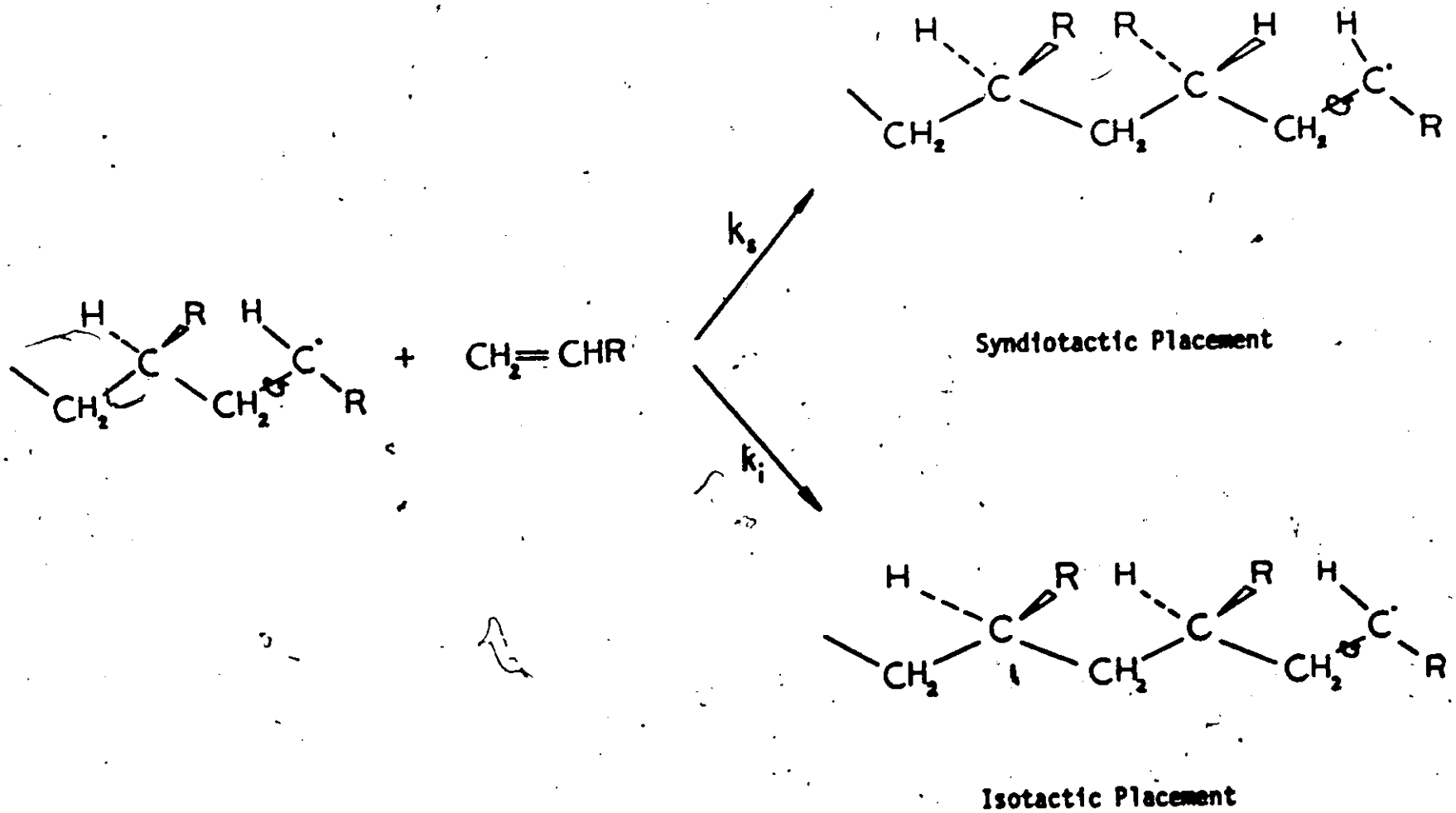

FIGURE (11-2)

molecule. The amount and type of stereo-regularity is determined by the value of k_i/k_s.

The ratio k_i/k_s depends on the polymerization temperature in the following manner:

$$\frac{k_i}{k_s} = \exp\left\{\frac{-\Delta(\Delta F_p)^*}{RT}\right\}$$

$$= \exp\left\{\frac{-\Delta(\Delta H_p)^*}{RT} + \frac{\Delta(\Delta S_p)^*}{R}\right\} \qquad (11\text{-}5)$$

$$\ln \frac{k_i}{k_s} = \frac{\Delta(\Delta S_p)^*}{R} - \frac{\Delta(\Delta H_p)^*}{R} \cdot \frac{1}{T} \qquad (11\text{-}6)$$

$$\Delta(\Delta F_p)^* = \Delta F_i^* - \Delta F_s^* \qquad (11\text{-}7)$$

$$\Delta(\Delta H_p)^* = \Delta H_i^* - \Delta H_s^* \qquad (11\text{-}8)$$

$$\Delta(\Delta S_p)^* = \Delta S_i^* - \Delta S_s^* \qquad (11\text{-}9)$$

where ΔF_i^*, ΔH_i^*, ΔS_i^* are the activation free energy, enthalpy, and entropy for isotactic placements and ΔF_s^*, ΔH_s^*, and ΔS_s^* are the corresponding quantities for syndiotactic placements.

Since the ratio $\frac{I}{S}$ or $\frac{1-S}{S}$ is proportional to the ratio k_i/k_s, we may write:

$$\ln \frac{1-S}{S} = \frac{\Delta(\Delta S_p)^*}{R} - \frac{\Delta(\Delta H_p)^*}{R} \cdot \frac{1}{T} \qquad (11\text{-}10)$$

Thus the quantities $\Delta(\Delta S_p)^*$ and $\Delta(\Delta H_p)^*$ may be obtained by carrying out a series of tacticity measurements for polymers prepared at different temperatures.

11.2.4 Distribution of Stereo-regular Sequence Lengths

Similar to the distribution of molecular weights in a polymer, there is a distribution of stereo-regular sequence lengths. The ratio k_s/k_i determines both the average sequence length and the sequence length distribution[20].

If the probability of having a syndiotactic sequence of n monomer units is the probability of having a sequence in which an initial syndiotactic placement is repeated (n-1) times followed by an isotactic placement, then this probability P_n^s is given by[20]:

$$P_n^s = S^{n-1}(1-S) \qquad (11\text{-}11)$$

The average length of the syndiotactic sequence $\bar{n}_s$ is given by:

$$\bar{n}_s = \sum_{n=1}^{\infty} n\, S^{n-1}(1-S) \qquad (11\text{-}12)$$

The fraction F_n^s of syndiotactic sequences of length greater than n monomer units is given by:

$$F_n^s = S^{n+1}\{1 + (1-S)n\} \qquad (11\text{-}13)$$

The fraction of the total polymer f_n^s which has a syndiotactic sequence length of n monomer units is given by:

$$f_n^s = n(1-S)^2 S^n \qquad (11\text{-}14)$$

Figure (11-3), from reference 20, shows the distribution given by equation (11-14) for different values of k_s/k_i. Polymers of high syndiotacticity have considerable amounts of short syndiotactic sequences. This explains why even the moderately high degree of syndiotacticity

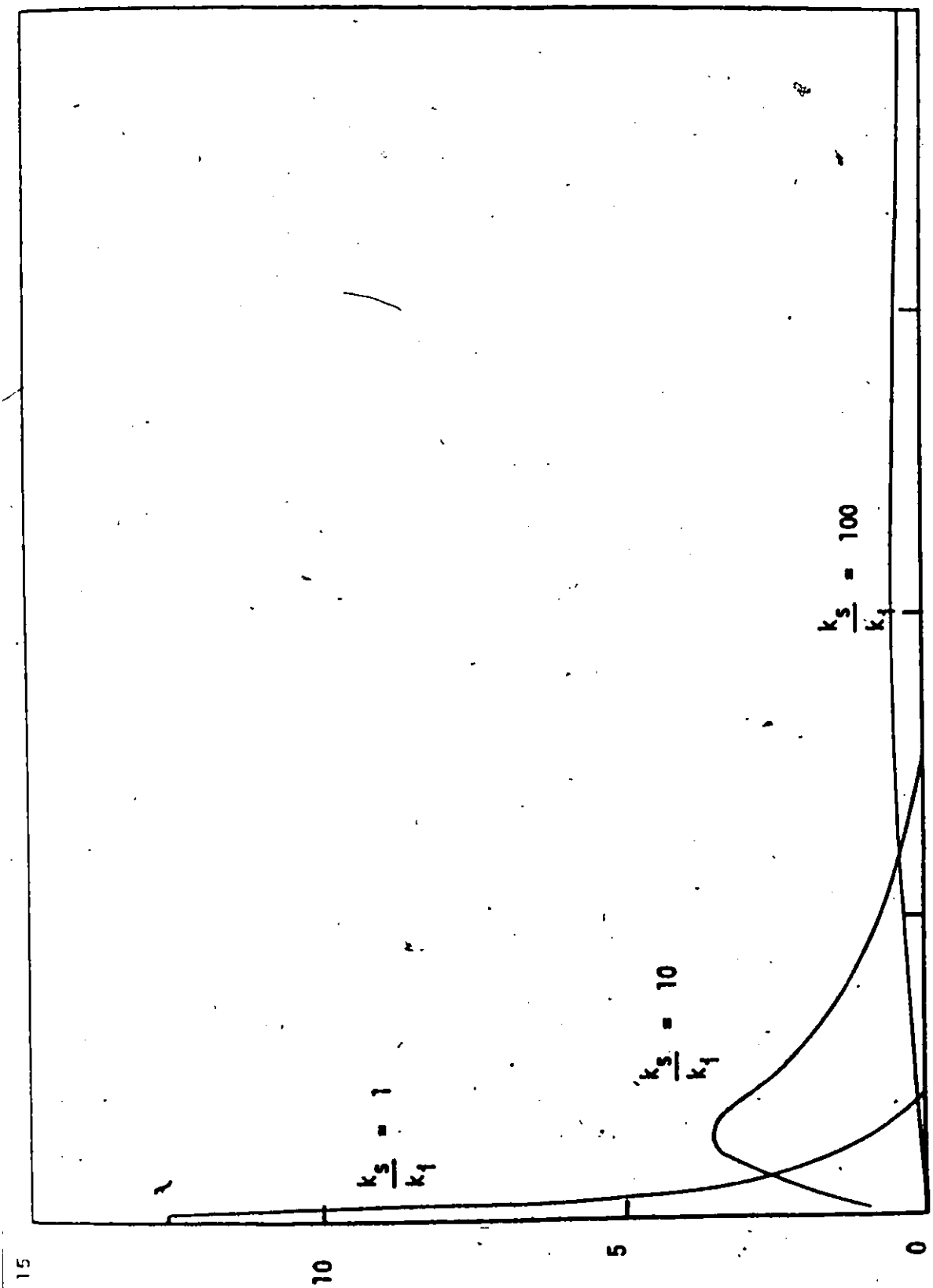
Fraction of polymer with sequence-length of $n, f^s_n \times 10^2$
15
10
5
0
0
50
100
150
200
Syndiotactic sequence - length, n
$k_s/k_t = 1$
$k_s/k_t = 10$
$k_s/k_t = 100$

FIGURE (11-3)

present in a polymer such as polymethyl methacrylate is not enough to allow it to crystallize extensively.

Although the ratio k_s/k_i is determined mainly by the polymerization temperature, it is possible to prepare polymers with very high degree of regularity by using special initiators. "Ziegler-Natta" type catalysts are examples. This type of polymerization known as coordination polymerization produces essentially pure syndiotactic or pure isotactic polymers[21,22].

11.3 Experimental

11.3.1 Materials

PVC samples were prepared in the temperature range, 30-70°C in bulk using chemical initiation (AIBN). Details of synthesis procedure are given in Part (I) of this thesis.

Low temperature PVC samples were polymerized in bulk using γ-ray initiation at -10°C, -30°C, and -50°C and were supplied for this investigation by G. Palma, Laboratorio di Fotochimica e Radiazioni d'Alta Energia C.N.R., Padova, Italy. Initiation involved a dose rate of 2.2 rad/sec giving conversions in the range 78 to 90%.

11.3.2 GPC Measurements

A Waters GPC model 200 was used. Operating conditions and column specifications are given in Part (I).

11.3.3 NMR Measurements

Measurements were done at the Ontario Research Foundation by Dr. Arthur Grey of the NMR Center. Specifications are:

220 - MH_z NMR

Solutions of PVC in O-dichlorobenzene (15 mg/ml)

2% HMDS as internal reference

Temperature: 120°C

Areas of peaks were measured by actual count and by the triangular method; both agree within 2% on the average.

11.4 Results and Discussion

11.4.1 NMR Analyses (Syndiotacticity)

To date, NMR is the most reliable tool to obtain tacticity data for PVC. In the present work it is shown that such data can also be obtained using GPC. Samples prepared at different temperatures were analyzed by NMR, tacticity data were obtained, in the form of diads, and are shown in Table (11-1). The Arrhenius plot of the tacticity data is shown in Figure (11-4), where $\ln \frac{1 - S}{S}$ is plotted vs. $\frac{1}{T}$. S being the syndiotactic fraction:

$$\ln \frac{1 - S}{S} = \frac{\Delta(\Delta S_p)^*}{R} - \frac{\Delta(\Delta H_p)^*}{R} \frac{1}{T}$$

From this plot, values of the difference in enthalpy and entropy of activation for isotactic and syndiotactic monomer placement can be obtained, it was found that: (see Appendix (11-1))

$$\Delta(\Delta H_p)^* = \Delta H_i^* - \Delta H_s^* \approx 694 \text{ cal/mole}$$

$$\Delta(\Delta S_p)^* = \Delta S_i^* - \Delta S_s^* \approx 1.68 \text{ eu}$$

These values are compared to literature values in Table (11-2).

TABLE (11-1)

TACTICITY DATA BY NMR

Polymerization Temperature °C		Syndiotactic Fraction S
Replicates 70	1	0.542
70	1	0.544
70	1	0.543
70	1	0.544
50	1	0.559
45	1	0.565
40	1	0.568
35	1	0.570
30	1	0.576
-10	2	0.615
-30	2	0.647
Replicates -50	2	0.673
-50	2	0.675
-50	2	0.673
-50	2	0.672

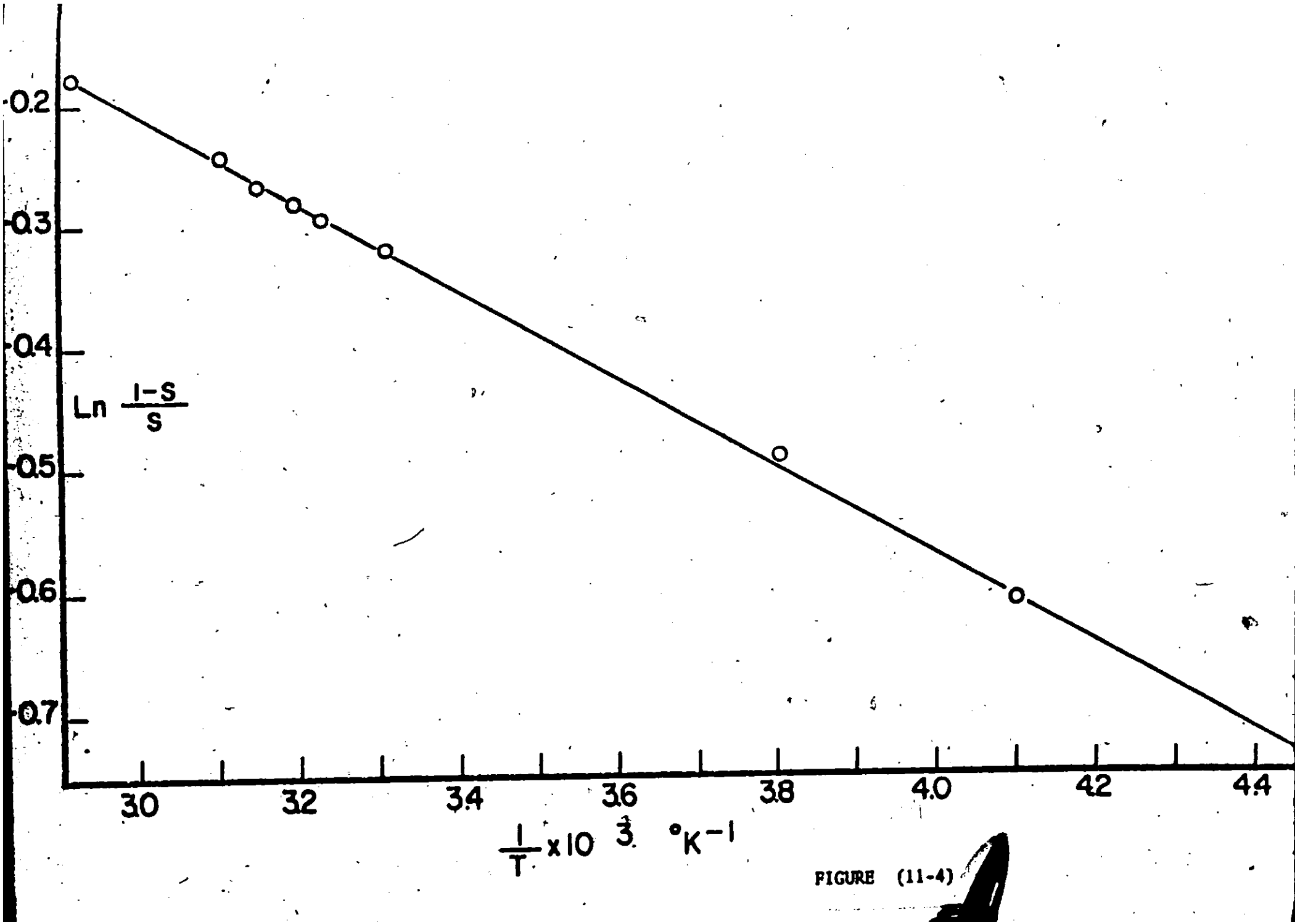

FIGURE (11-4)

TABLE (11-2)

$\Delta(\Delta H_p)^*$ and $\Delta(\Delta S_p)^*$ for PVC

Reference	$\Delta(\Delta H_p)^*$ $\frac{Cal.}{mole}$	$\Delta(\Delta S_p)^*$ eu.
Fordham, et.al. (23)	600	-
Bovey, et.al. (24)	310	0.6
Cavalli, et.al. (19)	630	1.5
Present work	694	1.68

11.4.2 GPC Analyses

Figure (11-5) is a flow diagram of the experimental procedure. PVC solutions, 0.2 wt. % in THF were prepared by mixing the appropriate amounts of polymer and THF. Dissolution was first tried at room temperature. At this stage different polymer samples showed different solubility behaviour. PVC prepared at 30°C and above (group 1 in Table 11-1) readily dissolved in THF at room temperature after stirring for about an hour or even less giving a clear solution of single molecules and aggregates. On the other hand, the low temperature (group 2 in Table 11-1, polymerization temperature -10°C and lower) did not give a clear solution at room temperature even with stirring for several days. The fraction of the polymer that remained in suspension was observed visually to be greater for the -50°C and -30°C PVC samples. Concentrations other than 0.2 wt. % were then tried to check whether concentration has any effect on the fraction in suspension. The results were the same, indicating that there is no concentration effect. This is expected as we are far below the saturation limit.

11.4.3 Aggregate Content in Group (1) Samples

Effect of Polymerization Temperature

It has been known[25] that the amount of aggregates in PVC increases as the polymerization temperature decreases. GPC analyses also show this. In figure (11-6) are shown GPC responses for six samples prepared at the same conversion and initiator (AIBN) concentration, 33%

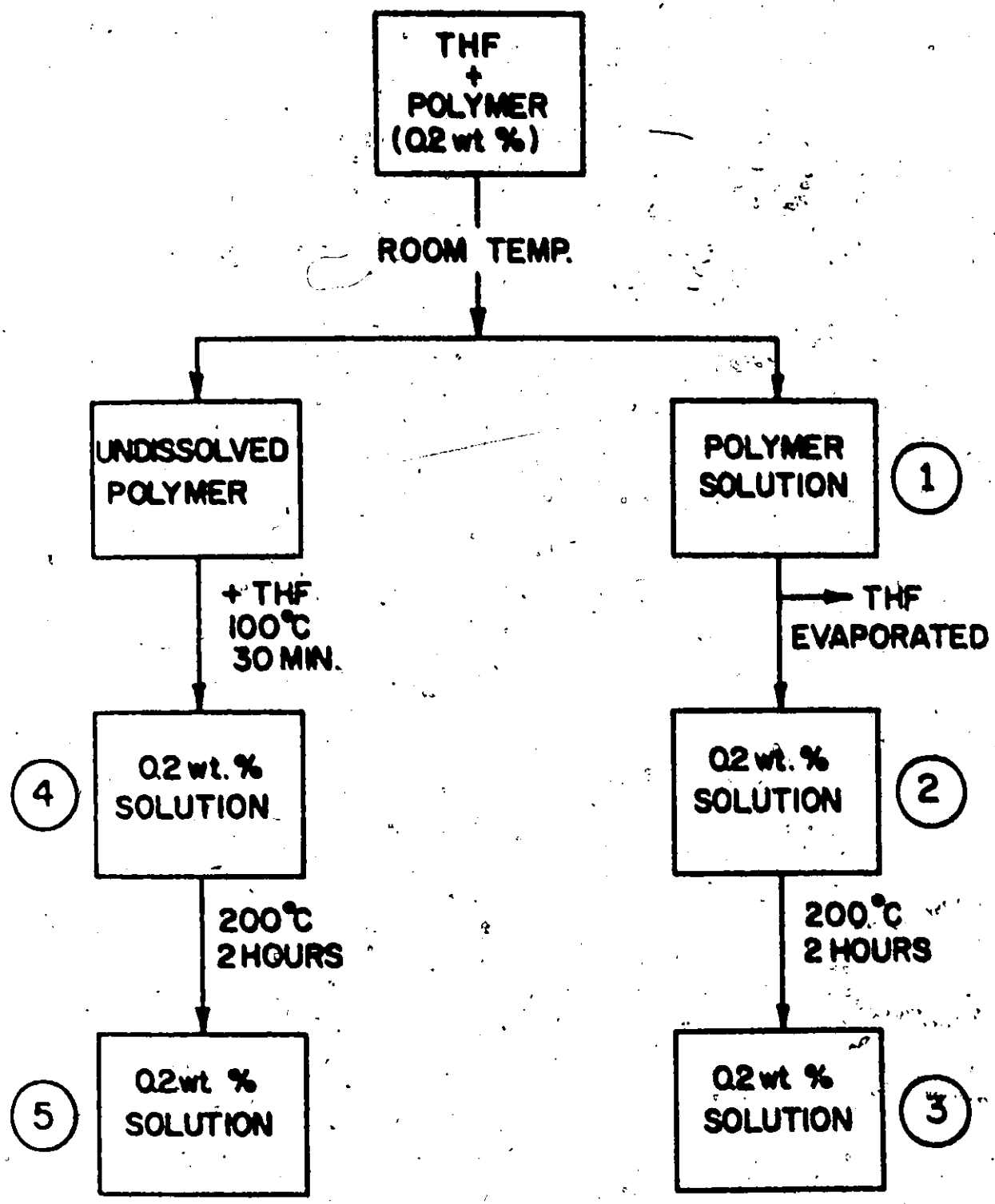
THF
+
POLYMER
(0.2 wt %)
ROOM TEMP.
UNDISSOLVED
POLYMER
POLYMER
SOLUTION
1
+ THF
100°C
30 MIN.
THF
EVAPORATED
4
0.2 wt. %
SOLUTION
0.2 wt. %
SOLUTION
2
200°C
2 HOURS
200°C
2 HOURS
5
0.2wt %
SOLUTION
0.2 wt %
SOLUTION
3

FIGURE (11-5)

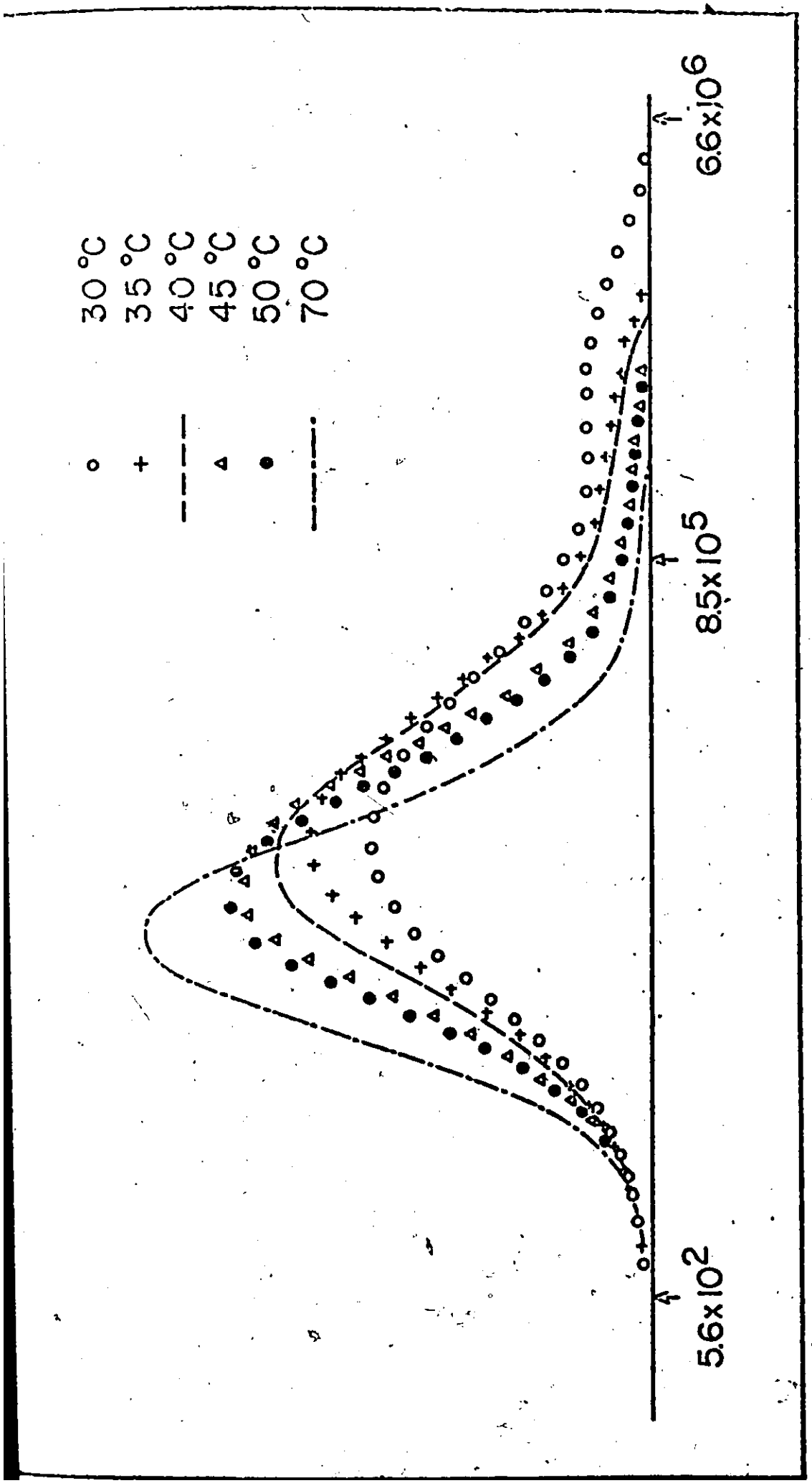

FIGURE (11-6)

and 0.27 mole % respectively, but at different temperatures, the GPC chromatograms show that the second peak at the high molecular weight end, gradually decreases in size with increase in polymerization temperature; at high temperatures, e.g. 70°C the chromatogram is essentially unimodal where the apparent high molecular weight peak is almost absent. The arrows shown on the base line in figure (11-6) give an indication of the molecular weight.

Effect of Heating the Solutions

It was reported[6-8] that heating dilute solutions of PVC dissolves the aggregates, Lyngaae-Jorgensen[26] noticed the disappearance of the second peak when the sample was reinjected in the GPC after heating at 120°C for 3 hours. However, in the present work, it was noticed that heating the solutions at 100°C for 10 minutes was enough to dissolve the aggregates. Figure (11-7a) shows the effect of heating on a sample prepared at 30°C, 93% conversion, 0.27 mole %. AIBN; it is noticed that after heat treatment (100°C for 10 minutes), the second peak was eliminated and the fraction of intermediate molecular weights was increased, a relatively more severe heat treatment did not lead to more disintegration to smaller molecules. The area between the two chromatograms in figure (11-7a), to the right of the intersection point (the hatched area) represents the gross change caused by heating; it is believed that such heat treatment would not lead to degradation[6-8], accordingly, the hatched area is a measure of the mass of aggregates in the sample.

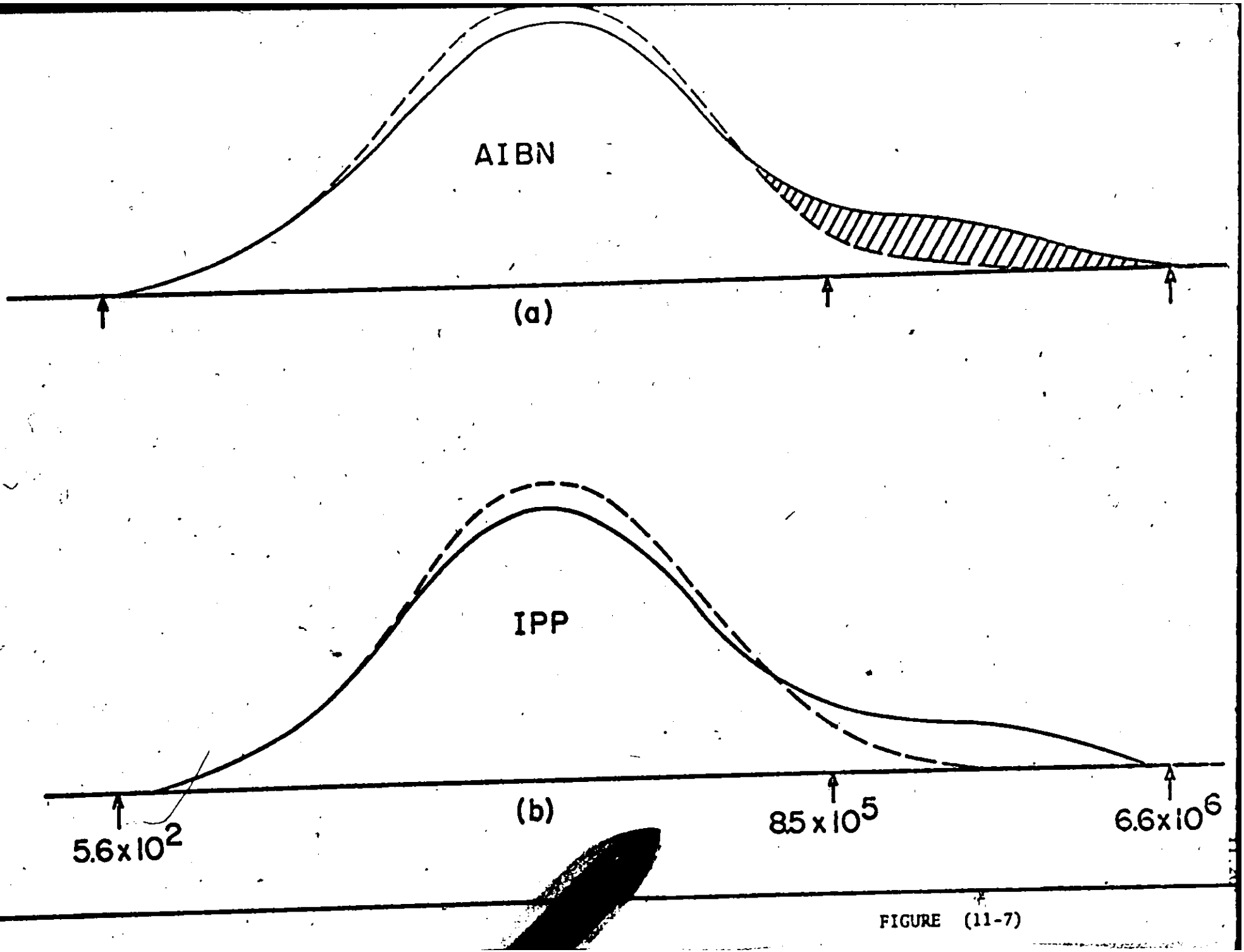

FIGURE (11-7)

11.4.4 Use of GPC to Measure Tacticity in the Temperature Range 30° - 70°C

It is believed that the aggregates found in PVC are made of relatively stable supermolecular structures linked together by crystalline bonds[25]. It is the syndiotactic placement that is responsible for the formation of these crystallites[14], accordingly as the polymerization temperature decreases, the fraction of syndiotactic placements increases[19] giving rise to higher content of crystallites and therefore more aggregates. This explains the appearance of a second peak at the high molecular weight end in GPC chromatograms for PVC samples prepared at relatively low temperatures. It was noticed in figure (11-6) that as the polymerization temperature increases, the second peak gradually decreases until it is almost absent at 70°C, this is in agreement with the above discussion.

The hatched area in figure (11-7a), represents the sample content of aggregates, as it is the area difference before and after heating at the high molecular weight end. This area, then, could be a measure of the syndiotactic fraction in the sample. If we define the quantity A as the fraction of the hatched area to the total chromatogram area, then we can plot an Arrhenius plot for

$$\ln \frac{1 - A}{A} \quad \text{vs.} \quad \frac{1}{T}$$

similar to that of tacticity data.

The measured values of A at different temperatures are shown in table (11-3) and the Arrhenius plot for group 1 samples in figure (11-8).

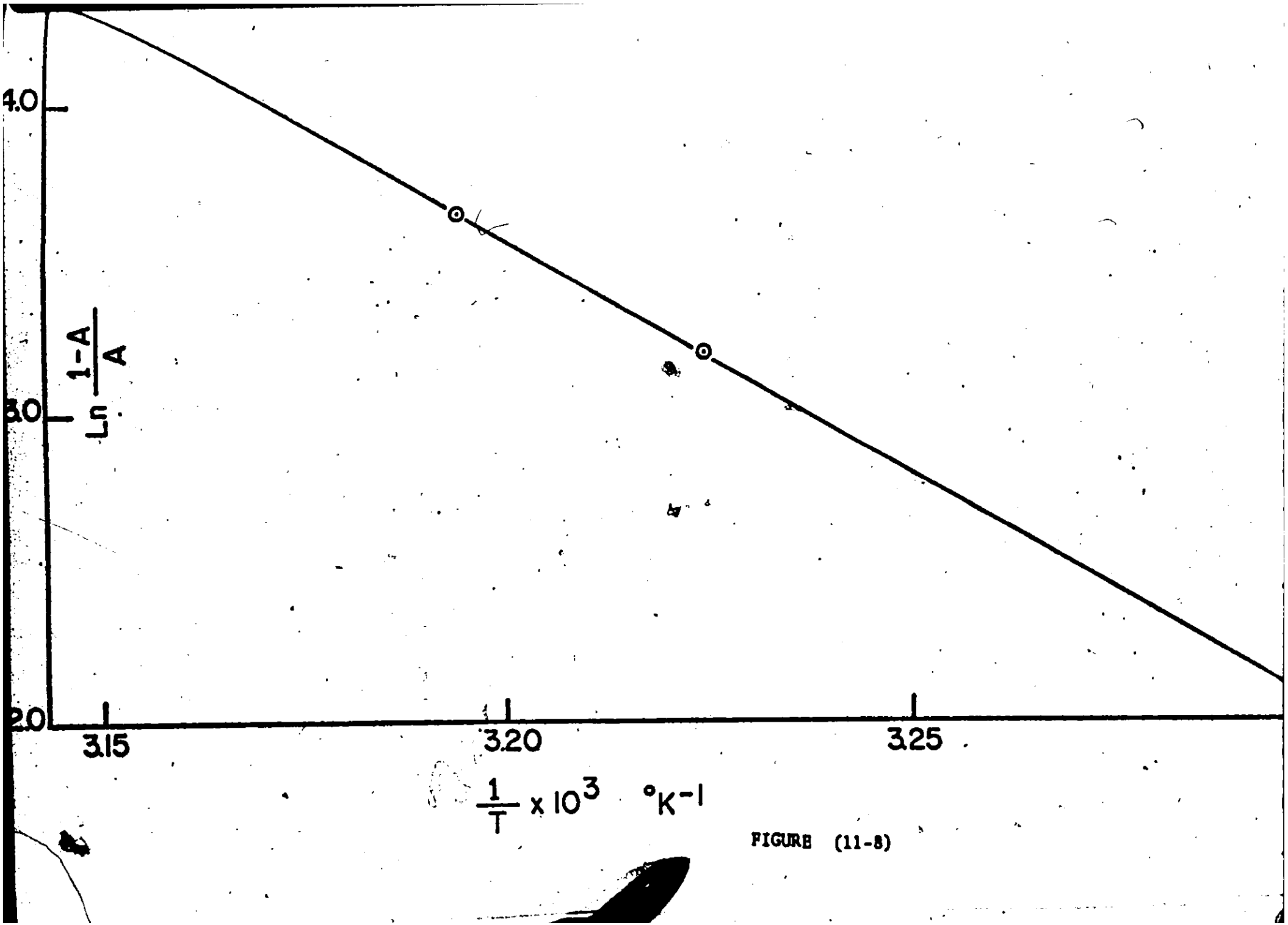

FIGURE (11-8)

The straight line of figure (11-8) has a slope of -1.48×10^4, while the slope of the tacticity data line, figure (11-4), has a value of -3.47×10^2. This big difference shows that A is much more sensitive to temperature than S. If the linear relations between $\ln \frac{1 - A}{A}$ and $\ln \frac{1 - S}{S}$ with $\frac{1}{T}$ are represented as follows:

$$\ln \frac{1 - S}{S} = a + \frac{b}{T}$$

$$\ln \frac{1 - A}{A} = c + \frac{d}{T}$$

then these two equations would give:

$$\left(\frac{1 - A}{A}\right) = k \left(\frac{1 - S}{S}\right)^h \qquad (11\text{-}15)$$

where

$$h = \frac{d}{b}$$

and

$$k = \exp(c - h.a)$$

A plot of this equation on a log-log scale is shown in figure (11-9). The slope $h = 42.7$ and the intercept $(c - h.a) = 15.2$ Such relationship between A and S would enable one to use the GPC to measure A and then tacticity data could be easily obtained.

11.4.5 Aggregate Content in Group (2) samples

With reference to figure (11-5); for group (2) samples the fraction of polymer that remained in suspension was measured in two ways, first by filtering, washing, drying and then weighing this material and second by injecting the solution (the filtrate) in GPC and calculating the area of the chromatogram which is proportional to the concentration of this

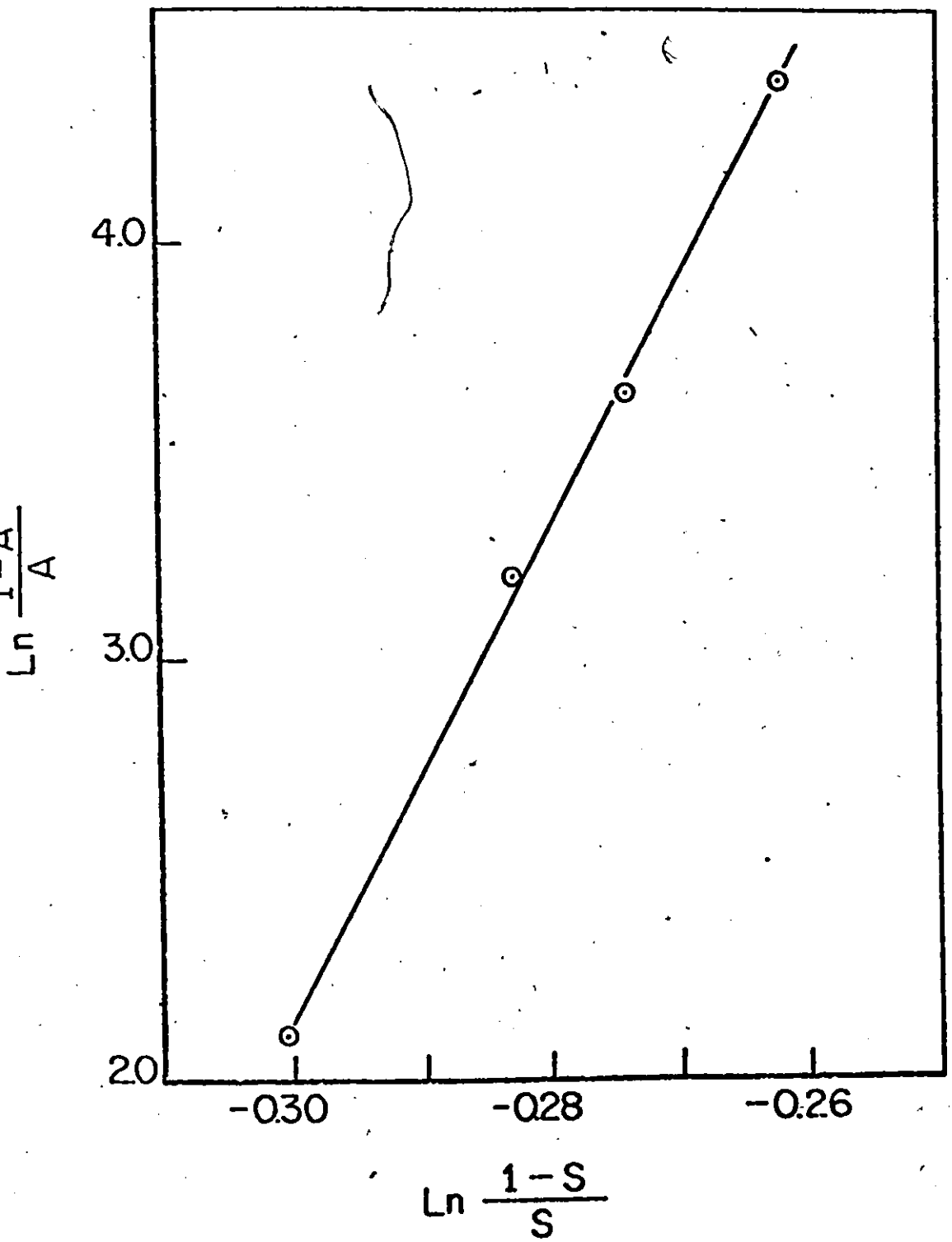

FIGURE (11-9)

solution and then comparing this area to the area corresponding to standard PVC solutions of 0.2 wt.% concentration. Results of the two methods agreed within experimental error. This first injection is called injection 1 as shown in figure (11-5). Following this, the undissolved polymer was mixed with calculated amounts of THF to make 0.2 wt.% solution, this time dissolution was done by heating the mixture at 100°C for 30 minutes under vacuum. This was found to be sufficient to dissolve the polymer. It should be mentioned here that the word dissolution does not imply making a true solution on the molecular scale. All it means is producing a clear solution free of suspended matters. This solution was then injected in GPC and this was called injection 4. The solubility behaviour of this fraction indicated that it was made of PVC aggregates due to molecular association of single molecules. This concept was proven to be true when these solutions (injection 4) were heated under vacuum for 2 hours at 200°C and then reinjected into the GPC (injection 5), this resulted in a different chromatogram shifted to the lower molecular weight side. Further heating did not result in further change. Heating at 150°C for 2 hours did not cause disintegration of the aggregates. This was also observed by other workers[9].

Going back to the first solutions (injection 1) knowing the concentrations of these solutions, calculated amounts of THF were evaporated to adjust the concentration to 0.2 wt.% (for easy comparison of areas). Injections of these solutions were called injections 2. As was done for group 1 samples, these solutions were heated to disintegrate aggregates. Injections after heat treatment were called injection 3. It

is worth mentioning here that heating of PVC solutions was performed in glass ampoules 10 m.m. O.D. and 8 m.m I.D. under vacuum. No degradation products (HCℓ or green coloration) was noticed upon heating.

GPC results are given in figure (11-10) for the -50°C PVC. The arrows on the base line indicate the molecular weight based on the molecular weight calibration curve of single PVC molecules. It is noticed that injections 2 and 3 are identical. This indicates that all of the aggregates were in suspension and were filtered from the solution of single molecules at room temperature. PVC polymerized at -50°C contains aggregates which do not dissolve in THF at room temperature. Comparison of injections 4 and 5 shows that the aggregates disintegrate on heating at 200°C. The distribution of injection 5 indicates that these aggregates are made preferentially of the longer molecules of the original polymer.

Figure (11-11) shows GPC results for the -30°C PVC. The size distribution of the aggregates and the molecular weight distribution of the single PVC molecules derived therefrom for the -50°C and -30°C PVC samples are identical. The wt.% aggregates at -50°C is larger, however. In figure (11-12), GPC results for the -10°C PVC show a different type of behaviour. Injections 2 and 3 are not the same indicating that some of the aggregates in this polymer dissolve (but not disintegrate) at room temperature. Actually these soluble aggregates disintegrated readily on heating at 100°C for 10 minutes; continuous heating at 200°C did not introduce further disintegration. The hatched area in figure (11-12) is a measure of the amount of these aggregates. However, some of the

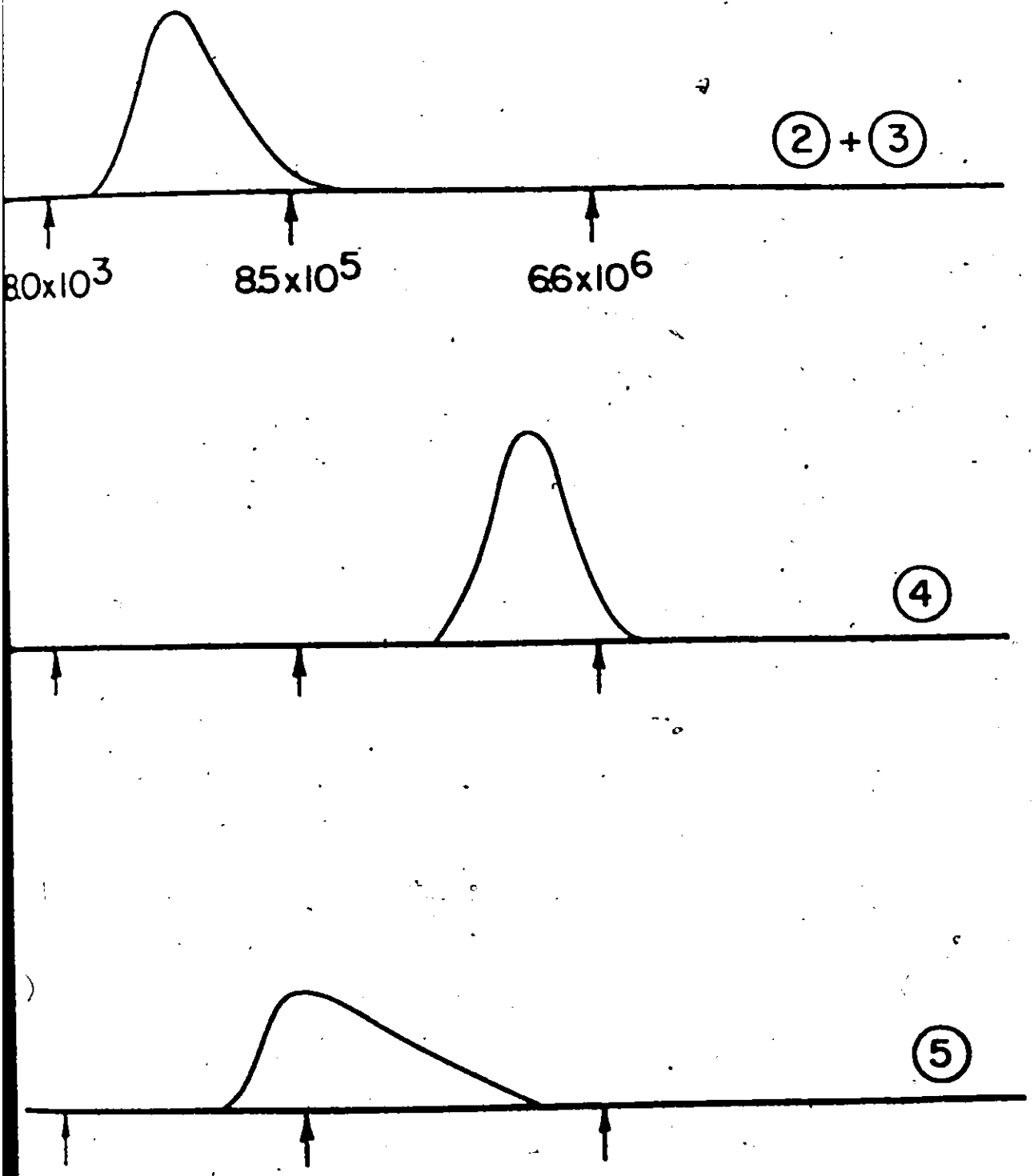

FIGURE (11-10)

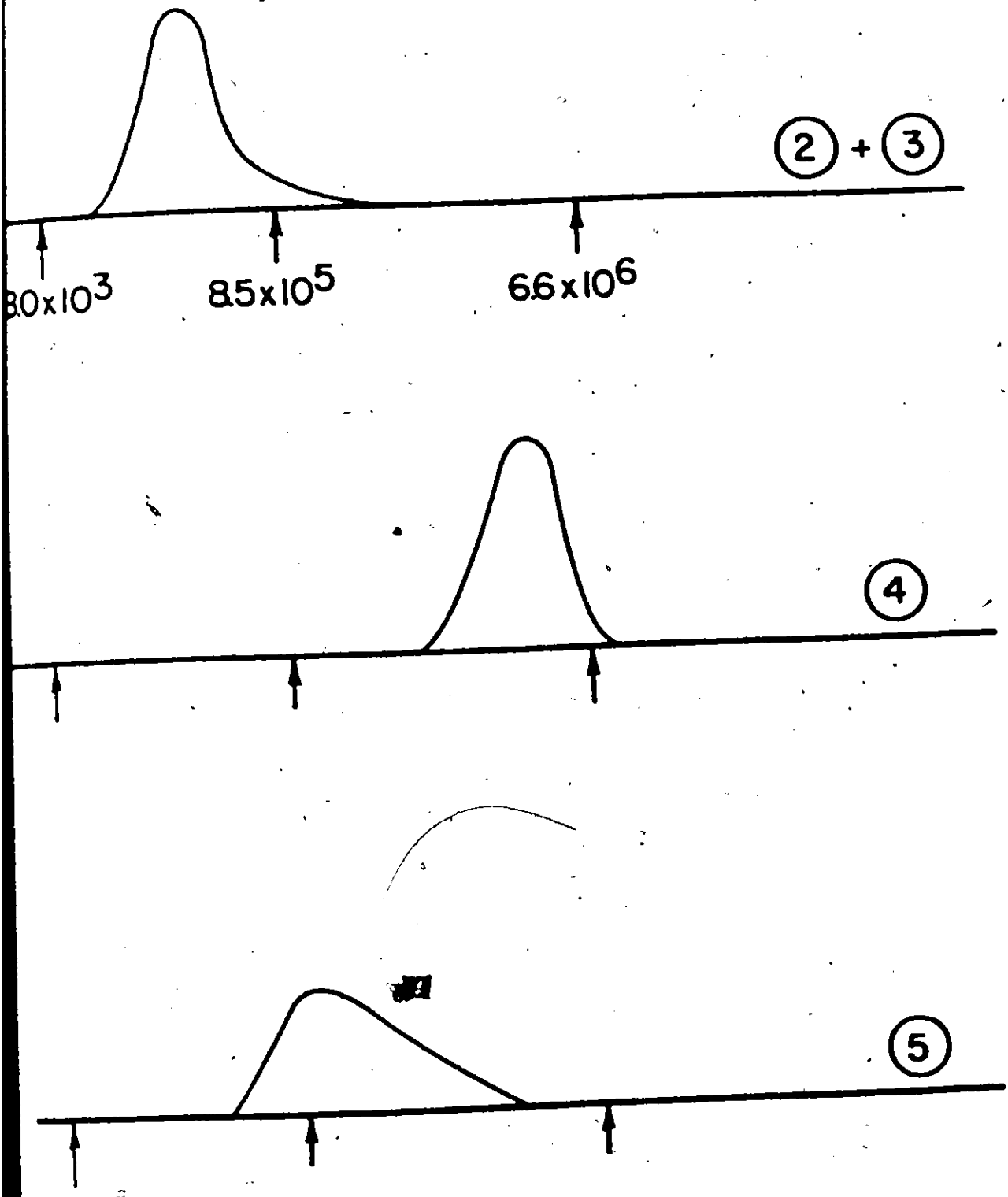

FIGURE (11-11)

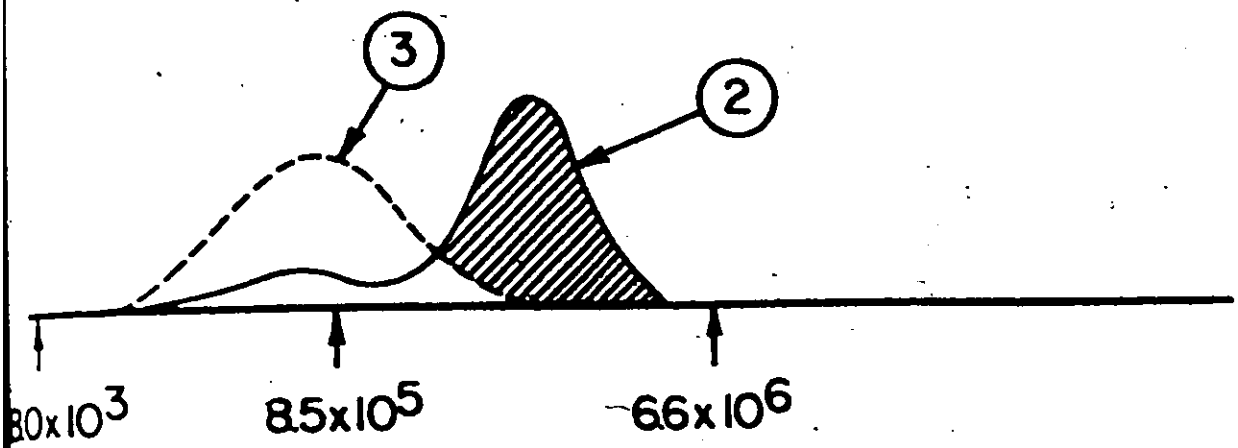

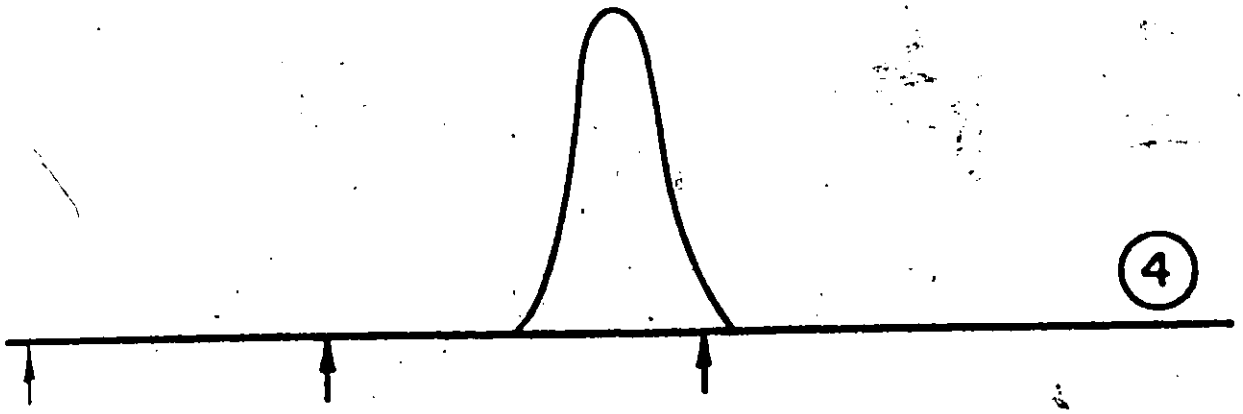

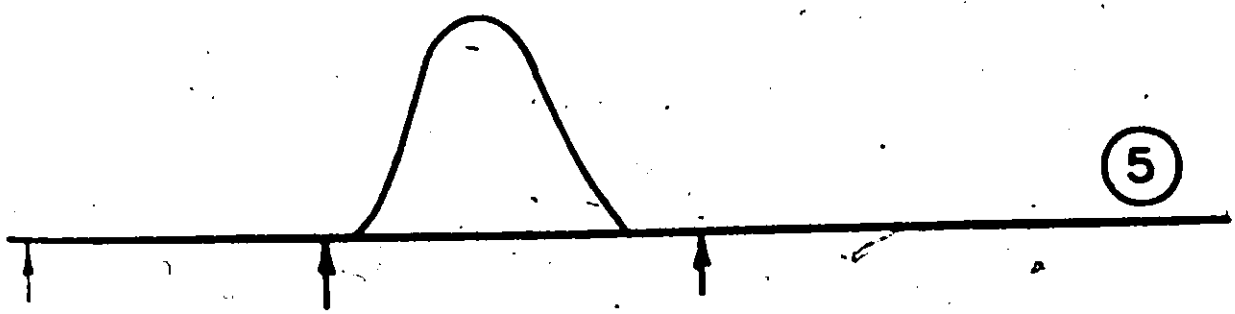

FIGURE (11-12)

aggregates in the -10°C PVC did not dissolve at room temperature and they showed similar behaviour to the aggregates in the -30°C and -50°C PVC. For group 1 samples it was noticed that aggregates present in PVC (polymerized at 30° - 70°C) dissolved completely at room temperatures giving clear solutions.

From the above observations it appears that there are at least two kinds of aggregates formed in PVC. At very low polymerization temperatures the aggregates are characterized by being insoluble in THF at room temperature, very stable towards heating, severe heating is needed to disintegrate them into single molecules and these aggregates are generally of large size, about 4300 Å in diameter (see appendices 11-2 and 11-3) and are made up of the longer molecules of the original polymer. Accordingly we shall call this kind a strong aggregate.

As polymerization temperature increases another kind of aggregate - weak aggregate - starts to form. This kind dissolves readily in THF at room temperature. It disintegrates into single molecules by heating at lower temperatures. These aggregates are smaller in size, about 2500 Å in diameter (see appendices 11-2 and 11-3) and they are made up of molecules of different molecular weights covering essentially the whole distribution of the original polymer.

The classification of the aggregates into two classes is arbitrary and depends on the heat treatment. A more reasonable picture is that PVC molecules come together as soon as they are produced and they form a whole spectrum of aggregates having different stability towards heat.

The application of a certain heat treatment enables us to classify the aggregates with respect to the severity of this particular heat treatment.

In Table (11-3) are listed the percent aggregates measured for the different PVC samples. The second column in the table is the percent of the strong aggregates. Weak aggregates are shown in the third column, and their sum, the total aggregate content is given in the fourth column.

The fractional total aggregate content (A) is plotted in an Arrhenius plot in figure (11-13). This figure shows an interesting feature. At higher polymerization temperatures a straight line is approached with a slope of -1.48×10^4 indicating that the amount of weak aggregates is very sensitive to polymerization temperature. At lower temperatures a second straight line is approached with a slope of -9.3×10^2 indicating that aggregate content increases slowly with falling polymerization temperature.

The extensions of the two lines in figure (11-13) intersect at a temperature of about 12°C. We then prepared a PVC sample at this temperature (using AIBN) and this PVC had only weak aggregates as shown in figure (11-14). The fraction of aggregates at this temperature was measured to be 0.55 and they were all of the weak type. This point was plotted on figure (11-13) and it lies in the transition region of the two types of behaviour.

Data from table (11-3) are plotted in figure (11-15) to show how the wt.% of each type of aggregate and the total aggregate content

TABLE (11-3)

AGGREGATE CONTENT IN PVC MADE AT DIFFERENT TEMPERATURES

Polymerization Temperature °C		Undissolved Polymer % (strong)	Aggregates by GPC % (weak)	Total Aggregate %
70	1	-	-	-
50		-	-	-
45		-	1.2	1.2
40		-	2.5	2.5
35		-	3.9	3.9
30		-	10.9	10.9
-10	2	14.2	64.3	78.5
-30		82.8	-	82.8
-50		87.1	-	87.1

TABLE (11-4)

EFFECT OF POLYMERIZATION TEMPERATURE ON MOLECULAR WEIGHT AVERAGES

Polymerization Temp. °C	$\bar{M}_n \times 10^{-5}$	$\bar{M}_w \times 10^{-5}$
70	0.19	0.44
50	0.51	1.03
30	0.94	1.98
12	2.21	4.37
-10	4.61	9.20
-30	4.70	9.41
-50	4.75	9.47

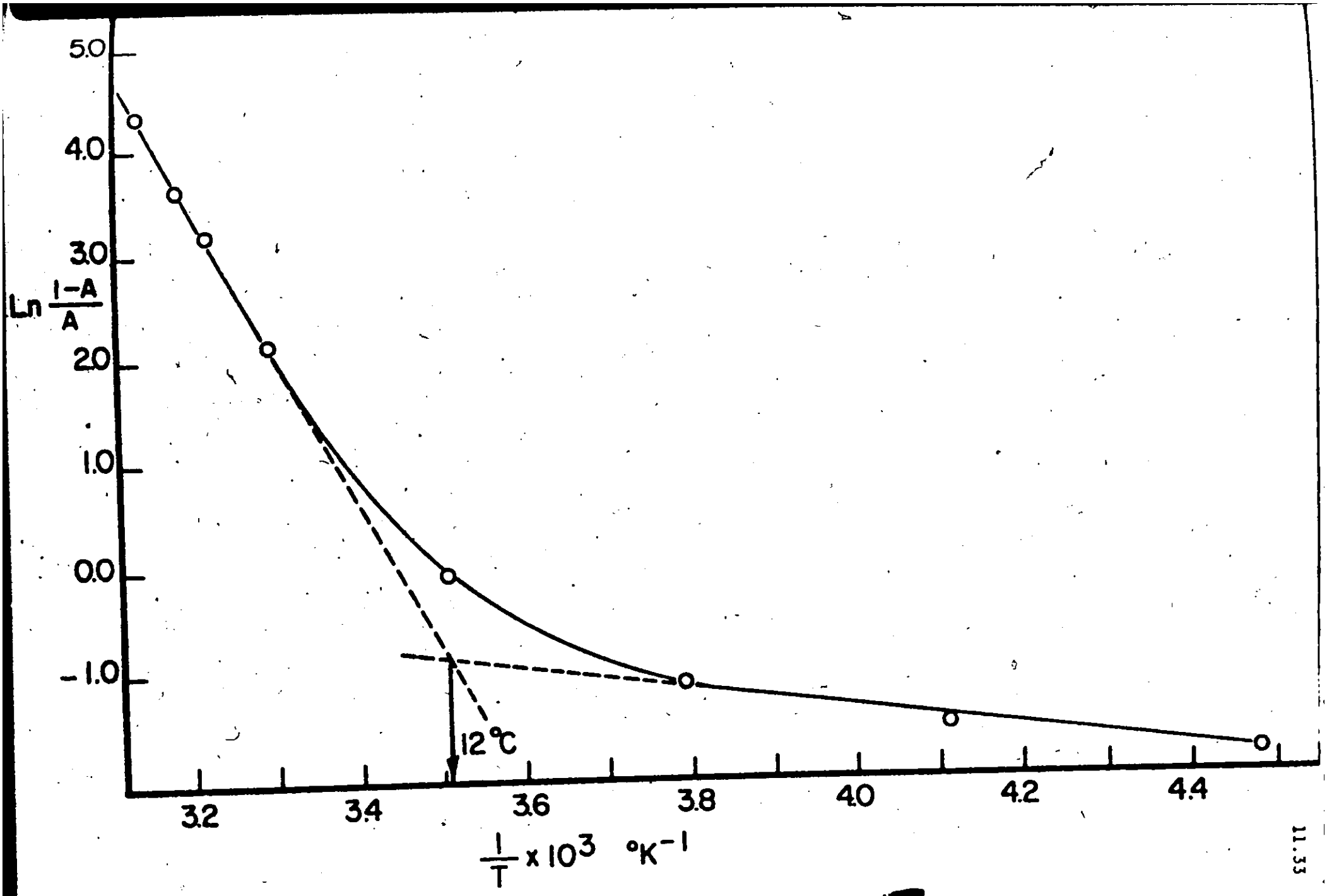

FIGURE (11-13)

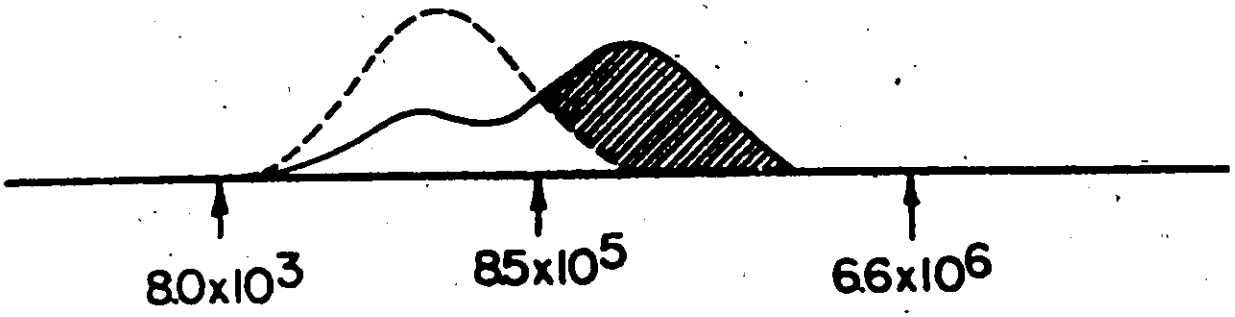

FIGURE (11-14)

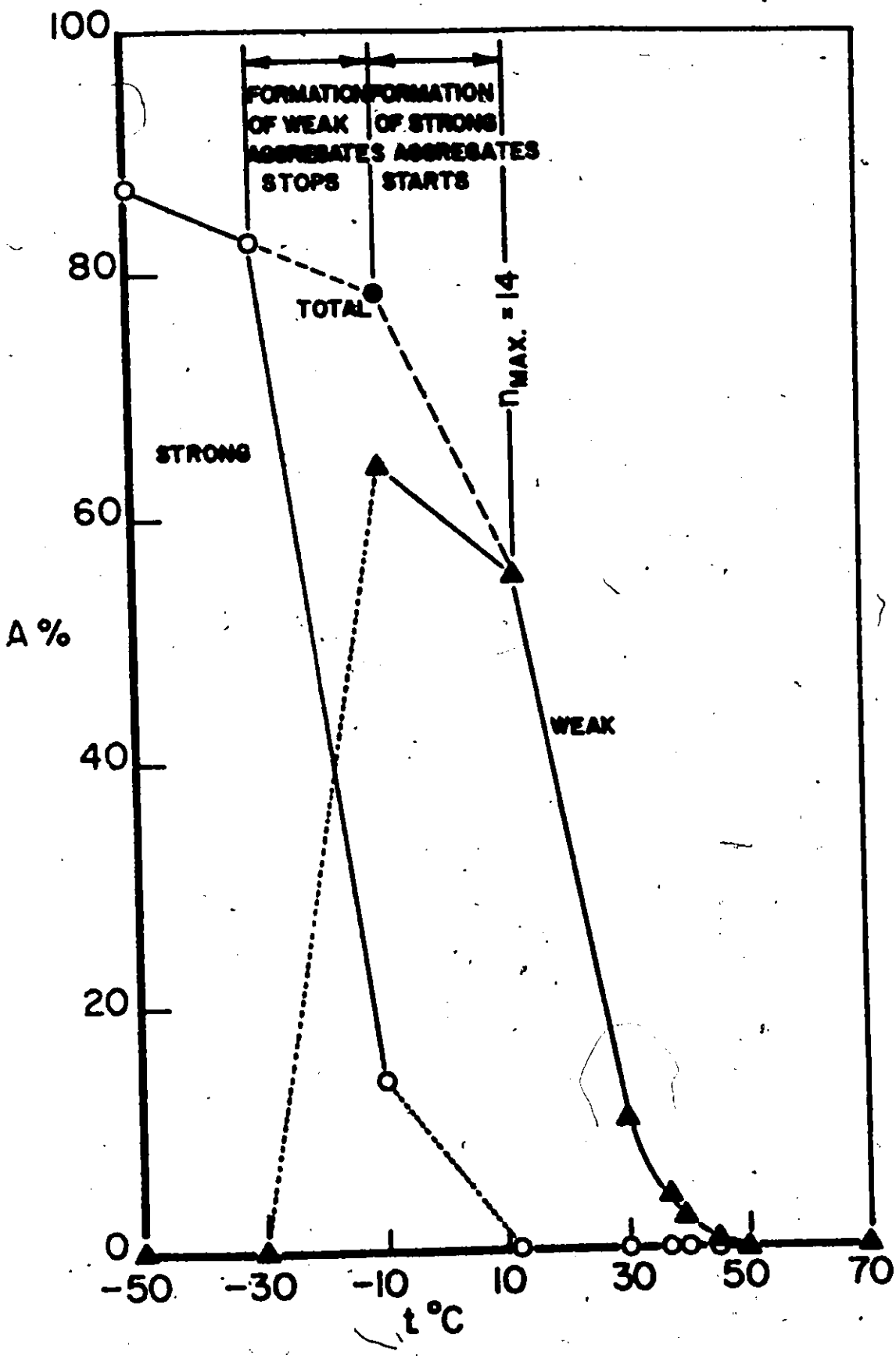
100
80
60
40
20
0
A %
FORMATION OF WEAK AGGREGATES STOPS
FORMATION OF STRONG AGGREGATES STARTS
TOTAL
STRONG
WEAK
$n_{MAX.} = 14$
-50
-30
-10
10
30
50
70
t °C

FIGURE (11-15)

varies with polymerization temperature. One can clearly see that for PVC prepared at very low temperatues (-50 and -30°C) aggregates are insoluble in THF at room temperature.

Dotted lines are used to emphasize the uncertainty in estimation of critical temperatures for the formation of weak and strong aggregates.. It is interesting to speculate on the reasons for the formation of two kinds of aggregates, Undoubtedly, syndiotacticity (sequence length distribution) and molecular weight of PVC play important roles in the formation of aggregates. It is well known that syndiotactic placements in PVC lead to crystallinity and aggregation[14]. The mere increase in the syndiotactic fraction with decreasing polymerization temperature does not fully explain the transition shown in figure (11-13). The syndiotactic sequence length distribution most probably is in part responsible for the formation of strong aggregates. At lower temperatures of polymerization, relatively long syndiotactic sequences are formed. in figure (11-16) the fraction (F_n^S) of syndiotactic sequences of length greater than n is plotted versus sequence length n (n monomer units) for a range of polymerization temperatures. This fraction is given by:

$$F_n^S = S^{n+1}\,(1 + (1-S)n)$$

where S is the syndiotactic fraction. F_n^S was calculated using the measured tacticity data. In figure (11-16) we see that the longer sequences are formed only at very low polymerization temperatures. At 12°C essentially all the sequences are shorter than 14 monomer units and this is shown in figure (11-15) (i.e. about 99.9% of the syndiotactic sequences are less than 14 monomer units long). At -10°C, n_{max} is about 16. This

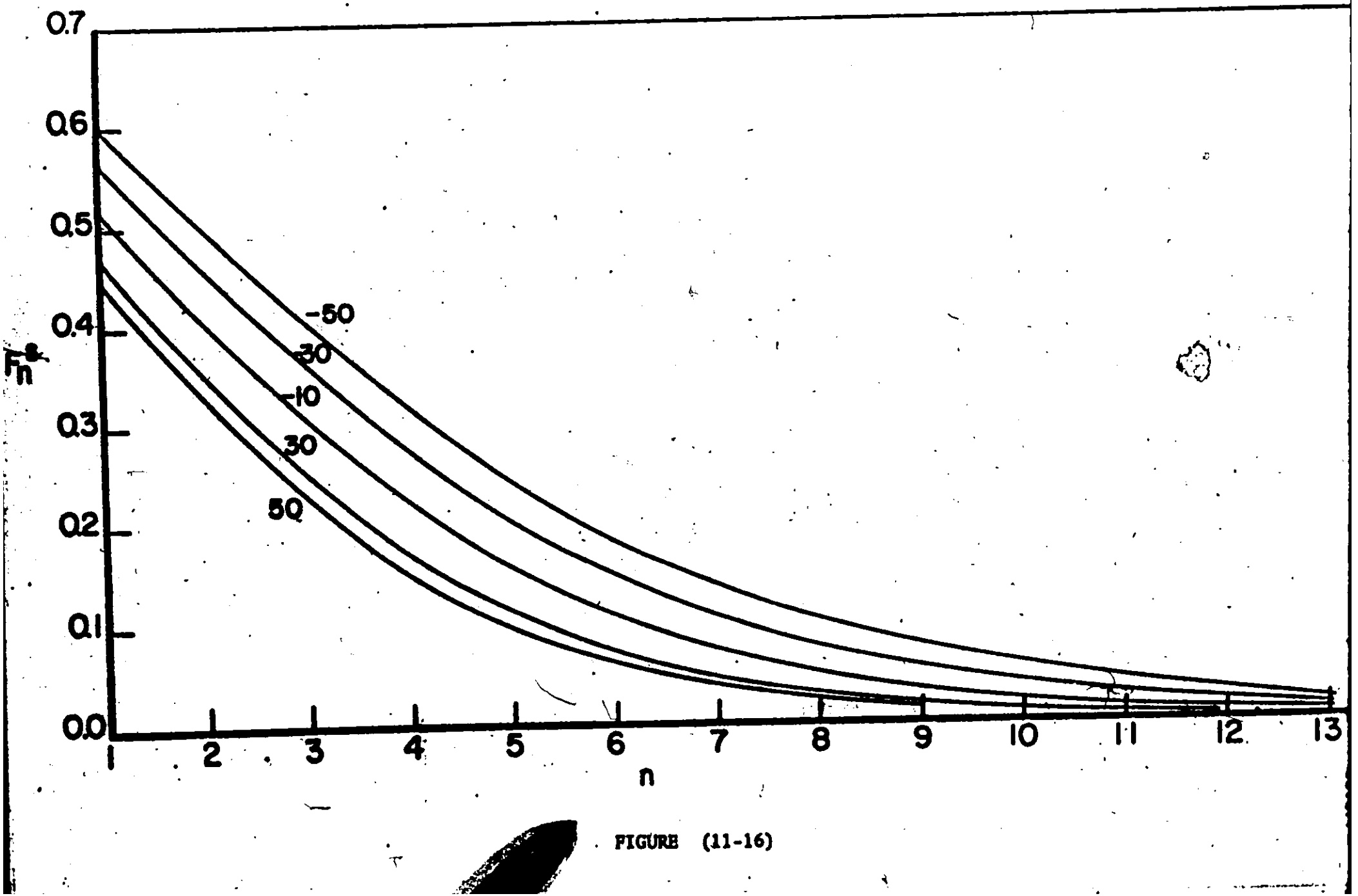

FIGURE (11-16)

suggests that syndiotactic sequence lengths of 14 to 16 monomer units are required for the formation of strong aggregates. The fact that weak aggregates do not form at low temperatures of polymerization leads us to believe that strong aggregate formation involves a nucleation-growth process where the long sequences are nucleation sites. The small sequence lengths participate in the growth process. Greater amount of syndiotacticity and longer sequences coupled with longer polymer chains all produced at lower polymerization temperatures create an environment which is suitable for the formation of strong aggregates. The longer polymer chains will contain more and longer syndiotactic sequences.

An examination of figures (11-13) and (11-15) shows that the formation of weak aggregates is much more temperature dependent that that for strong aggregates. The dependence of A on temperature is similar to that of $\bar{M}_n$ & $\bar{M}_w$ shown in figure (11-17). Typical numerical values for these molecular weight averages are tabulated in table (11-4). The range of conversions for these PVC samples was 70-90%. The polydispersity is constant at 2 over the temperature range, +50°C to -50°C. This is in excellent agreement with the model for the bulk polymerization of vinyl chloride developed in part (I) of this thesis. The molecular weight averages increase as the polymerization temperature falls and reach a plateau at the lower temperatures. This is in disagreement with published data[27,28] where maxima in molecular weight averages were found and with further reduction in polymerization temperature the averages began to fall. Talamini and Vidotto[28] found the maxima to occur at -30°C. They attributed this reduction at yet lower temperatures to be due to the occlusion of radicals in polymer particles with a concomitant reduction

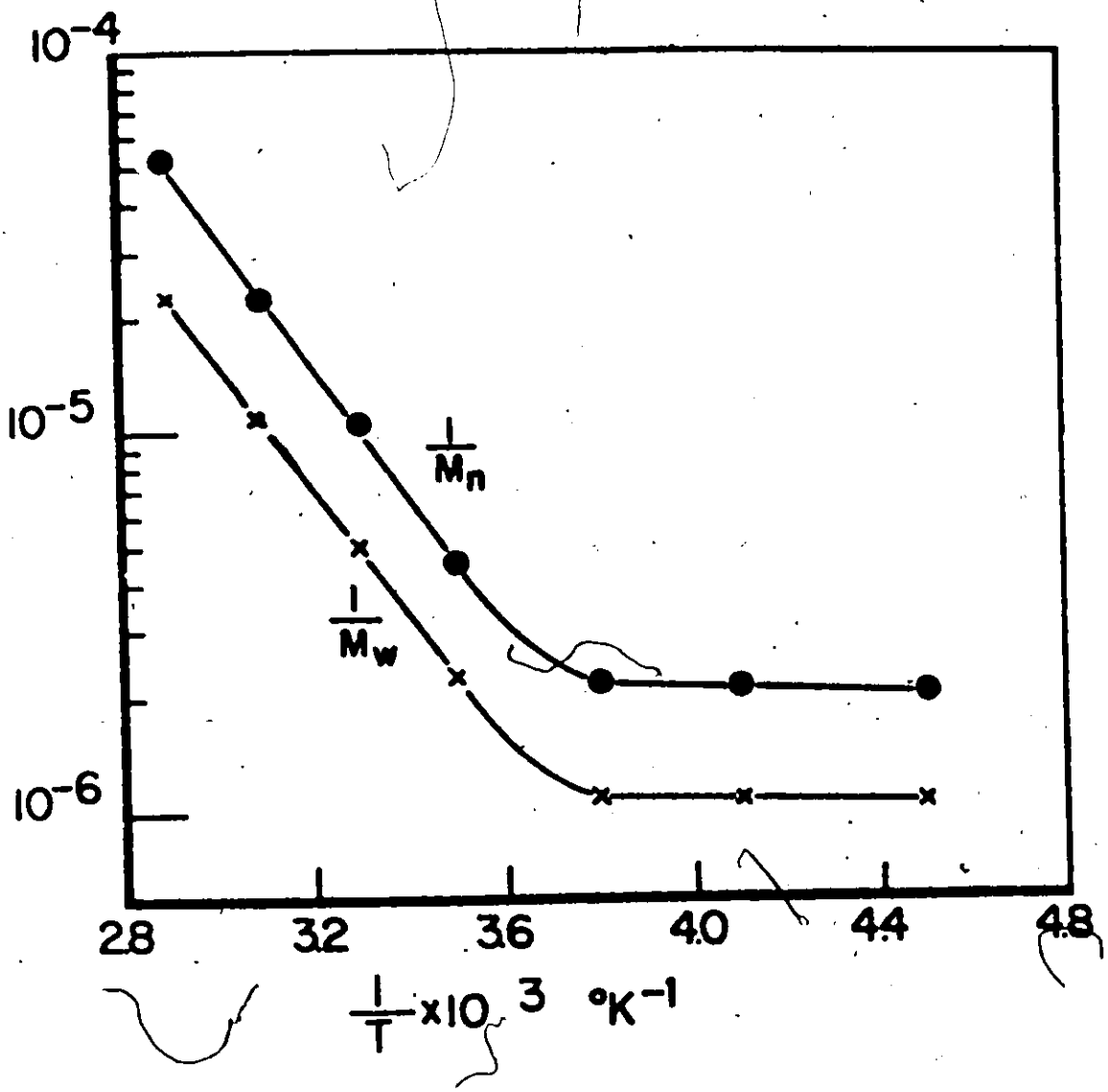
10^{-4}
10^{-5}
10^{-6}
$\frac{1}{M_n}$
$\frac{1}{M_w}$
2.8
3.2
3.6
4.0
4.4
4.8
$\frac{1}{T} \times 10^3$ °K^{-1}

FIGURE (11-17)

in the propagation rate constant. Carenza et.al.[27] found the maxima to occur at -10°C. We suspect that these disagreements are most probably due to the elimination of strong aggregates by these investigators [27,28] before their molecular weight measurements. These aggregates are formed preferentially from longer polymer chains and their elimination by filtration before molecular weight measurement would lead to measured $\bar{M}_n$ and $\bar{M}_w$ that are too small. On the basis of our experience we would recommend the use of our heat treatment procedures before measurement of molecular weight distribution or averages.

11.5 Summary

A novel experimental technique has been developed for the measurement of tacticity in polyvinyl chloride (PVC) using gel permeation chromatography (GPC). This GPC technique is much more sensitive than NMR at temperatures normally employed in the commercial production of PVC and the measurements of tacticity by both instruments correlate extremely well. This new analytical tool should find extensive use in the control of PVC reactors.

Molecular weight distributions and molecular aggregation for polyvinyl chloride (PVC) polymerized in bulk at 70°C to -50°C have been measured using gel permeation chromatography. The aggregate content in PVC polymerized at -50°C was found to be 87 wt.%. These spherical aggregates of mean diameter of 5000 Å are formed preferentially from PVC chains having high molecular weights and long syndiotactic sequence lengths. A temperature of 200°C was used to disintegrate these aggregates into single PVC molecules.

In disagreement with measurements of $\bar{M}_n$ and $\bar{M}_w$ published in the literature, the measured values do not reach a maximum but rather increase continuously with decreasing temperature of polymerization. This disagreement is most probably due to the phenomenon of molecular aggregation in PVC.

The following publications are based on Part (11) of this thesis:

1) Abdel-Alim, A.H., and A.E. Hamielec,
"Molecular Aggregation in Polyvinyl Chloride" - "A Novel Analytical Technique",
J. App. Poly. Sci., 16, 1093 (1972).

2) Abdel-Alim, A.H., and A.E. Hamielec,
"Molecular Aggregation in Polyvinyl Chloride" - Part II.
J. App. Poly. Sci. (in press).

3) Abdel-Alim, A.H., and A.E. Hamielec,
"Activation Energy and Entropy Change for tactic placements in PVC",
J. Poly. Sci. Part A-1 (in press)

11.6 Recommendations

1. It is recommended that the heat treatment procedures developed here be used before measurement of molecular weight distribution or averages of PVC. Inadequate disintegration of the aggregates leads to measurements that are highly in error.

2. The effect of different initiators on the stability of the aggregates should be further investigated. Some experimental data obtained in the present work suggests that different initiators may result in different polymer behaviour, a very interesting possibility for free radical polymerization.

11.7 Nomenclature

A	fraction of the total GPC chromatogram area due to aggregates, i.e. fraction of hatched area in figure (11-17a).
a,b,c,d,h, and K	constants
D	diameter of spherical aggregate in Å
f(V)	GPC calibration curve, V is retention volume
I	isotacticity (diads)
S	syndiotacticity (diads)
i	isotacticity (triads)
s	syndiotacticity (triads)
H	heterotacticity (triads)
ΔF^*	activation free energy change
ΔH^*	activation enthlapy change
ΔS^*	activation entropy change
R	gas constant
T	absolute temperature °K
k_i	propagation rate constant for isotactic placement
k_s	propagation rate constant for syndiotactic placement
p^s_n	probability of having a syndiotactic sequence of n monomer units.

$\bar{n}_s$	the average length of a syndiotactic sequence.
F_n^s	fraction of syndiotactic sequences of length greater than n monomer units
f_n^s	fraction of total polymer with syndiotactic sequence of n monomer units
$\bar{M}_n$	number average molecular weight
$\bar{M}_w$	weight average molecular weight
M	molecular weight
$\bar{r}^2$	mean square end-to-end distance
[η]	intrinsic viscosity
Φ	universal Flory's constant

Subscripts

i	refers to isotactic placement
s	refers to syndiotactic placement
p	refers to placement

11.8 References

1. Doty, P., H. Wagner, and S. Singer, J. Phys. Chem., 51, 32 (1947).

2. Kratochvil, P., V. Petrus, P. Munk, M. Bohdanecky, and K. Solc, J. Poly. Sci., C16, 1257 (1967).

3. Kratochvil, P., Collection Czech. Chem. Commun., 30, 683 (1965).

4. Kratochvil, P., Collection Czech, Chem. Commun., 29, 2290 (1964).

5. Hlousek, M., and J. Lanikova, J. Poly. Sci., C16, 935 (1967).

6. Hengstenberg, J.,and E. Schuch, Makromol. Chem., 74, 55 (1964).

7. Mencik, Z., and J. Lanikova, Collection Czech. Chem. Commun., 21, 257 (1956).

8. Gautron, R., and C. Wippler, J. Chim. Phys., 58, 754 (1961).

9. Crugnola, A., and F. Danusso, J. Poly. Sci., B6, 535 (1968).

10. Lyngaae-Jorgensen, J., J. Poly. Sci., C, 39 (1971).

11. Rudin, A., and I. Benschop-Hendrychova, J. Appl. Poly. Sci., 15, 2881 (1971).

12. Abdel-Alim, A.H., and A.E. Hamielec, J. Appl. Poly. Sci., 16, 1093 (1972).

13. Lyngaae-Jorgensen, J., Ph.D Thesis, The Tech. Univ. of Denmark, 1970.

14. Kockott, D., and Z. Kolloid, 198, 17 (1964).

15. Odian, G.,
"Principles of Polymerization",
McGraw-Hill, (1970).

16. Natta, G.,
J. Poly. Sci., 16, 143 (1955).

17. Bovey, F.A., and G.V.D. Tiers,
ibid., 44, 173 (1960).

18. Bovey, F.A.,
Accounts of Chem. Research, 1, (6), 175 (1968).

19. Cavalli, L., G.C. Borsini, G. Carrapo, and G. Confalonieri,
J. Poly. Sci., Part A-1, 8, 801 (1970).

20. Fordham, J.W.,
J. Poly. Sci., 30, 321 (1959).

21. Natta, G., I. Bassi, and P. Corradini,
Makromol. Chem., 18 - 19, 455 (1956).

22. Zeigler, K.,
Angew. Chem., 76, 545 (1964).

23. Fordham, J.W.L., P.H. Burleight, and C.L. Sturm,
J. Poly. Sci., 41, 73 (1959).

24. Bovey, F.A., F.P. Hood, E.W. Anderson, and R.L. Kornegay,
J. Phys. Chim., 71, (Nr. 2), 312 (1967).

25. Kratochvil, P., M. Bohdanecky, K. Solc, M. Kolinsky, M. Ryska,
and D. Lim,
J. Poly. Sci., Paar C, 23, 9 (1968).

26. Lyngaae-Jorgensen, J.,
J. Chrom. Sci., 9, 331 (1971).

27. Carenza, M., G. Palma, and M. Tavan,
IUPAC, Helsinki, July 2-7 (1972).

28. Talamini, G., and G. Vidotto,
Die Makromolekulare Chemie, 50, 129 (1961).

11.9 Appendices

APPENDIX (11-1)

Statistical Estimation of $\Delta(\Delta H_p)^*$ and $\Delta(\Delta S_p)^*$

It was shown in the main text that $\Delta(\Delta H_p)^*$ and $\Delta(\Delta S_p)^*$ may be obtained from the equation:

$$\ln \frac{\Phi - S}{S} = \frac{\Delta(\Delta S_p)^*}{R} - \frac{\Delta(\Delta H_p)^*}{R} \cdot \frac{1}{T} \qquad (11\text{-}10)$$

by linear least square fitting.

However, it is better to estimate $\Delta(\Delta H_p)^*$ and $\Delta(\Delta S_p)^*$ by non-linear least squares regression from:

$$\frac{1 - S}{S} = \exp\left(\frac{\Delta(\Delta S_p)^*}{R} - \frac{\Delta(\Delta H_p)^*}{RT}\right) \qquad (11\text{-}16)$$

for the following reason:

$$\text{Variance}\left(\ln \frac{1-S}{S}\right) \simeq \left(\frac{\partial}{\partial S} \ln \frac{1-S}{S}\right)^2 \text{variance (S)}$$

$$\therefore \quad \text{var}\left(\ln \frac{1-S}{S}\right) \simeq \frac{\text{var}(S)}{S^2(1-S)^2} \qquad (11\text{-}17)$$

while

$$\text{var}\left(\frac{1-S}{S}\right) = \left[\frac{\partial}{\partial S}\left(\frac{1-S}{S}\right)\right]^2 \text{var (S)}$$

$$= \frac{\text{var}(S)}{S^4} \qquad (11\text{-}18)$$

Since in the present work S is always greater than 0.5; equation (11-18) indicates that $\frac{1-S}{S}$ will have smaller variance than $\ln\left(\frac{1-S}{S}\right)$. The difference may not be very large however since S is always close to 0.5.

Non-linear estimation was carried out by the method described in appendix (I-2). Pure error variance was obtained from the replicates shown in table (11-1)

The estimated values were:

$$\Delta(\Delta S_p)^* = 1.68 \pm 0.13 \quad \text{eu.}$$

$$\Delta(\Delta H_p)^* = 694 \pm 34 \quad \text{cal/mole}$$

Table (11-5) shows the analysis of variance. The pure error sum-of-squares may be obtained directly from replicates of $\frac{1-S}{S}$, or from replicates of S but converting var(S) to var($\frac{1-S}{S}$) by using equation (11-18).

The "F" test shown in table (11-5) indicates the absence of lack of fit at 95% confidence level.

TABLE (11-5)

ANALYSIS OF VARIANCE FOR TACTICITY DATA

Polymerization Temperature °C	Syndiotacticity S	$\frac{1-S}{S}$	$(\frac{1-S}{S})_{fitted}$	Residuals
70.	0.542	0.845	0.840	0.005
70.	0.544	0.838	0.840	-0.002
70.	0.543	0.842	0.840	0.002
70.	0.544	0.838	0.840	-0.002
50.	0.559	0.789	0.788	0.001
45.	0.565	0.770	0.775	-0.005
40.	0.568	0.761	0.762	-0.001
35.	0.570	0.754	0.753	0.001
30.	0.576	0.736	0.734	0.002
-10.	0.615	0.626	0.616	0.010
-30.	0.647	0.546	0.552	-0.006
-50.	0.673	0.486	0.486	0.000
-50.	0.675	0.482	0.486	-0.004
-50.	0.673	0.486	0.486	0.000
-50.	0.672	0.488	0.486	0.002

Source	Sum of Squares (SS)	Degrees of Freedom (ν)	Mean Squares MS=SS/ν	$\frac{(L.O.F)MS}{(P.E.)MS}$	$F_{0.95}(\nu_{L.O.F}, \nu_{P.E.})$
Residuals	236×10^{-6}	13	18.2×10^{-6}		
Pure Error (P.E.)	54.8×10^{-6}	6	9.13×10^{-6}	2.84	4.21
Lack of Fit (L.O.F.)	181.2×10^{-6}	7	25.9×10^{-6}		

APPENDIX (11-2)

Aggregate Size Calculation Based on GPC Measurements

The following calculations enable one to obtain a rough estimate of the aggregate size. If $\overline{r^2}$ is the mean square chain end to end distance, then the hydrodynamic volume is related to the molecular weight, M and intrinsic viscosity $[\eta]$ by the Flory equation:

$$[\eta]M = \Phi(\overline{r^2})^{3/2} \qquad (11\text{-}19)$$

where Φ is the universal Flory's constant = 2.5×10^{23} mole^{-1}. Assuming the aggregate of molecular weight M to be a sphere of diameter D, then,

$$[\eta]M = \Phi \frac{\Pi}{6} D^3 = f(v) \qquad (11\text{-}20)$$

where $[\eta]M = f(v)$ is the universal calibration curve for GPC. We can therefore relate D to retention volume as

$$D = \left(\frac{6f(v)}{\Pi \Phi}\right)^{1/3} \text{Å} \qquad (11\text{-}21)$$

and this modified GPC calibration curve may be used to find the size distribution of the molecular aggregates. It was found that weak and strong aggregates have mass mean sizes of about 2500 Å and 4300 Å, respectively. Kratochvil et.al.[2,3,4] using light scattering techniques also estimated the size of PVC aggregates to be of the order of 2500 Å. These workers most probably experienced weak aggregates in their measurements.

APPENDIX (11-3)

Investigation of Aggregate Geometry by Electron Microscopy

It was of interest to estimate the shape and size of weak and strong aggregates and to compare the latter with those measured by GPC. Micrographs of PVC samples at various stages of preparation (see figure 11-5) were made using scanning and transmission electron microscopes.

Figures (11-18) and (11-19) show micrographs taken with the scanning electron microscope. This particular PVC was polymerized at -50°C. The fraction of the polymer in figures (11-18) and (11-19) is undissolved polymer at room temperature collected on 15 micron filter paper. A lump of this dried PVC was placed in a metal base, coated with carbon and palladium and analyzed with a scanning electron microscope. The micrograph in figure (11-18) indicates that the polymer is made up of agglomerates of about 5 microns in diameter connected together by bridges of PVC to form a 3-dimensional network. These groups of 5 micron agglomerates would understandably not pass through 15 micron filter paper. Figure (11-19) shows an enlarged section of figure (11-18). The little shiny white dimples are probably smaller sized strong aggregates.

Figure (11-20) shows a micrograph of a strong aggregate taken with a transmission electron microscope (dark sphere of about 5000 Å diameter). The smaller spheres are probably smaller strong aggregates. A solution of strong aggregates (-50°C PVC in THF at 100 ppm concentration) were sprayed onto Formvar on copper mesh. After a suitable period for THF evaporation the sample was coated with carbon and palladium.

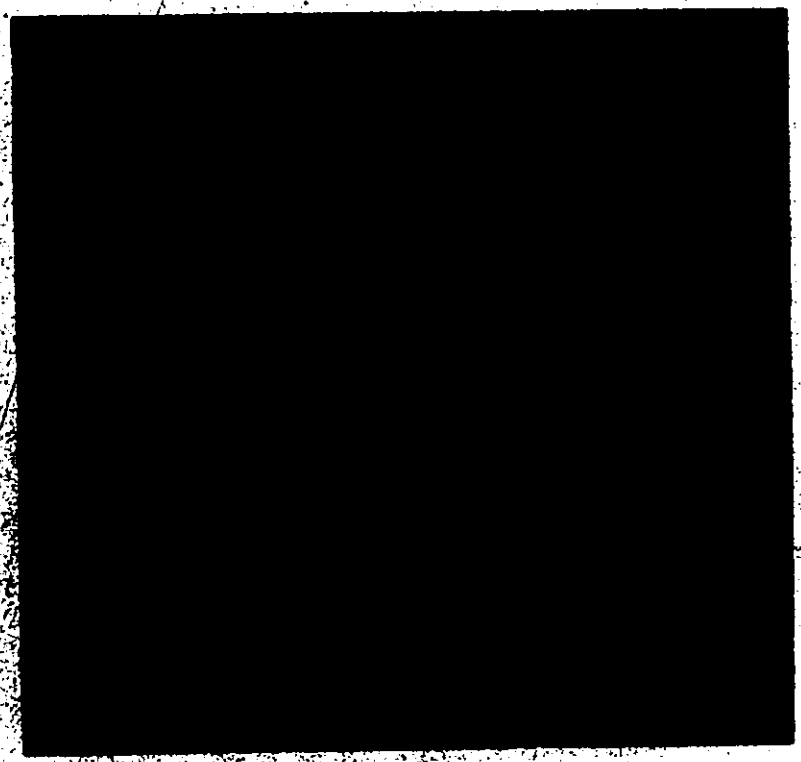

FIGURE (11-19)

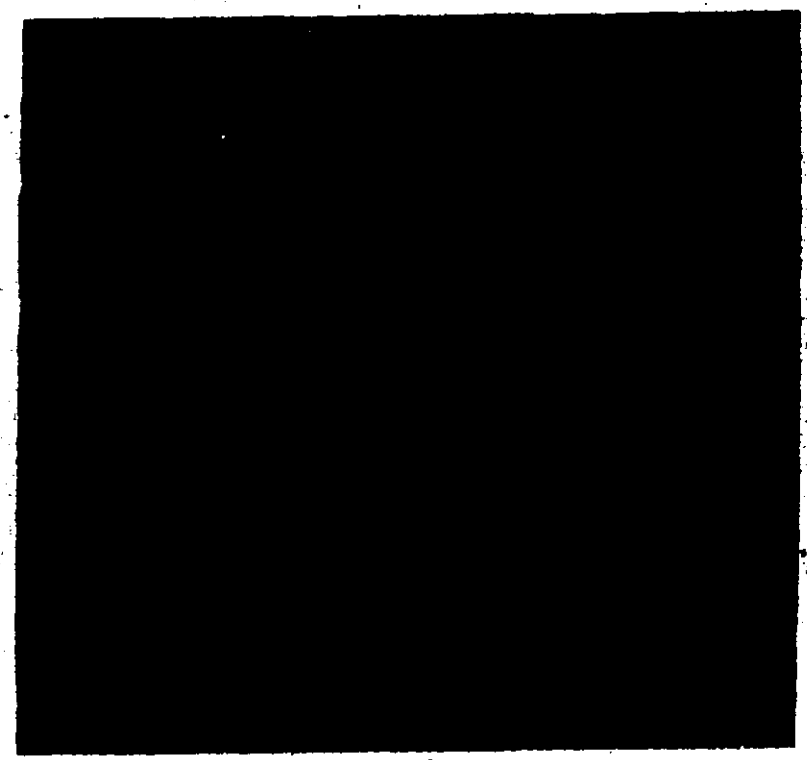

FIGURE (11-18)

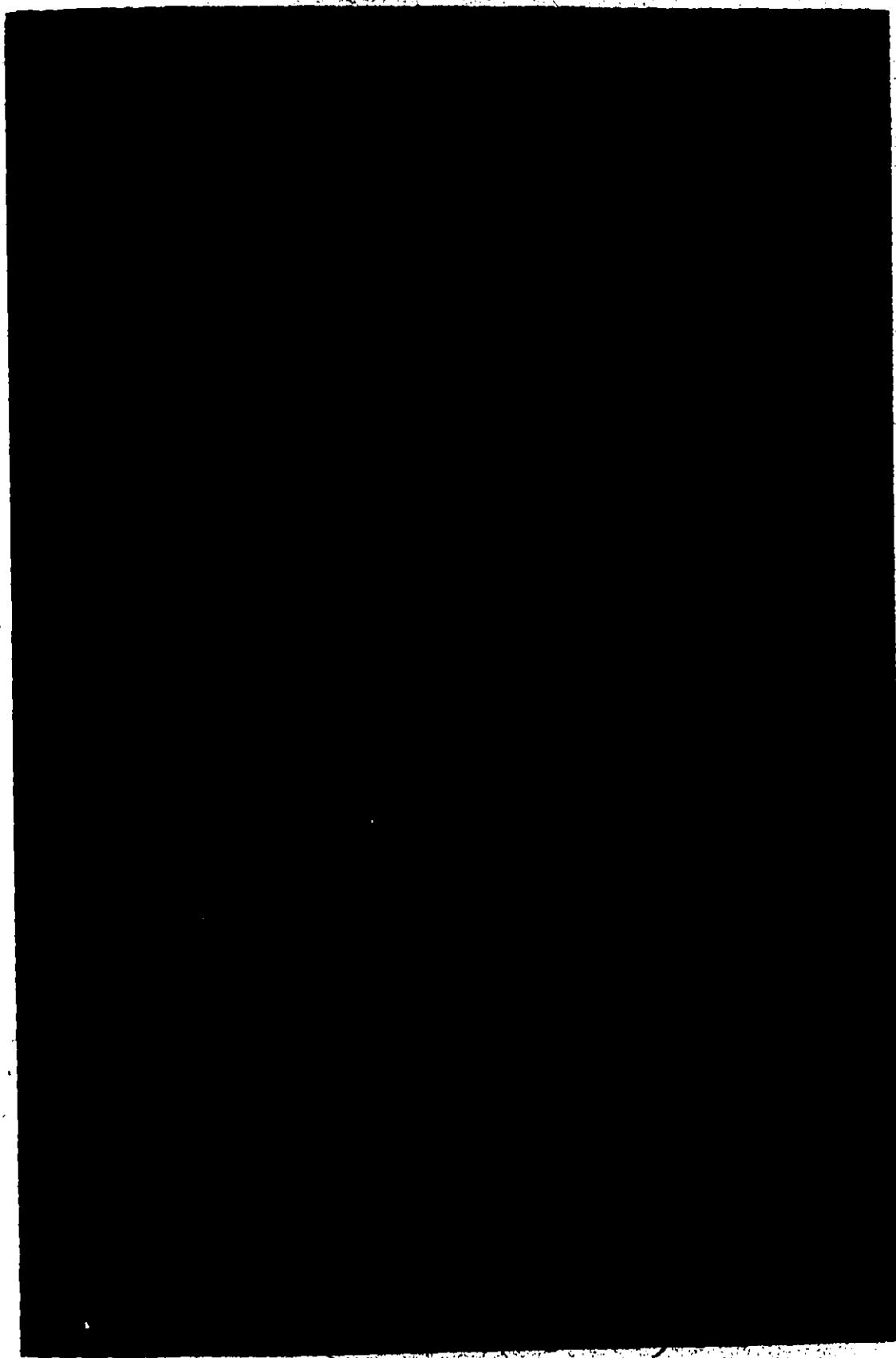

FIGURE (11-20)

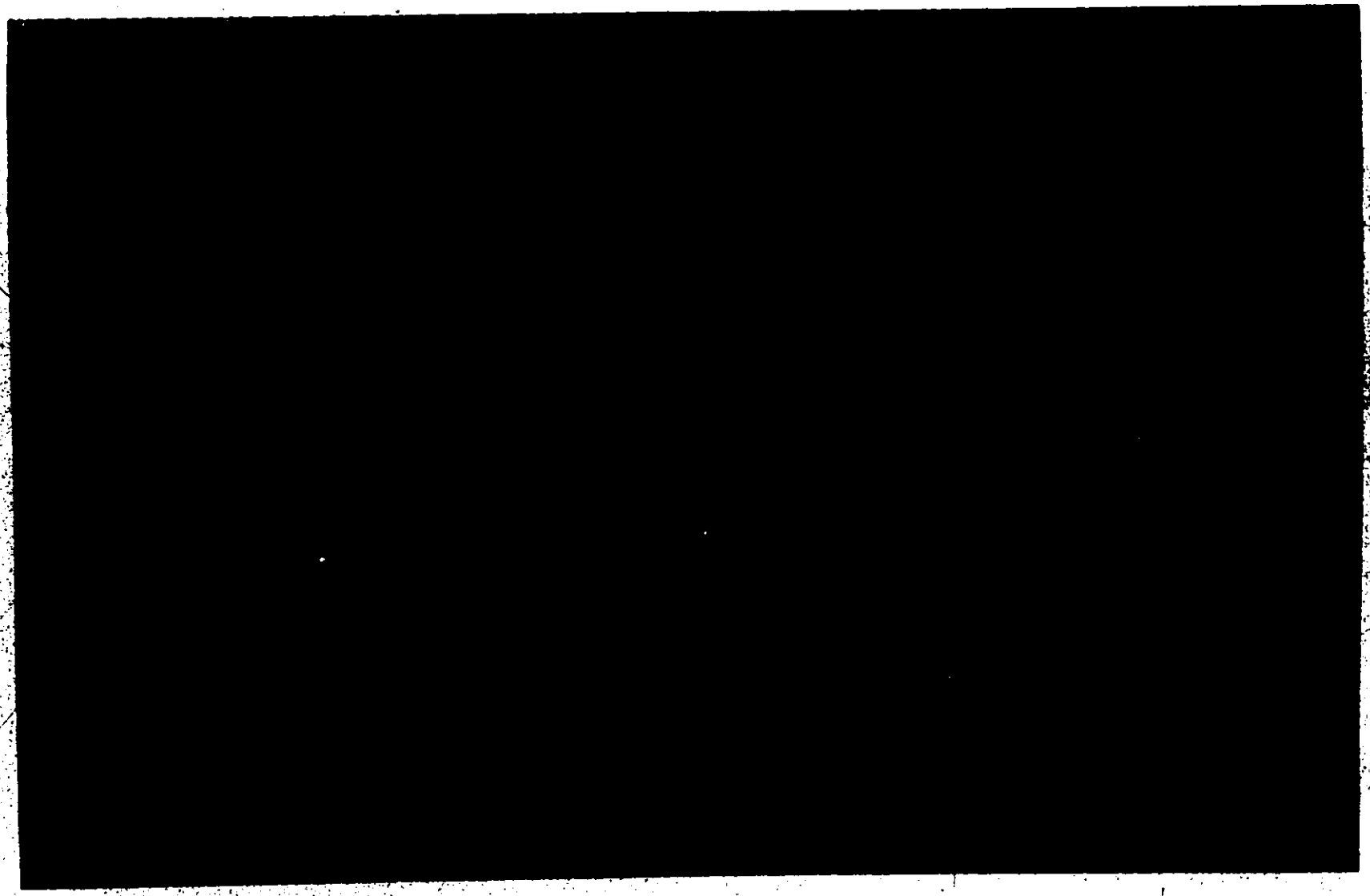

FIGURE (11-21)

Shadow dimensions indicate that the strong aggregate has an approximately spherical shape with a diameter of about 5000 Å. The weight average mean diameter of the strong aggregates estimated from GPC measurements was about 4300 Å.

Figure (11-21) shows a micrograph of weak aggregates taken with a transmission electron microscope. Some of the small particles shown may be individual PVC molecules. The polymerization temperature of the polymer was -10°C. A solution of weak aggregates and individual PVC molecules in THF (100 ppm) was used to prepare samples for electron microscopy. Similar spraying and coating procedures were used as with strong aggregates (figure 11-20). The weight average mean diameter of weak aggregates measured by GPC was about 2500 Å. The larger weak aggregates in figure (11-21) approach this size.

APPENDIX (11-4)

Effect of Using Different Initiators on Aggregate Stability

It was of interest to study the effect of different initiators on the heat stability of the aggregates. Beside AIBN the following initiators were used:

IPP

A : Dicyclohexyl peroxy - dicarbonate

B : Di (sec-butyl) peroxydicarbonate

C : Di (2-Ethylhexyl) Peroxydicarbonate

Polymers were prepared at 93% conversion, 0.27 mole % initiator at 30°C. Solutions of the polymers in THF were injected before and after heating at 100°C for 10 minutes. It was possible to differentiate between two types of behaviours, in figure (11-7a and b), the results for AIBN and IPP are shown; almost complete elimination of the second peak is observed.

For the same heat treatment, however, the other initiators show different behaviour, figure (11-22) indicates that the aggregates formed with these initiators are more stable towards heating, elimination of the second peak was not complete, initiator "B" gives aggregates having a greater stability than the others, since the very high molecular weight end was almost unaffected. Whether the physical properties of the PVC produced by these various initiators is significantly different, as suggested by the GPC measurements is not known. Further work is required to answer this question.

The arrows in figure (11-22) indicate the apparent molecular weight. The figure shows that the aggregates have a molecular weight in the order of one million, a value of 10^8 was reported by Kratochvil[2,3,4] using light scattering.

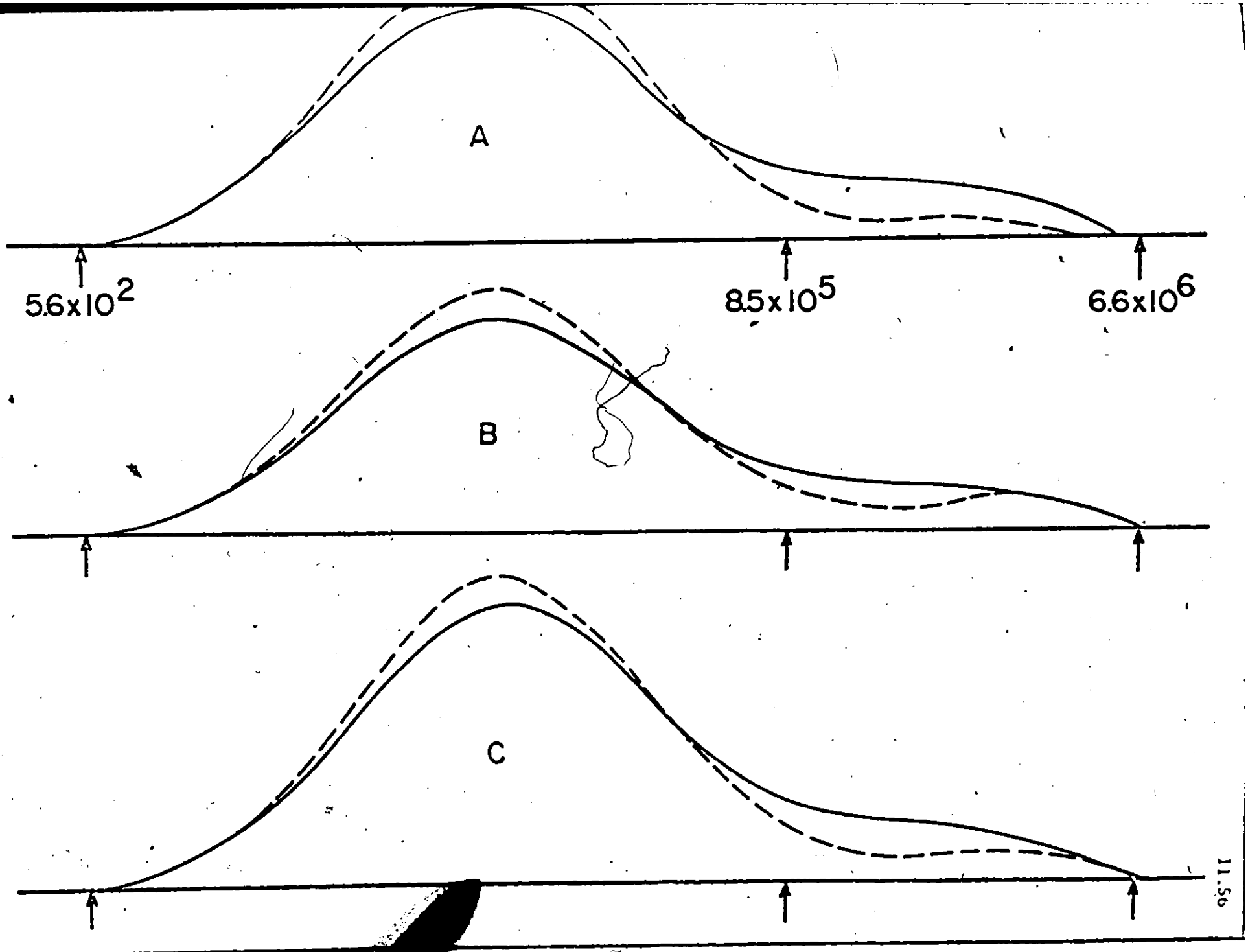

FIGURE (11-22)

PART (111)

HIGH SHEAR VISCOMETRY

111.1 Introduction

The study of polymeric fluids is but a small part of the broader field called rheology. Literally, rheology means the study of flow, but the science of rheology has become much broader than this. It has come to include almost every aspect of the study of the deformation of matter under the influence of imposed stress; it is the study of the internal response of materials to forces.

Between the extremes of simplicity of the newtonian fluid and the hookean solid lie materials of great interest. It is fair to say that commercial interest in synthetic polymeric materials has given the greatest impetus to the rapid growth of the science of rheology.

In the processing of fluids, rheology is an important consideration. The constitutive equation of the fluid (the relationship between shear stress and rate of deformation) is necessary if the flow behaviour is to be described through solution of the equations of motion. Newton's law of viscosity has been found to provide this relationship for some fluids at low shear conditions. However, the situation for many fluids, particularly polymers, and for all materials under very high shear conditions, can be more complicated and is much less well known, despite its industrial importance.

With polymers a basic cause of this situation is the long chain nature of their molecules. Through chain entanglements in concentrated solutions for example, non-Newtonian viscoelastic behaviour can result[1].

Three reasons for the difficulties in elucidating the flow behaviour of polymers at very high shear rates are:

(1) Polymer chains are liable to degrade

(2) The characterization of polymers (MWD, branching and chemical composition) is difficult

(3) Instruments for measuring flow behaviour, particularly at high shear, have design limitations which can cause data obtained using them to be difficult if not impossible to accurately interpret.

Part (111) of this thesis reports on the development of a high shear couette viscometer. The instrument was first tested using Newtonian standards. It was then employed in a study of two areas of significant importance in polymer rheology. These two areas were chosen to utilize the unique advantages of such an instrument. One feature is the ability to produce very high and well defined shear fields, up to about 10^5 - 10^6 sec^{-1}. Another feature is that very small amounts of polymer can be used (amounts which can readily be synthesized isothermally in a small glass ampoule). Accordingly the two chosen topics were:

1) Flow properties of polystyrene solutions under high shear rates.

2) Shear degradation of polyacrylamide (a water soluble polymer).

111.2 Design Considerations[2]

111.2.1 General

The object in designing an instrument to measure flow properties is usually to obtain "simple shear flow". That is, flow in which there is a significant component of velocity in only one direction[3]. Both shear stress and normal stress may be significant as a result of this velocity component. Analysis of simple shear flow is the most practical route to establishing a constitutive equation because the Equations of Motion can be solved in terms of the unknown shear stress and rate of deformation tensor components to give a relationship between these unknowns. However, the results obtained from only one instrument cannot be considered general enough to determine a complete constitutive equation, since this latter relationship must involve all of the components of the rate of deformation tensor.

Simple shear flow is often obtained by either flow through a capillary (poiseuille Flow), flow between a cone and plate, or flow between concentric cylinders (Couette Flow). All of these instrument

types have advantages and disadvantages to a greater or lesser extent depending on their design details. A high shear concentric cylinder instrument was a reasonable choice for the work done here. In particular, it has the potential of giving a uniform, well defined shear field, and data which reflects no undesirable effects (notably temperature gradients) [4]. Furthermore the instrument could be based on a design which was proven practical for extremely high shear rates ($\sim 10^5 sec^{-1}$) by several investigators [4-5]. The original blueprints for the instrument were those of Porter et.al. [7].

The prime design considerations for high shear operation are discussed below.

111.2.2 Fluid Mechanics

The derivation and notation which follow are largely based on that of Middleman [3].

For Couette flow, the velocity vector $\underline{v}$, has one component:

$$\underline{v} = (v_\theta, 0, 0) \tag{111-1}$$

and

$$v_\theta = v_\theta(r) = r\omega(r) \tag{111-2}$$

where r is distance in the radial direction, v_θ is the tangential component of velocity and ω is the angular velocity (radians/sec). Also the rate of

deformation tensor Δ has only the components

$$\Delta_{12} = \Delta_{21} = r \frac{d\omega}{dr} \equiv - \dot{\gamma} \qquad (111\text{-}3)$$

Let

$$f(\tau) \equiv - r \frac{d\omega}{dr} = \dot{\gamma} \qquad (111\text{-}4)$$

The objective in examining a fluid is to determine this relation from the experimental data: Torque and Shear Rate.

If the inner cylinder is driven with angular velocity Ω then the torque Q required to restrain the outer cylinder from moving when the gap is filled with the fluid is

$$Q = \tau_{R_o} 2\pi R_o^2 L = \tau_{R_o} 2\pi \frac{R^2}{S^2} L \qquad (111\text{-}5)$$

where

τ is shear stress

R is the radius of the inner cylinder (the rotor)

R_o is the radius of the hole in the outer cylinder (the stator)

$S = R/R_o$

For this simple shear flow the only informative equation of motion will be the one in the θ-direction (tangential), which reduces to:

$$r^2 \tau = \text{constant}$$

Differentiation with respect to r shows that

$$\frac{d\omega}{dr} = - \frac{2\tau}{r} \frac{d\omega}{d\tau} \qquad (111\text{-}6)$$

Then

$$f(\tau) = \dot{\gamma} = - r \frac{d\omega}{dr} \tag{111-7}$$

$$= 2\tau \frac{d\omega}{d\tau} \tag{111-8}$$

Using the boundary condition that

$$\omega = 0 \text{ at } r = R_o \tag{111-9}$$

and with τ_R the shear stress at the inner cylinder then at $r = R$ by integration of Equation (111-8):

$$\Omega = \frac{1}{2} \int_{\tau_{R_o}}^{\tau_R} \frac{\dot{\gamma}}{\tau} d\tau \tag{111-10}$$

where Ω is the angular velocity of the inner cylinder.

Equation (111-10) is the basic relationship of interest. From

$$\tau_{R_o} R_o^2 = \tau_R R^2 \tag{111-11}$$

$$\frac{d\tau_{R_o}}{d\tau_R} = \left(\frac{R}{R_o}\right)^2 = \frac{\tau_{R_o}}{\tau_R} = S^2 \tag{111-12}$$

and differentiation of (Equation (111-10)) with respect to τ_R a difference equation for $f(\tau_R)$ results. Without assuming any relation for $f(\tau_R)$ the difference equation can be solved so that determination of $\frac{d \ln \Omega}{d \ln \tau_R}$ from the experimental data along with Ω, S, and τ_R yields $f(\tau_R)$.

If a power law relation is assumed

$$\tau = K \dot{\gamma}^n \tag{111-13}$$

$$= K f(\tau)^n \tag{111-14}$$

$$f(\tau) = \frac{1}{K^{\frac{1}{n}}} \tau^{\frac{1}{n}} = a\tau^m \tag{111-15}$$

Substituting $f(\tau)$ into (111-10) and integrating using $\tau_{R_o} = S^2\tau_R$ gives

$$\Omega = \frac{1}{2} a \left(\frac{1-S^{2m}}{m}\right) \tau_R^m \qquad (111\text{-}16)$$

$$f(\tau_R) = \frac{2\,\Omega\, m}{(1-S^{2m})} = a\,\tau_R^m \qquad (111\text{-}17a)$$

Another expression for the shear rate given by Krieger and Elrod[10] was used for the Non-Newtonian runs:

$$\dot{\gamma} = \Omega / \ln S(1 + m \ln S) \qquad (111\text{-}17b)$$

The difference between using equation (111-17a) and equation (111-17b) was insignificant since the polymer solutions were almost power-law fluids.

For a Newtonian Fluid; $m = 1$

$$f(\tau_R) = \dot{\gamma}_R = \frac{2\,\Omega}{(1-S^2)}$$

$$= -\,r\,\frac{d\omega}{dr} \qquad (111\text{-}18)$$

Then, using the relationship between the measured torque and the shear stress on the surface of the outer cylinder:

$$\tau_R = \frac{\tau_{R_o}}{S^2} = \frac{Q\,S^2}{S^2 R^2\, 2\pi L} = \frac{Q}{R^2\, 2\pi L} \qquad (111\text{-}19)$$

Thus, if Newtonian standards of known viscosity are used then the gap can be calculated from

$$\dot{\gamma}_R = \frac{2\,\Omega}{(1-S^2)} = \frac{Q}{\mu R^2\, 2\pi L} \qquad (111\text{-}20)$$

$$S = \sqrt{1 - \frac{2\,\Omega\mu R^2\, 2\pi L}{Q}}$$

Although Reches[9] used a very similar instrument to the one used here, he considered the measured torque to be

$$Q' = \tau_R \, 2 \pi R^2 L \qquad (111\text{-}21)$$

This is actually the torque at which the inner rotor is driven and hence the torque balanced by the fluid on the face of the inner rotor. The measured torque is actually that torque required to hold the outer cylinder stationary and hence the torque exerted by the fluid at the inner face of the outer cylinder and is given by equation 111-5. The result of this was that instead of obtaining $\frac{1}{1-S^2}$ explicitly from Equation (111-20) Reches obtained $\frac{S^2}{1-S^2}$ and even approximated this by $\frac{1}{2}\left(\frac{S}{1-S}\right)$ since S was close to unity. The results of all these discrepancies are insignificant if S is very close to unity.

111.2.3 Viscous heating and temperature rise

There are two important aspects of the results of temperature rise due to viscous dissipation:

(1) the temperature at the film edges, and

(2) the maximum temperature rise through the film

Calculation of the first mentioned can be accomplished reliably using measured values of temperature. The second can only be estimated since it depends on the unknown constitutive equation and thus effort should be made in the instrument design to make it of probable insignificance.

Film Edge Temperature

As Reches[9] shows, from a straightforward heat balance and use

of Fourier's Law the temperature T_f at R_o (the radius of the hole) is calculated from the following equation when T_{R_1} (temperature at the outer radius of the outer cylinder (R_1)) and T_c (temperature at radial distance R_2) have been measured.

$$T_f = T_{R_1} + (T_{R_1} - T_c) \frac{\ln (R_o/R_1)}{\ln (R_1/R_2)} \qquad (111\text{-}22)$$

By having cooling fluid on the inside of the inner cylinder as well as the outside of the outer cylinder and having the heat path to the film the same distance in each case then the assumption that the other edge of the film (at least for a very narrow gap) is at the same temperature, is reasonable. Then, if the maximum temperature rise through the film is negligible, T_f is considered as the isothermal film temperature.

Often the film temperature cannot be precisely set to a constant value at all shear rates because of the inadequacy of the temperature control system. To obtain data all at one temperature, it is then necessary to find some way of interpolating or extrapolating the result from data obtained at one or more temperatures.

Andrade's equation is often assumed for the variation of viscosity with temperature:

$$\eta = A' e^{B'/T} \qquad (111\text{-}23)$$

where η is apparent viscosity, T is absolute temperature and A' and B' are constants.

Runs at different temperatures but the same shear rate provide sufficient data to calculate B'. Then this can be used to calculate the

viscosity at the desired temperature. It was noticed that B' is not a function of shear rate[4] (i.e. parallel lines on a log η - versus - $\frac{1}{T}$ plot). If the visocisty is already known at several other temperatures for the sample (as for Newtonian Standards) a plot of log η versus $\frac{1}{T}$ can be used for interpolation. A universal plot of log η versus the reciprocal of absolute temperature can also be used and is valuable once established for a type of material since it then requires only one experiment to obtain the viscosity at different temperatures if a material is a member of that type[11].

The ratio of the viscosity at a desired temperature T to the viscosity at any temperature at which shear stress was actually measured T_m has been termed a "viscosity factor" and was used to change the shear stress value from T_m to that at the desired temperature, T[9].

Maximum Temperature Rise

Although maximum temperature rise in the film may be estimated, if a simple form for the constitutive equation is assumed, by simultaneous solution of the momentum and energy equations,[3] since these forms are generally uncertain except for Newtonian Standards, probably the best course of action here is to calculate the maximum temperature rise for Newtonian fluids with viscosities similar to the apparent viscosities to be encountered with non-Newtonian materials, and then to make this temperature rise negligible by altering the instrument design or operating conditions.

For Newtonian fluids the maximum temperature rise (ΔT) is given by[2]:

$$\Delta T \propto \frac{\mu v_1^2}{8k} \qquad (111\text{-}24)$$

where

μ is Newtonian viscosity, v_1 is velocity, and k is thermal conductivity of the film.

For very narrow gaps the shear rate may be approximated as follows by the assumption of a linear velocity profile:

$$\dot{\gamma} \approx \frac{v_1}{b} \qquad (111\text{-}25)$$

$$\Delta T = \frac{\mu b^2 \dot{\gamma}^2}{8K} \qquad (111\text{-}26)$$

where

b is film thickness.

As already pointed out by other investigators[4-9], equation (111-26) shows that high shear rates are best obtained by narrower gaps rather than higher RPM.

111.2.4 End Effects

Shear stress on the ends of the rotating cylinder can contribute significantly to the measured torque. In this instrument the film is suspended by surface tension in the annular gap. There is an air liquid interface above and below the film. It should be noted that as with capillary rise, surface tension, not viscosity, is the important parameter in attaining suspension against the force of gravity. This design effectively eliminates end effects.

111.2.5 Concentricity

Concentricity of the inner cylinder in the concentric cylinder viscometer is not often considered as a problem in the rheology literature. In one case[12] it was noted that causing deliberate eccentricity in the particular apparatus resulted in no significant difference in results. The problem is not mentioned in previous publications[4-9] regarding the narrow gap high shear concentric cylinder viscometer (the instrument used in this study). The consistent and considerable discrepancies between annular gaps measured by micrometer and those calculated by running Newtonian standards in the instrument when very narrow gaps are used were always attributed to the fact that micrometer measurement tended to emphasize high spots on the surface.

Roches[9] considered the long secondary drive shaft to be a safety factor (meant to shear if the inner cylinder seized). Although he did point out that this shaft was balanced and periodically checked for alignment, he did not state how. Porter[13] in a seminar at the University of Toronto, emphasized that the drive shaft was long and thin (actually a 1/8 inch O.D., 17 inch long steel drill rod) to provide self centering of the inner cylinder by the action of viscous forces in the gap. In a discussion of the Stormer Viscometer, a popular rheology text[14] mentions that two universal joints are supplied in the rotor shaft to permit self alignment by the action of viscous forces in the narrower portion of the gap but that this sometimes resulted in an undamped pendulum-like motion of the rotor. The only reference quoted by this text on the concentricity problem is the 1939 publication of Inglis[15].

Inglis derived an approximate relation for the effect of simple (two dimensional) eccentricity on the measured torque for a concentric cylinder viscometer containing a Newtonian fluid. Using a simplified Navier Stokes equation for the flow which neglected curvature:

$$\frac{\partial p}{\partial x} = \mu \frac{\partial^2 v_0}{\partial y^2} \qquad (111\text{-}27)$$

where

μ = Newtonian viscosity

v_0 = velocity in the angular direction

p = pressure

x = distance in the angular direction

y = distance in the radial direction

He assumed narrow gap dimensions (compared to the radius of the inner cylinder) and solved for the pressure distribution as a function of angle due to the eccentricity. From this solution he derived the following expression for the viscous torque per unit height on the outer cylinder:

$$\frac{\Theta}{L} = \frac{2 \pi \mu v_1 R^2 (1-c^2)}{b} \qquad (111\text{-}28)$$

where

v_1 = the velocity at the inner cylinder

b = the film thickness with zero eccentricity

c = the eccentricity ratio (distance between cylinder centers ÷ b) = 0 for concentricity

R = radius of the inner cylinder

Qualitatively speaking, the eccentricity makes the gap wider in one portion than another. This results in a net decrease in fluid transport, a decrease in the average velocity of fluid and, since the finite velocity of the moving boundary and the zero velocity of the stationary boundary are fixed, an increase in shear rate near the moving boundary and a decrease near the stationary boundary. Thus shear stress on the stationary boundary is decreased while that on the moving boundary is increased.

Equation (111-28) shows that, as it should, for zero eccentricity it reduces to the expression given by Equation (111-20). However, it is clearly evident that torque measurement at high shear rates (narrow gaps and high velocities) can be severely affected by eccentricity. Since most instruments to date operate at low shear rate, or have wide gaps which cause other more obvious problems (e.g. temperature gradients) and end effects (since the film is then not suspended) it is easy to see why the problem of eccentricity has been given little attention.

A better understanding of the results and causes of eccentricity can be obtained from the Mechanical Engineering literature regarding vibration of rotating shafts[16] and lubrication of journal bearings[17]. A journal bearing may be considered as a horizontal concentric cylinder viscometer used to support a vertical load on the outer cylinder. It has been found that seizing or rough operation of the bearing can occur because of the combination of oil forces, shaft vibration and misalignment. The first mentioned topic is the main concern of lubrication

theory. The problem is dealt with by numerical solutions of the Reynolds Equation (this equation is really a momentum equation phrased in terms relevent to the thin film problem (e.g. film thickness and eccentricity) as well as velocity and pressure)[17]. The pressure distributions obtained (most uncertain for non-Newtonian fluids)[18] indicate that a film force tends to center the inner cylinder for an absolutely zero load[19] situation but that this centering is unstable. This conclusion is by no means certain[20] because of the inherent complexity of the force situation, in particular the interaction of shaft vibration with oil forces. Whirl or whip (usually defined as a self perpetuating, often violent movement of the center of the inner cylinder with respect to the center of the outer cylinder) is often observed to be a problem in bearings at frequencies corresponding to one half shaft speed. The reason for this is unknown. With the concentric cylinder viscometer there is no gravitational load (unlike the usual bearing situation). The load is rotational and originates primarily from unbalancing or presence of a bend in the shaft or misalignment or interaction of the shaft movement with the oil forces. Balancing of such a shaft is still a subject of research as is the whole field of vibration in rotating shafts and lubrication of bearings.

From a polymer rheologist's point of view the state of the art is particularly unsatisfactory, since what progress there has been made towards this problem emphasizes the avoidance of actual bearing failure, or rough running, rather than exact prediction of the location of the inner cylinder center relative to the outer cylinder center. Design of bearings which encourage stable running at the expense of a well defined velocity profile is the main result.

Thus from the above discussion it is evident that eccentricity is complex, critical, and difficult to predict or eliminate for a narrow gap high shear concentric cylinder viscometer. The most practical course is either to measure it or to prove it negligible with respect to the desired torque measurement. The second choice was taken in the present work. Steady torque measurements free of oscillations were obtained by using a semi-flexible drive shaft. Details of the design are given the next section.

111.2.6 Static Friction

"Friction is the resistance to motion which exists when a solid object is moved tangentially with respect to the surface of another which it touches or when an attempt is made to produce such a motion."(21) When movement is induced by a friction force F then the following expression may be written:

$$F = \tau_{av} * A_r \qquad (111\text{-}29)$$

where

τ_{av} = average shear stress over the real area of contact

A_r = real area of contact

Thus the uncertainties of friction are lumped into A_r. The magnitude and variation of A_r is the unknown at which many explanations of friction are aimed. A_r is influenced by many factors: the nature of the materials in contact, the presence of lubricant and the time of application of the force F. It is well known that the F required to start sliding is usually greater than that required to maintain sliding. This has given rise to the simplification that a static friction and a kinetic friction exists.

With viscometers the only value of shear stress desired is that applied to the fluid whose viscosity is to be measured. Friction can add to the measured value of shear stress and therefore must either be made insignificant or measured. The main source of friction in the concentric cylinder viscometer is the contact between the support bearings and the outer cylinder. This can be made negligible by using an air bearing or by working at such high shear stresses that the frictional component is negligible.

Barber et.al.[4] in experiments with the high shear concentric cylinder viscometer, claimed that torques measured while moving the support table in one direction and then in the other, are shearing torque plus, and shearing torque minus, support bearing friction. He mentioned that this cancellation procedure was significant only for the lowest torques. Reches[9] extrapolated the torque measured values to zero RPM to obtain estimates of static friction.

111.3 Development of the High Shear Viscometer[2]

111.3.1 Description of the Original Instrument

The high shear viscometer constructed is basically the same as that used by Barber[4], Reches[9] and Porter[7]. The original blueprints were those of Porter. The design considerations implemented in the instrument have already been outlined.

The apparatus can be considered to consist of the following main components; figures (111-1) and (111-2):

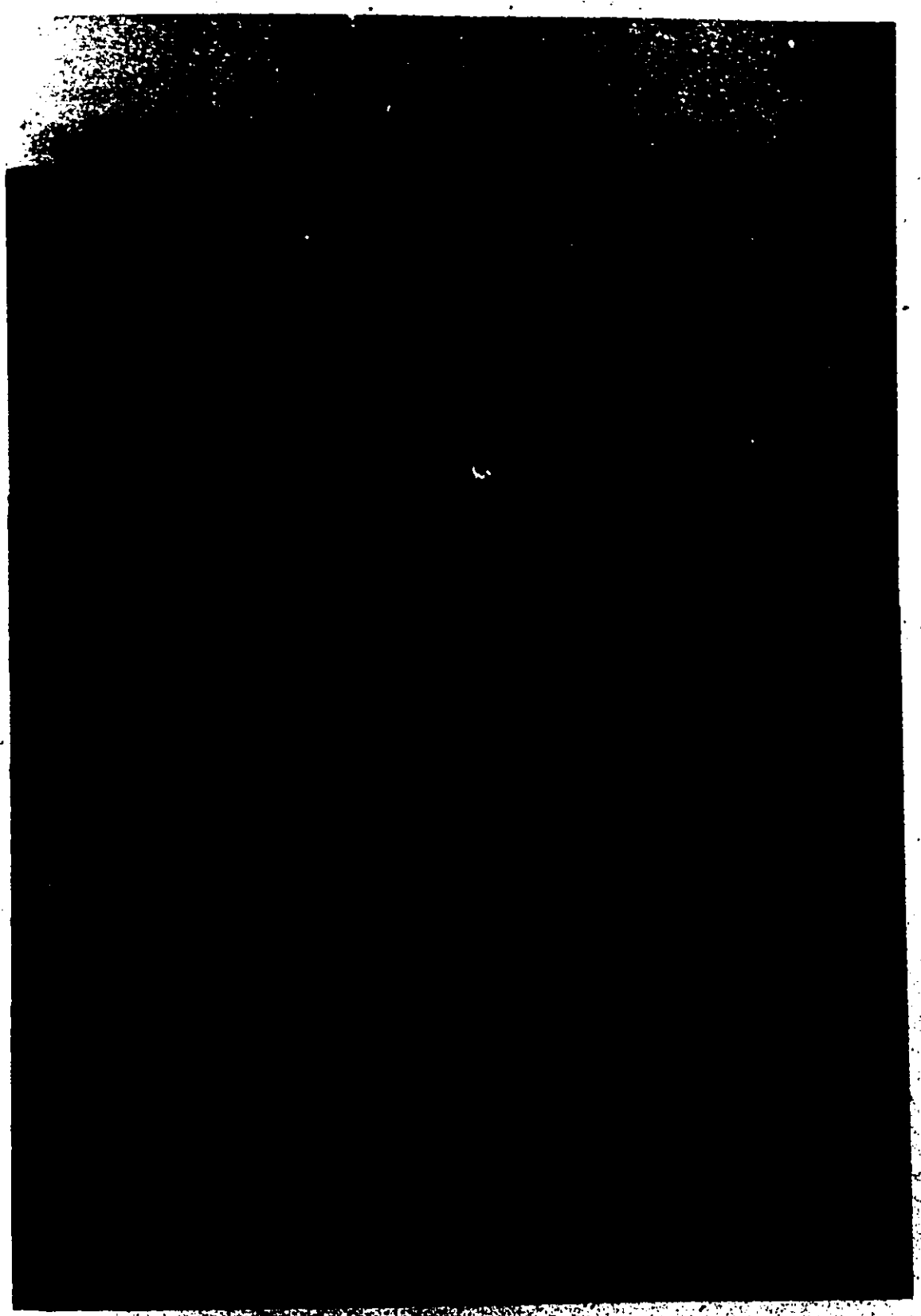

FIGURE (III-1)

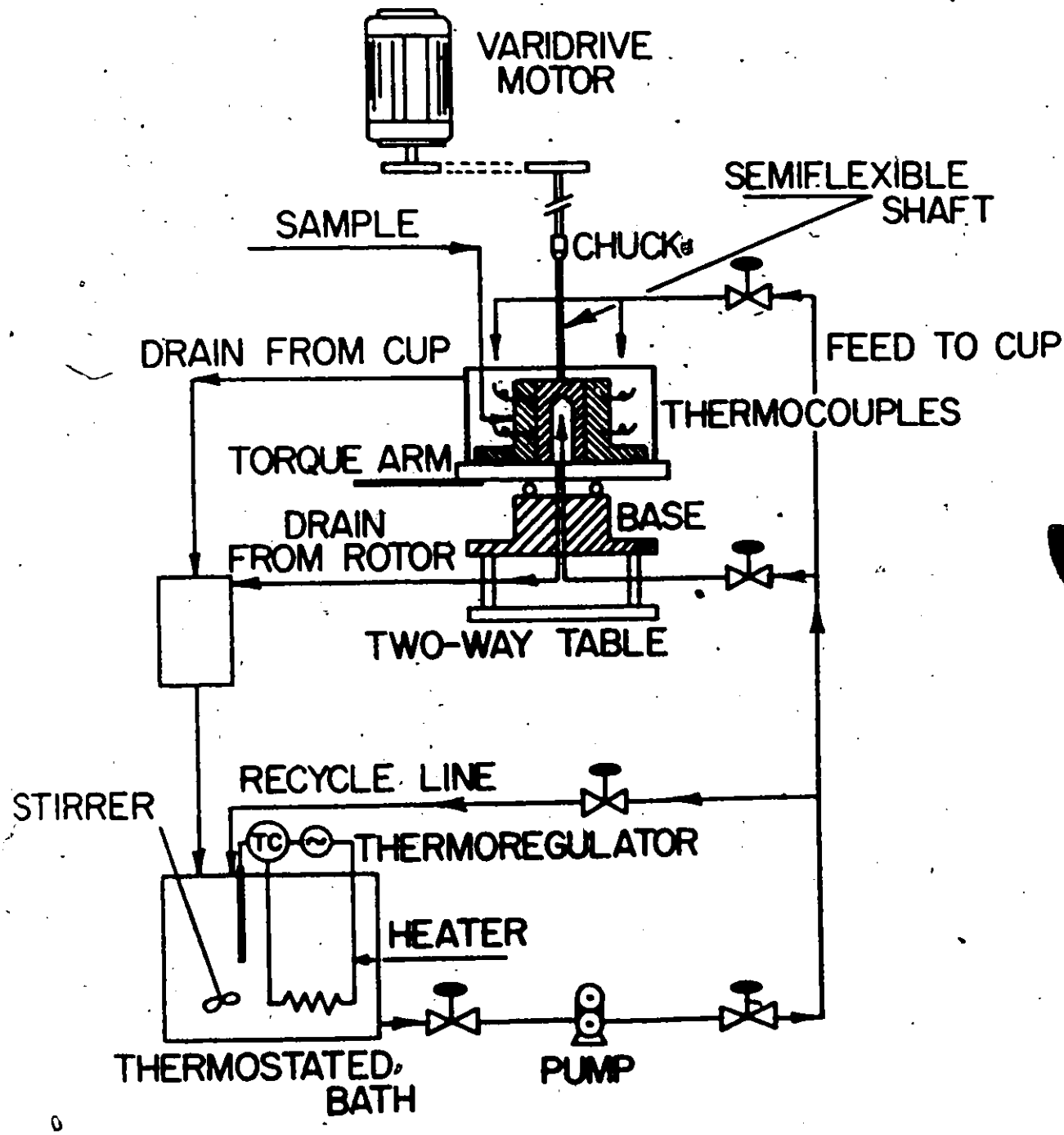
VARIDRIVE MOTOR
SEMIFLEXIBLE SHAFT
SAMPLE
CHUCKS
DRAIN FROM CUP
FEED TO CUP
THERMOCOUPLES
TORQUE ARM
BASE
DRAIN FROM ROTOR
TWO-WAY TABLE
RECYCLE LINE
STIRRER
TC
THERMOREGULATOR
HEATER
THERMOSTATED BATH
PUMP

FIGURE (111-2)

(1) the thermostating system

(2) the transducing cell, the outer viscometer cylinder and its mountings

(3) the console containing the electronic controls

(4) the drive system

The Thermostating System

This system was similar to that of Reches[9]. The bath was a Blue M-Magni Whirl Model MW-1145A-1 Utility Oil Bath. Union Carbide UNICON HTF-30 heat transfer fluid was used. An Albany Model Gear Pump circulated the fluid. Control of flow rate was effected by adjusting the valves in the line. The fluid circulated around the outer cylinder in a brass retaining cup and was prevented from entering the film by a steel guard. Fluid also was sprayed into the inside of the inner cylinder.

Viscometer Table and Transducing Cell

The outer cylinder and its attachments were mounted on self alighing ball bearings. Shear stress was obtained by measuring the force exerted by the torque arm. This measurement was accomplished by positioning a Strathan UC3 Transducing Cell along the arm at one of seven positions. Two pulleys were mounted opposite each other on needle bearings at the end of the torque arm. They permitted calibration of the transducing cell against known weights and accurate positioning of the arm. The transducing cell permitted a range of zero to 0.5 lbs. and zero to 5 lb. force depending on the cell adapter used. The power supply used for the cell was very similar to that used by Porter except, for these

cells, a 7 volt excitation was required. Figure (111-3) shows the cylinders.

Both inner and outer cylinders were originally constructed of SAE4140 carbon steel. A range of shear clearances were available by varying the diameter of the inner cylinder. Two rotors were used; dimensions are given in table (111-1).

TABLE (111-1)

CYLINDER DIMENSIONS

Effective Shear Area:		
	Length:	1.875 in.
	Diameter:	1.0000 in.
Rotor # 1:		Gap 0.00220 ± 0.00001 in.
Rotor # 2:		Gap 0.00100 ± 0.00001 in.

Samples were injected by using a glass syringe connected through a Luer-Lok fitting to the sample inlet tubes.

Electronic Controls

A Sargent Two Pen Recorder Model DSRG was used to record torque and temperature. RPM control was the same as Porter's. Measurement of RPM was directly by stroboscope.

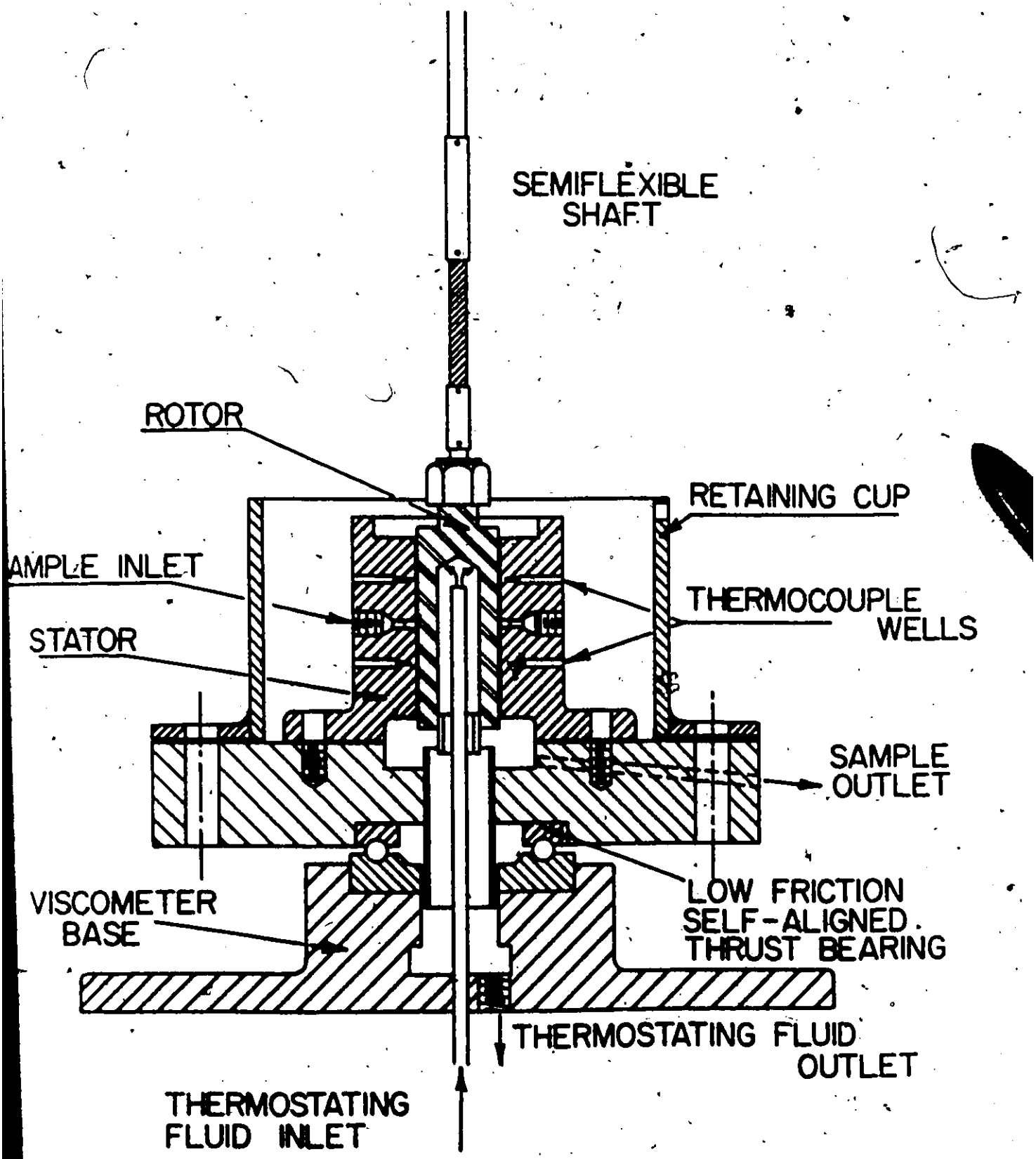
SEMIFLEXIBLE SHAFT
ROTOR
RETAINING CUP
AMPLE INLET
THERMOCOUPLE WELLS
STATOR
SAMPLE OUTLET
VISCOMETER BASE
LOW FRICTION SELF-ALIGNED THRUST BEARING
THERMOSTATING FLUID OUTLET
THERMOSTATING FLUID INLET

FIGURE (111-3)

Drive System

A 1 HP Reliance Electric Co. Type T DC Motor was used to drive overhead pulleys which in turn drove a secondary shaft. This secondary shaft held a chuck which attached to a 17" long 1/8 inch diameter flexible steel shaft which was in turn attached to the top of the inner cylinder. Speed control and drive ratio changes were identical to Porter's.

111.3.2 Development of the Instrument

The following major modifications were found to be necessary:

(1) The I HP drive motor was mounted on a concrete pillar to reduce vibrations (Porter's plans had called for this motor to be on the floor). Reches[9] also found this modification necessary.

(2) The material of construction was changed to Stainless Steel 430. The mild steel originally used corroded very easily. Use of the new material sacrificed some temperature control (the thermal conductivity of SS430 is 15.1 BTU/hr.ft.°F at 212°F).

(3) The reservoir for coolant fluid was shortened and the fluid guard removed to permit cleaning of the top of the viscometer previous to removing and washing the inner cylinder with solvent for analysis by injection into the GPC. (The instrument could also be run using continuous feed if necessary to obtain more material for analysis.) For room temperature runs the effect of this modification is negligible. For higher temperature runs presence of an undesirable axial temperature gradient along the film is possible. Its presence would be indicated by the thermocouple measurements.

(4) The 1/8 inch O.D. 17" long drill rod used by all previous investigators gave large "measured torque" vibration which were evidently due to eccentricity, and most severe at low RPM's.

Two other shafts were then tried:

(a) a similar rod equipped with a universal joint at the cylinder end, and

(b) a completely flexible shaft made from the flexible attachment to a portable electric drill.

The first provided no improvement in torque measurement - erratic vibrations were still evident. The second provided smooth measurement at low RPM's but was obviously too flexible for use at high RPM's. The shaft finally used was semi flexible, figures (111-4) and (111-5). It consisted of a 29.7 cm length of 0.65 cm O.D. steel tubing attached to 3.1 cm of flexible shaft at each end. It provided good results apparently for several reasons. The central rigid portion is tubular so that unbalance was less severe. The flexible end pieces allowed for imperfect alignment and provided damping of shaft vibrations. The net effect was that the rotational load to the inner cylinder was reduced. Soft iron pins at each end served as safety measures by shearing if the inner cylinder seized in the outer.

111.3.3 Development of Experimental Procedure

Preliminary Procedure

(a) The pump in the thermostating system was started up about three hours previous to the actual run.

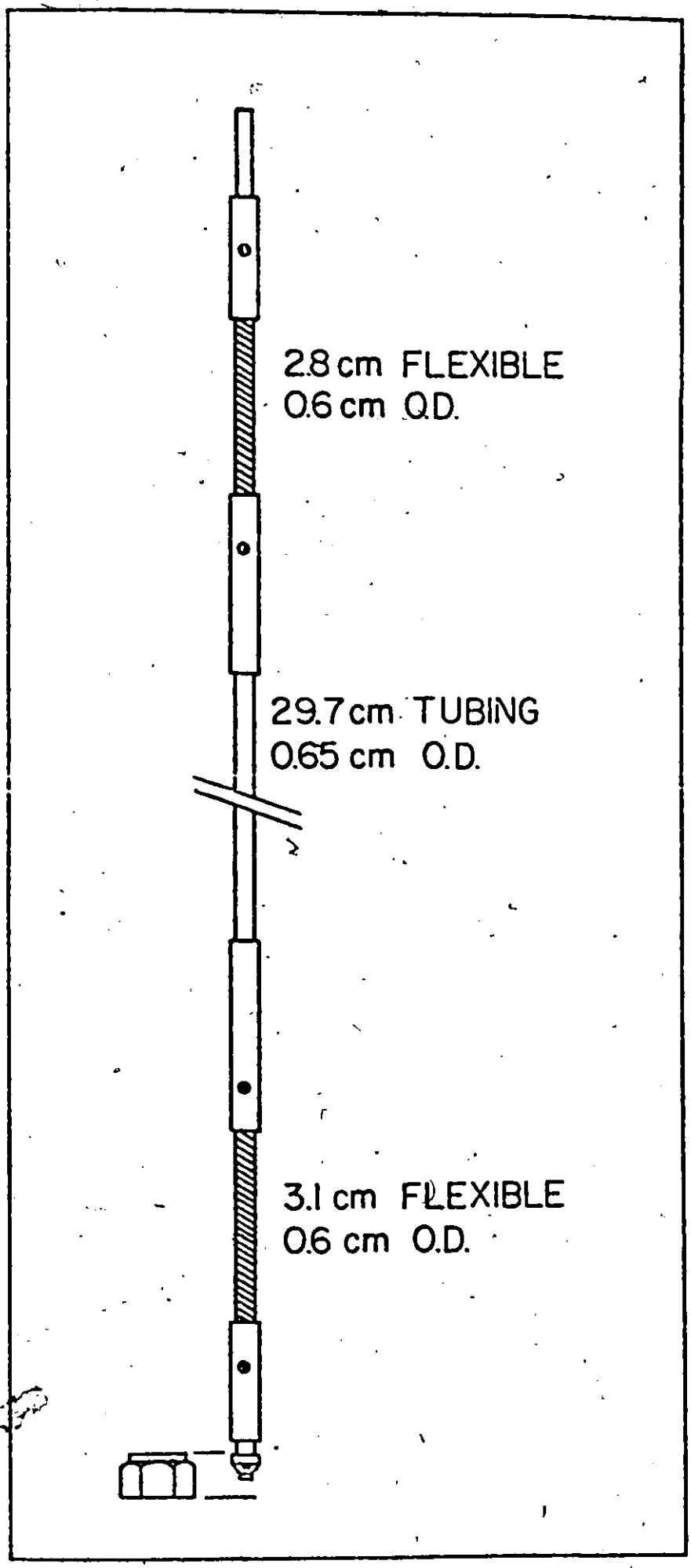
2.8 cm FLEXIBLE
0.6 cm O.D.
29.7 cm TUBING
0.65 cm O.D.
3.1 cm FLEXIBLE
0.6 cm O.D.

FIGURE (111-4)

FIGURE (111-5)

(b) The flow rate of temperature control liquid from the spray was maintained at greater than the minimum required to obtain a true spray in the inner rotor. (33 ml/min. at room temperature for the system used.)

(c) The sample was injected at least 15 minutes in advance of the run.

(d) The run was begun when all thermocouples registered no change in temperature.

Calibration of the Transducer Cell

(a) Sufficient weight was attached to the foreward pulley to cause a positive response on the recorder from the pressure on the transducer cell by the torque arm.

(b) Known weights were hung on the other pulley and the pen deflection of the recorder was recorded. These data provided the calibration curve.

Two points are worthy of note here:

(1) More reproducible results were obtained by the above procedure than by trying to tare (balance) the torque arm in step (a) by addition of weights to both pulleys (the good linearity of response of the transducer cells combined with the nature of the static friction were the likely reasons for this situation), and

(2) The rate of application of the force (both in calibration and later with non zero RPM's) was kept reasonably uniform by gently easing the torque arm on to the transducer after the weight had been hung, (or after the RPM had been set). This was accomplished by having the arm resting against the flat of a disc which was threaded to the cell mounting. The arm was applied against the cell by wheeling the disc towards the cell

after force was present on the torque arm.

Measurement of Sample Flow Properties

(a) An RPM was set and measured by stroboscope.

(b) The force required to maintain the outer cylinder stationary was measured by allowing the torque arm to contact the transducer cell (as in calibration).

(c) All thermocouple readings were registered by one pen of the two pen recorder by using a consecutive switching arrangement.

(d) The torque arm was then moved back from the cell.

(e) The above steps (a) through (d) were repeated for another RPM.

Calibrations were carried out before and after each run. RPM's were begun low, raised into steps the highest value to be used for the run and then taken down in steps.

111.3.4 Testing the Instrument with Newtonian Standards[2] (Table 111-2):

Temperature

From the thermocouple measurements presence of an axial temperature gradient was checked. Temperature at the edges of the film was calculated using Equation (111-22). Maximum temperature rise was estimated using Equation (111-26). No axial temperature gradient was observed and temperature rise across the film was low (in the order of 1°F).

TABLE (111-2)

NEWTONIAN OIL STANDARDS* USED TO TEST THE COUETTE VISCOMETER

Standard	Viscosity No.
A	S - 3 - 65 - ij
B	S - 20 - 68 - 2b
C	S - 200 - 68 - 1i
D	S - 2000 - 68 - 1e
E	S - 30000 - 67 - 1g

*Supplied by "Cannon Instrument Company", P.O. Box 16, State College, Pa. 16801.

Torque

The calculations required for torque calculation were as follows:

(a) A calibration curve for the transducer cell response for the run was obtained by a least squares fit of pen deflection, G, on the recorder chart versus weight required to obtain the deflection (placed on the back pulley) W. Response was linear so

$$G = A + B * W \qquad (111\text{-}30)$$

(b) The weight on the pan (W_o) at zero pen deflection was calculated from equation (111-30) by setting G = 0. That is, forces above this value were assumed to be sufficient to overcome both static friction of the self aligning ball bearings on the outer cylinder and the weight hung on the foreward pulley.

(c) Pen deflection at different RPM's were used along with the calibration curve (equation (111-30)) to obtain the total measured force (= the result of shear stress exerted by the liquid in the gap on the inner wall of the outer cylinder plus the result of shear stress exerted by the ball bearings rubbing against the bottom of the outer cylinder (static friction) plus the force of the weights hung on the foreward pulley, equals the desired force + W_o).

(d) Torques were calculated by multiplying each measured force and W_o by the distance from the point at which the string over the pulleys was attached, to the centre of the rotor.

(e) The desired torque (that due to liquid flow) was obtained by subtracting the torque due to W_o from the measured torque at each RPM.

(f) The torque at the desired reference temperature could then be obtained by multiplying by the viscosity factor.

Gap Estimate

Point estimates of gap width may be obtained using equation (111-20). Figure (111-6) (from reference 2) shows torque versus RPM at 20°C for Newtonian Standards B and C. A variety of symbols for data points was used to indicate runs carried out on different days. Gap estimate agreed within 6% error with micrometer measurements.

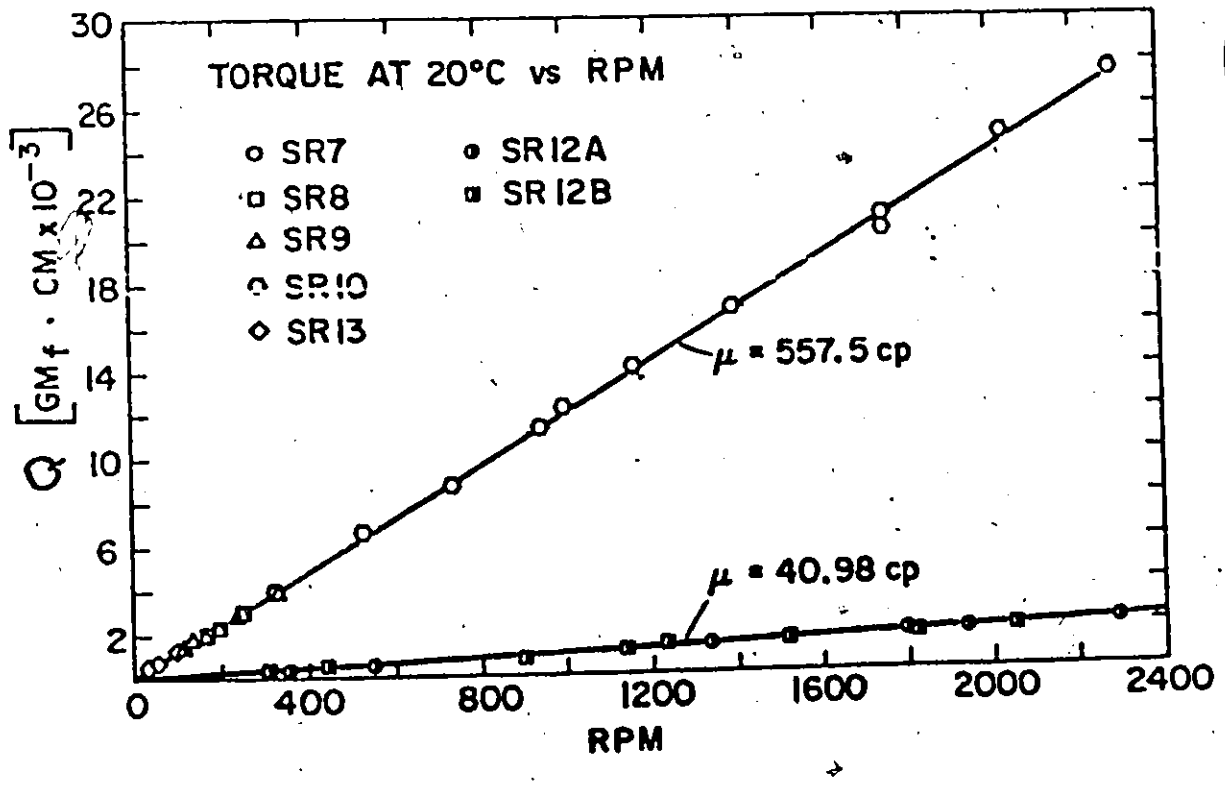
TORQUE AT 20°C vs RPM
SR7
SR8
SR9
SR10
SR13
SR12A
SR12B
μ = 557.5 cp
μ = 40.98 cp
Q [GMf · CM x 10⁻³]
RPM
0
400
800
1200
1600
2000
2400
2
6
10
14
18
22
26
30

FIGURE (111-6)

111.4 Flow Properties of Polystyrene Solutions Under High Shear Rate

111.4.1 Introduction[3]

The non-Newtonian viscosity of polymers and their solutions has been studied extensively during the past several years. For most systems in steady shearing flow the viscosity coefficient depends on the shear rate in a rather characteristic manner. At sufficiently low shear rates the viscosity is independent of the shear rate (the Newtonian region). However, Within some critical range of shear rates the viscosity begins to decrease and continues to decrease as the shear rate is increased to still higher values, approaching power-law behaviour. Most of the experimental work done so far was limited to shear rates up to about 10^3 sec^{-1}, through the use of either capillary or cone and plate viscometers. The high shear couette viscometer offers an excellent opportunity to extend this range to about 10^5 sec^{-1}. The main purpose for obtaining data covering a wide range of shear rates is to check on the validity of the available theories that describe the non-Newtonian viscosity behaviour of polymeric solutions.

Most molecular theories, imply that the viscosity shear rate curve is a universal function when plotted as η/η_o versus $\dot{\gamma}\lambda$, where η_o is the viscosity at zero shear rate and λ is a characteristic relaxation time for the fluid. Different theories give different expressions for this relaxation time. A review of these theories for monodisperse polymers follow:

A) The Bueche Theory of Viscosity[22,23]:

The starting point is the Debye picture of the free draining coil rotating in a simple shear field. This molecule is supposed to rotate with

a frequency of one-half the shear rate. With reference to figure (111-7), from reference (3), it can be seen that the monomer units along the line AA' experience a drag force which tends to extend the chain. Along the line BB', however, the drag force tends to compress the chain. Hence, as a monomer unit rotates about the center of gravity of the molecule, it experiences a sinusoidally alternating tension and compression. Bueche imagined the polymer molecule to be subdivided into a large number of "sub-molecules", each of which behaves mathematically like a small mass attached to a linear spring. This allows the development of a formal solution for the displacement of each sub-molecule relative to its equilibrium position. Since the forcing function is periodic, the displacements of the monomer units are also periodic. The viscosity then is given by the average dissipation for the whole molecule calculated over a period of rotation.

The final expression given by Bueche follows:

$$\frac{\eta - \eta_s}{\eta_o - \eta_s} = 1 - \frac{6}{\pi^2} \sum_{n=1}^{N} \frac{(\dot{\gamma}\lambda)^2}{n^2(n^4 + \dot{\gamma}^2 \lambda^2)} \left(2 - \frac{(\dot{\gamma}\lambda)^2}{n^4 + \dot{\gamma}^2 \lambda^2}\right) \quad (111\text{-}31)$$

where

η_s is the solvent viscosity, N is the degree of polymerization, λ is a relaxation time, given by:

$$\lambda = \frac{12(\eta_o - \eta_s)M}{\pi^2 C R T} \quad (111\text{-}32)$$

where

M is the molecular weight, C is the solvent concentration, R is the gas constant, and T is the absolute temperature.

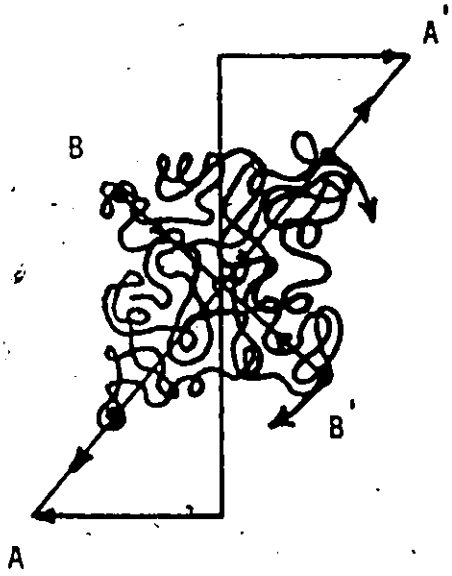

Bueche's picture of a rotating molecule

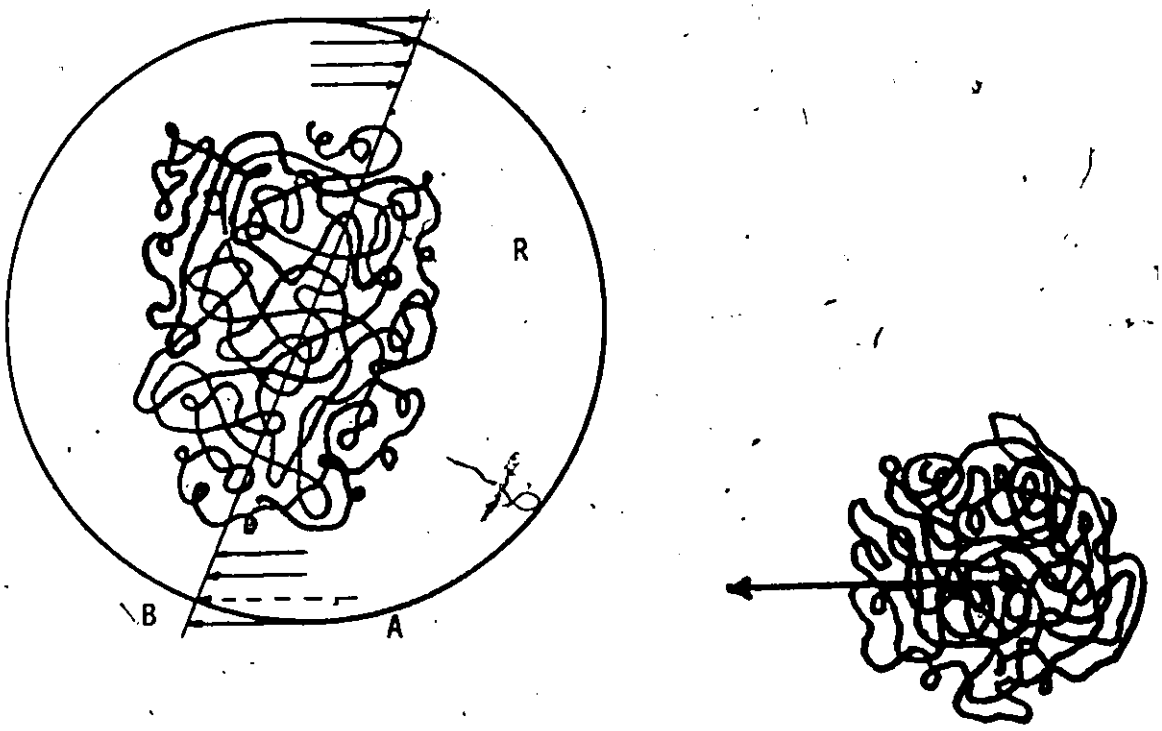

Graessley's entanglement theory

FIGURE (111-7)

At large values of $\dot{\gamma}\lambda$, the theory predicts a limiting slope of -0.5 when log η/η_o is plotted versus log $\dot{\gamma}\lambda$. It also shows that the reduced viscosity $(\eta - \eta_s)/(\eta_o - \eta_s)$, is a function only of $\dot{\gamma}\lambda$.

B) Graessley's Molecular Entanglement Theory[24]:

Graessley offered an alternative picture of polymer behaviour which leads to a non-Newtonian viscosity without requiring rotation. He envisioned events between molecular segments during which interaction, which he considered to be entanglement, occurs leading to increased dissipation of energy.

The kinetics of the actual events are unknown. Graessley adopted a very simple mechanistic picture. For an entanglement to exist, two molecules must first be within a certain distance of each other, say within a sphere of radius R. Second, the molecules must remain within this sphere for a finite time λ, or else no entanglement occurs. The greater the shear rate, the more rapidly two molecules move relative to one another. Hence, the entanglement density is reduced by high shear rate, since fewer molecules will remain in the "entanglement sphere" for a sufficiently long time at high shear rate. The result is a reduction in the viscosity. Figure (111-7) pictures this process, the polymer molecules move relative to one another because of a velocity gradient. If the center of mass of one molecule moves through the sphere centered about the second molecule, entanglement may occur. The duration of the entanglement depends upon the time required to move along the path AB, and is reduced as the velocity gradient increases. When the details of this dynamic picture are worked

out, the following is obtained:

$$\eta/\eta_o = h = \frac{2}{\Pi}\left\{\cot^{-1}\theta + \frac{\theta(1-\theta^2)}{(1+\theta^2)^2}\right\} \qquad (111\text{-}33)$$

where

$$\theta = \frac{\dot{\gamma}\tau_o}{2}\left(\frac{\eta}{\eta_o}\right) \qquad (111\text{-}34)$$

τ_o is the entanglement formation time, reduced to $\dot{\gamma} = 0$, it is a constant of the system. τ_o is related to the Rouse relaxation time of a chain[25] τ_r by:

$$\tau_o = C.\,\tau_r \qquad (111\text{-}35)$$

where C is a constant that depends on the entanglement density and is in the order of unity. τ_r is given by[25]:

$$\tau_r = \frac{6}{\Pi^2}\frac{\eta_o M}{CRT} \qquad (111\text{-}36)$$

For large values of $\dot{\gamma}\tau_o$ (>> 1), equation (111-33) takes the limiting form:

$$\eta/\eta_o = \text{constant}\left(\frac{\dot{\gamma}\tau_o}{2}\right)^{-\frac{3}{4}} \qquad (111\text{-}37a)$$

This shows that the limiting slope will be -0.75 instead of -0.5 given by Bueche's theory.

Graessley then modified his theory by relaxing some assumptions. The results are[26]:

$$\eta/\eta_o = h\,g^{3/2} \qquad (111\text{-}37b)$$

h is defined as before (111-33), g is given by:

$$g = \frac{2}{\Pi}\left\{\cot^{-1}\theta + \frac{\theta}{1+\theta^2}\right\}$$

θ is defined as in equation (111-34). At large values of θ, Graessley shows that:

$$\eta/\eta_o = \text{constant } (\frac{\dot{\gamma}\tau_o}{2})^{-\frac{9}{11}} \qquad (111\text{-}37c)$$

The limiting slope according to (111-37c) is $-\frac{9}{11}$ or -0.818.

C) The Molecular Theory of Williams[27]:

Unlike the theories prposed by Bueche and Graessley, Williams proposed a theory that does not give a detailed mechanistic picture of the interaction between the molecules. His theory simply assumes that there is some kind of interaction and the force of interaction can be expressed in terms of a potential function and a segment distribution function. The result of William's analysis could be put in the usual form:

$$\frac{\eta - \eta_s}{\eta_o - \eta_s} = F(\lambda\dot{\gamma}) \qquad (111\text{-}38)$$

At high shear rates η/η_o as predicted by this theory should decrease in proportion to $\frac{1}{\lambda\dot{\gamma}}$. This means that the limiting slope will be -1.

111.4.2 Experimental

The purpose of this study was to produce data covering a wide range of shear rates to be able to check on the validity of the available theories.

Graessley, in his experimental work[28], used solutions of narrow polystyrene standards in n-butylbenzene and he employed a Weissenberg plate and cone viscometer.

In the present study the same solutions used by Graessley were prepared. Narrow polystyrene standards were used of molecular weights 97,200, 411,000, and 860,000. The concentration ranged from 0.08 g/cc to 0.5 g/cc, as shown in table (111-3). Experimental procedure was described in detail earlier. Each run was done by increasing the RPM up to the maximum and then reducing it. This was to check for polymer degradation. The results indicate no degradation since the run followed the same path in both directions. For some runs this was checked further by GPC analysis of the sample before and after shearing; no difference was noticed.

111.4.3 Results and Discussion

Experimental results are shown in table (111-4) in the form of viscosity versus shear rate for the different solutions listed in table (111-3). All the data were referred to 30°C for easy comparison with literature[24,28]. These data are also plotted in figures (111-8) and (111-9). The straight lines in figure (111-9) have a slope of -0.83. This indicates that the experimental limiting slope is -0.83 which agrees well with the modified entanglement theory of Graessley. Experimental limiting slope of -0.82 was reported by Stratton[29] using polystyrene melts in a capillary rheometer. He noticed that at high shear rates, the viscosity is not a function of molecular weight. This was also observed in the present study, as shown in figures (111-8) and (111-9); runs of the same concentration and different molecular weights show almost the same viscosity. Stratton postulated that the decrease in viscosity with increasing shear rate is due to an increase in the spacing of coupling entanglements[29].

TABLE (III-3)

Rheological Data for Polystyrene Standards*

Run	M	C gm/cc	η_o(Poise)	τ_o sec. x 10^3	τ_r sec. x 10^3	τ_r/τ_o	E
PS1 X	97,200	0.5	120	1.19	0.56	0.471	0.96
PS2 ▲	411,000	0.08	2.2	0.67	0.27	0.403	0.65
PS3 Δ	411,000	0.125	5.4	0.89	0.43	0.483	1.0
PS4 ■	411,000	0.3	250	12.0	8.28	0.690	2.4
PS5 □	860,000	0.08	8.8	4.16	2.29	0.551	1.4
PS6 O	860,000	0.22	425	43.7	40.18	0.926	3.7
PS7 ●	860,000	0.3	3600	209	249.6	1.19	5.1

*Polystyrene standards were supplied by "Pressure Chemical Company", 25 Smallman St., Pittsburg, Pa. 15201. They all have polydispersity of less than 1.06.

TABLE (111-4)

VISCOSITY VERSUS SHEAR RATE FOR POLYSTYRENE STANDARDS AT 30°C

PS1 X		PS2 ▲		PS3 Δ		PS4 ■		PS5 □		PS6 O		PS7 ●	
$\dot{\gamma} \times 10^{-4}$ sec^{-1}	η poise	$\dot{\gamma} \times 10^{-4}$ sec^{-1}	η poise	$\dot{\gamma} \times 10^{-4}$ sec^{-1}	η poise	$\dot{\gamma} \times 10^{-4}$ sec^{-1}	η poise	$\dot{\gamma} \times 10^{-4}$ sec^{-1}	η poise	$\dot{\gamma} \times 10^{-4}$ sec^{-1}	η poise	$\dot{\gamma} \times 10^{-4}$ sec^{-1}	η poise
0.252	73.2	0.432	1.32	0.326	2.97	0.193	42.5	0.279	2.29	0.248	20.4	0.364	31.3
0.429	54.0	0.509	1.23	0.640	2.38	0.275	30.1	0.409	1.72	0.293	16.2	0.526	24.5
0.571	43.8	0.719	1.03	0.989	1.67	0.550	17.5	0.664	1.28	0.503	10.2	0.672	19.8
0.826	36.0	1.20	0.771	1.48	1.29	0.917	11.3	1.08	0.827	1.05	5.95	0.995	13.7
1.33	26.4	1.94	0.602	2.47	0.918	1.42	7.89	2.36	0.431	1.65	4.16	1.82	8.64
1.85	15.6	2.92	0.407	4.18	0.578	2.05	5.50	3.38	0.317	2.24	2.98	3.54	4.90
3.50	13.4	3.88	0.341	5.73	0.454	3.17	4.02	5.11	0.233	3.75	2.08	5.75	3.60
5.21	9.36	6.21	0.227	7.87	0.405	5.25	2.50	7.45	0.176	6.68	1.36	9.19	3.17
10.1	4.91	10.1	0.145	9.42	0.310	10.1	1.49	10.1	0.128	10.1	0.940	10.1	3.02

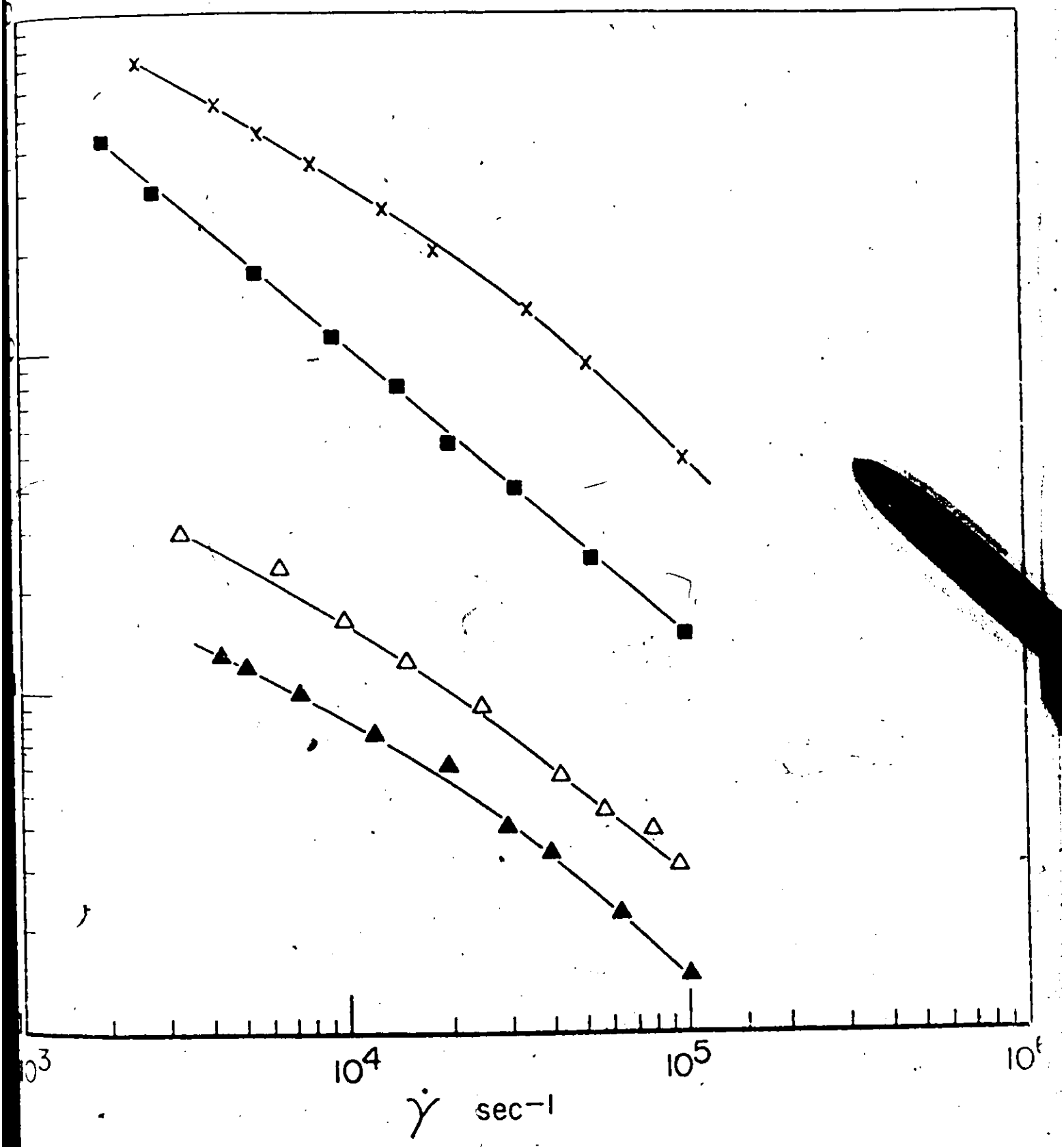

FIGURE (111-8)

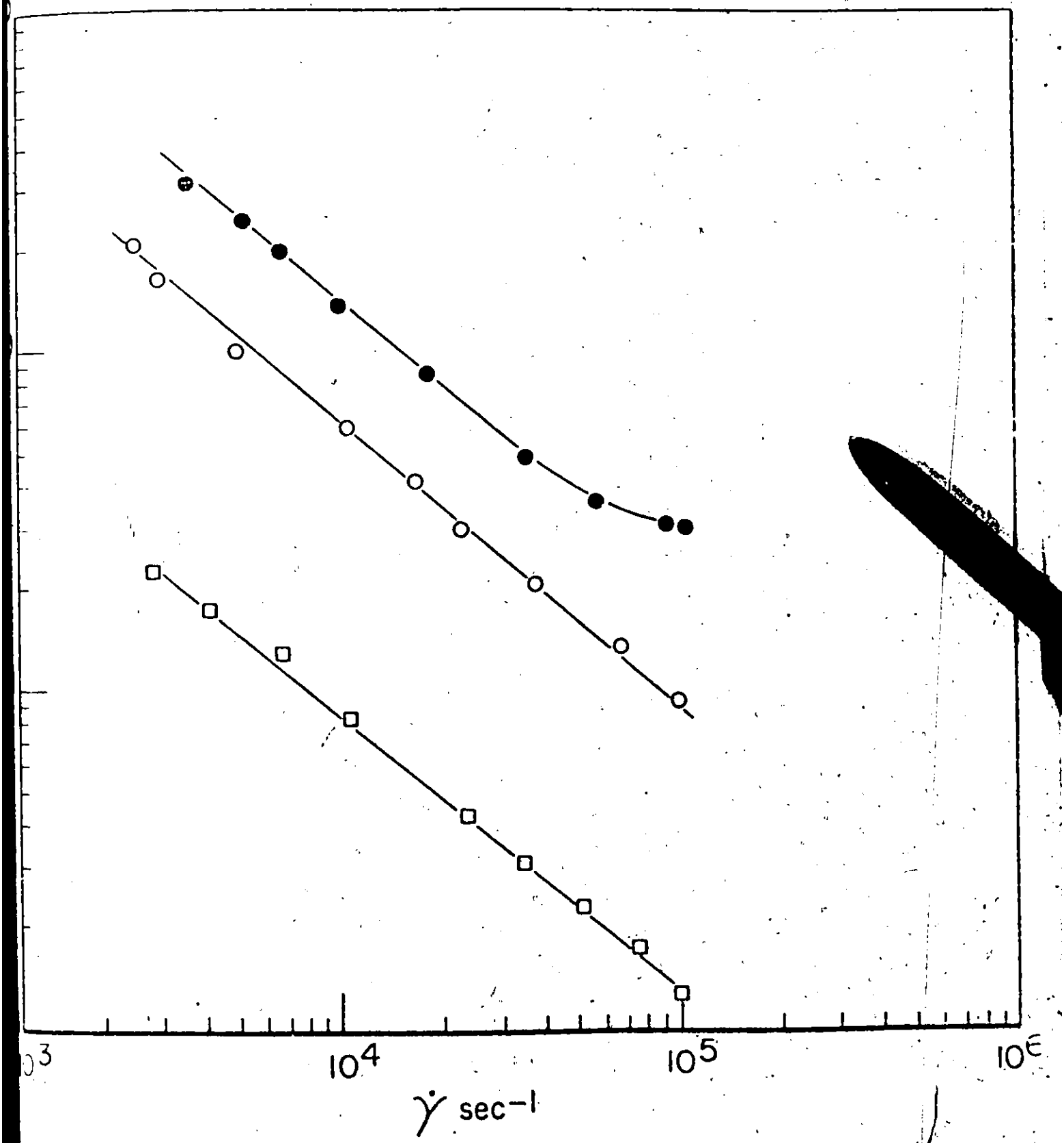

FIGURE (111-9)

The present results were analyzed by the method of Graessley[28]. The values of η_o, the viscosity at zero shear rate, we extracted from reference (28) since our instrument was not capable of giving data to cover the Newtonian range as well as the non-Newtonian range. Measurements below shear rates of about 10^3 sec^{-1} were not accessable.

The data were then fitted to the modified entanglement theory by applying a one parameter search (as given in appendix I.2). This parameter is the relaxation time τ_o in equation (111-34). This is a more precise way of shifting the data horizontally only - η_o being fixed - to fit the master curve given by equation (111-37b). Values of τ_o - experimental relaxation time - obtained this way are shown in table (111-3), for the different runs. In the same table also are shown the corresponding Rouse relaxation times τ_r given by equation (111-36) and η_o values obtained from reference (28).

Figure (111-10) is a universal plot of η/η_o versus $\frac{\dot{\gamma}\tau_o}{2}$ as given by the different theories. The data from figures (111-8) and (111-9) are also plotted in the dimensionless coordinates and it shows good agreement with the modified entanglement theory.

At about $\frac{\dot{\gamma}\tau_o}{2}$ of 10^4 there seems to be some leveling of the curve. This was noticed in run PS7 of the highest molecular weight. Unfortunately, only this run could reach $\frac{\dot{\gamma}\tau_o}{2}$ of 10^4. Further work at higher shear rates is needed before any conclusions can be made.

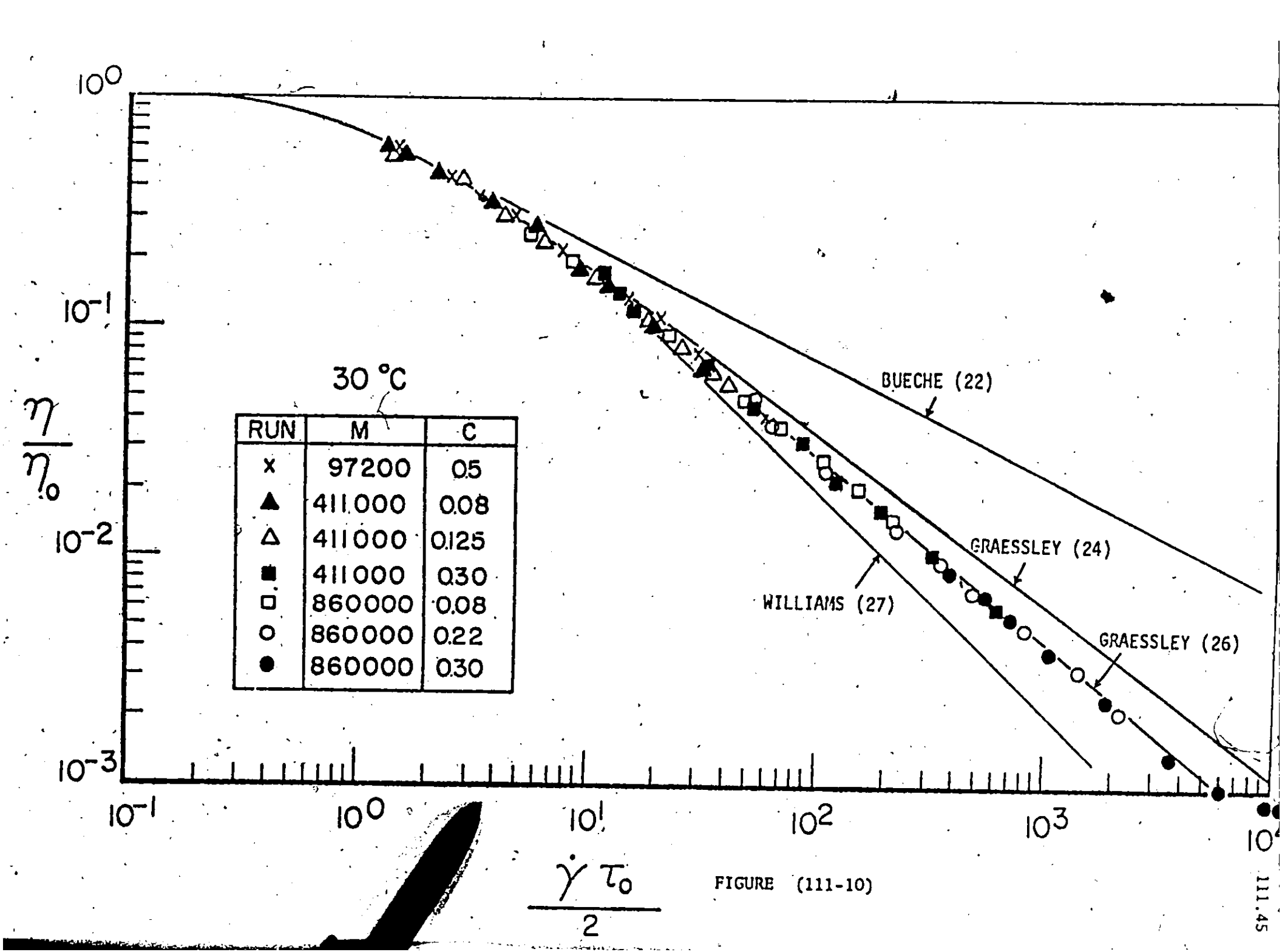

FIGURE (111-10)

It was shown that when η_o is plotted versus molecular weight M on a log-log plot, a broken straight line is obtained[28]. The value of M_b at the break point depends on the concentration C. The product CM_b is a constant however, The break in the line corresponds to a chain entanglement point along the molecule. Accordingly for any polymer-solvent system, the product CM is proportional to the number of entanglement points along the chain[30], which is defined as the entanglement density E:

$$E = \frac{CM}{(CM_b)} \qquad (111\text{-}39)$$

For the system polystyrene - n butylbenzene at 30°C , Graessley[28] obtained an average value of CM_b of 50,500. He also plotted τ_r/τ_o versus E, defined in equation (111-39) and obtained a straight line given by:

$$\frac{\tau_r}{\tau_o} = 0.28 + 0.19\ E \qquad (111\text{-}40)$$

Table (111-3) shows the ratios τ_r/τ_o obtained and also the entanglement density E given by:

$$E = \frac{CM}{50{,}500} \qquad (111\text{-}41)$$

τ_r/τ_o were plotted versus E in figure (111-11). The least-squares line is given by:

$$\frac{\tau_r}{\tau_o} = 0.30 + 0.17\ E \qquad (111\text{-}42)$$

The correlation coefficient between these two parameters (0.3 and 0.17) is equal to -0.81.

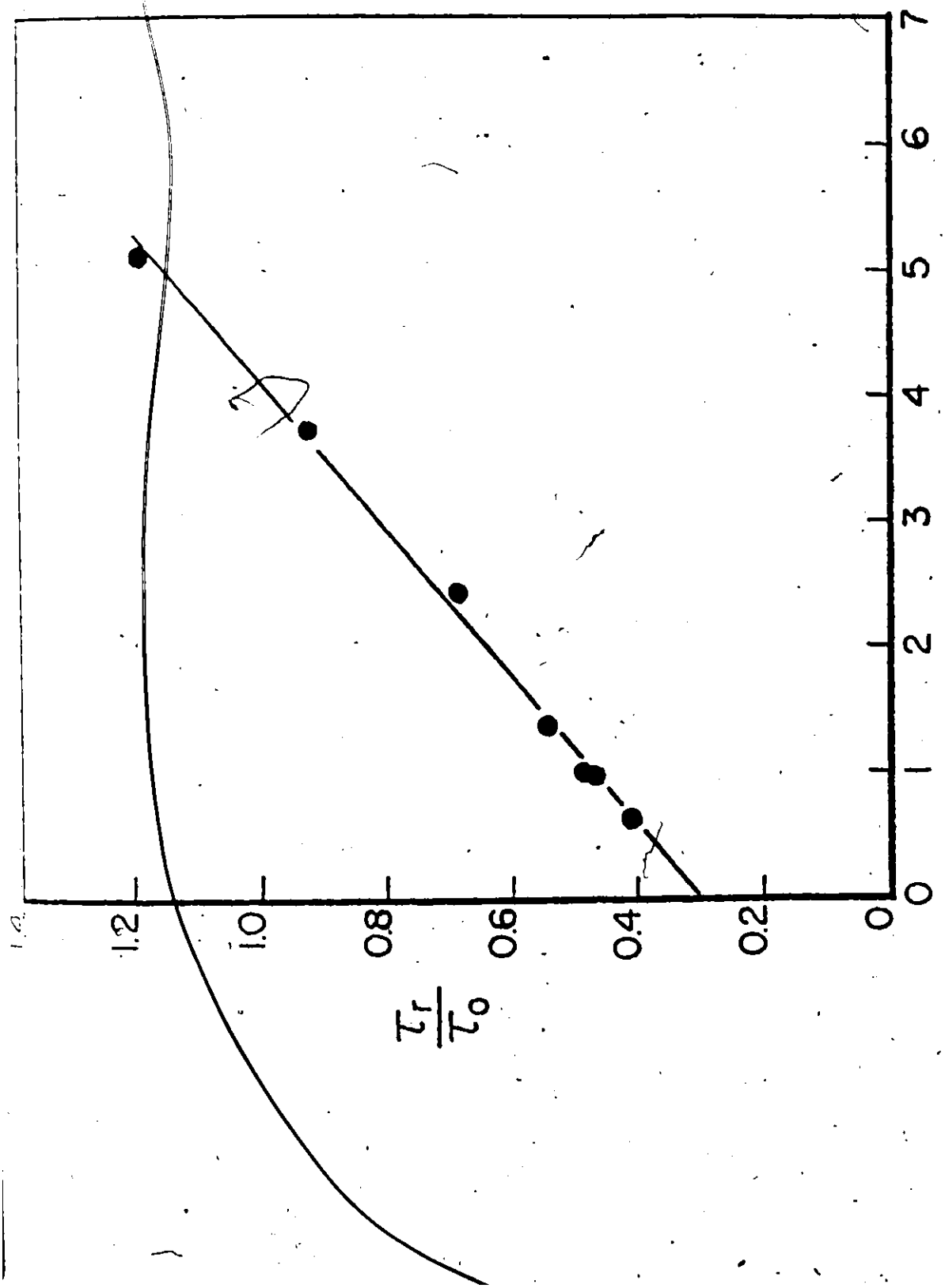

FIGURE (111-11)

111.5 Shear Degradation of Polyacrylamide

111.5.1 Introduction

Mechanical degradation of high polymers has become increasingly important as new applications for super molecular weight polymers develop.

It was shown recently that some water soluble polymers, e.g., polyacrylamide, have a unique property. It was noticed that small amounts of such polymers when added to water flowing in pipes, cause a considerable drag reducation. Many interesting features regarding drag reduction in dilute solutions of high polymers have been investigated and during the past few years a number of publications have appeared on this subject[31]. Interestingly enough, a decline in the capacity for drag reduction was noticed on repeated use of the polymer solution. This is thought to be due to polymer degradation.

Another very important application of polyacrylamide is in the field of waste water treatment. It has been shown that this polymer acts as an excellent flocculant in sewage treatment. Care must be taken in dissolving and stirring polyacrylamide-water solutions to prevent degradation of long chains. In these applications, polymer molecules are exposed to shear action which can cause chain degradation. Larger molecules contribute more in the aforementioned applications; it is therefore important to study the shear degradation of these molecules to establish limits for their use.

Thus, from an engineering point of view, a degradation study of polyacrylamide in dilute solution is interesting in that it provides some evidence on the life-time of the dilute polymer solution exposed to shear. Only very recently has shear degradation of this polymer received attention. Wade and Kumar[31] degraded dilute aqueous solutions of polyacrylamide by forcing the solutions through a fine capillary. They used electron microscopy to follow the molecular weight distribution variation with number of passes through the capillary. In capillary flow the shear field is not uniform and only a small fraction of the polymer experiences the wall shear stress per pass. The polymer experiences a distribution of shear stress across the radius of the capillary and makes interpretation of degradation measurements very difficult. The same holds true with the use of an ultrasonic generator.

In the present work, the high shear Couette flow viscometer with its very narrow gap was used. As stated before this offers many advantages e.g., a well-defined and uniform shear field, high rates of shear up to about 10^6 sec^{-1}, no corrections for end effects and very small amounts of the polymer are needed. This viscometer enables one to vary the shear rate simply by changing the RPM of the inner cylinder and so it offers the opportunity to perform a series of equilibrium degradation experiments at different shear rates. Equilibrium degradation is achieved in less than a minute.

Porter, Cantow and Johnson[6,8,32,33] used a similar high shear viscometer to study shear degradation of polyisobutene. They used gel permeation chromatography (GPC) to measure the molecular weight distribution at different stages of degradation. GPC was also used in this work and this made it possible to follow the molecular weight distribution change with shear stress.

From a practical point of view, the goal to be achieved through such studies, is to obtain a quantitative relationship between the shear stress applied to the system and the MWD of the polymer that survives these conditions. Such relationship would tell the user what chain sizes he should expect to have under the shear conditions he is applying. Relationships of this kind are highly desirable and valuable for industrial applications.

III.5.2 Experimental

Materials and Experimental Conditions

Polyhall 402, a non-ionic polyacrylamide (supplied by Stein-Hall Ltd.) was used. The polymer is water soluble and solutions in water are very viscous even in dilute concentrations. This puts an upper limit on the concentrations to be used, in fact a solution of concentration more than 2% by weight is essentially a solid gel. Two concentrations were investigated in this work, 0.2 and 0.7% by weight. Temperatures employed were 25°C and 40°C.

GPC Measurements

A Waters ALC/GPC 301 was used, under the following conditions: sample volume injected 2 mls; solvent, distilled water (25°C); polymer concentration, 0.01 wt%; max. sensitivity; flow rate, 3 ml/min; and five columns in series of the following specifications:

CPG-10, 2500 Å

CPG-10, 2000 Å

PORASIL DX, 400-800 Å

PORASIL CX, 200-400 Å

CPG-10, 125-240-370 Å

Due to the lack of water soluble narrow standards the columns were calibrated using broad standards of polyacrylamide of known molecular weight distribution employing a technique that was developed to calibrate GPC for water soluble polymers (appendix III-1).

Procedure

The polymer solution was injected into the viscometer using a glass syringe fitted with a filter. The inner cylinder was then removed and washed carefully with a known amount of distilled water, the concentration of the wash liquid was adjusted to about 0.01 wt% prior to GPC analysis. This first GPC injection is considered the undegraded polymer. In this way we eliminate the error due to possible degradation caused by the injection process. The viscometer is then cleaned and the gap is refilled with polymer solution. The shear rate is then increased by rotating the inner cylinder at increasing RPM in steps. At each shear rate

equilibrium conditions were established when the recorded torque levelled off to a steady state value. This never required more than one minute of time. After equilibrium was reached, the RPM was decreased again to the previous value, degradation is indicated by a permanent loss in viscosity. A reversible path indicates no degradation. When degradation was noticed at certain shear conditions, the instrument was stopped, the inner cylinder taken out, washed as described above and a GPC injection was made. Following this the instrument was cleaned and refilled. Shear rate was increased to a higher level this time and the process repeated.

111.5.3 Results

Figure (111-12) shows the effect of shear rate on the viscosity of the 0.7 wt % solution at 25°C. The viscosity was recorded at a shear rate of 2.6×10^3 sec^{-1}. The shear rate was increased to 5.2×10^3 sec^{-1}. On going back to 2.6×10^3 sec^{-1} a lower viscosity was recorded indicating shear degradation. The solid lines with arrows at both ends indicate reversible paths, while dashed lines with arrows at one end indicate irreversible paths or degradation paths.

Figure (111-13) shows the results for the 0.2 wt % solution at 25°C. Figures (111-14) and (111-15) are for the 0.2 and 0.7% solutions respectively at 40°C. It is interesting to note that in Figure (111-14) we do not get any degradation at all in the range of shear rates used.

Figure (111-16) shows the molecular weight distributions (differential and cumulative) for the undegraded polymer and for two of the degraded polymers corresponding to Runs 28 and 32 in table (111-5). Table (111-5)

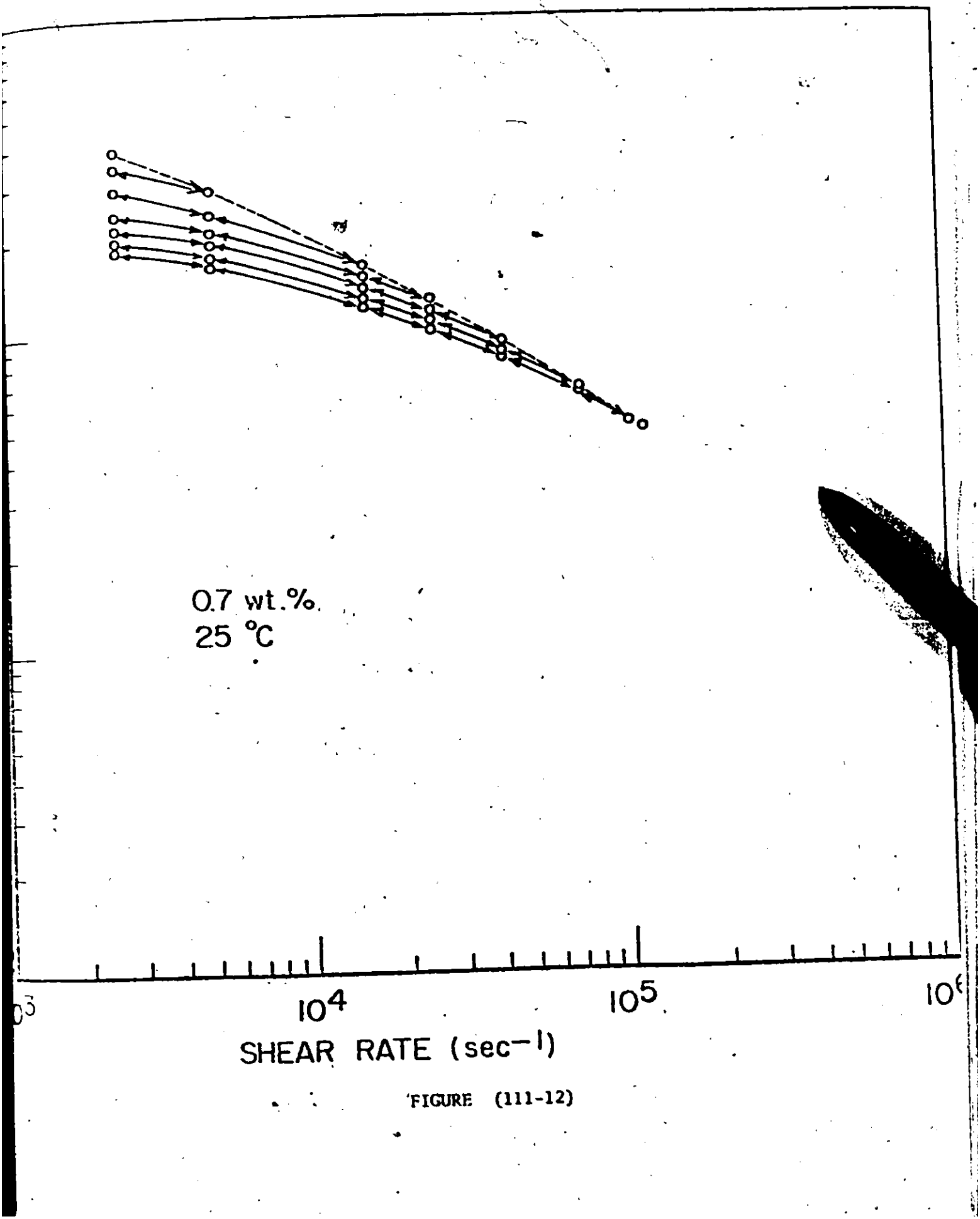

FIGURE (111-12)

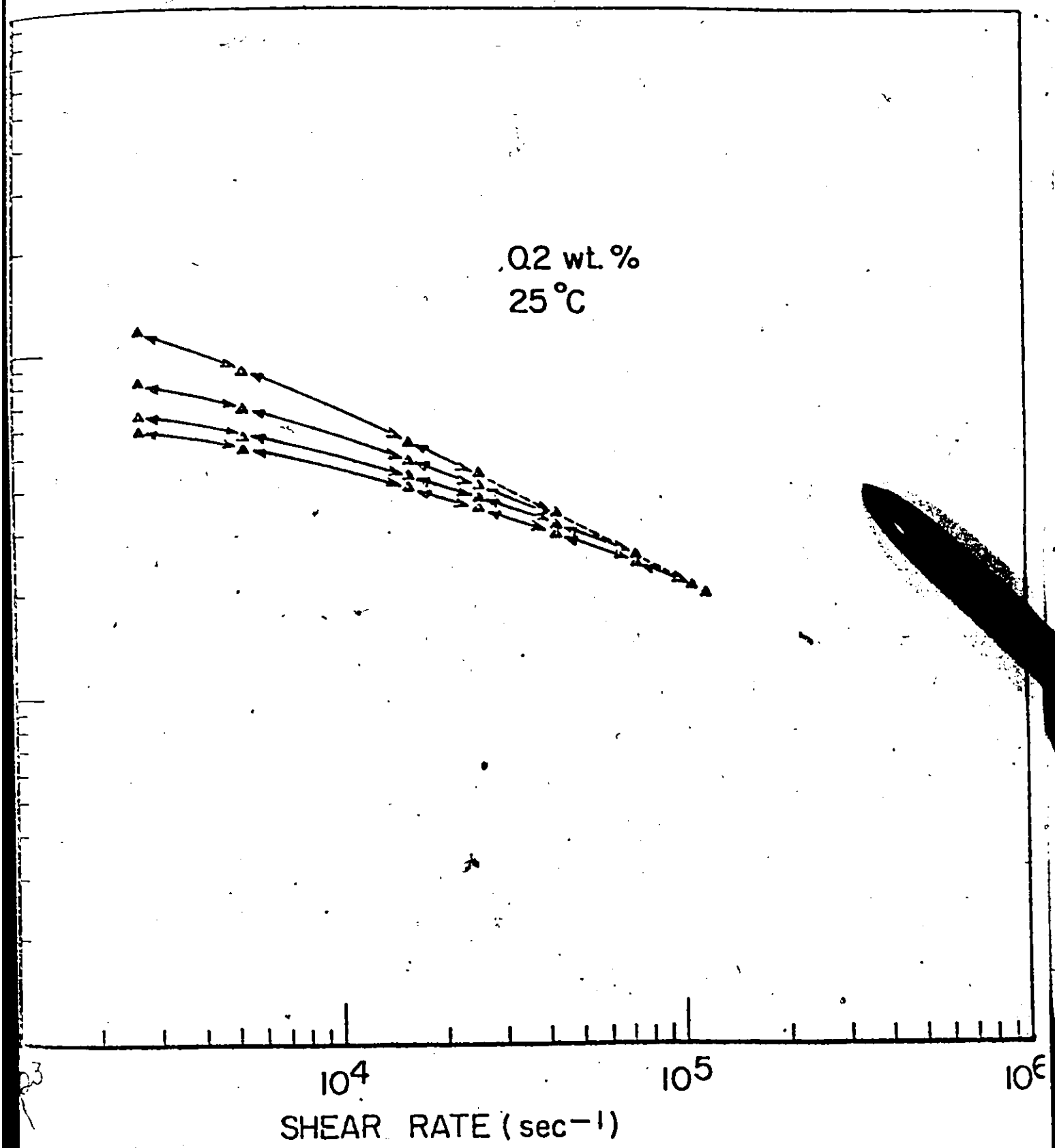

FIGURE (111-13)

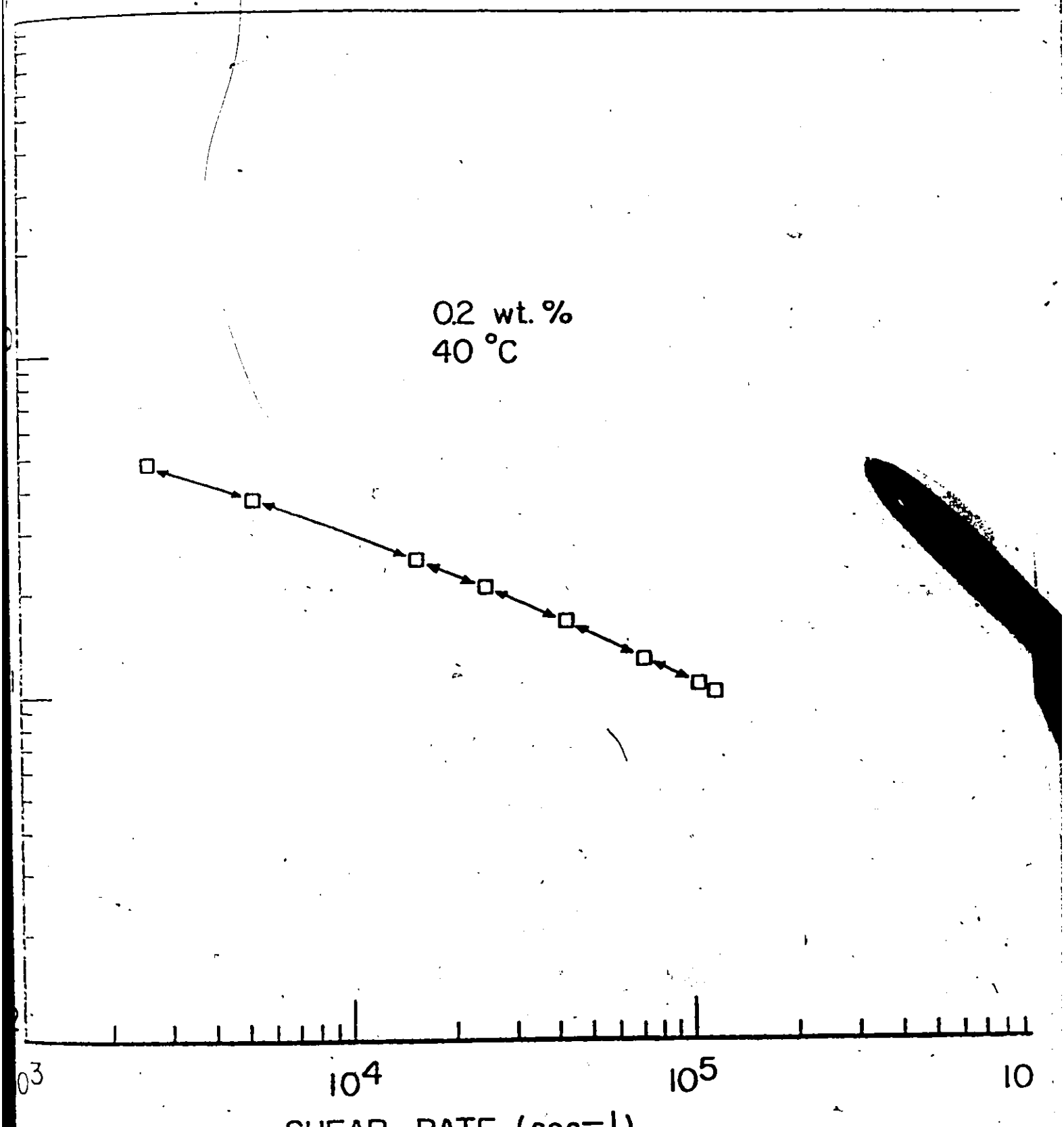

FIGURE (111-14)

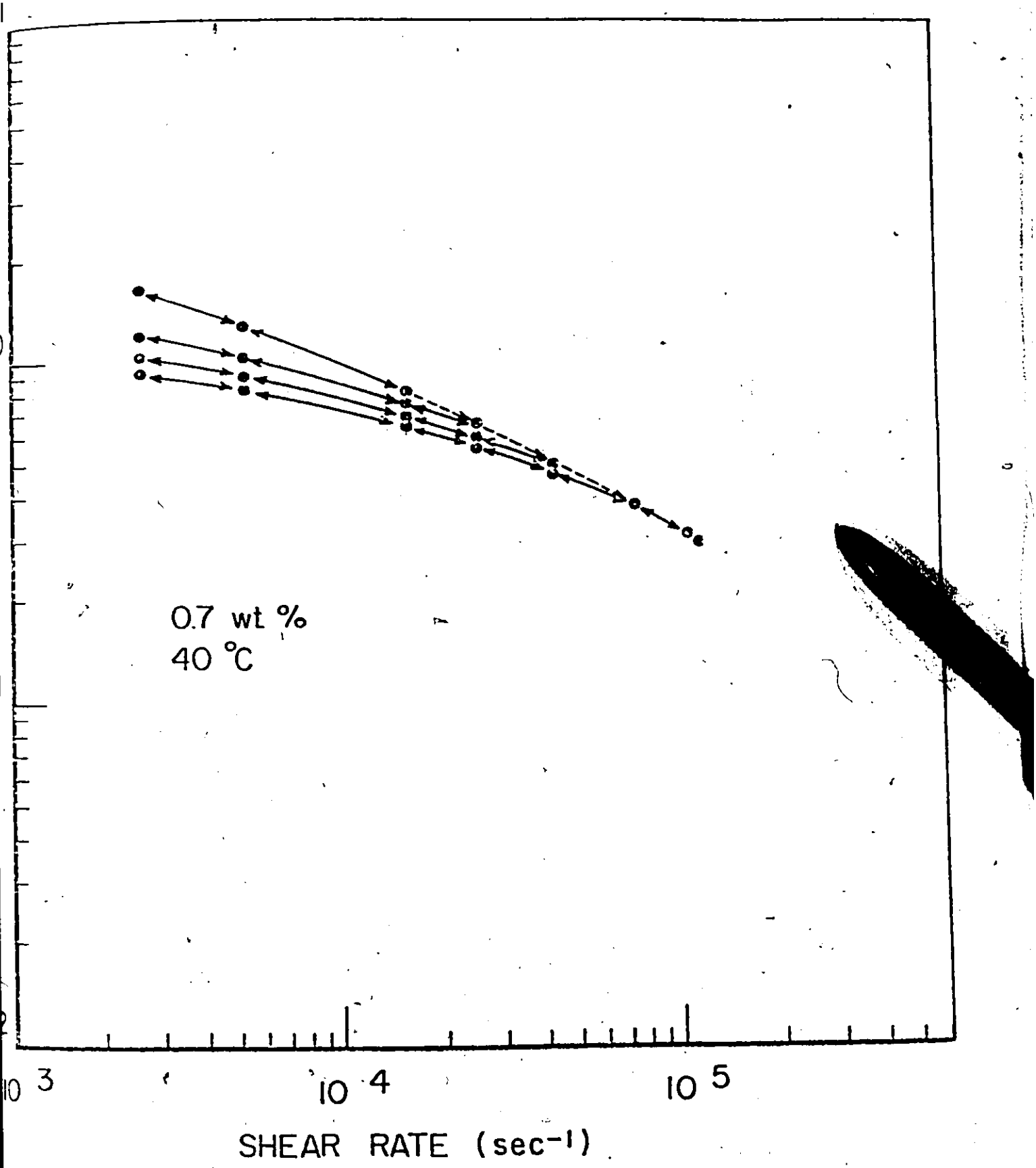

FIGURE (111-15)

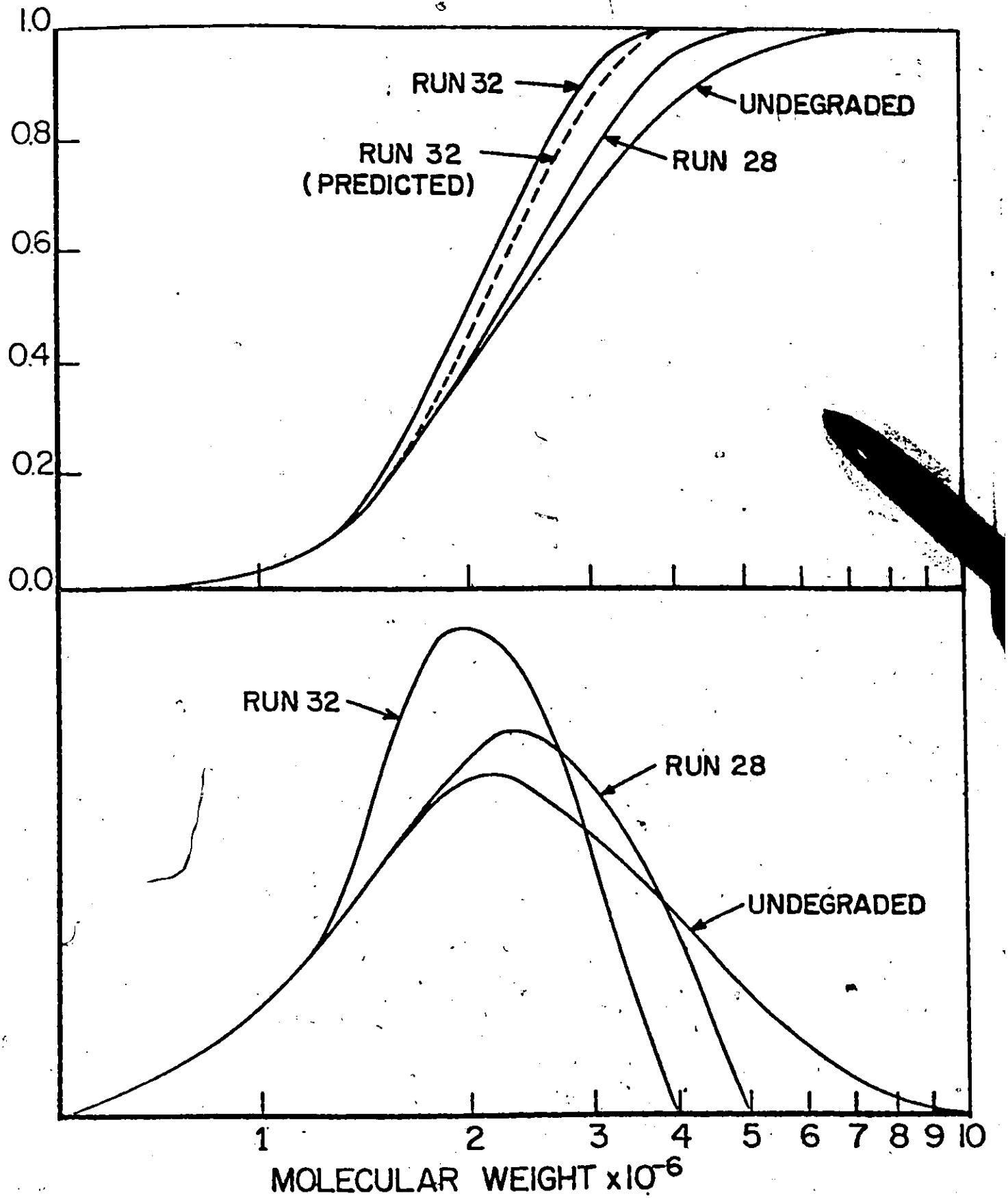

FIGURE (111-16)

summarizes all the degradation results. The sixth column in the table is the degrading shear stress obtained directly from the measured torque. The viscosity in the fifth column is obtained by dividing the shear stress by the shear rate. In the table also is the critical molecular weight (M_c) which is the maximum molecular weight present at the specified shearing conditions, obtained from the GPC analysis (99.9% of the area).

In Runs 31 and 32 (highest shear stresses), GPC analyses of degradation products indicated the formation of a low molecular weight peak made up of molecules of chain lengths ranging between 5 and 20 monomer units. In a similar study of shear degradation of polyisobutene, Porter et al[8] noticed such a low molecular weight peak in their degradation products. Figure (111-17) shows the molecular weight distribution for degraded polymer Run 32. The area of the low molecular weight peak is about one third (33%) of the larger one. Comparison of the distribution of Run 32 with the less severe runs indicates that the low molecular weight products come from molecules covering essentially the whole range of the big peak. In other words the low molecular weight products do not seem to come from a certain molecular size of the degraded polymer.

Figure (111-18a) is a plot of the critical molecular weight as defined above and obtained from the GPC trace, versus the degrading shear stress. Figure (111-18b) is the same plot on log ordinates, the relation is reasonably linear on a logarithmic plot.

TABLE (III-5)

EXPERIMENTAL DEGRADATION RESULTS

Run	Concentration wt%	Temperature °C	Shear Rate x 10^{-4} sec^{-1}	Equilibrium viscosity (poise)	Shear Stress x 10^{-4} $\frac{dynes}{cm^2}$	Critical Molecular Wt. x 10-6 M_c	$M_n x10^{-6}$	$M_w x10^{-6}$	M_w/M_n
13	0.2	25	4.20	0.34	1.43	6.79	2.38	5.76	2.42
14	0.2	25	7.32	0.25	1.90	6.50	2.35	5.36	2.28
15	0.2	25	10.4	0.21	2.18	5.82	2.21	4.79	2.17
16	0.2	25	11.5	0.20	2.30	5.61	2.23	4.75	2.13
20	0.7	40	2.51	0.66	1.65	6.50	2.34	5.41	2.31
21	0.7	40	4.20	0.51	2.14	5.91	2.24	5.08	2.27
22	0.7	40	7.32	0.38	2.78	5.50	2.15	4.54	2.11
23	0.7	40	10.4	0.31	3.22	4.94	2.05	4.16	2.03
24	0.7	40	11.5	0.30	3.45	4.92	2.02	3.98	1.97
26	0.7	25	0.52	2.84	1.48	6.80	2.43	5.83	2.40
27	0.7	25	1.56	1.65	2.57	5.55	2.14	4.49	2.10
28	0.7	25	2.51	1.29	3.24	5.00	2.08	4.16	2.00
29	0.7	25	4.20	0.95	3.99	4.50	1.93	3.67	1.90
30	0.7	25	7.32	0.67	4.90	4.25	1.91	3.38	1.77
31	0.7	25	10.4	0.53	5.51	3.95	1.82	3.19	1.75
32	0.7	25	11.5	0.50	5.75	3.90	1.84	3.13	1.70

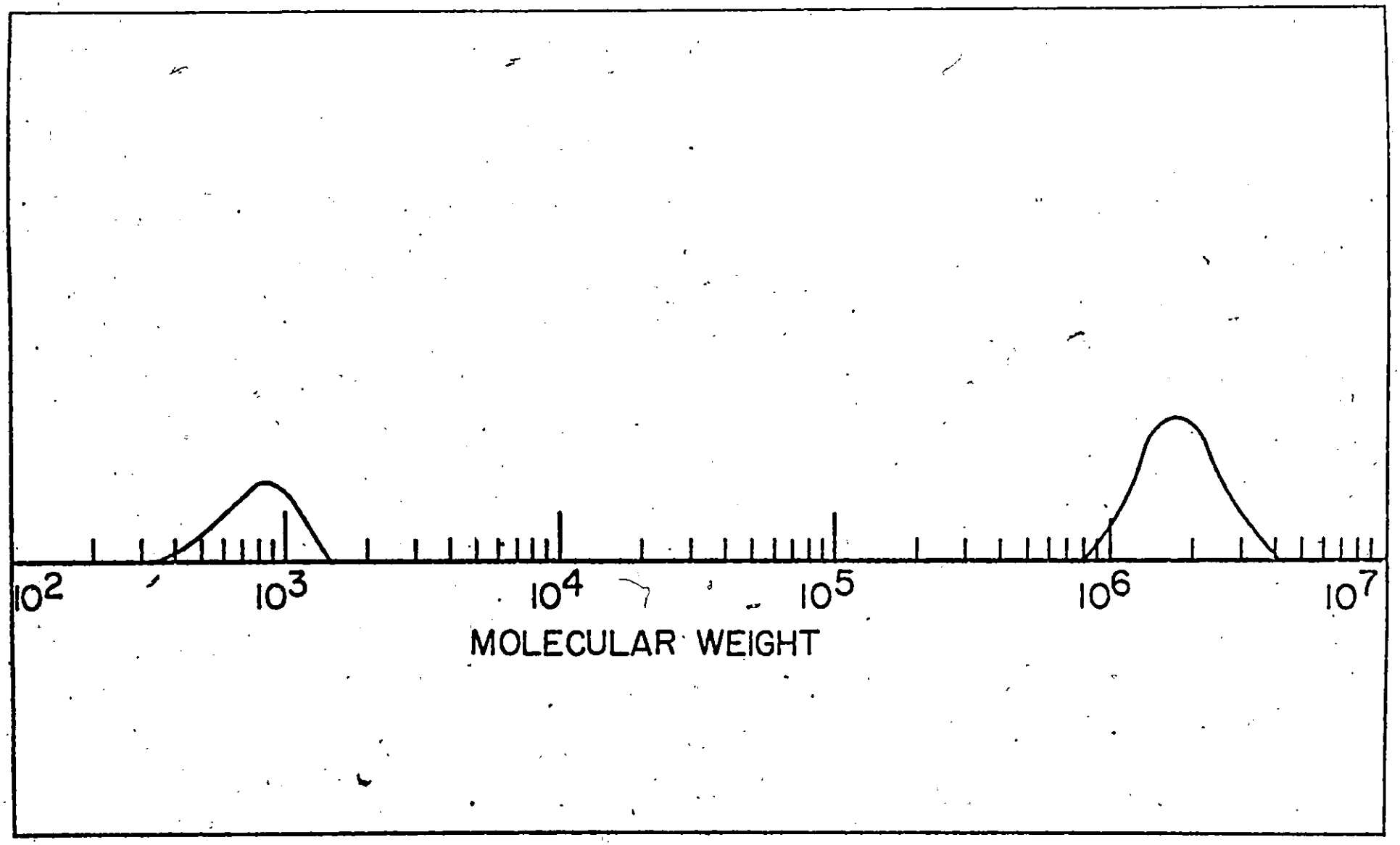

FIGURE (111-17)

111.5.4 Discussion

As mentioned above, it was noticed that figure (111-14) does not show any degradation for the 0.2 wt % solution at 40°C. The highest shear stress obtained under these conditions was 1.17×10^4 dynes/cm^2 corresponding to shear rate of 1.15×10^5 sec^{-1}. From table (111-5) we see that the minimum shear stress noticed to cause polymer degradation is 1.43×10^4 dynes/cm^2 (the first line in the table). From this it becomes evident that shear stress not shear rate is the controlling factor in shear degradation. Some degradation effects were obtained at equal shear stresses regardless of the value of the shear rate in the range studied. The effect of temperature and concentration on degradation is then simply a result of their effect on viscosity. At a constant shear rate, a decrease in temperature or increase in concentration leads to higher viscosity and higher shear stress and accordingly more degradation. GPC analyses show that the low end of the molecular weight distribution does not change under degradation. The high end, however, shows a continuous decrease in molecular weight with increasing the shear stress. This results in a narrowing of the distribution. These results seem to support Bueche's theory[34] of mechanical degradation. According to this theory chain breaking does not take place at random along the chain but occurs predominantly in the central portion of the chain where the extending forces are maximum. The theory assumes the presence of molecular entanglements to be necessary for shear degradation. In the case of polyacrylamide, entanglements should persist even at low concentrations due to the polar nature of the polymer. The theory states that for a polydispersed polymer,

all the chains with molecular weight higher than a certain critical size M_c will be broken down into low-molecular weight material. All the original polymer having molecular weight $M_1 > M_c$ will appear in the final product as molecular weight $M_1/2^n$ where n is the smallest integer to make $M_1/2^n < M_c$. The value of M_c depends on the shear rate and the viscosity. The higher the viscosity and shear rate the lower will be M_c.

M_c is easily measured at any degrading shear stress by injecting the degraded polymer in GPC, M_c will be the highest molecular weight in the distribution. For degraded polymer GPC indicates a well defined critical molecular weight. This is shown in figure (111-16) for Runs 28 and 32. The undegraded polymer has a high molecular weight end which is less well-defined. Values of degrading shear stresses and the corresponding M_c are given in table (111-5). A logarithmic plot of these data is shown in figure (111-18b). The relationship between M_c and τ will then take the form:

$$M_c = A/\tau^B \qquad (111\text{-}43)$$

where τ is the degrading shear stress in dynes/cm^2.

Equation (111-43) may be written as:

$$\log M_c = \log A - B \log \tau$$

The constants A and B may then be estimated by linear regression. When this is done we obtain:

$$M_c = \frac{3.59 \times 10^8}{\tau^{0.41}}$$

The correlation coefficient between A and B is -0.99 which is very high.

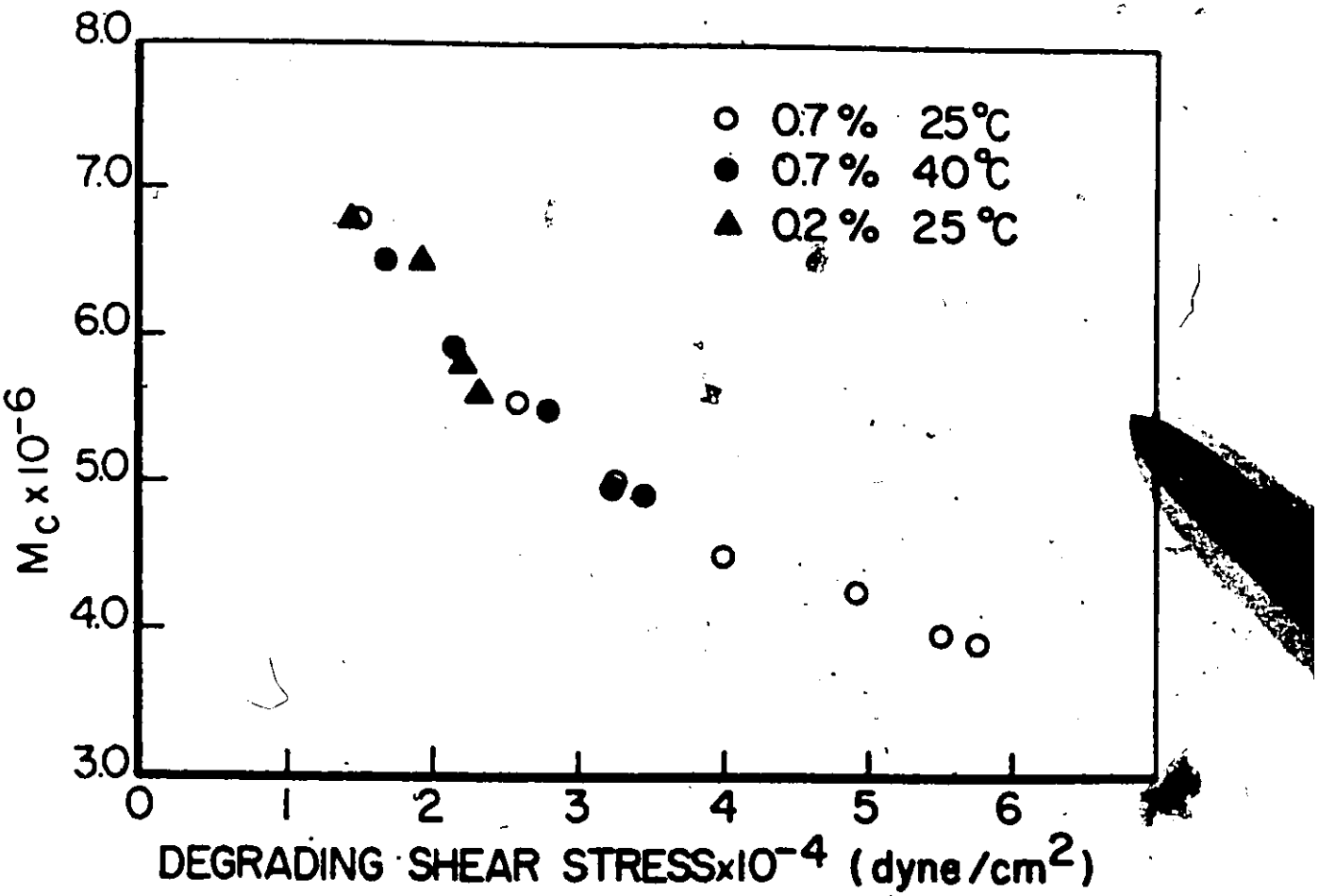

FIGURE (111-18a)

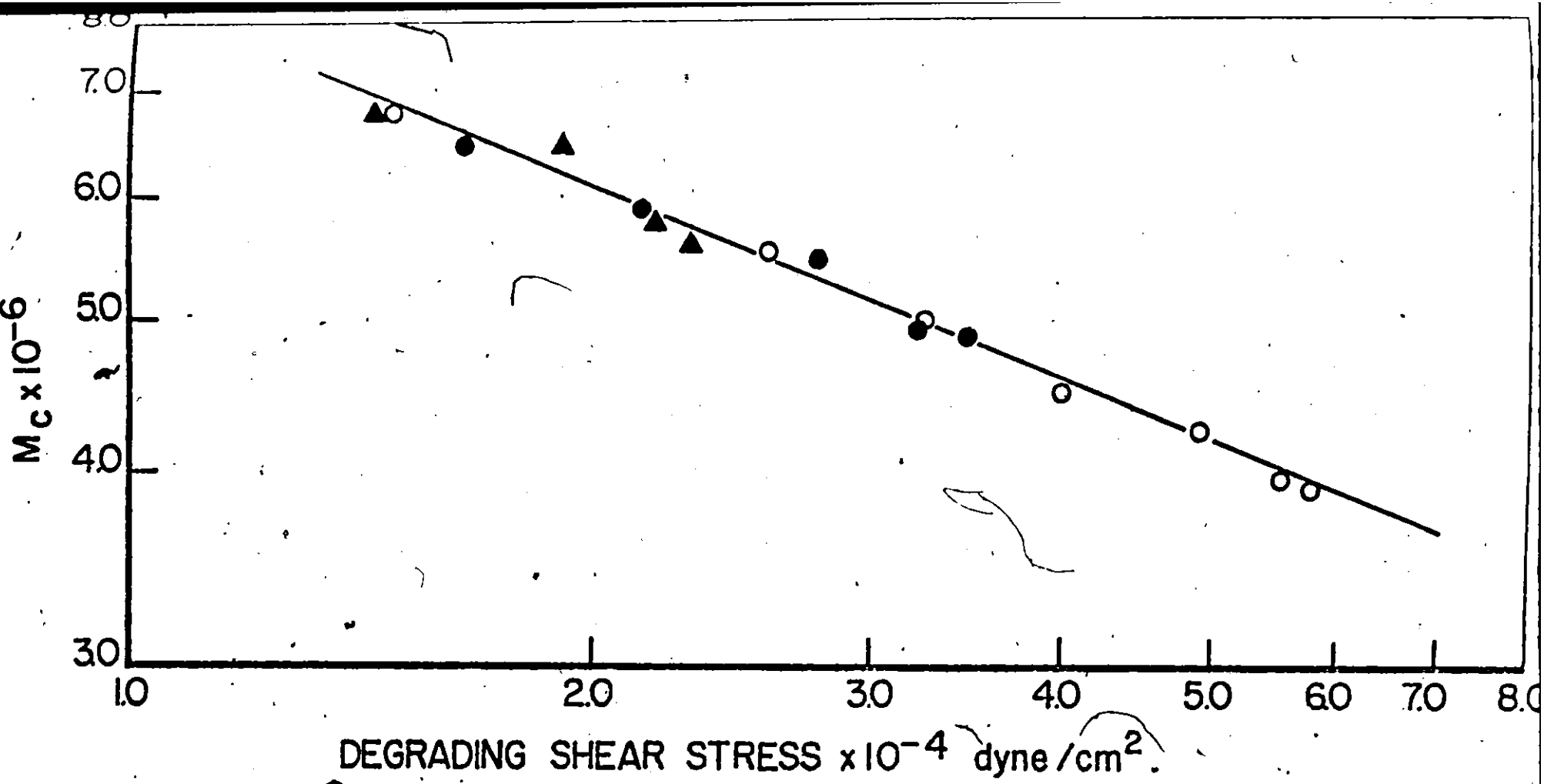

FIGURE (111-18b)

As explained before (section 1.6.3) the data are shifted far away from the origin which gives rise to the high correlation. If, however, the origin is moved near the middle value of the range of τ values available, the equation takes the form:

$$\log M_c = \log A' - B \log \frac{\tau}{\tau'}$$

In the above form, the constant A' is simply M_c at $\tau = \tau'$, while the constant A in equation (111-43) was M_c at $\tau = 1$ which is completely out of the range. The latter form gives, on regression, for $\tau' = 2.78 \times 10^4$ dynes/cm^2:

$$A' = 5.49 \times 10^6, \text{ and } B = 0.41$$

The correlation coefficient between A' and B is 0.017. Assuming the above correlations are valid for low shear stresses we can see that low shear stresses would degrade only very high molecular weight material. For example:

τ dynes/cm^2	M_c
10	13.98×10^7
100	5.44×10^7
1000	2.11×10^7

The above correlation should find use for the estimation of the stability to mechanical degradation of a polymer in applications involving a shear field.

These relatively low shear stresses are more likely to prevail in certain applications, for example in settling basins. To justify the validity of equation (111-43) in this range, degradation experiments should be carried out under these conditions. This requires the use of polymers of very high molecular weights as shown above. These polymers may be very difficult to obtain, and even then, GPC will not be an adequate tool for analysis due to its resolution limitations.

The dashed line in figure (111-16) is a theoretical prediction of the cumulative molecular weight distribution for Run 32. It was obtained from the cumulative distribution of Run 28 by straight forward application of the idealized theory of midpoint break. The original undegraded polymer has a disperse high molecular weight tail.

M_c for Run 32 is 3.9×10^6, according to the theory all molecules ranging between 3.9×10^6 and 5.0×10^6 (N_c for Run 28) should break in the middle. In this case n = 1 since 5.0/2 is less than 3.9. Since molecules of molecular weigth 5.0×10^6 would yield molecules of molecular weight 2.5×10^6 on breaking, then the fraction of the polymer of molecular weight between 2.5 and 3.9×10^6 should not change and graphically this means that the fraction of the original distribution between 2.5 and 3.9 is projected unchanged onto the

new distribution. The fraction of the new distribution having molecular weight in the range 1.95×10^6 to 2.5×10^6 is simply that in the original polymer plus the fraction of the original polymer between 3.9×10^6 and 5.0×10^6. In this way, the predicted distribution can be constructed. The agreement between theory and experiments is not very good. In fact some of the molecules will break at different distances from the center of the chain and this should lead to a distribution broader than the midpoint theory prediction. Such a distribution would agree better with experimental observations.

The low molecular weight material observed in Runs 31 and 32 is further evidence that Bueche's theory is not valid, particularly at higher shear rates. A possible explanation for the formation of very short chains, however, could be that at these elevated shear stresses the polymer chain breaks before it has time to extend appreciably. At lower shear stresses degradation does not occur until the polymer chain has extended its conformation appreciably. In other words, chain degradation occurs before equilibrium conformation is obtained and during the approach to conformational equilibrium a polymer chain can experience many breaks.

In a recent study of degradation of polystyrene using ultrasonics, Glynn et al[35,36] also found that their experimental MWD's were in disagreement with calculated MWD's based on a model which allows breakage at the mid point of the polymer chain only. A Gaussian probability distribution for the location of rupture sites along the chain and centered around the mid point gave good agreement with experiment for up to 15 breaks per original polymer molecule. For our lower shear rate experiments this approach appears promising. However, the results at high shear rates where a second MWD of very low molecular weight polymer is formed as a degradation product are radically different and would require a distribution with mean near the chain end.

III.6 Summary

This part of the thesis reports on the development of a high shear couette flow viscometer with a very narrow gap. Attention is drawn to the importance of the concentricity problem. The main design considerations are reviewed and discussed.

The instrument was first tested and calibrated using Newtonian standard oils. Two research projects were then carried out.

The first one is the study of the flow behaviour of polystyrene solutions under high shear rates ranging from 10^3 to 10^5 sec^{-1}. The results obtained agreed very well with the molecular entanglement theory.

The second project was a study of the shear degradation of polyacrylamide, a member of the water soluble polymer family. An equilibrium-type of study was carried out. Molecular weight distributions

at different stages of degradation were measured by GPC and a correlation was obtained between the critical molecular weight and the applied shear stress.

The following publications are based on Part (111) of this thesis:

1) Abdel-Alim, A.H., S.T. Balke, and A.E. Hamielec, "Flow Properties of Polystyrene Solutions under High Shear Rates", J. App. Poly. Sci., 17, 1431 (1973).

2) Abdel-Alim, A.H., and A.E. Hamielec, "Shear Degradation of Water-Soluble Polymers: I - Polyacrylamide with a High Shear Couette Viscometer", J. App. Poly. Sci., (in press).

3) Abdel-Alim, A.H., and A.E. Hamielec, "Calibration of GPC for Water-Soluble Polymers", J. App. Poly. Sci., (in press).

111.7 • Recommendations

It is recommended that smaller gaps be used in the future work to obtain higher shear rates. This will be helpful in clarifying the following questions:

1. At very high shear rates the viscosity of polymer solutions might level off to another Newtonian region. One run in the present study (PS7) indicated this, but more points at higher shear rates are needed to confirm it.

2. In the shear degradation work, very high shear stresses and degradation caused the formation of very low molecular weight material. The change in the degradation mechanism is not fully understood. Further work is required to elucidate the mechanism of degradation.

3. Similar degradation studies with different polymers should be done to obtain expressions similar to equation (111-43). A general correlation may then be generated for a range of polymer types. The effect of geometrical factors such as bulky side groups situated on the polymer chain would be most interesting.

111.8 Nomenclature

a	constant in Power Law
A,B	constants in transducer cell calibration curve
A_r	real area of contact (cm^2)
A',B'	constants in Andrade Equation
b	film thickness (in)
c	eccentricity ratio, also solution concentration
E	entanglement density
F	friction force (dynes)
$f(\tau)$	function of shear stress defined by Eq. (111-4)
G	recorder pen deflection due to force
k	thermal conductivity (BTU ft/ft^2 sec°F)
K	constant in Power Law - Eq. (111-13)
L	length of shear area (in)
M	molecular weight of monodisperse polymer
MWD	molecular weight distribution
M_c	critical molecular weight
m	constant in Power Law
n	constant in Power Law
p	pressure (psi)
Q	Torque at outer cylinder surface (dyne cm)
Q'	Torque at inner cylinder surface (dyne cm)
r	radial coordinate (in)
R_o	inner radius of outer cylinder (radius of hole)(in)
R_1	outer radius of outer cylinder (in)

R_2	radial distance to thermocouples in outer cylinder (in)
R_1	radius of inner cylinder (in)
S	R/R_o
T	temperature (°C)
T_f	temperature at R_o(°C)
T_c	temperature at R_2(°C)
T_{R_1}	temperature at R_1(°C)
T_m	temperature at which shear stress was measured (°C)
T_1, T_2, T_3, T_4	temperature in outer cylinder (averaged to obtain T_c)(°C)
$\underline{v}$	velocity vector
v_1	velocity of inner cylinder (in/sec)
v_0	tangential component of velocity, (in/sec)
W	weight (gms)
W_o	weight at zero pen deflection (gms)
x,y	cartesian co-ordinates - Eq. (111-27)

Greek Symbols

τ_{av}	average shear stress of real area of contact (dynes(cm)$^{-2}$)
τ	shear stress (dynes(cm)$^{-2}$)
τ_r	rouse relaxation time
τ_o	observed relaxation time
ω	angular velocity across gap (radians/sec)
θ	angular co-ordinates (radians)
$\dot{\gamma}$	shear rate (sec)$^{-1}$
$\underline{\Delta}$	rate of deformation tensor
ΔT	maximum temperature rise (°C)

Ω	angular velocity of inner cylinder (radians/sec)
μ	Newtonian viscosity (poise)
η	non-Newtonian viscosity (poise)
η_o	viscosity at zero shear rate
λ	relaxation time
Γ	Gamma function

111.9 References

1. Graessley, W.W.,
"Molecular Aspects of Viscoelasticity in Concentrated Polymer Systems",
ACS Polymer Preprints, 13, 35 (1972).

2. Balke, S.T.,
Ph.D. Thesis,
McMaster University (1972).

3. Middleman, S.,
"The Flow of High Polymers",
Interscience Publishers, New York (1968).

4. Barber, E.H., J.R. Muenger, and F.J. Villforth,
Anal. Chem., 27, 3 (1955).

5. Porter, R.S., and J.F. Johnson,
J. Phys. Chem., 63, 202 (1959).

6. Porter, R.S., and J.F. Johnson,
J. Appl. Phys., 35, 3149 (1964).

7. Porter, R.S., J.F. Johnson, and R.F. Klaver,
Rev. Scientific Inst., 36, 1846 (1965).

8. Porter, R.S., J.F. Johnson, and M.J.R. Cantow,
J. Polymer Sci., 16, 1 (1967).

9. Reches, E.,
"Studies of the Flow Properties Under High Shear Rates of Selected Organic Compounds in the Molecular Weight Range of Lubricating Oils",
Ph.D. Thesis, University of Cincinatti, Cincinatti, Ohio, (1967).

10. Krieger, I.M., and H. Elord,
J. Appl. Phys., 24, (2), 134 (1953).

11. Pierce, P.E.,
J. Paint Technology, 41, 383 (1969).

12. Harper, J.C.,
Rev. Scientific Inst., 32, 425 (1960).

13. Porter, R.S.,
Seminar,
University of Toronto, (1968).

14. Van Wazer, J.R., J.W. Lyons, K.Y. Kim, and R.E. Colwell, "Viscosity and Flow Measurement", Interscience Publishers, New York (1963).

15. Inglis, D.R., Phys. Rev., 56, 1041 (1939).

16. Bishop, R.E.D., and A.G. Parkinson, Appl. Mech. Rev., 21, 439 (1968).

17. Cameron, A., "The Principles of Lubrication", John Wiley and Sons Inc., New York (1966).

18. Tao, F.F., and W. Philippoff, ASME Trans., 10, 302 (1967).

19. Hori, Y., J. Appl. Mechanics, Trans. of ASME, 189 (1959).

20. Martin, F.A., Paper No. 63-LUBS-8, "Steady-State Whirl in Journal Bearings for a Vertical Flexible Rotor System", 1963 ASME Lubrication Symposium.

21. Rabinowicz, E., "Friction and Wear of Materials", John Wiley and Sons, Inc., New York (1965).

22. Bueche, F., J. Chem. Phys., 22, 1570 (1954).

23. Bueche, F., "Physical Properties of Polymers", Interscience, New York (1962).

24. Graessley, W.W., J. Chem. Phys., 43, 2696 (1965).

25. Rouse, P.E., J. Chem. Phys., 21, 1272 (1953).

26. Graessley, W.W., J. Chem. Phys., 47, 1942 (1967).

27. Williams, M.C., AIChE J., 12, 1064 (1966).

28. Graessley, W.W., R.L. Hazleton, and L.R. Lindeman,
Trans. Soc. Rheol., 11, (3), 267 (1967).

29. Stratton, R.A.,
J. Colloid Interface Sci., 22, 517 (1966).

30. Porter, R.S., and J.F. Johnson,
Chem. Rev., 66, 1 (1966).

31. Wade, J.H.T., and P. Kumar,
J. Hydronautics, Vol. 6, No. 1, 40 (1972).

32. Porter, R., M. Cantow, and J. Johnson,
Polymer, 8, 87 (1967).

33. Cantow, M., R. Porter, and J. Johnson,
J. Poly. Sci. C, 16, 13 (1967).

34. Bueche, F.,
J. App. Poly. Sci., Vol. IV (10), 101 (1960).

35. Glynn, P.A.R., B.M.E. Van der Hoff, and P.M. Reilly,
J. Macromol. Sci. - Chem. A6(8), 1653 (1972).

36. Glynn, P.A.R., and B.M.E. Van der Hoff,
"Degradation of Polystyrene in Solution by Ultrasonation - A Molecular Weight Distribution Study",
J. Macromol. Sci. - Chem. (1973). In press.

37. Ishige, T., and A.E. Hamielec,
"Solution Polymerization of Acrylamide to High Conversion",
J. Applied Polymer Sci., 17, 1479 (1973).

38. Swartz, T.D., D.D. Bly, and A.S. Edwards,
"A Valid Method of Calibration which Includes Correction for Dispersion in GPC",
J. Applied Polymer Sci., 16, 3353 (1972).

39. Cantow, M.J.R., R.S. Porter, and J.F. Johnson,
J. Polymer Sci., A-1, 5, 1391 (1967).

40. Flory, P.J.,
"Principles of Polymer Chemistry",
6th Edition (1967) p 312, Cornell University Press.

111.10 Appendices

APPENDIX (111-1)

GPC Calibration for Water-soluble Polymers

In a recent investigation of the free radical polymerization of acrylamide in aqueous solution[37], it was found that classical kinetics accurately predict the molecular weight distribution (MWD) of the synthesized polymer. Transfer to monomer controls molecular weights giving a linear polymer having the most probable distribution. This presents a convenient method of synthesizing water-soluble standards for GPC calibration. The linear polyacrylamide has a very broad MWD which is the most probable distribution. This broad MWD standard can be used to determine the GPC molecular weight calibration over a wide range of molecular weights. Mark-Houwink constants are available for polyacrylamide in water[37] and these can then be used to construct a universal calibration curve for GPC. The universal calibration curve may then be used to construct molecular weight calibration curves for other water-soluble polymer. This statement should be qualified somewhat. To date, Benoit's universal calibration curve concept has not been proven valid for water-solube polymers. It is likely, however, that the wide applicability of the universal calibration curve for water-soluble polymers will be experimentally verified in the near future.

Two broad MWD polyacrylamides, Standards A and B were synthesized in aqueous solution using a free-radical initiator, 4,4' azobis-4-cyanovaleric

acid (ACV) and isothermal polymerization[37]. The synthesis conditions were:

Standard A

T = 40°C, monomer concentration = 0.281 moles/liter,

ACV concentration = 714 x 10^{-4} moles/liter

Standard B

T = 50°C, monomer concentration = 0.563 moles/liter

ACV concentration = 1.43 x 10^{-3} moles/liter.

Standard A, with theoretical differential MWD,

$$W(M) = \frac{M}{\bar{M}_n^2} \exp\left(-\frac{M}{\bar{M}_n}\right) \qquad (111\text{-}44)$$

where M is molecular weight and W(M) is weight fraction, and $\bar{M}_n$ = 2.52 x 10^6, $\bar{M}_w$ = 5.04 x 10^6, $\bar{M}_z$ = 7.56 x 10^6 was used to find the GPC molecular weight calibration curve. Figure (111-19) shows the cumulative most probable distribution and cumulative GPC chromatogram for Standard A. The use of these curves as shown provided the molecular weight calibration curve which adequately corrects for axial dispersion was recently successfully applied by Swartz, Bly and Edwards[38] and was first suggested by Cantow, Porter and Johnson[33].

The calibration curve in figure (111-20) was then used to determine the MWD and molecular weight averages of Standard B. Figure (111-21) shows a comparison of the MWD measured by GPC and equation

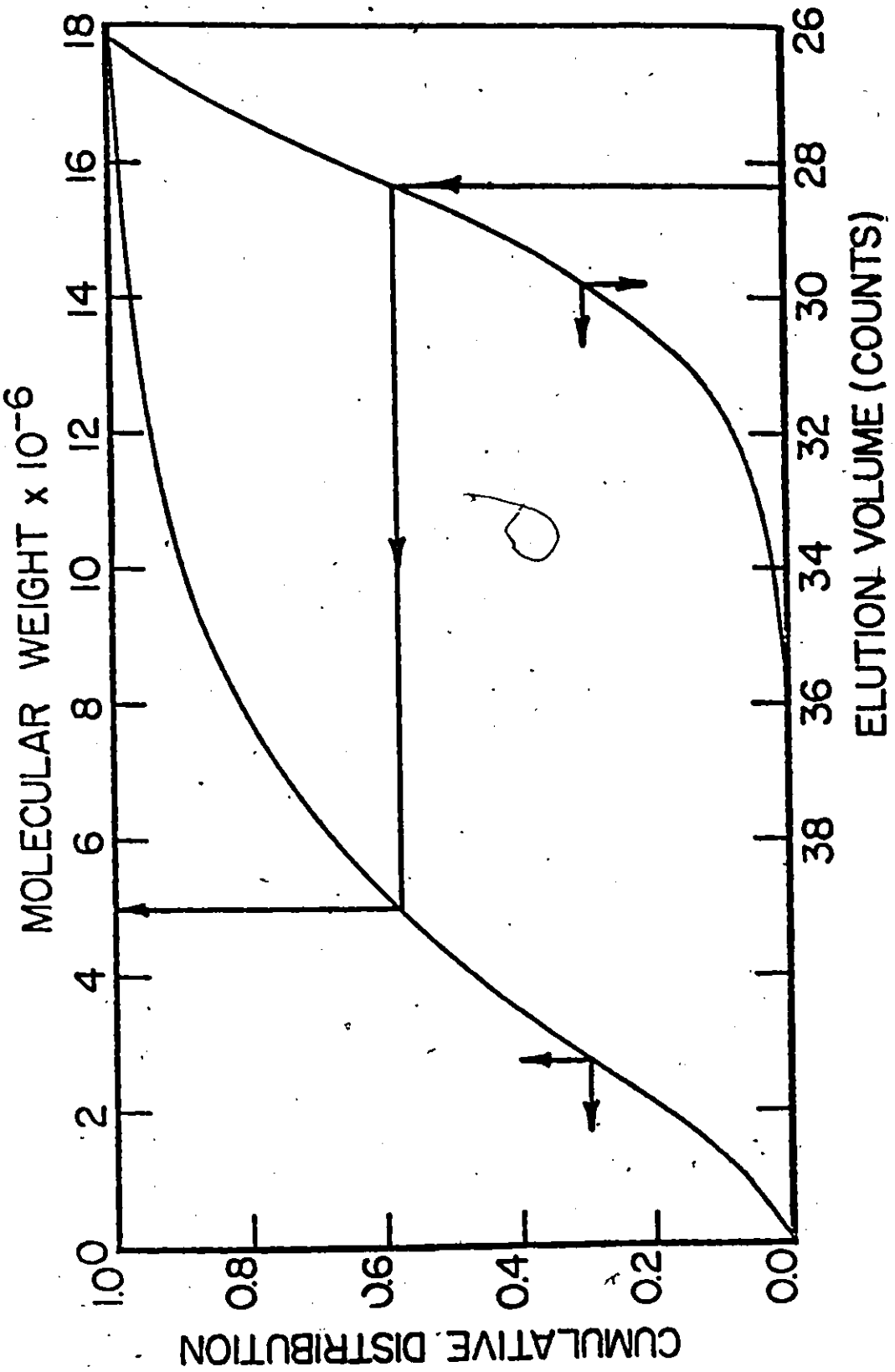

FIGURE (111-19)

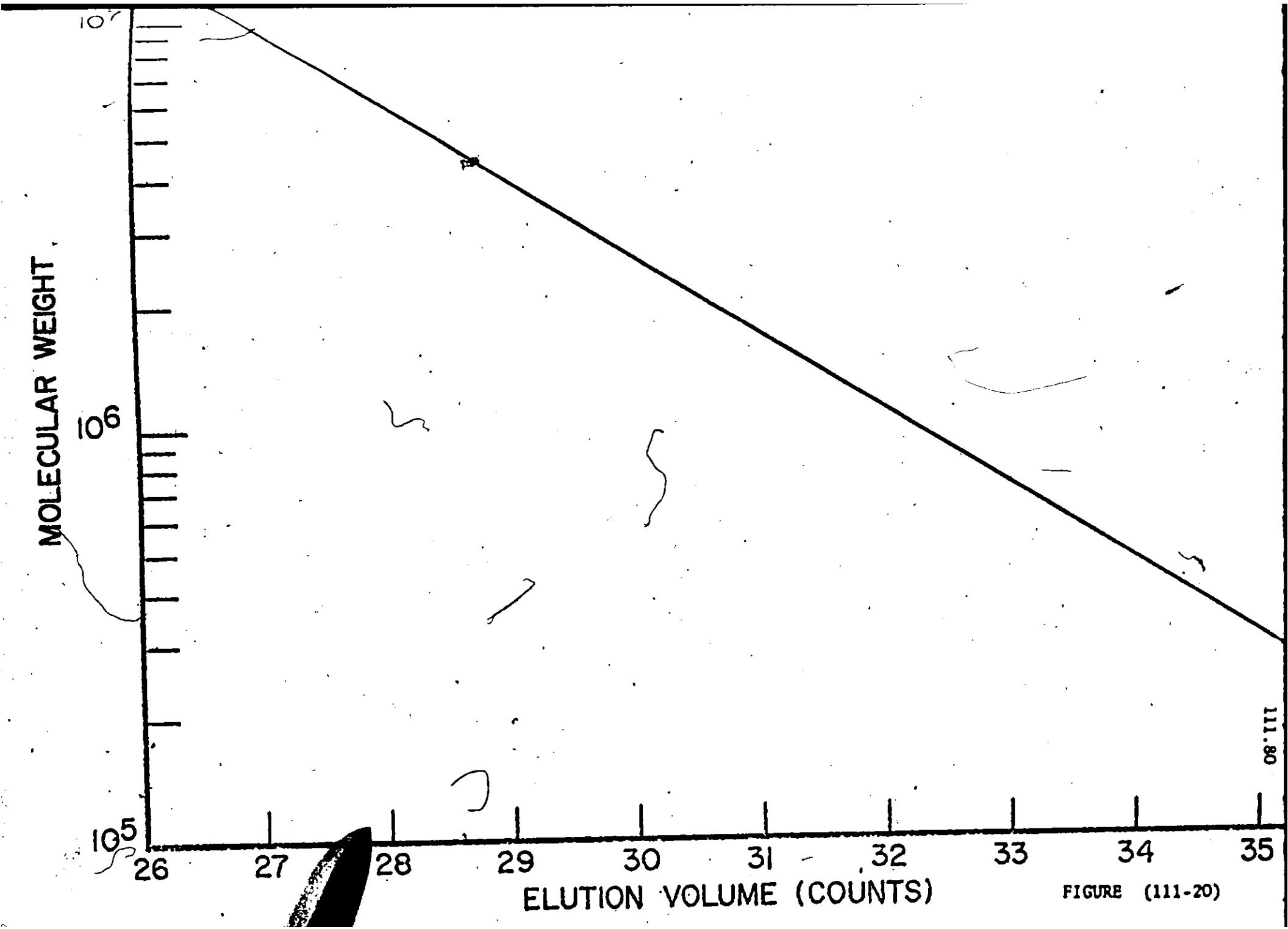

FIGURE (111-20)

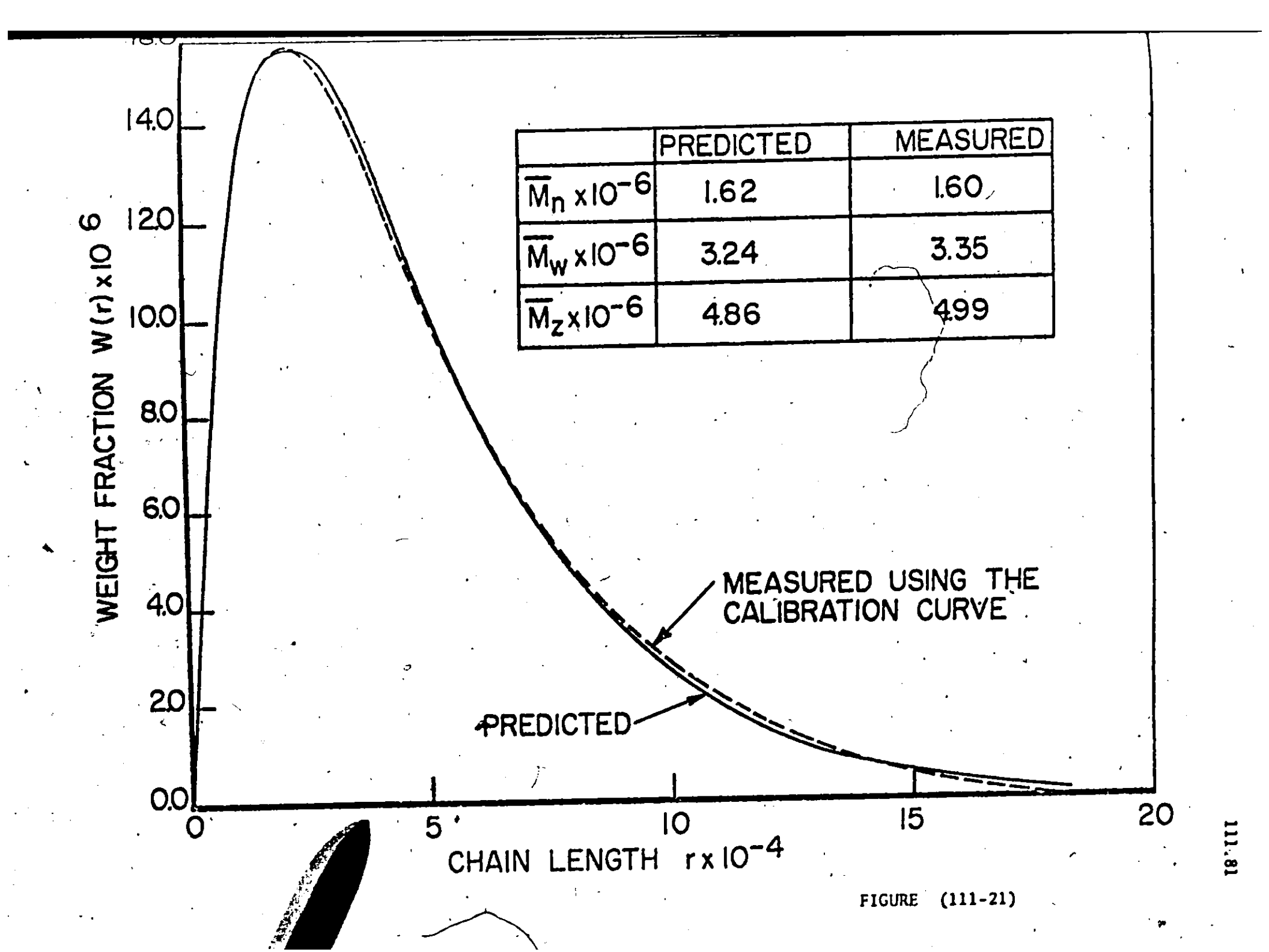

FIGURE (111-21)

(111-44) with $\bar{M}_n = 1.620 \times 10^6$. Also shown is a comparison of molecular weight averages, $\bar{M}_n$, $\bar{M}_w$ and $\bar{M}_z$. The good agreement gives validity to the molecular weight calibration curve in figure (111-20).

Viscometry

Mark-Houwink equations for linear polyacrylamide in aqueous solution at T = 25°C follow (37):

$$[\eta] = 6.80 \times 10^{-4} \bar{M}_n^{0.66} \qquad (111\text{-}45)$$

$$[\eta] = 4.54 \times 10^{-4} M^{0.66} \qquad (111\text{-}46)$$

where

$$4.54 \times 10^{-4} = \frac{6.80 \times 10^{-4}}{\Gamma(2+a)} \quad \text{and } a = 0.66$$

Equation (111-45) was proven valid for polyacrylamide having the most probable distribution[37] and accordingly equation (111-46) can be derived from equation (111-45).

To further test the validity of the GPC molecular weight calibration curve in figure (111-20), Standard B was characterized by viscometry. Its intrinsic viscosity at 25°C in water was measured to be 8.17. The intrinsic viscosity of Standard B measured by GPC was found to

$$[\eta]_{GPC} = 4.54 \times 10^{-4} \int_0^{\infty} F(v)\, M(v)^{0.66}\, dv = 8.21$$

where F(v) is the normalized GPC detector response and V is the retention volume. The basis for this calculation may be found in Flory's text[40].

Finally using equation (111-45)

$$[\eta]_{Eq.(111-45)} = (6.80 \times 10^{-4})(1.60 \times 10^{6})^{0.66} = 8.45$$

This excellent agreement confirms the validity of the GPC calibration curve in figure (111-20).